Design and control of an energy storage system for voltage flicker caused by clouds passing over photovoltaic systems

Master Thesis Report

Lynrick Wix

Delft University of Technology

Design and control of an energy storage for voltage flicker caused by clouds passing over photovoltaic systems

Master Thesis Report

by

Lynrick Wix

Student number 4534654

Project duration 14 February 2023 — November 9 2023

Thesis committee:			
	Prof. dr. ir. Pavol Bauer	Delft University of Technology	Chairman
	dr. ir. Gautham Ram Chandra Mouli	Delft University of Technology	Supervisor
	dr. ir. Arjan van Voorden	Stedin	Supervisor
	dr. ir. Milos Cvetkovic	Delft University of Technology	External Member

External supervisor: Ing. Henk Fidder, Stedin

In partial fulfilment of the requirements for the degree of

Master of Science
in Electrical Engineering

at Delft University of Technology.

To be publicly defended on Thursday 9 November 2023 at 3:00PM CET

An electronic version of this thesis is available at `http://repository.tudelft.nl/`.

STEDIN.NET

TU Delft Delft University of Technology

Abstract

As more and more solar panels are installed on households, a problem arises when the power from the solar panels fluctuating throughout the day due to clouds passing over the solar panels. This in turn causes voltage flickers in the household, which can be visible/irritable to the human eye and damage appliances in the household. These voltage flickers can exceed limits set by the IEC standard 61000-3-7 or the visible flicker threshold on the Low Voltage (LV) network set by Qualtech [1]. This problem can be solved by making use of an Energy Storage System (ESS) which delivers active power in order to reduce and avoid the voltage fluctuations above the visible flicker threshold.

In this report, a novel control algorithm is designed and implemented in two different ways to control the active power dispatch of the ESS. The main goal for the control algorithm is to reduce or avoid any visible voltage flickers from occurring and minimizing energy usage as much as possible in order to open the possibility for a Supercapacitor Energy Storage System (SESS) application in the future. For this, a power to energy ratio of higher than 70 is needed to achieve this. The primary control algorithm makes use of a moving average with a weight distribution that is optimised for smoothness and accuracy. Furthermore, extra layers of control was added to the control algorithm to minimize energy usage. The first implementation of the control algorithm, called power control, makes use of the Photovoltaic (PV) system output power to dispatch the appropriate amount of power from the ESS. The second implementation, called voltage control, makes use of the measured voltage at Point of Common Coupling (PCC) to dispatch the ESS power.

Simulation results using pre-existing PV system data showed that the power control implementation was not able to fully eradicate all of the measured visible and annoying voltage flickers. The voltage control implementation was able to do so within the window of operation. Furthermore, simulation results showed that the energy usage from the control algorithm with a power control implementation uses 87% percent less energy than a control algorithm using conventional moving average. The energy usage from the control algorithm with a voltage control implementation uses 95% less energy than the conventional moving average control algorithm. Furthermore, the power to energy ratio of the control algorithm with a power control implementation was around 98.9 and with a voltage control implementation the power to energy ratio was around 190.2. This shows a clear implementation of a SESS in the future.

Two different experimental setups were built and commissioned. The first setup having the Battery Energy Storage System (BESS) connected via an inverter on the same Alternating Current (AC) bus with the PV system. The second setup has the BESS connected on the same Direct Current (DC) bus with the PV system which is then connected to an inverter. Experiment results showed that the DC connected ESS experiment setup operating in power control mode had the best performance in terms of avoiding any visible voltage flickers from occurring. While the AC experimental setup and mode of operation (voltage and power control mode) did not operate properly due to the slow inverter response time. In terms of energy usage, both experimental setups had very low ESS energy usage. Although the results showed that power to energy ratio from both experimental setups using both power and voltage control did not exceed the set goal of 70 due to the limitations of both experimental setups.

Finally, a conclusion based on the results is given with future work and as well as recommendations for the continuation on this research topic.

Acknowledgment

This thesis has been produced as the final work to obtain my Master in Science degree in Electrical Power Engineering at Delft University of Technology. First off, I want to express my gratitude towards Arjan and Henk for given me the opportunity to work on this thesis in collaboration with Stedin and for their continuous support throughout the project with their priceless advice, guidance and financial contribution to the experimental setup(s). I would also want to express my gratitude to Gautham for his constant support and advice throughout the project, I really appreciate our brainstorming sessions and feedback you have given me. Furthemore, I would like to thank Prof. Bauer and Dr. Cvetkovic for being part of the committee and evaluating my work.

Furthermore, a lot of this project would not be possible without the help of the lab technicians of the ESP lab and for that I want to thank Bart, Joris and Harrie for their constant support. You guys really helped me allot with the practical aspect of my thesis but also guiding me as to what can be achieved within the timeframe of the thesis and providing valuable advice for my thesis report and presentation. I also really appreciate you guys' readiness to always help whenever I am stuck with something and small talks we had about anything during the breaks at the ESP lab.

I also want to thank Sharmila for not only setting up everything for my defense and helping out with the forms that had to be handed in to the examination committee, but also arranging the storage for the material used for the shade experiments and giving me priceless advice for my career in the future.

The shade experiment was done with the help of multiple people, otherwise this would not have been possible. For that I want to thank the following people in no particular order. Lyndon, Sara, Xiangyu, Bart, Joris, Hitesh, Rohan, Bob, Koen, Tjeu, Avinash and Henk. You guys were ready to help me out for this experiment whether it be during, before or after the experiment and for that I express my gratitude to all of you.

This thesis was also not possible without the support I have from my family and friends. I want to thank my mom Maybeline, my dad Eduardo, my brother Lyndon, my cousins Danielle and Alexander and other family members for their support and advice throughout this period of my life. Friends that have also been there throughout this period such as my day ones from way back during my bachelor Henk, Avinash and Laura. My good friends whom I studied with and call family these days Xiangyu, Sara, Francesca and David. My gym buddies Jacopo and Patrick. Friends from my time during Delft Hyperloop Bob, Tjeu, Sebas and everyone else. Friends from the office during my thesis period Rohan, Jeroen, Patrick, Nikolina, Nestor, Hitesh, Fan Xie and everyone else. Also I want to thank all of the amazing people I met during my time at Lightyear, Tesla, Stedin and during my time as a juror at the European Hyperloop week. You guys were not only amazing and fun people, but also I have learned so much from you all that I will forever take this with me for the rest of my career.

Sin ningun di bosnan, lo mi nunca a yega na unda mi ta awe como un persona y como un ingeniero. Masha danki na cada un di bosnan!

Pa mi Abe stima.

Contents

List of Figures 8

List of Tables 10

1 Introduction 13
1.1 Problem statement for research topic . . . 14
1.2 Motivation for research . . . 17
1.3 Main research goal and sub research goals . . . 18
1.4 Outline report . . . 18
1.5 Conventions and general terms . . . 19

2 Existing research review 20
2.1 Existing design of test setups and setting for research topic . . . 21
2.2 Types of ESS considered . . . 22
2.3 Control algorithm . . . 23
2.4 Research gap for this thesis . . . 24

3 Control algorithm design and simulation 25
3.1 Control algorithm choice . . . 25
3.2 Control algorithm design . . . 25
3.2.1 Moving average algorithm . . . 26
3.2.2 Window of operation . . . 28
3.2.3 State of Charge (SoC) power reduction curve . . . 29
3.2.4 Idle charge/discharge . . . 30
3.3 Voltage sensitivity calculation . . . 31
3.4 Power control design . . . 32
3.5 Voltage control design . . . 34
3.6 Simulation setting and assumptions . . . 35
3.7 Simulation results of power control . . . 36
3.7.1 Moving average type simulation results . . . 36
3.7.2 Window of operation check simulation results . . . 38
3.7.3 State of Charge (SoC) power reduction curve simulation results . . . 39
3.7.4 Idle charge and discharge simulation results . . . 39
3.7.5 Summary of simulation results and performance results during different seasons . . . 41
3.8 Simulation results of voltage control . . . 43
3.8.1 Moving average type simulation results . . . 43
3.8.2 Window of operation check simulation results . . . 44
3.8.3 State of Charge (SoC) power reduction curve simulation results . . . 45
3.8.4 Idle charge and discharge simulation results . . . 45
3.8.5 Summary of simulation results and performance results during different seasons . . . 46

4 Experimental setup design 49
4.1 AC connected ESS experimental setup . . . 49
4.2 DC connected ESS experimental setup . . . 52
4.3 Graphical User Interface (GUI) design . . . 55
4.3.1 'Initialize Connections' button . . . 56
4.3.2 Drop down menu for choosing control algorithm . . . 56
4.3.3 'Read/write registers' button . . . 57
4.3.4 'Pause' and 'Export data to CSV file' button . . . 57
4.3.5 Safety features implemented through the Graphical User Interface (GUI) . . . 57

5 Experimental results 59
5.1 Measured voltage sensitivity . . . 59
5.2 Voltage flicker avoidance . . . 59
5.2.1 AC connected ESS experimental setup . . . 60
5.2.2 DC connected ESS experimental setup . . . 61

5.2.3 Full day experiment . . . 63
5.2.4 Summary of results . . . 64
5.3 Energy usage . . . 64
5.3.1 AC connected ESS experimental setup . . . 64
5.3.2 DC connected ESS experimental setup . . . 65
5.3.3 Summary . . . 66
5.4 Comparison between the experimental setups and control algorithm implementations . . . 66
5.5 Limitations of experimental setups . . . 67
5.5.1 Inverter response time delay . . . 67
5.5.2 Inverter power setpoint reaction . . . 68
5.5.3 Measurement devices limitation . . . 69
5.5.4 Connected loads at the DC connected ESS experimental setup . . . 69

6 Conclusion and Recommendation for future research 70
6.1 Conclusion . . . 70
6.1.1 Voltage fluctuation below visible flicker using ESS and control algorithm . . . 70
6.1.2 Minimization of the ESS energy usage with the control algorithm . . . 70
6.1.3 Design, build and commission two experimental setups . . . 71
6.1.4 Compare the performance of both experimental setup with both implementation of the control algorithm . . . 71
6.2 Recommendation for future research . . . 71
6.2.1 Fast responding inverter . . . 71
6.2.2 Implementation of a SESS . . . 72
6.2.3 Cost analysis . . . 73
6.2.4 Sensitivity analysis of the control algorithm with experimental setups . . . 74
6.2.5 Simulation of the control algorithm with an ESS at a distribution level . . . 74
6.2.6 Simulation of the control algorithm with an ESS at a utility level . . . 75
6.3 Final thoughts . . . 76

Bibliography 77

A Appendix, Simulation 80
A.1 Simulation results . . . 80
A.1.1 Energy usage throughout the day with different layers - Power control . . . 80
A.1.2 Energy usage throughout the day with different layers - Voltage control . . . 81
A.2 Matlab script for simulation . . . 81
A.2.1 Voltage control simulation Matlab script . . . 81
A.2.2 Power control simulation Matlab script . . . 81
A.2.3 Full year power control simulation Matlab script . . . 81
A.2.4 Full year voltage control simulation Matlab script . . . 81
A.2.5 Voltage flicker curve mapping Matlab script . . . 81

B Appendix, Experimental setup & results 82
B.1 Final parameters used for the experimental setups . . . 82
B.1.1 Power control for AC connected ESS experimental setup . . . 82
B.1.2 Voltage control for AC connected ESS experimental setup . . . 83
B.1.3 Power control for DC connected ESS experimental setup . . . 83
B.1.4 Voltage control for DC connected ESS experimental setup . . . 84
B.2 Configuration file for experimental setups . . . 85
B.2.1 Configuration file for DC experimental setup . . . 85
B.2.2 Configuration file for AC experimental setup . . . 86
B.3 Matlab script for GUI and data processing . . . 86
B.3.1 Graphical User Interface (GUI) Matlab code for DC connected ESS experimental setup . . . 86
B.3.2 Graphical User Interface (GUI) Matlab code for AC connected ESS experimental setup . . . 86

C Appendix, Datasheets 87
C.1 Datasheets . . . 87
C.1.1 Power optimizer datasheet . . . 87
C.1.2 DC circuit breaker datasheet . . . 90
C.1.3 ATEPS battery module datasheet . . . 93
C.1.4 Victron lead acid battery module . . . 96
C.1.5 Battery cells used for ATEPS module datasheet . . . 101
C.1.6 Victron compatible energy meters datasheet . . . 106

C.1.7 Pylontech Lithium-Iron-Phosphate (LFP) battery pack datasheet . . . 108
C.1.8 SkelMod 102V88F Electric Double Layer Capacitor (EDLC) Supercapacitor module datasheet . . . 111
C.1.9 Eltek 48V DC/DC Converter datasheet . . . 114
C.1.10 Victron Multiplus II datasheet . . . 117
C.1.11 Victron Multiplus II - GX datasheet . . . 120
C.1.12 PV system cost for Delft . . . 123

D Cost analysis 132
D.1 Existing PV system setup and assumptions made . . . 132
D.2 Types of ESS considered. . . . 133
D.3 Cost of an upgraded solution . . . 134
D.3.1 AC connected BESS system cost . . . 134
D.3.2 DC connected BESS system cost . . . 135
D.3.3 AC connected SESS system cost . . . 136
D.3.4 DC connected SESS system cost . . . 137
D.4 Cost of an integrated solution . . . 137
D.4.1 AC connected BESS system cost . . . 138
D.4.2 DC connected BESS system cost . . . 138
D.4.3 AC connected SESS system cost . . . 139
D.4.4 DC connected SESS system cost . . . 140
D.5 Summary of findings . . . 141

List of Figures

1.1 Different types of application of photovoltaic systems. . . . 13
1.2 Examples of the PV output power on cloudy and clear sky summer day. . . . 14
1.3 Simplified electrical diagram of a household with a PV system is installed. V_{PCC} is the voltage at PCC and P_{PV} is the power delivered by the PV system. . . . 14
1.4 Example illustrating PV power fluctuation and voltage flickers from collected PV data. . . . 15
1.5 Illustration of how fast the PV system fluctuates with 30% of its power capacity from collected PV data. . . . 16
1.6 Flicker curve as described in the paper published by QualTech [1]. . . . 16
1.7 Voltage quality study done in the Paddepoel area of Groningen. The x-axes denotes the measured values of the P_{lt} with respect to the maximum allowable value from the Distribution System Operator (DSO). Plt_95% (highligthed by the red rectangle) denotes the measured P_{lt} with the orange line denoting the maximum allowable value define by the Distribution System Operator (DSO)'s and grid codes and standards . . . 17
1.8 The two different connection types for the ESS. The red and black line indicates the DC positive and negative poles. The orange line indicates the AC line connection to the grid. Finally the dashed black lines indicate a communication line between the control algorithm and inverter. . . . 18

2.1 Expermintal setup designs of which the highlighted parts will be discussed in this section. . . . 20
2.2 System design and simulation results from Kakimoto et al [2]. . . . 21
2.3 Simulation results of the voltage at PCC and the delivered power from ESS presented by the authors[3]. . . . 21

3.1 Order in which each control layer is implemented for the control algorithm. . . . 26
3.2 Weight distribution of the simple moving average algorithm. . . . 26
3.3 Different weight distribution considered for the moving average control algorithm, the window size for each graph is thirty. . . . 27
3.4 Weight distribution calculated by the author and used for this research. The author illustrated an example of the weight distribution using fifty element for the window for the moving average calculation. While the example given for this research has a window of 30 elements. . . . 27
3.5 Performance of the two types of moving averages. The red line in the graph is the moving average line using the optimised weight distribution and the green line is the simple moving average line. Finally the blue line is the stock prices which is used for the moving average calculation. . . . 28
3.6 Summer operating window compared to PV system generation during the summer. . . . 29
3.7 State of Charge (SoC) power reduction curve for both charge and discharge power. . . . 30
3.8 Example of idle charge/discharge control layer, the upper and lower threshold denotes 40 and -40W respectively. 31
3.9 Example of voltage flickers exceeding the visible and annoying flicker curve, highlighted by the yellow rectangle. 32
3.10 Example of a power control implementation with the designed control algorithm. . . . 32
3.11 Power control sequence of action. . . . 33
3.12 Example of a voltage control implementation with the designed control algorithm. . . . 34
3.13 Voltage control sequence of action. . . . 35
3.14 System design and simulation results from Kakimoto et al. . . . 36
3.15 PV output power compared to the simple moving average output and the moving average with optimised weights output. . . . 37
3.16 Energy usage throughout the day with idle charge and discharge . . . 40
3.17 Voltage flickers measured before and after applying power control. . . . 42
3.18 Energy usage throughout the day with idle charge and discharge. . . . 46
3.19 Voltage flickers measured before and after applying voltage control. . . . 47

4.1 Locations of PV systems used for the experimental setups. The map is a satellite image of the Electrical Engineering Mathematics Computer Science (EEMCS) faculty. . . . 49
4.2 AC connected ESS experimental setup design. . . . 50
4.3 Pictures of the actual AC connected ESS experimental setup. . . . 51
4.4 DC connected ESS experimental setup design for the research. . . . 53
4.5 Pictures of the actual DC connected ESS experimental setup. . . . 54
4.6 Graphical User Interface (GUI) for the AC connected ESS experimental setup. . . . 55
4.7 Graphical User Interface (GUI) for the DC connected ESS experimental setup. . . . 56
4.8 Example of the measured ESS power that is continuously plotted in real time. . . . 57

5.1 Summary of the procedure to measure the voltage sensitivity as explained in section 3.3. . . . 59
5.2 Illustration of how the shade experiments were conducted. The planks were moved up and down along the PV panels by pulling on a rope that is attached to the planks and runs all the way behind the PV system. . . . 60
5.3 Reference measurement from the the PV system from the AC connected ESS experimental setup. A 400 W increase resulted in a visible voltage flicker highlighted by the red rectangle. . . . 60
5.4 Power control performance for the AC connected ESS experimental setup. . . . 61
5.5 Voltage control performance for the AC connected ESS experimental setup. . . . 61
5.6 Reference measurement from the shade experiment onto the PV system from the DC connected ESS experimental setup. . . . 62
5.7 Power control performance for the DC connected ESS experimental setup. . . . 62
5.8 Voltage control performance for the DC connected ESS experimental setup. . . . 63
5.9 Voltage flickers measured from both experimental setup operating in power and voltage control mode. . . . 63
5.10 Two sequential annoying voltage flickers measured by both experimental setups. . . . 64
5.11 SoC of the BESS from the AC connected ESS experimental setup. . . . 65
5.12 SoC of the BESS from the DC connected ESS experimental setup. . . . 65
5.13 SoC of the BESS from the AC connected ESS experimental setup with the window of analysis given . . . 66
5.14 Power setpoint experiment with the inverter from the AC connected ESS test setup. . . . 68
5.15 Power setpoints sent to the inverter from both experimental setups whenever a PV power fluctuation occurred. 68
5.16 Example of the inverter from the AC connected ESS experimental setup not delivering zero power when the setpoint was 0 W. . . . 69

6.1 Simulation results for both control algorithm implementations with a time lag introduced for the power delivered by the ESS. . . . 72
6.2 Open Circuit Voltage (OCV) versus SoC curve of the different types of ESS. . . . 72
6.3 Summary of the cost for different ESS implementations. . . . 73
6.4 AC connected ESS experimental setup example to perform the sensitivity analysis. . . . 74
6.5 ESS and control algorithm implementation at a distribution level. . . . 75
6.6 Indicative representation of an ESS implementation at a utility level. . . . 76

A.1 Energy usage with different control layers applied using power control . . . 80
A.2 Energy usage with different control layers applied using voltage control . . . 81

D.1 Typical PV system installed for a household. . . . 133
D.2 Open Circuit Voltage (OCV) versus SoC curve of the different types of ESS used for the cost analysis. . . . 134
D.3 Electrical diagram of an AC connected BESS for the upgraded solution. The devices highlighted in yellow are the devices that needs to be installed for the upgrade with a BESS. . . . 134
D.4 Electrical diagram of an DC connected BESS for the upgraded solution. The devices highlighted in yellow are the devices that needs to be installed for the upgrade with a BESS. . . . 135
D.5 Electrical diagram of an AC connected SESS for the upgraded solution. The devices highlighted in yellow are the devices that needs to be installed for the upgrade with a SESS. . . . 136
D.6 Electrical diagram of an DC connected SESS for the upgraded solution. The devices highlighted in yellow are the devices that needs to be installed for the upgrade with a SESS. . . . 137
D.7 Electrical diagram of an AC connected BESS for the upgraded solution. The devices highlighted in yellow are the devices that needs to be installed for the upgrade with a BESS. . . . 138
D.8 Electrical diagram of an DC connected BESS for the upgraded solution. The devices highlighted in yellow are the devices that needs to be installed for the upgrade with a BESS. . . . 139
D.9 Electrical diagram of an AC connected SESS for the upgraded solution. The devices highlighted in yellow are the devices that needs to be installed for the upgrade with a SESS. . . . 140
D.10 Electrical diagram of an DC connected BESS for the upgraded solution. The devices highlighted in yellow are the devices that needs to be installed for the upgrade with a BESS. . . . 141
D.11 Summary of the cost for an upgraded and integraded solution using BESS or SESS at two different connection points. . . . 142

List of Tables

2.1 Comparison between different types of BESS and SESS that is considered for this application. 23

3.1 Specification of the data from the PV system used for the simulation. 35
3.2 Simulation results using the simple moving average. 36
3.3 Simulation results using the moving average with optimised weights. 37
3.4 Voltage flickers after applying the simple moving average with different window sizes. 38
3.5 Voltage flickers after applying the moving average with optimised weights with different window sizes. 38
3.6 Effect on voltage flicker reduction after implementing window of operation check. 38
3.7 Energy usage of the ESS after applying different correction factors for the SoC power reduction curve. 39
3.8 Voltage flickers after applying different correction factors for the SoC power reduction curve. 39
3.9 Energy usage from the ESS after applying different idle charge and discharge power values. 40
3.10 Voltage flickers after applying different idle charge and discharge power values. 40
3.11 Summary of the energy usage when each each control layer is applied. 41
3.12 Summary of the voltage flicker reduction when each each control layer is applied. 41
3.13 Energy usage from the ESS when using power control in different days from different seasons. 42
3.14 Final parameter list for the control algorithm implemented for power control. 43
3.15 Simulation results using the simple moving average. 43
3.16 Simulation results using the moving average with optimised weights. 43
3.17 Voltage flickers after applying the simple moving average with different window sizes. 44
3.18 Voltage flickers after applying the moving average with optimised weights with different window sizes. 44
3.19 Effect on voltage flicker reduction after implementing window of operation check. 44
3.20 Energy usage of the ESS after applying different correction factors for the SoC power reduction curve. 45
3.21 Voltage flickers after applying different correction factors for the SoC power reduction curve. 45
3.22 Energy usage from the ESS after applying different idle charge and discharge power values. 45
3.23 Voltage flickers after applying different idle charge and discharge power values. 46
3.24 Summary of the energy usage when each each control layer is applied. 46
3.25 Summary of the voltage flicker reduction when each each control layer is applied. 47
3.26 Energy usage from the ESS when using power control in different days from different seasons. 48
3.27 Final parameter list for the control algorithm implemented for voltage control. 48

4.1 Components used for the AC connected ESS experimental setup. 51
4.2 Specifications of the ATEPS AB5050 battery module [C.1.3]. 52
4.3 Specifications of the Victron Energy Gell Accu [C.1.4]. 54
4.4 Components used for the DC connected ESS experimental setup. 54

5.1 Measured voltage sensitivity for both experimental setups. 59
5.2 Summary of the shade test for both experimental setups operating in either power or voltage control. 66
5.3 Summary of the full day experiment to analyse the voltage flicker avoidance performance for both experimental setups operating in either power or voltage control. 67
5.4 Summary of the full day experiment to analyse the ESS energy usage performance for both experimental setups operating in either power or voltage control. 67

B.1 Final parameters for power control for the AC connected ESS experimental setup 82
B.2 Final parameters for voltage control for the AC connected ESS experimental setup 83
B.3 Final parameters for power control for the DC connected ESS experimental setup 83
B.4 Final parameters for voltage control for the DC connected ESS experimental setup 84

D.1 Cost of an AC connected BESS system upgrade. 135
D.2 Cost of an DC connected BESS system upgrade. 136
D.3 Cost of an AC connected SESS system upgrade. 136
D.4 Cost of an DC connected SESS system upgrade. 137
D.5 Cost of an AC connected BESS integrated solution. 138
D.6 Cost of an DC connected BESS integrated solution. 139
D.7 Cost of an AC connected SESS integrated solution. 140

D.8 Cost of an DC connected SESS integrated solution. 141

List of Abbreviations

AC Alternating Current

BESS Battery Energy Storage System

CSV Comma-Seperated Values

DC Direct Current

DSO Distribution System Operator

EDLC Electric Double Layer Capacitor

EEMCS Electrical Engineering Mathematics Computer Science

EOL End of Life

ESP Electrical Sustainable Power

ESS Energy Storage System

GUI Graphical User Interface

HV High Voltage

LFP Lithium-Iron-Phosphate

LV Low Voltage

MPC Model Predictive Control

MPPT Maximum Power Point Tracker

MV Medium Voltage

NMC Nickel-Manganese-Cobalt

OCV Open Circuit Voltage

PCC Point of Common Coupling

PV Photovoltaic

SESS Supercapacitor Energy Storage System

SOA Safe Operating Area

SoC State of Charge

1

Introduction

As of today, the need for more sustainable energy generation is increasing at a rapid pace to transition the world to a more sustainable future. One of the primary sources of sustainable generation are photovoltaic panels. These photovoltaic panels comprise of photovoltaic cells connected in series and parallel to form one single panel with a single photovoltaic cell being able to generate electric current through the conversion of sunlight to electricity. This is primarily done through the conduction electrically charged electrons and holes through the semiconductor that is the photovoltaic cells.
This process is done using primarily cheap and vastly available material such as silicon. This makes the manufacturing of photovoltaic very cost effective and thus very attractive for project developers and ordinary inhabitants to invest in a large scale solar plant or photovoltaic system at their home respectively. By making use photovoltaic panels connected in series and/or parallel, photovoltaic inverters and a maximum power point trackers, one could install a photovoltaic system at their home for electricity generation for their consumption.
For solar plants, project developers make use of the above mentioned components with a transformer for connection to the high voltage grid in order to provide electricity to an area of thousands of inhabitants. Figure 1.1a and 1.1b illustrates a photovoltaic system at a residential home and a large solar plant respectively.

(a) Residential photovoltaic system.

(b) Large scale solar plant.

Figure 1.1: Different types of application of photovoltaic systems.

Within neighbourhoods in Europe, many inhabitants are opting to install their own photovoltaic system for their homes. With the Netherlands being at the forefront of this with around 25% of all households having a PV system installed [4]. Furthermore there are more incentives in the Netherlands to install more large scale solar plants, with the most recent in 149 MWp solar plant in Dorhout Mees becoming operational in August 2022[5].
Though the main disadvantage of solar power generation is the intermittent nature of the power generation. During the day there is high power generation from the solar panels due to the high solar irradiation and at night there would be little to no power generation due to the sun setting. To tackle this issue, many sustainable energy companies install battery energy storage systems with the photovoltaic system for their clients. The goal of this is to charge the battery whenever there is an excess of power generation from the photovoltaic system during the day and discharge the battery to provide electricity to the household at night.
Another aspect of photovoltaic system that is not considered is the intermittent nature of the power generation during the day aswell. Whenever clouds pass over photovoltaic system, a shadow is casted over the panels. This results in a lower power

generation from the panels and returns back to normal when the clouds has passed. Figure 1.2a illustrates a PV system power generation during the summer where the cloud overheads were at its worst throughout that year and figure 1.2b illustrates the same PV system power generation when there was a clear sky throughout the day.
This could then result in a inconsistent power generation for households and could lead to power and voltage quality issue as more households rely on solar power generation for electricity generation. This issue was thoroughly investigated in Schuurmans et al [6] where the main consequence would be high voltage fluctuations in many households across the Netherlands. This issue is further elaborated in section 1.1

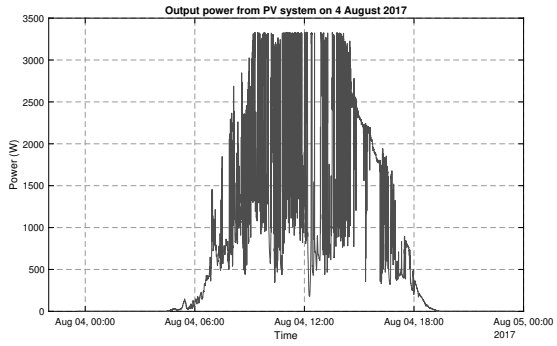

(a) Example of the power output of a PV system throughout the day during a cloudy summer day.

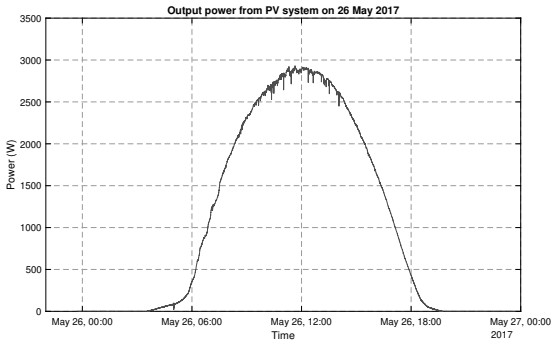

(b) Example of the power output of a PV system throughout the day during a clear sky summer day.

Figure 1.2: Examples of the PV output power on cloudy and clear sky summer day.

1.1. Problem statement for research topic

Based on line and grid behaviour, it was established that the reactive power of generation unit directly affects the voltage at the point of common coupling. This is due to the very low $\frac{R}{X}$ ratio of the line (resistance to reactance ratio), the cause of this is due to the inductance of the cable having a larger influence at the operation frequency of 50 Hz than the resistance of the cable. In the Netherlands at Medium Voltage (MV) and High Voltage (HV) this is very much the case, yet at LV this is not the case. For this report LV is considered to be the mains voltage within a household. The voltage at PCC and power from the PV system can be best described in simplified electrical diagram given in figure 1.3.

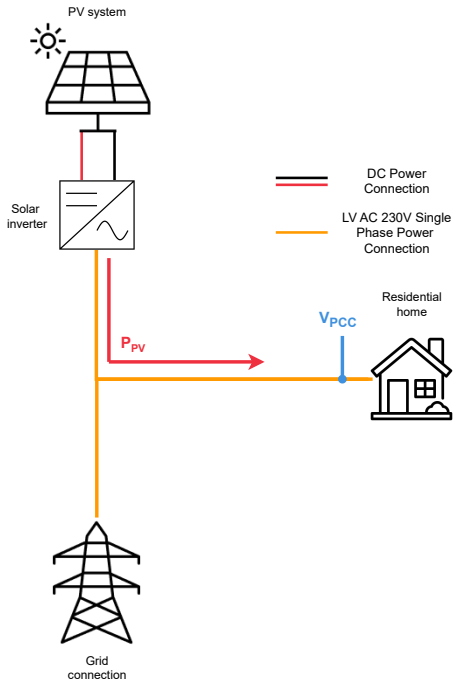

Figure 1.3: Simplified electrical diagram of a household with a PV system is installed. V_{PCC} is the voltage at PCC and P_{PV} is the power delivered by the PV system.

At LV, the $\frac{R}{X}$ ratio is much higher which causes the active power of the generation unit having a larger influence on the voltage at PCC. This is due to the LV cables in the Netherlands running above ground instead of underground such as in the case for

the greater part of the world. This relation between the active power of the generation unit and the voltage at PCC can be deduced as follow [7].

$$V_R = V_S + dP \cdot \frac{R}{V_R} + dQ \cdot \frac{X}{V_R} \tag{1.1}$$

$$\Delta V = V_R - V_S \tag{1.2}$$

From equation 1.1, the relation between the active/reactive power and the voltage at PCC is described. Where V_R is the voltage at PCC or load voltage and V_S is the voltage of the source or generation unit in this case. Equation 1.2 describes the difference between the source voltage and the voltage at PCC which describes the voltage fluctuation used for this research. Based on the described equations, the relation between the active/reactive power and the voltage fluctuation as follow.

$$\Delta V = dP \cdot \frac{R}{V_R} + dQ \cdot \frac{X}{V_R} \tag{1.3}$$

Based on equation 1.3 and the assumption that the $\frac{R}{X}$ ratio is very high, then the following reduction to the equation can be done.

$$\Delta V \approx dP \cdot \frac{R}{V_R} \tag{1.4}$$

Based on equation 1.4, the relation between the active power of the generation unit and the voltage fluctuation at LV in the Netherlands was deduced. This can also be seen from data acquired from a PV system installed at a household in figure 1.4, when the output power of the PV system (ΔP_-) dips with 1766 W then the voltage at PCC (ΔV_-) dips with 1.7 V. Similarly when the power of the PV system rises back up when the cloud has passed (ΔP_+) with 1758 W, then the voltage at PCC (ΔV_-) rises with 1.7 V.
Most of these voltage fluctuations violations occur at a residential level, which can cause health risks to the inhabitants[8][9]. As more photovoltaic panels are installed at a residential level, the higher the penetration of these panels are onto the grid. This will eventually result into increase number of voltage fluctuations at a residential level. Finally for the rest of this report, the $\frac{R}{V_R}$ constant is described and equated to the $\frac{dV}{dP}$ value as this is a constant value called voltage sensitivity which will be used for the simulation and experimental setup design of this report.

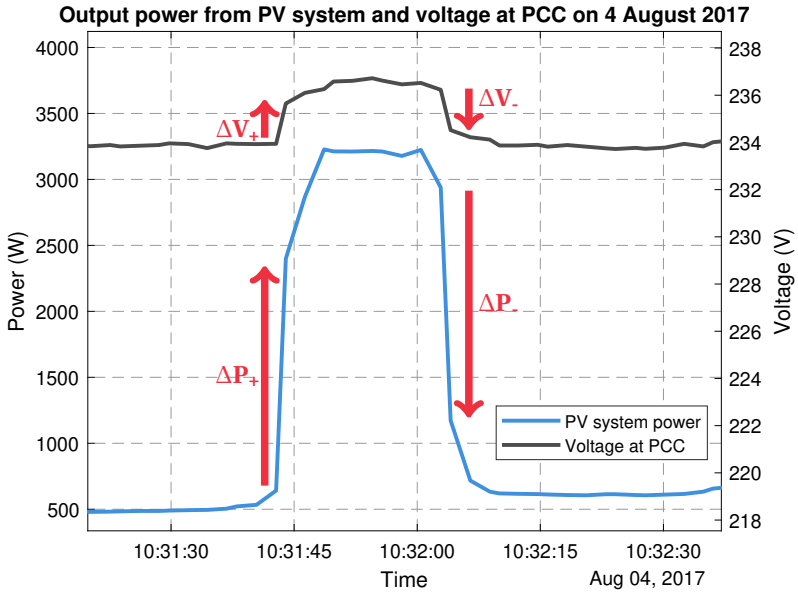

Figure 1.4: Example illustrating PV power fluctuation and voltage flickers from collected PV data.

The effect of voltage fluctuation on human perception has been extensively researched and grid code standards were introduced to tackle such an issue. For a PV system, it was widely expected for the PV power not to fluctuate in the orders of a few seconds or milliseconds yet this is what actually occurs when the PV power fluctuates due to clouds passing by and is highlighted by figure 1.5. The figure illustrates the amount of times the PV power fluctuated by more than 30% of its power capacity and how many seconds it took for the fluctuation to occur. This data is taken from the PV power output of figure 1.2a between the hours of 8 AM and 4 PM as these are the hours when the irradiation levels are at its highest during the day. Finally, the sampling rate of the data is an average of two seconds.

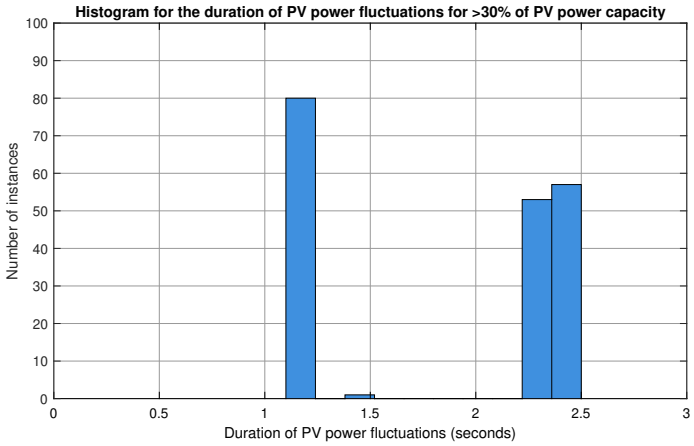

Figure 1.5: Illustration of how fast the PV system fluctuates with 30% of its power capacity from collected PV data.

As can be seen from the figure above, the power fluctuations occured many times throughout the analysed period and the duration of it are between 1 to 2 seconds, though it must be pointed out that the average sample rate of the data is 2 seconds. Thus if the power fluctuates that quickly then the voltage at PCC might also vary at same speed and can thus lead to the flickering of the lights in a household. In a report by QualTech [1], the flickering of lights was highlighted based on prior research with human experimentation as to what the threshold for an annoying flicker and visible flicker is. The Qualtech curve is primarily based on a P_{st} value of 1 and is given in figure 1.6, where the annoying flicker curve is considered to be a P_{st} of 1 and the visible flicker is considered to have a lower P_{st} value. The P_{st} values is thoroughly explained in the IEC standard 61000-4-15 [10] (and further explained in IEC 61000-3-7[11] and IEC 61000-3-11[12]) and the value of P_{st} describes how irratating flicker is thought when measured over a period of 10 minutes. When looking at the flicker longterm, this is expressed as cubic mean of the P_{st} values over a period of 2 hours which is thus called the P_{lt}. Since the value of P_{st} that the load/client shall have on the grid is set around 1 according to the the IEC standard 61000-4-15[10], an experimental equation was setup by Mombauer [13] for which it is illustrated in figure 1.6 as the 'borderline of irritation' flicker curve. Equation 1.5 illustrates how the P_{st} is calculated according to Mombauer.

$$P_{st} = 0.36 \cdot R \cdot F \cdot d_{max} \cdot r^{0.31} \tag{1.5}$$

R is the correction factor, F is the form factor of the fluctuation and is thus 1 for stepwise fluctuation. d_{max} is the absolute value of voltage fluctuation and r is the amount of fluctuations every minute. It must be highlighted that equation 1.5 is only for the case when the P_{st} is 1. According to the IEC standard 61000-4-15:2011[10], a specialized flicker meter can be used and is described in the standards. The meter reads in the measured voltage values and computes the P_{st} values according to the IEC standards, which can be used for the research.

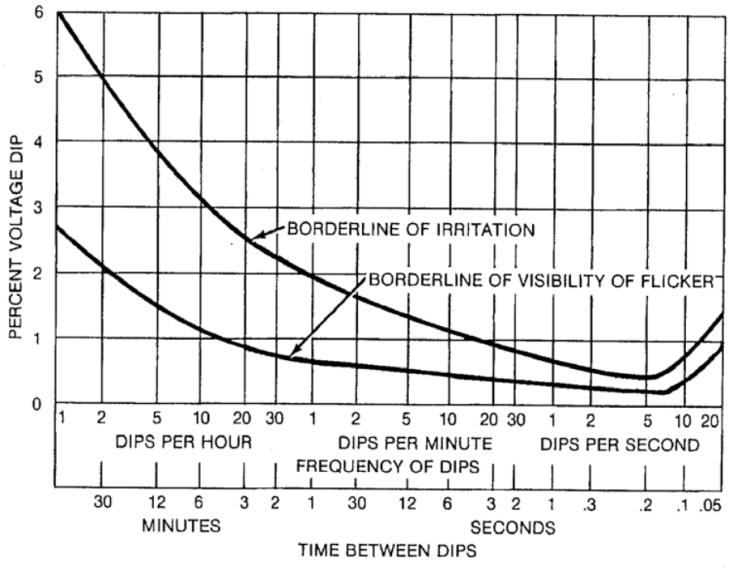

Figure 1.6: Flicker curve as described in the paper published by QualTech [1].

1.2. Motivation for research

The main motivation for this research and reason why to address this issue is to ensure that if the transition to a more sustainable future shall occur, a keen amount of effort has to also be put in to ensure a high power/voltage quality generated by the renewable energy sources. Thus if more photovoltaic panels shall be installed to deliver more renewable energy to households, we must ensure that no harm shall be done to the inhabitants themselves. Furthermore based on recent study done by the DSO about the voltage quality across the Netherlands, it was found that in a high PV penetration area in Groningen called Paddepoel the P_{lt} value during a summer week in June was around 0.6, figure 1.7 illustrates the graph of the results in the Paddepoel area. The maximum value for the P_{lt} at any given moment shall be 1 as stated in the IEC standard with the clients contribution to the long term flicker set at a maximum of 0.8. This information is readily available at netbeheernederland.nl.

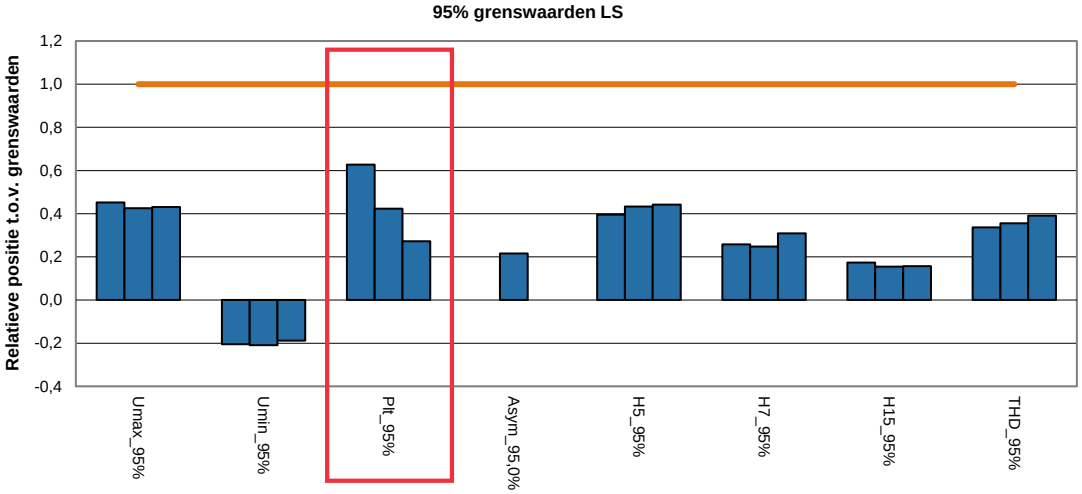

Figure 1.7: Voltage quality study done in the Paddepoel area of Groningen. The x-axes denotes the measured values of the P_{lt} with respect to the maximum allowable value from the Distribution System Operator (DSO). Plt_95% (highligthed by the red rectangle) denotes the measured P_{lt} with the orange line denoting the maximum allowable value define by the Distribution System Operator (DSO)'s and grid codes and standards

This phenomena in the Paddepoel area is only in an area with a PV penetration of around 30% per household, should the PV penetration increase in the future the voltage fluctuations and P_{lt} shall increase aswell. The former being proven by Schuurmans [6]. Furthermore based on existing research papers [14][15], most authors presented that the power fluctuations from PV systems (at a utility scale or residential scale) causes the P_{st} to go above the threshold of 1 several times a day.
The main beneficiary of this research will be the Distribution System Operator (DSO)'s in and around the Netherlands. The main reason why DSO's will benefit from this research is that this is one of the means to ensure robustness of the grid which is increasing in flexibility and renewable energy penetration in the coming years. By ensuring robustness of the grid, DSO's can ensure to all of their clients that they will receive the highest power quality from power generated by renewable energy sources.
Within this research area, several mitigations procedures to address these voltage fluctuations violations were investigated and published by Schuurmans [6]. Out of the considered mitigation procedures, the best option to reduce the voltage fluctuations were to make use of a supercapacitor bank which will compensate the sudden reduction of active power from the photovoltaic panels due to passing clouds. Supercapacitors are one of the types of ESS considered for this research due to its high power to energy ratio of more than 70, very low response time and high cycle lifetime. The specifications for a supercapacitor is explained more in depth in chapter 2. Furthermore in another paper published by Brinkel et al [16], the battery pack of electric vehicles were used to reduce the voltage fluctuations induced by the photovoltaic panels. The main issue with using electric vehicles is the availability of these vehicles and the level acceptance by the vehicle owner for the usage of reducing the voltage fluctuations. The type of ESS considered for this application is further investigated in section 2.2, yet supercapacitors is mostly seen as an ideal ESS type for this due to their specifications matching for what is needed for this application.
Furthermore various research and simulations were done using different types of energy sources that can be used to reduce the voltage fluctuations. Many of which used a different type of control strategy with different degrees of complexity. Some of the papers even presented that the voltage fluctuations was reduced through the use of an ESS, yet mainly simulations results were presented to validate the functionality of the control scheme[3][17][18][19][20].
Another aspect for this research is the connection type for the ESS. This will be further elaborated in chapter 2 and in chapter 4, yet in most household with a PV system and an ESS there are two types of connection for the ESS. There is the connection type where the ESS is connected on the same DC bus with the PV system to the inverter and there is the connection type where there is a separate inverter and ESS connected to the same AC bus as the PV inverter and PV system. These connection types were considered in similar papers found regarding this research area, yet these mostly provided simulation results or

when an experiment was conducted by the authors no results were provided as to how much the voltage fluctuations were reduced as a result of implementing an ESS. This is further investigated in section 2.1. Hence increasing the motivation to conduct a research as to which connection is most suitable to implement in the future to tackle this issue. Figure 1.8 shows a simple illustration of how the different connection type for the ESS are electrically connected.

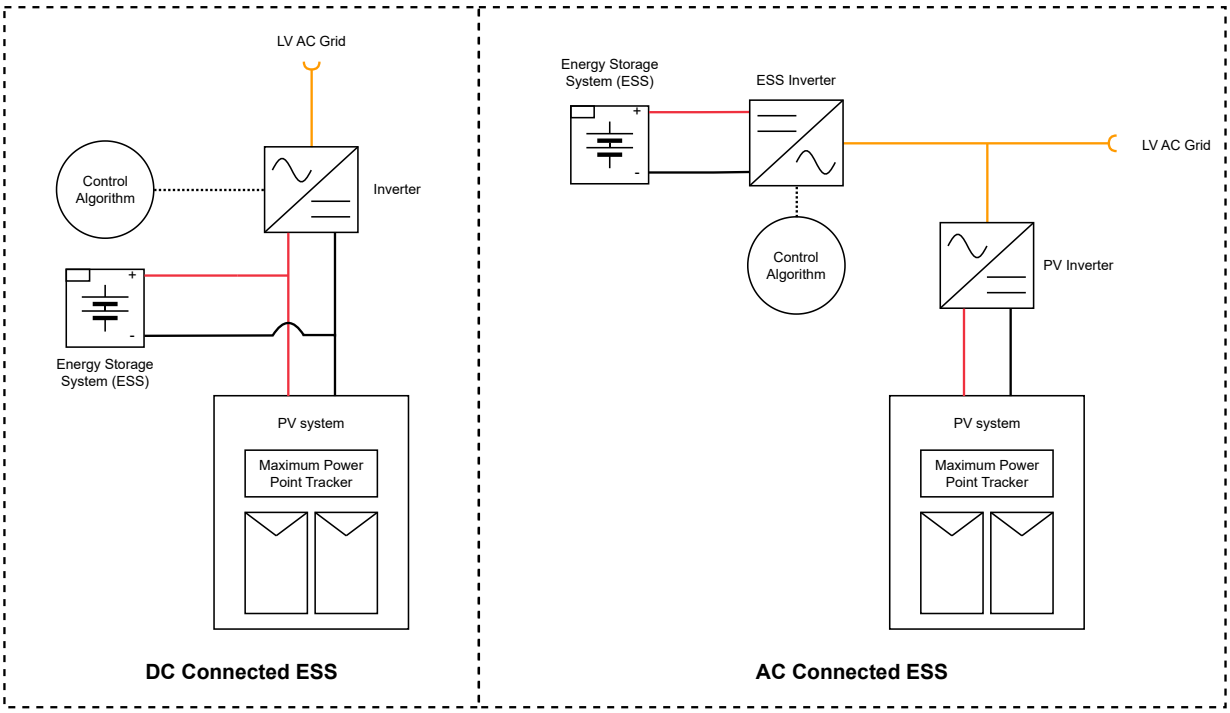

Figure 1.8: The two different connection types for the ESS. The red and black line indicates the DC positive and negative poles. The orange line indicates the AC line connection to the grid. Finally the dashed black lines indicate a communication line between the control algorithm and inverter.

It should be noted that for the AC connection type, the Maximum Power Point Tracker (MPPT) could also be combined with the PV inverter, yet for illustration purposes these two components are separated from each other. The same was done for the DC connection type, where a DC/DC converter could be connected to the ESS and then to the main DC bus. This could be done to maintain the voltage level at the DC bus relatively constant.

1.3. Main research goal and sub research goals

Based on the problem definition and motivation for this research, the following main research goal was formulated.

Develop a control algorithm which uses an energy storage system to reduce voltage fluctuations ,caused by photovoltaic panels due to clouds passing by, to values below the visible flicker curve.

Furthermore, the following sub research goals was also formulated as a means to support the findings that will be used to achieve the main research goal.

1. Design the control algorithm in such a way that the ESS energy usage is minimized and the measured power to energy ratio used throughout the day is more than 70. The latter is in order to have an implementation of a SESS for this application in the future.

2. Design and build two experimental setups setups which mimics a household with a PV system connected for electricity generation and an extra ESS to reduce the voltage flickering. The main difference between the two test setups is the ESS connected at the DC bus or at the AC bus.

3. Compare the performance of the control algorithm implementation with the two constructed test setups to verify which setup and control algorithm implementation has the best performance in terms of flicker reduction and ESS energy usage

1.4. Outline report

Chapter 2 — This chapter gives an in depth review on already existing research surrounding this topic. Based on prior research, a final research gap is proposed in this chapter. Furthermore, an in depth analysis is done regarding the type of ESS that will be used for the test setup. Based on the analysis, a decision is then made as to which type of ESS is more appropriate

to use for the test setup.

Chapter 3 — This chapter explores which primary control is most appropriate to use based on preliminary simulations and elaborates on the extra layers of control added to the primary control in order to reduce energy usage of the ESS. Furthermore, two types of controls are introduced in this chapter which are the voltage control and power control. These two types of control makes use of the same primary control with different set parameters. Finally a full simulation is done to illustrate the performance of both types of control using preexisting PV data.

Chapter 4 — This chapter elaborates the detailed test setup design and the reasoning behind implementing certain devices in the test setup. Furthermore, the Graphical User Interface (GUI) used for the test setup is explained and which features are implemented in the GUI.

Chapter 5 — This chapter presents the test results from the test setup and elaborates if the main research goal for the thesis is achieved using an ESS coupled with a novel control algorithm.

Chapter 6 — This chapter presents the conclusion of the research and gives an answer on the main research question. Furthermore, a recommendation regarding future work regarding this research topic is explained.

1.5. Conventions and general terms

For this report, it is important to highlight the conventions and terms used throughout the report. These are as follow.

1. For active power, whenever power is flowing from a power source to the grid (ESS discharge) then the sign convention for power is positive. Whenever power is flowing from the grid or another power source to a power source (ESS charge) then the sign convention for power is negative.
2. When considering LV power from the AC grid, the voltage level is considered to be around 230V. Since this is the mains voltage in most households in the Netherlands.

2

Existing research review

For the literature review, the main idea is to investigate existing research done in the area of the research topic. From there a what is called a research gap has to be found, this is an idea for the research topic that has not been done or seen in literature before. Since the main task of this research is to validate the ESS functionality through lab verification, the main focus should be around the experimental setups which are illustrated in figure 2.1. Already existing experimental setups made to investigate the research area is reviewed in section 2.1. Furthermore, the most optimal type of ESS has to be chosen for the experimental setup (highlighted by the blue rectangles in figure 2.1) based on a set of criteria for its application in this research area. This is investigated in section 2.2. Finally, different control algorithms used for this research area (highlighted by the green rectangles is investigated in section 2.3. Finally a research gap for this research is established and will be further investigated throughout this report.
It is important to note that it was decided not to investigate the inverter design needed for this application. The reason being that the main goal of this research is to design a novel scheme that reduces the voltage flickers and is energy efficient. Thus researching and designing an inverter for this application was considered not to be within the scope of this research and was thus not further investigated.

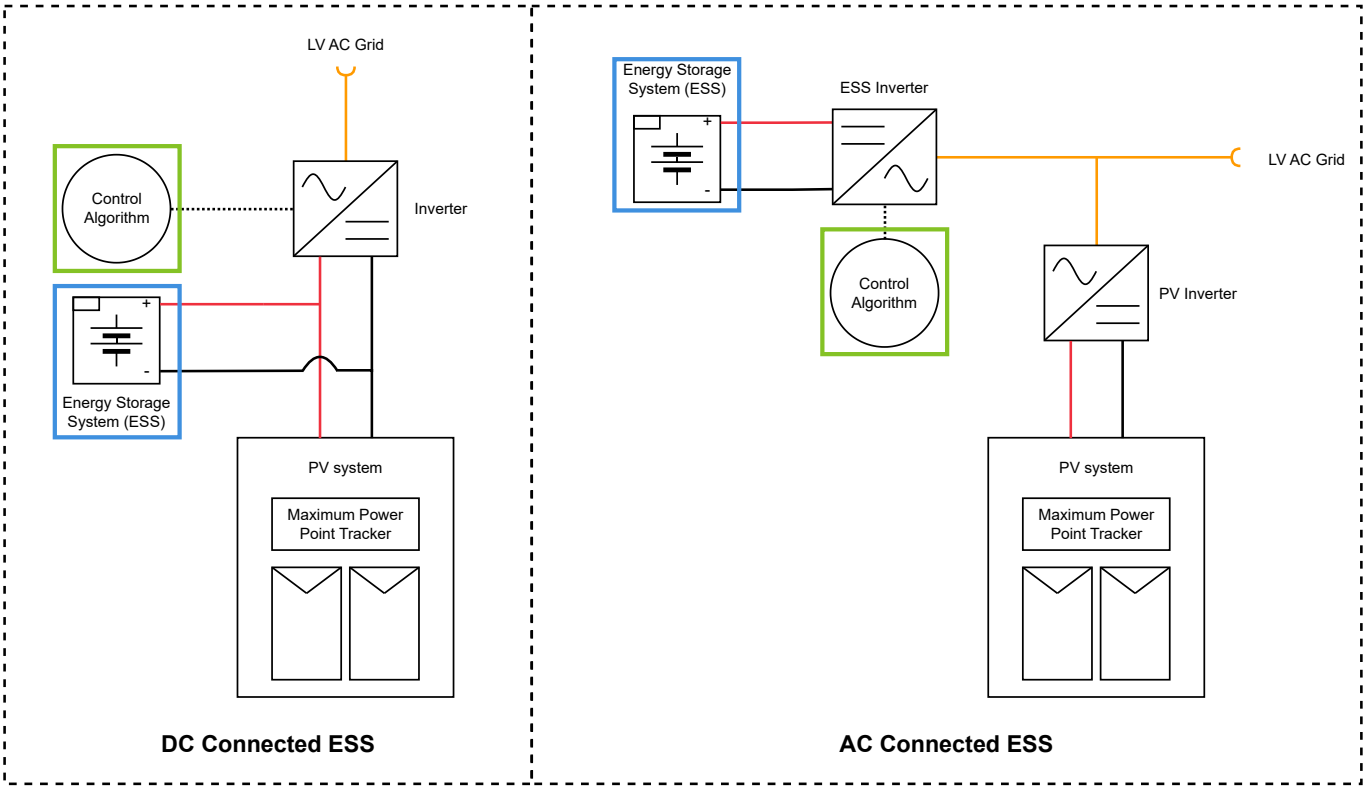

Figure 2.1: Expermintal setup designs of which the highlighted parts will be discussed in this section.

2.1. Existing design of test setups and setting for research topic

Based on the literature research done so far, there were a few application of an ESS with a PV system to reduce the power/voltage fluctuation. Most papers only presented simulation results to show and validate that the implemented control scheme reduces the power/voltage fluctuations at PCC. While only a handful of papers presented experimental results that further validates their implemented control scheme and system design.

In Kakimoto et al [2], a simulation and experiments were done with a supercapacitor bank that was connected on the same DC bus with a DC-DC converter connected PV system to reduce the power fluctuation at PCC. The control scheme used in this setup was a moving average control with an extra layer of control which limits the active power of the supercapacitor based on the voltage of the supercapacitor and maximum allowable charge/discharge current. Figure 2.2 illustrates the PV generation system used for the test setup and the power fluctuation results ($^{W}/_{min}$) from the experiments. The main takeaway from this research is that the supercapacitor successfully reduced the power fluctuations caused by clouds passing over the PV system and was kept for the most part within the 50 $^{W}/_{min}$ requirement set by the authors. Though the main shortcoming from this paper is that the authors did not present how the voltage at PCC is affected by the smoothing of the output power and the time resolution used throughout the paper was in minutes instead of seconds or even milliseconds.

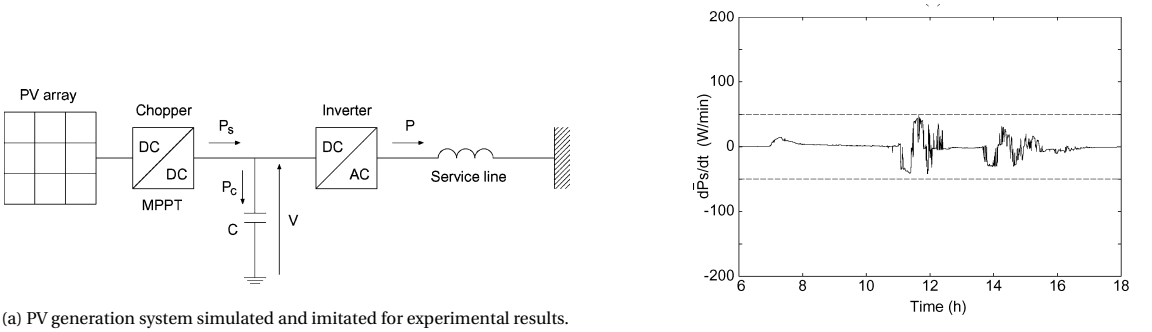

(a) PV generation system simulated and imitated for experimental results.

(b) Power fluctuation simulation result after the applied control.

Figure 2.2: System design and simulation results from Kakimoto et al [2].

In Marcos et al [21], the operators implemented a BESS with a moving average control to reduce the power fluctuations caused the 1.1 MW PV plant. The article stated that the power fluctuations were reduced with 312 kWh used annually by the BESS. As to how much the power or voltage fluctuations were reduced and further results from this implementation of the BESS, this was not explained in the article.

In Alam et al [3], the authors presented a control scheme which uses a moving average control with an extra layer of control to limit the ramprate of power at PCC and the maximum allowable charge/discharge power of the battery system. This was tested using a simulation of a residential area with voltage measurements taken at the PCC of residential homes. Furthermore a characteristic power fluctuation model of the PV system was used in order to accurately calculate the amount of active power compensation needed to reach the maximum allowable power ramprate at PCC. The design of the system also included a BESS connected on the same DC bus as the PV system. Figure 2.3 illustrates the simulation results of the voltage at PCC and the power delivered by the ESS. It can be deduced that the proposed control scheme reduces the voltage fluctuations at PCC. Unfortunately, the authors did not present thorough experimental results and the the experimental setup used did not consist of an actual PV system but rather a programmable AC load.

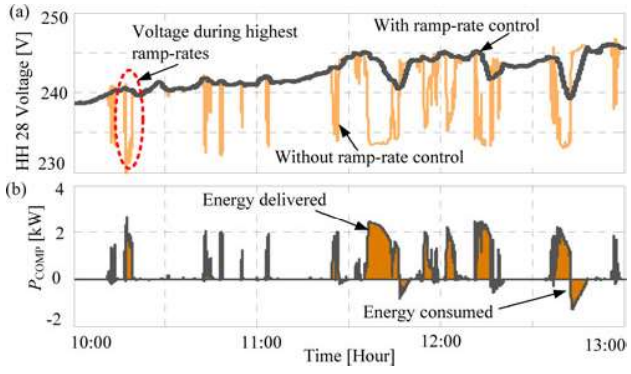

Figure 2.3: Simulation results of the voltage at PCC and the delivered power from ESS presented by the authors[3].

For this research, the main decision for the setting for which the experimental setup is based on is between emulating a large

scale solar plant or a PV system for a household. Emulating a large scale solar plant which provides electricity to thousands of homes is very costly and simply not feasible within the timeframe of the research and not feasible to build in the lab of TU Delft. Furthermore as explained in section 1.1, the main issue lies within households with its own PV system and the induced voltage fluctuations because of the PV system. As shown in the area of Paddepoel, around 30% of all households has PV systems installed at their home of which the P_{lt} value reach very critical values during cloudy summer days.

2.2. Types of ESS considered

For the type of ESS used for the test setup and research, the following types were considered for implementation :

- BESS
- SESS
- Hydrogen storage system
- Flywheel storage system
- Redox flow battery

With the main criteria for making a choice between the different types of ESS being the following :

- **Fast response time**
  Based on data sets from PV systems, the measured power fluctuations occurred between 1 to 3 seconds. This is important as when a fluctuation occurs the ESS should be fast enough to react and deliver power for compensation.
- **High cycle lifetime**
  Since the ESS is expected to undergo between 0.5 to 1 cycle everyday based on preliminary simulations, it is expected for the ESS to be able to last atleast 5 years of operation before reaching End of Life (EOL). Thus an ESS with high cycle lifetime is needed for this research and experimental setup.
- **High power to energy ratio**
  Since the ESS is expected to output and receive high power and be as energy efficient as possible with the control algorithm. It is important for the ESS to have a high power to energy ratio in order to be as energy efficient as possible. This would then result in a lower ESS energy capacity needed and thus lower the overal cost of the system.
- **Low cost**
  For the type of ESS, the cost to manufacture 1 kWh ($/kWh) is considered to lower the overal cost of the test setup.

Based on preliminary research considering the different types of ESS with the set criteria. The following decisions were made.

- It was decided not to implement a hydrogen storage system for the research and test setup as the response time of such a system is typically around 7 seconds [22]. This response time is way too slow for this research.
- It was decided not to implement a flywheel storage system for the research due to the response time and lack flexibility and availability on the market. The response time of a flywheel storage system is less than 4 seconds [23], which is not sufficient for the research. Furthermore based on preliminary research, the flywheel cost is around 1500 $/kWh [24] which is acceptable yet many flywheel storage system on the market are in the regions of hundreds of kW to MW. Which is not applicable to the use case of this research, which is at residential level that only needs an ESS of only a few kW.
- It was decided not to implement a redox flow battery for the research as the power to energy ratio is very poor with a calculated value of [25][26] and the cost of such a system is around 1000 $/kWh[25].

Based on the previous decision and considering the performances of the other types of ESS, it was then decided to further consider BESS or SESS for this research. Since there are many types of chemistry available for BESS and SESS, the following chemistry were considered for further implementation for the research and their performances are given in table 2.1.

Type of chemistry for supercapacitor and battery cells	Response time	Cycle lifetime (# cycles)	Power to energy ratio	Cost ($/kWh)
Electric Double Layer Capacitor (EDLC)	very high	500000 [27, p.953]	500 [27, p.953]	5000[28]
Pseudo supercapacitor	very high	20000 [29]	66.67 [29]	5000[28]
Lithium-Iron-Phosphate (LFP) battery cells	very high	4000[30]	13.33 [27, p.954]	87[31]
Nickel-Manganese-Cobalt (NMC) battery cells	very high	1500[30]	2.31 [27, p.801]	90[31]
Nickel-Cobalt-Aluminium battery cells	very high	750[30]	3.41 [27, p.801]	75[31]
Lithium-Titanium-Oxide battery cells	very high	>5000[32]	20 [27, p.954]	218[33]

Table 2.1: Comparison between different types of BESS and SESS that is considered for this application.

Based on the performances of the different types of SESS and BESS considered, Electric Double Layer Capacitor (EDLC) is the best type of ESS to use for the research and experimental setup as it has the best power to energy ratio and cycle lifetime (highlighted in blue). Though the main drawback of SESS is the high cost of around 5000 $/kWh (highlighted in red), thus increasing the overal cost of the experimental setup. Though a SESS would be the ideal case to use for this research, it was opted not to use a SESS as the cost per module are very high and several types of BESS are already available at the Electrical Sustainable Power (ESP) lab. Since both these types of ESS can be used to achieve the main thesis goal due to both having a fast response time and the experimental setups are initial prototypes, it was thus opted to use a BESS instead. Nonetheless, the control algorithm design shall be designed such that a SESS can be used for this application in the future.

2.3. Control algorithm

Based on previous work where an energy storage source(s) was used to reduce the power and voltage fluctuations of LV grid caused by PV panels. Most of the control algorithm included the following.

- **Moving average control [2][34][21][35][20][36][37]**
  This is where the power output of the combined ESS and PV panel system is calculated based on the previous measured output power values of the PV system. The calculated value from the moving average control is thus used as a reference point for the ESS to discharge or charge to meet the reference value for the power. This type of control is advantages as the power output of the combined system or at the point of common coupling smoothes out the power fluctuations of the PV system. Equation 2.1 illustrates the equation for calculating an expected output power using a simple moving average [38].

$$\overline{X_{n+1}} = \frac{\sum_{n=1}^{\infty} X_n}{n} \tag{2.1}$$

  Where $\overline{X_{n+1}}$ denotes the averaged expected output in the next time interval with X_n and n being the preceding values in the window and window size respectively. This type of control or calculation is primarily used in the financial sector to accurately predict the stock market price, but can be used for this research.

- **Low pass filter control[36][37][39][40]**
  In this control scheme, a generic low pass filter is applied to calculate a new reference point for the power output of the combined system. Much like the moving average control, the previous measured output power values from the PV system is used to calculate the reference value power value at the point of common coupling when the low pass filter is applied. Since the low pass filter filters out the high frequency fluctuations of the PV panels, a smoothed output power at the point of common coupling is produced by using the ESS to compensate and achieve a smoothed output power. Equation 2.2 illustrates an example of a low pass filter used for the smoothing of the PV system output power, this based from a paper from Senjyu et al[39].

$$f(s) = \frac{0.9}{20s+1} \tag{2.2}$$

  By applying this low pass filter, the author showed that the power at PCC was smoothed out with a BESS.

- **Model Predictive Control (MPC)[36][41]**
  For this control algorithm, a plant model (which in this case is the PV system model) is used to predict the expected behaviour of the PV system. Knowing the expected behaviour, the ESS can thus compensate to limit the ramp rate of the output power at PCC. Equation 2.3 illustrates the MPC objective function used for the MPC to reduce the power fluctuation at PCC in a paper published by Aryani et al[41].

$$J(u(k)) = \alpha(y(k) - y_{ref}(k))^2 + \beta(u(k))^2 \tag{2.3}$$

  Where u(k) is defined as the control unit, α and β are the sampling parameters. Furthermore, y(k) is the measured PV system output power at time interval k and $y_{ref}(k)$ is the averaged expected value of the output power at PCC.

- **Optimization control [42][18]**
  This type of control is used in order to limit ramprate of the output power at the point of common coupling by using constraint set by the system such as state of charge of the ESS, maximum output power of the ESS etc. By setting an objective function that minimizes the power fluctuation or voltage fluctuation, an optimal output power from the ESS can be used which limits energy usage and thus a lower size or capacity of the ESS would then be needed. Equation 2.4 illustrates the objective function used by Wang et al [18] to reduce the voltage fluctuation at PCC caused by the PV system using a battery storage.

$$J = \Delta V_{PV} + \frac{dV}{dP}\Delta P_B + \frac{dV}{dQ}(\Delta Q_B + \Delta Q_{PV}) + \alpha|P_B + \Delta P_B| \tag{2.4}$$

  Where is J is the outcome of the objective function to minimize the voltage fluctuation, V_{PV} and ΔV_{PV} is the voltage and the voltage fluctuation of the PV system respectively, $\frac{dV}{dP}$ and $\frac{dV}{dQ}$ is the voltage sensitivity to active power and reactive power respectively. Finally α denotes a weight factor with P_B, ΔP_B, Q_B and ΔQ_B denotes the measured and difference in active and reactive power from the ESS. The author used such a optimization control algorithm in order to minimize the usage of the ESS and thus be more energy efficient with the ESS.

Furthermore based on the explanation in section 1.1, a further research should be done in order to establish if active power control or voltage control is needed for the ESS. What is meant by active power control, is that the active power at the point of common coupling is controlled by injecting active power from the energy source. The expected result is that most (if not all) voltage flickers are eliminated due to smoothed output power at PCC due to the $\frac{dV}{dP}$ relation as explained in section 1.1. For voltage control, the voltage at PCC is smoothed out and the resulting compensating power that needs to be delivered by the energy source is calculated through the $\frac{dV}{dP}$ relation. The main criteria for choosing which type of control and if it should be active power or voltage control are as follow.

- **Low energy usage**
  It is important to keep the size of the energy source is small as possible due to cost of such a system if implemented in a real life scenario. Thus the control algorithm shall use the energy of the ESS very efficiently to keep the size of the ESS relatively small.

- **Amount of voltage flickering reduced/avoided**
  Based on research conducted by Qualtech, the visible and annoying flickering of lights values seen by human beings are very dependent from the frequency at which the flickering occurs. Based on the sampling rate of our used data and simulation, it shall be checked if the chosen control scheme has eliminated most if not all voltage flicker.

- **Feasibility for implementation on hardware**
  Since the expectation is to build a experimental setup to validate the ESS application, it is expected that the control algorithm shall be simple yet effective. This is due to the expected high response time of the control scheme to swiftly correct the sudden power/voltage fluctuation at PCC. For an ideal control algorithm, the hardware shall not take too long to compute what action needs to be taken from the ESS

Furthermore, multiple layers of control can be added to the primary control in order to reduce the ESS energy usage. Such controls were investigated in papers where an State of Charge (SoC) control was implemented to reduce energy usage. These extra layers of control are further discussed in section 3.2, where are new novel layers of control is implemented for the primary control system.

2.4. Research gap for this thesis

Based on the already existing experimental setups from research papers and their shortcomings, the following research gaps were found and will be investigated in this thesis.

1. The main goal of this research is to build the two experimental setups highlighted in figure 1.8 and to provide not only power but also voltage fluctuations experimental data and how these are reduced using an ESS. These experimental setups are designed in such a way that it mimics a household which has a PV system installed and an ESS is installed to avoid the voltage flickers from occurring. This is due to most papers presenting a solution to this voltage flicker problem at a distribution or utility level and not a residential LV level.

2. Furthermore it is important to achieve a high time resolution for the experimental data as the measured power fluctuations from the PV systems are in the order of a few seconds and not minutes as was used in several papers.

3. Another gap within this research topic is the control algorithm used to reduce the power and voltage fluctuations as the different types of control algorithms discussed in the papers are used throughout the day. Even when the PV system is not delivering any power. This as a consequence can unnecessarily use energy from the ESS and due to the low energy density of SESS (as highlighted in section 2.2), this type of ESS cannot be used for this application. Thus a novel control algorithm has to be conceived and designed in such a way that the energy usage from the ESS is kept to a minimum.

3

Control algorithm design and simulation

For this chapter, the control algorithm design is explained in detail. Firstly, the main concept for the control algorithm is chosen and explained in section 3.1. Then the control algorithm design is explained in section 3.2 with each control layer explained thoroughly. Then the voltage sensitivity calculation procedure is explained in section 3.3 as to how the voltage sensitivity was calculated from the PV data used for the simulation. This same procedure can be used for the measuring the voltage sensitivity of the experimental setups. In section 3.4 and 3.5, the power and voltage control design is explained as to how each was implemented using the designed control algorithm. Before the simulation results are presented, section 3.6 explains the assumptions and setting for the simulations. Finally in section 3.7 and 3.8, the simulation results for power and voltage control implementations is given with the effect of each control layer explained. Then the final parameters used for power and voltage control implementation is given at the end of each section.

3.1. Control algorithm choice

Based on the criteria explained in section 2.3 for the control system design, several decision were made as to which control algorithm shall be used for this research. Firstly it was decided not to pursue an MPC controller design as a perfect plant model is needed which describes the PV system. Since PV systems from different households differ allot with regards to inverter brand and photovoltaic material used, it was decided not to pursue such a design since it would introduce allot of variables which reduces the chances of the control design being implemented on hardware in the future.
It was also decided not to pursue an optimization function control design for the main control algorithm, as when solving an optimization function the time it takes to solve might differ each time. This is dependent on how fast the solver can find the optimal solution. Furthermore if there is an convergence issue to find the most optimal solution, the response time of control algorithm would become too large to fix the power/voltage fluctuations.
Finally a low pass filter solution for the control algorithm was also considered unfeasible, as the performance of such a control algorithm would result in 'over-smoothing' of the power/voltage at PCC[37]. The result of this would be that the energy usage of the ESS would be very high since the ESS shall always be active to achieve the 'over-smoothed' power and voltage at PCC.
Based on the explanation above, it was decided to pursue a control algorithm using moving average since it would have a faster response, simpler design and much more feasible to implement successfully on hardware. The specific type of moving average used for the control system is explained in section 3.2.1.

3.2. Control algorithm design

Apart from the main control algorithm being the moving average control, extra layers of control was also added to reduce the overal energy usage for the ESS. The layers added are as follow :

- Window of operation control, explained in section 3.2.2.
- SoC power reduction curve, explained in section 3.2.3.
- Idle charge/discharge, explained in section 3.2.4.

The order in which the extra control layers are given by the enumeration in figure 3.1. The input could be either the measured PV power or the measured AC voltage at PCC as there is two types of control algorithm implementation used for this research, this being power control and voltage control. The former is explained in section 3.4 and in section 3.5, both of which uses the same control layers but with different inputs.

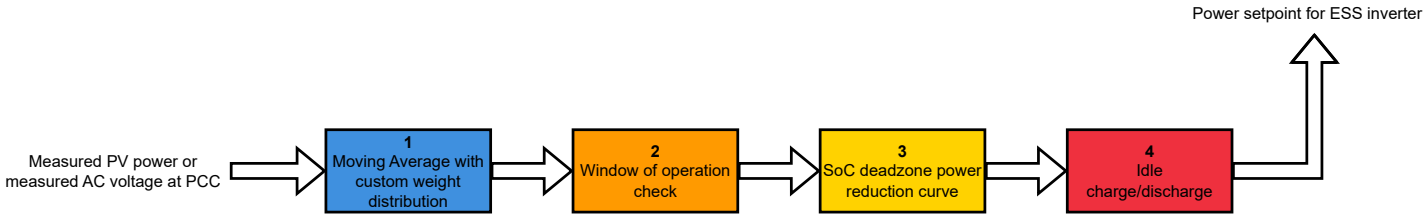

Figure 3.1: Order in which each control layer is implemented for the control algorithm.

3.2.1. Moving average algorithm

For the moving average algorithm, the fundamental idea behind is using past measurements to predict what the measurement in the next sample shall be. Since this is a very powerful tool to predict the outcome of a scenario, it is widely used within the financial sector to predict stock market prices. The most widely used type of moving average is the conventional simple moving average. The equation for the simple moving average is given as follow.

$$\overline{X_{n+1}} = \frac{\sum_{n=1}^{\infty} X_n}{n} \tag{3.1}$$

Where $\overline{X_{n+1}}$ is the calculated predicted value, X_n are the measurements from the past used for the calculated predicted value and n is the amount of past measurements used for the calculation. Alternatively the equation can be rewritten to indicate the weight distribution of the moving average equation.

$$\overline{X_{n+1}} = \begin{bmatrix} 1/n & 1/n & \dots & 1/n \end{bmatrix} \begin{bmatrix} X_1 \\ X_2 \\ \dots \\ X_n \end{bmatrix} \tag{3.2}$$

As can be seen from this reformulation of the equation, the weights for the simple moving average is the same for each element used for the calculation with a value of $1/n$. These weight values are illustrated in the figure 3.2.

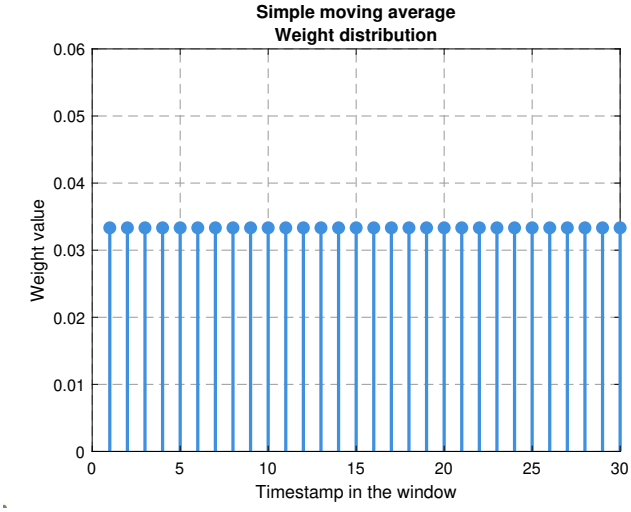

Figure 3.2: Weight distribution of the simple moving average algorithm.

From all of the papers using the moving average algorithm to reduce power and voltage fluctuation, all of them only considered the simple moving average for the control algorithm. Though there are different types of moving average used in the financial sector, all of which have its own advantages and disadvantages with regards to predicting the stock market prices. These different types of moving averages have their own weight distribution, hence why the general equation for the moving average calculation can be reformulated as follow.

$$\overline{X_{n+1}} = \begin{bmatrix} w_1 & w_2 & \dots & w_n \end{bmatrix} \begin{bmatrix} X_1 \\ X_2 \\ \dots \\ X_n \end{bmatrix} \tag{3.3}$$

Where w_n are the weights value assigned to a particular measurement from the past. It is very important to note that the sum of all of the weight should be equal to one, such is the case for the weight distribution for the simple moving average. If

the sum is not equal to one, then the calculated predicted value will start to diverge from the measurements. Hence for the weight distribution of the moving average, the following rule must be adhered to.

$$\sum_{n=1}^{\infty} w_n = \sum_{n=1}^{\infty} \frac{1}{n} = 1 \tag{3.4}$$

For this research, the different weight distributions were considered as a means to increase accuracy and smoothness of the predicted values. This would then result in a reduced energy usage from the ESS as the ESS would to provide less power to compensate for the power and voltage fluctuation whenever the PV system is outputting constant power. The different types of weight distribution considered for this research is given in figure 3.3.

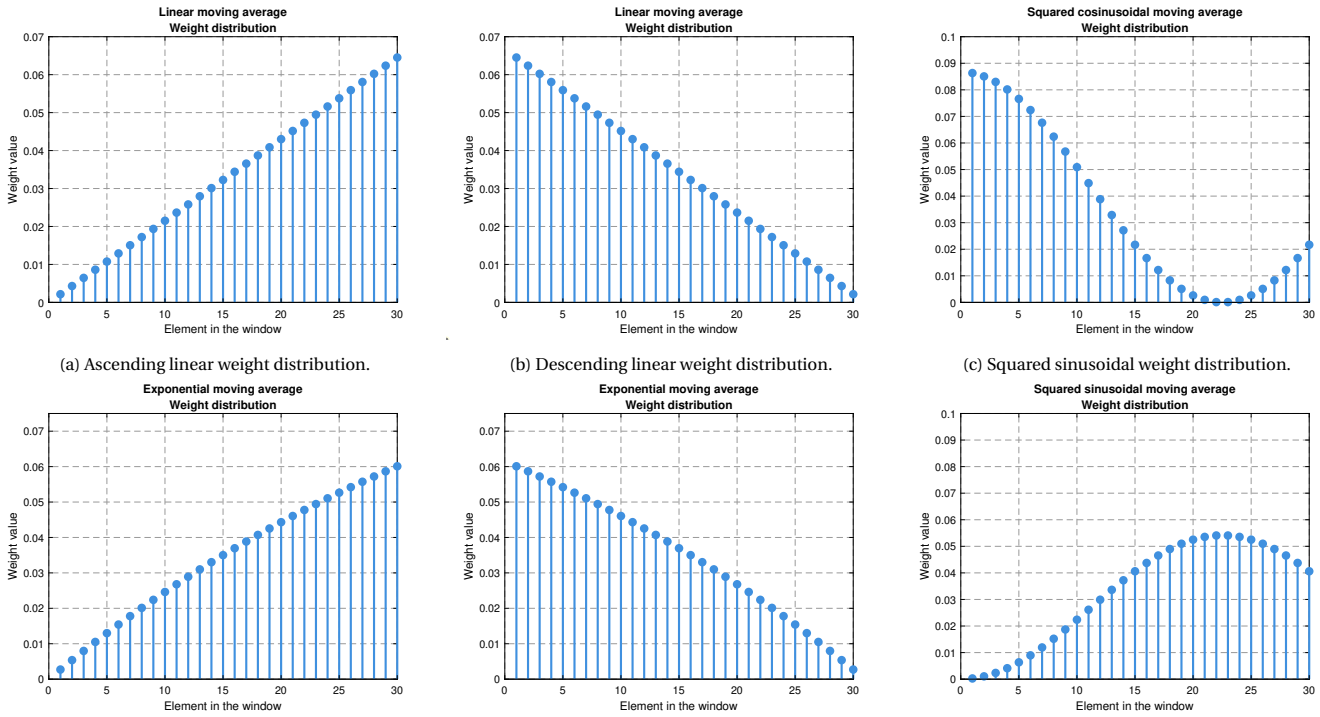

(a) Ascending linear weight distribution.

(b) Descending linear weight distribution.

(c) Squared sinusoidal weight distribution.

(d) Ascending exponential weight distribution.

(e) Descending exponential weight distribution.

(f) Squared cosinusoidal weight distribution.

Figure 3.3: Different weight distribution considered for the moving average control algorithm, the window size for each graph is thirty.

Eventually a paper was found by Raudys et al [38] where the author calculated the optimal weight distribution for the moving average calculation to be used to accurately calculate and predict the stock market prices. The author used gradient descent to calculate the optimal weights for each element in the window for the moving average calculation. The optimal weight distribution was found by the author and is given in figure 3.4a. Based on this, it was decided to test this out on a slightly altered version of the weight distribution for this research. This weight distribution is given in 3.4b.

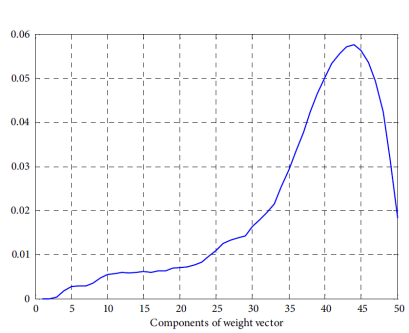

(a) Optimised weight distribution calculated by Raudys et al[38].

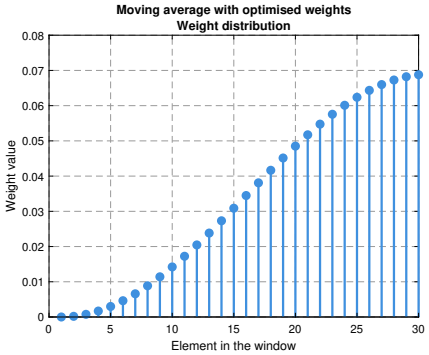

(b) Slightly altered version of the optimised weight distribution used for this research.

Figure 3.4: Weight distribution calculated by the author and used for this research. The author illustrated an example of the weight distribution using fifty element for the window for the moving average calculation. While the example given for this research has a window of 30 elements.

Furthermore, the author also illustrated the performance of the moving average using the optimised weight distribution and

compared it to the performance of the conventional simple moving average. Figure 3.5 illustrates the performance of both types of moving average.

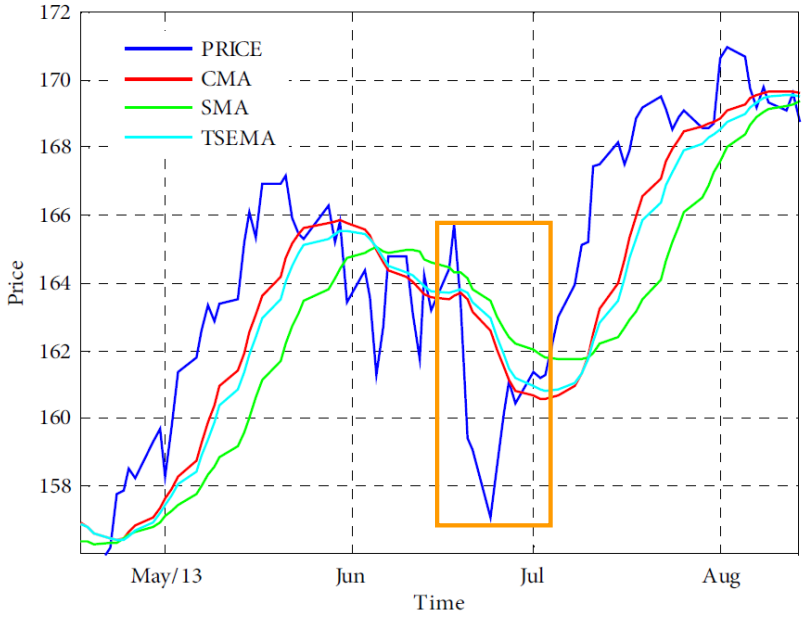

Figure 3.5: Performance of the two types of moving averages. The red line in the graph is the moving average line using the optimised weight distribution and the green line is the simple moving average line. Finally the blue line is the stock prices which is used for the moving average calculation.

As can be seen from the graph, the optimised weight distribution has a higher accuracy than the simple moving average and lags less than the simple moving average. This is important for this research as whenever there is no power or voltage fluctuation the calculated moving average value should also reflect this in a way that ensure that the ESS will not discharge/charge any power. Resulting in less energy consumption from the ESS. Furthermore, the moving average using the optimised weight distribution also achieved a smoothed output even if the stock price fluctuated. This is highlighted with an orange rectangle. This is also important for our application since this method for the control algorithm must ensure that the power or voltage at PCC be smoothed out using the ESS.
To test the hypothesis that the optimised weight distribution will ensure for a more energy efficient control algorithm, simulation using pre-existing PV system data was used and all of the considered weight distribution were used to smooth out the voltage or power at PCC. The simulation setup and the performance of two types of weight distribution is highlighted in sections 3.7 and 3.8.

3.2.2. Window of operation

For this layer of control, the main idea is for the algorithm to check if the time of the day at that exact moment is within the operating window for the control algorithm to operate. If the the time of the day is within the operating window range, then the control algorithm shall calculate power setpoint for the next control layer. If not then the control algorithm does not output a power setpoint for the next control layer and instead sends a zero power setpoint.
This layer is important as the operating window corresponds to when there is sunlight during that time of day. The operating window can very throughout the seasons of the year, since the time for sunrise and sunset can vary between winter and summer time in the Netherlands. For simulation of the controls, a different operating window for the different seasons are as follow.

- **Winter**
  Operating window : 08:00:00 — 17:00:00
- **Spring**
  Operating window : 06:00:00 — 20:00:00
- **Summer**
  Operating window : 05:00:00 — 22:00:00
- **Fall**
  Operating window : 08:00:00 — 19:00:00

For testing purposes since the experiments shall occur during the summertime, the operating window used for the experi-

ments is summer time operating window. Figure 3.6 illustrates the operating window on a summer day and as can be seen the summer operating window (highlighed by the orange area in the graph) is well within the time of day when the PV generates power.

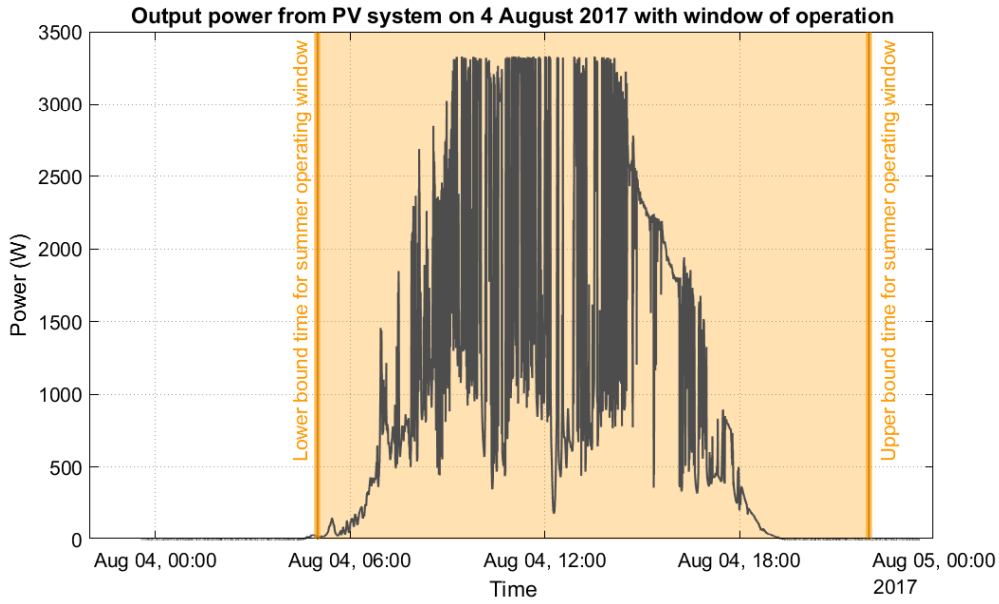

Figure 3.6: Summer operating window compared to PV system generation during the summer.

3.2.3. SoC power reduction curve

For this layer of control, the function of it is to reduce the power based on measured SoC values so as to not overcharge or overdischarge the ESS and to keep the ESS' operation within its Safe Operating Area (SOA). The idea for this control layer was first presented by Senjyu et al[39] and is where the design for this control layer is based from. In essence how this control layer works is that a reduction factor is applied to the calculated power to reduce the power. The reduction factor scales linearly with the measured SoC as given in figure 3.7. Furthermore it was set that within a certain SoC range no power reduction shall occur, since it is expected that within this SoC range the calculated power value shall not exceed the ESS' SOA. Equation 3.5 and 3.6 illustrates how the calculation for the power reduction can be done for discharge and charge power respectively.

$$P_{\text{ESS,DISCH,SoC}} = \begin{cases} P_{\text{ESS,DISCH}} \cdot (1 - K_{\text{DISCH}} \cdot |SoC_{\text{measured}} - SoC_{\text{lower limit}}|), & \text{if } SoC_{\text{measured}} < SoC_{\text{lower limit}} \\ P_{\text{ESS,DISCH}}, & \text{otherwise} \end{cases} \tag{3.5}$$

$$P_{\text{ESS,CH,SoC}} = \begin{cases} P_{\text{ESS,CH}} \cdot \left(1 - K_{\text{CH}} \cdot |SoC_{\text{measured}} - SoC_{\text{upper limit}}|\right), & \text{if } SoC_{\text{measured}} > SoC_{\text{upper limit}} \\ P_{\text{ESS,CH}}, & \text{otherwise} \end{cases} \tag{3.6}$$

In both equations, the K_{DISCH} and K_{CH} are the correction factors used for the calculation. The $P_{\text{ESS,DISCH}}$ and $P_{\text{ESS,CH}}$ being the calculated discharge and charge power from the previous control layer, window of operation check control layer, with $P_{\text{ESS,DISCH,SoC}}$ and $P_{\text{ESS,CH,SoC}}$ being the calculated discharge and charge power after the power reduction calculation. Lastly, SoC_{measured} is the measured SoC with $SoC_{\text{upper limit}}$ and $SoC_{\text{lower limit}}$ being the upper and lower SoC limit of which the range in between those values are the values where no power reduction shall occur.
An example for how this control layer works can be the following. Consider the calculated power is 1000 W and the measured SoC is 30%. Furthermore the SoC range with which there is no power reduction is between 49.8% and 50.2%. Lastly, given in figure 3.7b the correction factor to be used for this example shall be 0.01. Based on these parameters and using equation 3.5, the calculated power from this control layer can be calculated as follow.

$$P_{\text{ESS,DISCH,SoC}} = 1000 \cdot (1 - 0.01 \cdot |30 - 49.8|) \approx 802W \tag{3.7}$$

From this calculation, it can be deduced that the power reduction was around $\frac{1000-802}{1000} \cdot 100 \approx 19.8\%$. This corresponds to the value given in the graph in figure 3.7b.

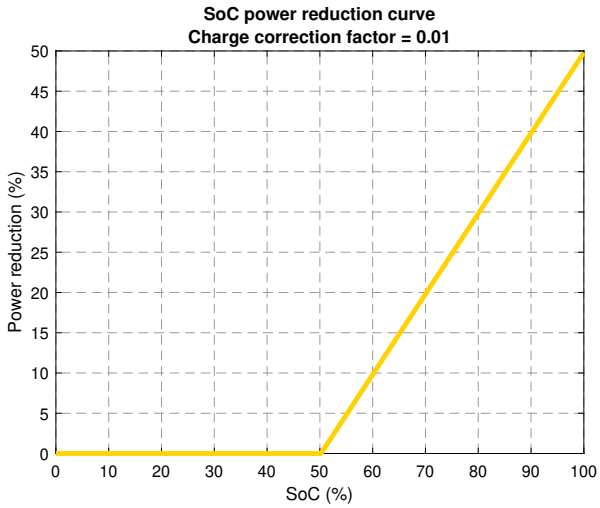

(a) SoC power reduction curve for charge power from the ESS.

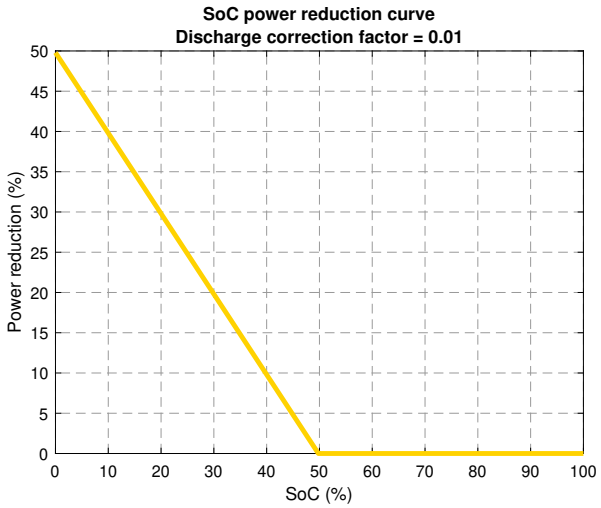

(b) SoC power reduction curve for discharge power from the ESS.

Figure 3.7: SoC power reduction curve for both charge and discharge power.

It is important to highlight that when simulating this control layer, the energy usage is used instead of the measured SoC. It was decided to only use the energy usage since for both setups the ESS' used had a different capacity value and thus would not be beneficial to use SoC for the simulation of this control layer and the next control layer called idle charge and discharge. Once the energy threshold is set after simulation results, then this value is translated to a SoC value using the ESS capacity from the test setups. The equations used for calculating the new power setpoint using energy usage instead of the measured SoC is given in equation 3.8 and 3.9.

$$P_{\text{ESS,DISCH,SoC}} = \begin{cases} P_{\text{ESS,DISCH}} \cdot \left(1 - K_{\text{DISCH}} \cdot |E_{\text{usage}} - E_{\text{lower limit}}|\right), & \text{if } E_{\text{usage}} < E_{\text{lower limit}} \\ P_{\text{ESS,DISCH}}, & \text{otherwise} \end{cases} \tag{3.8}$$

$$P_{\text{ESS,CH,SoC}} = \begin{cases} P_{\text{ESS,CH}} \cdot \left(1 - K_{\text{CH}} \cdot |E_{\text{usage}} - E_{\text{upper limit}}|\right), & \text{if } E_{\text{usage}} > E_{\text{upper limit}} \\ P_{\text{ESS,CH}}, & \text{otherwise} \end{cases} \tag{3.9}$$

3.2.4. Idle charge/discharge

The main idea for this control layer is to ensure that the SoC of the ESS throughout the day will always remain around the starting SoC of the ESS as set in at the beginning of the day. In order to achieve this, this control layer will charge or discharge the ESS when the power setpoint has a value that is deemed not significant to influence the voltage fluctuation at PCC. Furthermore if the SoC of the ESS is higher than a specified value, then this control layer will ensure that the ESS discharges at a specified discharge power if there is an insignificant power setpoint calculated by the previous control layer. Likewise if the SoC of the ESS is lower than a specified value, then this control layer ensures that the ESS charges at specified charge power if there is an insignificant power setpoint calculated. Equations 3.10 illustrates how the idle charge and discharge is implemented. It is important to point out that from the previous layer the variables $P_{\text{ESS,DISCH,SoC}}$ and $P_{\text{ESS,CH,SoC}}$ are combined to a single variable called $P_{\text{ESS,SoC}}$ which is then fed into the equation and thus the control layer.

$$P_{\text{ESS,Idle}} = \begin{cases} P_{\text{Idle discharge}}, & \text{if } P_{\text{lower limit}} \geq P_{\text{ESS,SoC}} \leq P_{\text{upper limit}} \\ & \text{and } SoC_{\text{measured}} > SoC_{\text{upper limit}} \\ P_{\text{Idle charge}}, & \text{if } P_{\text{lower limit}} \geq P_{\text{ESS,SoC}} \leq P_{\text{upper limit}} \\ & \text{and } SoC_{\text{measured}} < SoC_{\text{lower limit}} \\ P_{\text{ESS,SoC}}, & \text{otherwise} \end{cases} \tag{3.10}$$

As an example, figures 3.8a and 3.8b illustrates idle charging and idle discharge for 30% and 70% SoC respectively. The SoC threshold for charge and discharge was 49.8% ($SoC_{\text{lower limit}}$) and 50.2% ($SoC_{\text{upper limit}}$) respectively. Furthermore the power threshold was set at ± 40W ($P_{\text{upper limit}}$ and $P_{\text{lower limit}}$) and the idle charge and discharge value was set at ± 50W ($P_{\text{Idle discharge}}$ and $P_{\text{Idle charge}}$).

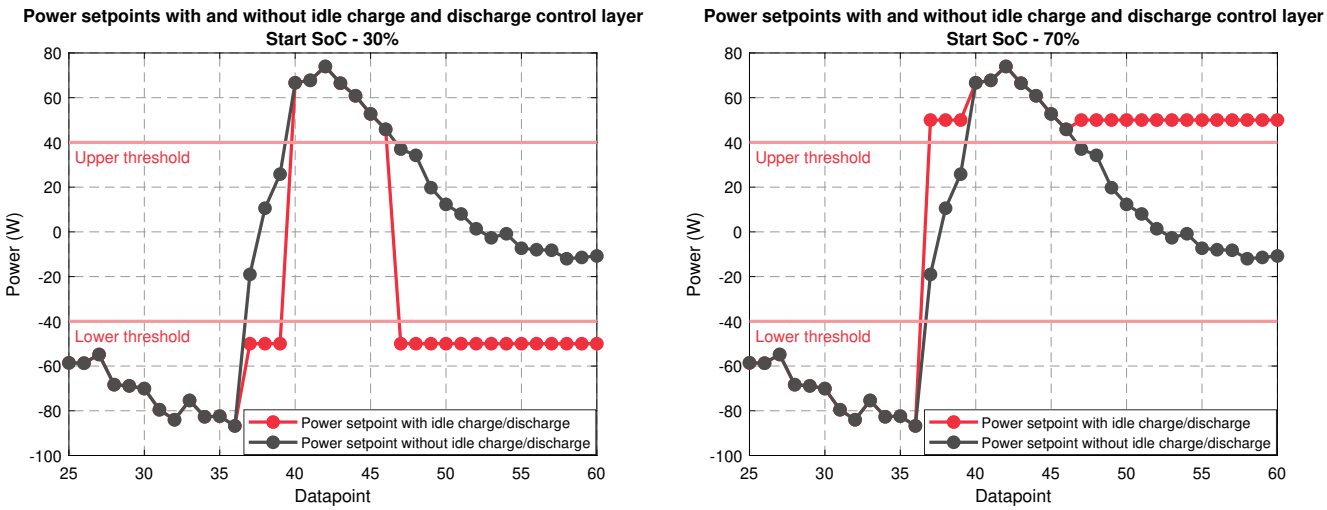

(a) Power setpoint before and after applying idle charge control layer.

(b) Power setpoint before and after applying idle discharge control layer.

Figure 3.8: Example of idle charge/discharge control layer, the upper and lower threshold denotes 40 and -40W respectively.

As can be seen from both figures, whenever the calculated power setpoint value from the previous control layer is within -40 and 40W then the ESS either charges or discharges 50W as given by the red line.

3.3. Voltage sensitivity calculation

As explained in chapter 1, the voltage sensitivity of the circuit is an important metric used to quantify how much influence the power fluctuation of the PV system will have on the measured PCC voltage. This value was first mentioned in a paper written by Wang et al[18], yet the difference between the application for this thesis and the one used in the paper is that the voltage sensitivity used in this thesis is at a LV level. While the setting for the simulation in the paper is at MV level. Nonetheless due to simplicity for applying this value to benchmark the performance of the two control algorithms, it was decided to use this value for the simulation and test setup design.
The value of voltage sensitivity is used primarily by the voltage control algorithm to output a power setpoint for the ESS, for which this is further explained in section 3.5. Furthermore this value is then used to quantify how many visible and annoying voltage flickers were avoided by using the two control algorithms, which is an important performance metric that was explained in chapter 1.
The method for quantifying the voltage sensitivity value can be described as follow.

1. Firstly the dataset used must contain the measured PV output power, PCC voltage and the exact time of day when each measurements were taken. Then the change in PCC voltage, PV output power and elapsed time between the samples is calculated.

2. Using the calculated change in PCC voltage and elapsed time between the samples, these values are then mapped onto a Matlab recreated version of the voltage flicker curve described in figure 1.6. The values that exceed the visible flicker curve are then recorded. An example of this is given in figure 3.9.

3. The recorded values are then used to calculate the voltage sensitivity of each recorded values by dividing the change in PCC voltage with the change in PV output power.

4. Since some of the visible or annoying voltage flickers are caused by external factors (load connection for example) and not by the PV system, some of the calculated voltage sensitivity would have a value that is close to infinity. This is deemed implausible and thus some of the values have to be filtered out. Through research regarding LV cabling in household in the Netherlands and how much the resistance of such cables would be, it was decided to filter out any voltage sensitivity values above 0.01.

5. Filtering out the implausible voltage sensitivity values would result in more meaningful values. These meaningful values are then averaged out to a single value which is thus the overal voltage sensitivity value of the circuit in which the PV system is connected to.

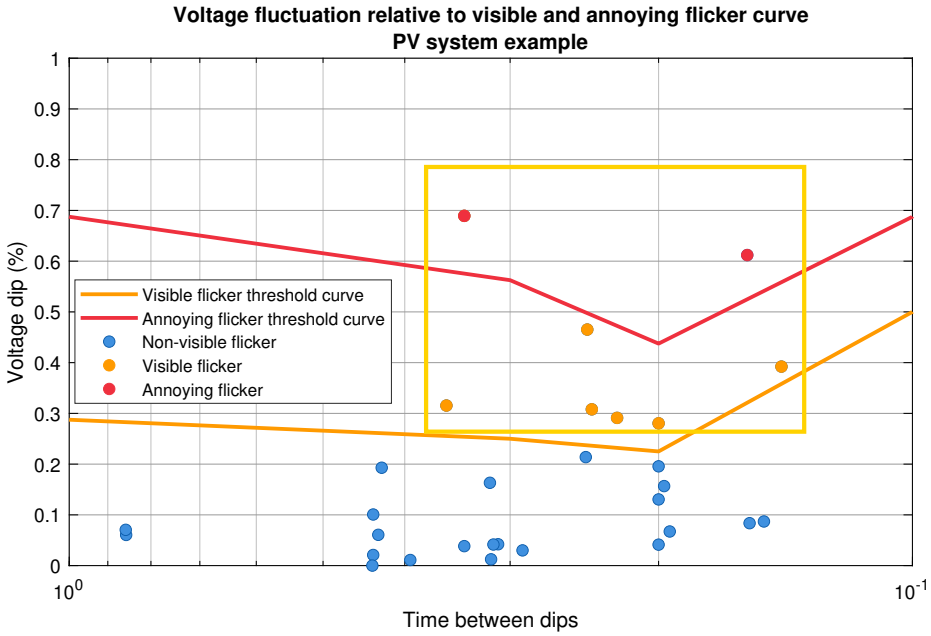

Figure 3.9: Example of voltage flickers exceeding the visible and annoying flicker curve, highlighted by the yellow rectangle.

3.4. Power control design

For the power control, it was designed such that it would only react and compensate for the power fluctuations from the output power of the PV system based on control algorithm using moving average. Figure 3.10 illustrates an example of this, where the grey line is the measured PV output power and the blue line is the calculated power using the moving average control algorithm. Whenever there is a difference between the calculated power and the measured PV power, the ESS must be able to compensate for the difference between the two which is the ΔP highlighted in figure 3.10. This ensures that the power at PCC would the calculated power from the moving average control algorithm.

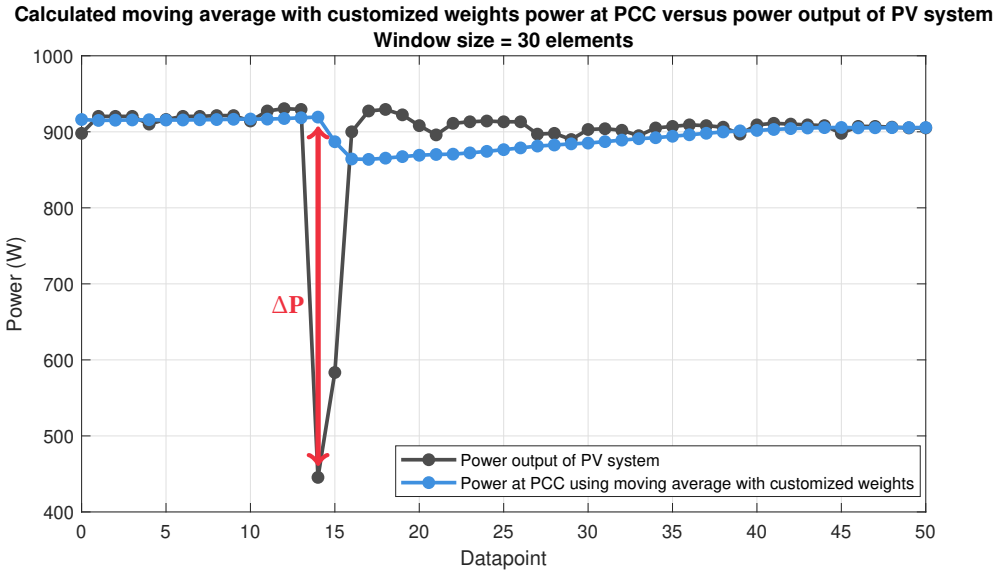

Figure 3.10: Example of a power control implementation with the designed control algorithm.

How the power control sequence of action was simulated is given in figure 3.11 and each step can be described in detail as follow.

1. During the first step, the PV output power is constantly measured and each new measurement is added to the moving average window. Until the moving average window is completely filled up, a calculated power value that is equal to the measured PV power is sent to the next step. This is to ensure that proper and current values are filled into the moving average window first before sending out a power setpoint command to the ESS inverter. When the moving average window is filled up, then a proper calculated power from the moving average control algorithm is sent to the next step.

2. For this step, the calculated power from the control algorithm (given by $P_{MA,PCC}$ in the equation) is subtracted from the measured PV power at the time instance (P_{PV}). The resulting value is the power that the ESS must deliver to compensate and avoid any voltage flickering from occurring. This value is then sent to the next step.

3. During this step, the calculated ESS power goes through the extra layers of control from the control algorithm. These layers of control were described in figure 3.1. The final value which is sent to the ESS inverter comes after the final layer of control.

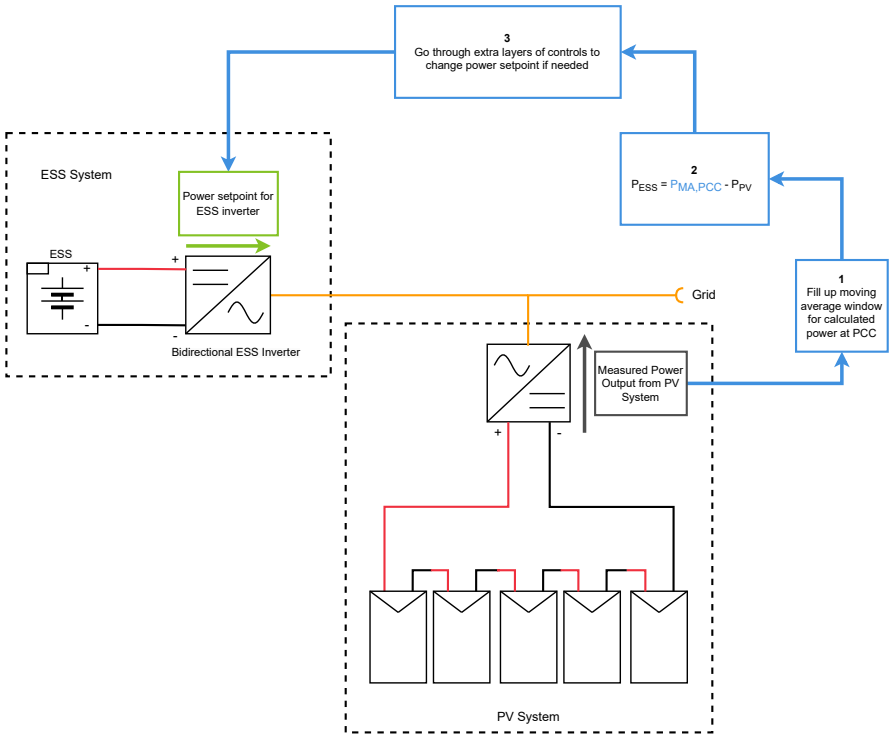

Figure 3.11: Power control sequence of action.

After sending the power setpoint to the ESS inverter, the power at the DC input of the inverter which is the power that ESS exactly delivers is calculated using the ESS inverter's efficiency value. For charge and discharge power of the ESS, the calculation is as follow in equations 3.11 and 3.12.

$$P_{\text{ESS,DC,charge}} = P_{\text{ESS,AC,charge}} \cdot \eta \tag{3.11}$$

$$P_{\text{ESS,DC,discharge}} = \frac{P_{\text{ESS,AC,discharge}}}{\eta} \tag{3.12}$$

From this the energy usage of the ESS can be calculated using the cumulative trapezoidal method given in equation 3.13. This method is used to calculate the energy used during a time instance, then this value is to either add or subtract from the previous energy value. Furthermore, this can then be used to calculate the new SoC value for the ESS, which is given in equation 3.14.

$$E_{\text{used}} = \frac{1}{2} \cdot \frac{(P_{\text{ESS,i}} - P_{\text{ESS,i-1}}) \cdot (t_{\text{i}} - t_{\text{i-1}})}{3600} \tag{3.13}$$

$$SoC_i = SoC_{i-1} - 100 \cdot \frac{E_{\text{used}}}{E_{\text{ESS capacity}}} \tag{3.14}$$

Where $P_{\text{ESS,i}}$ and $P_{\text{ESS,i-1}}$ is the measured DC power of the ESS at the moment it was measured and the measured value previously. Furthermore t_{i} and $t_{\text{i-1}}$ is the elapsed time measured now and the previous value respectively. From the calculated energy usage (E_{used}), the SoC of the ESS can then be calculated by dividing the calculated energy usage with the energy capacity of the ESS and then subtracting it from the previous measured SoC value. After the energy usage and power setpoint values are calculated for the full day simulation, the power to energy ratio can be calculated using equation 3.15.

$$\text{Power to energy ratio} = \frac{\text{Max}(|P_{\text{ESS,DC,charge}}|, P_{\text{ESS,DC,discharge}})}{E_{\text{total}}} \tag{3.15}$$

Where E_{total} is total energy usage from the ESS throughout the whole day with the maximum value between the charge $P_{\text{ESS,DC,charge}}$ and discharge $P_{\text{ESS,DC,charge}}$ power being used to calculate the power to energy ratio. Then the calculated energy

is divided by 3600 in order convert the calculated energy from Ws to Wh.
It is important to highlight this step of the simulation as the energy usage is directly used for the other layers in the control algorithm to adjust the power setpoint accordingly. The results of the simulation is explained in section 3.7.

3.5. Voltage control design

For the voltage control, it was designed such that it would only react and compensate for the voltage fluctuations from the voltage at the PCC based on a control algorithm using the moving average. Figure 3.12 illustrates an example of this, where the grey line is the measured PCC voltage and the blue line is the calculated PCC voltage using the moving average control algorithm. Whenever there is a difference between the calculated voltage and the measured PCC voltage (highlighted by (ΔV in figure 3.12), the ESS must be able to compensate enough power to ensure that the calculated PCC voltage is reached.

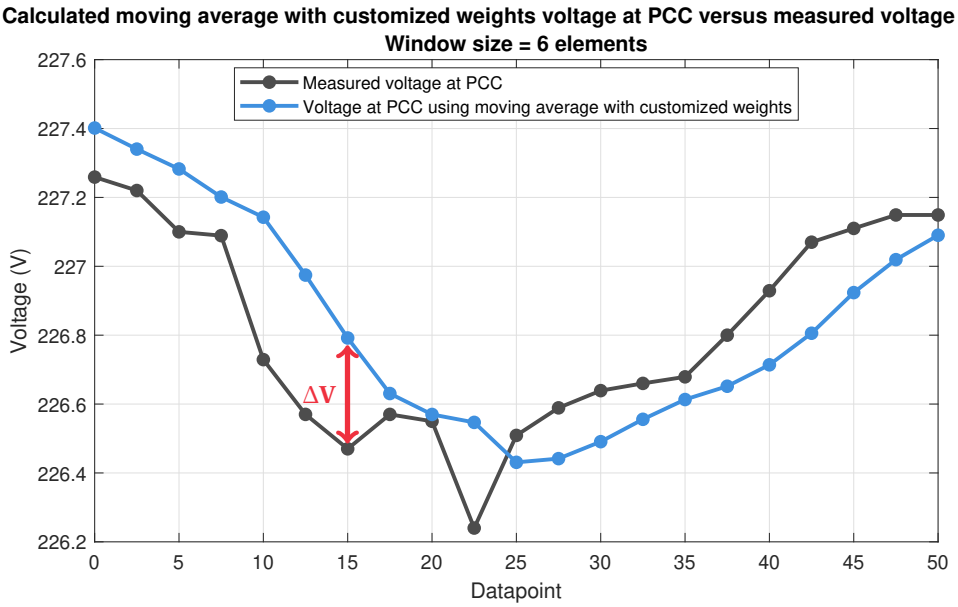

Figure 3.12: Example of a voltage control implementation with the designed control algorithm.

How the voltage control sequence of action was simulated is given in figure 3.13 and each step can be described in detail as follow.

1. During the first step, the PCC voltage is constantly measured and each new measurement is added to the moving average window. Until the moving average window is completely filled up, a calculated power value that is equal to the measured PCC voltage is sent to the next step. This is to ensure that proper and current values are filled into the moving average window first before sending out a power setpoint command to the ESS inverter. When the moving average window is filled up, then a proper calculated voltage from the moving average control algorithm is sent to the next step.

2. Once the calculated voltage at PCC is sent through by the moving average control algorithm. The difference between the calculated voltage and measured voltage at the time instance is then calculated (ΔV) using equation 3.16.

$$\Delta V = V_{\text{MA,PCC}} - V_{\text{Measured}} \tag{3.16}$$

   In order to translate this to a power setpoint for the ESS, the difference between the calculated and measured voltage at PCC is divided by the measured voltage sensitivity of the circuit ($^{dV}/_{dP}$), this is highlighted using equation 3.17. Then this value is sent through to the next step.

$$P_{\text{ESS}} = \frac{\Delta V}{^{dV}/_{dP}} \tag{3.17}$$

3. During this step, the calculated ESS power goes through the extra layers of control from the control algorithm. These layers of control were described in figure 3.1. The final value which is sent to the ESS inverter comes after the final layer of control.

As explained in section 3.4 regarding the energy usage and SoC estimation, the same is applied for the simulation of voltage control aswell. The simulation results are explained in section 3.8.

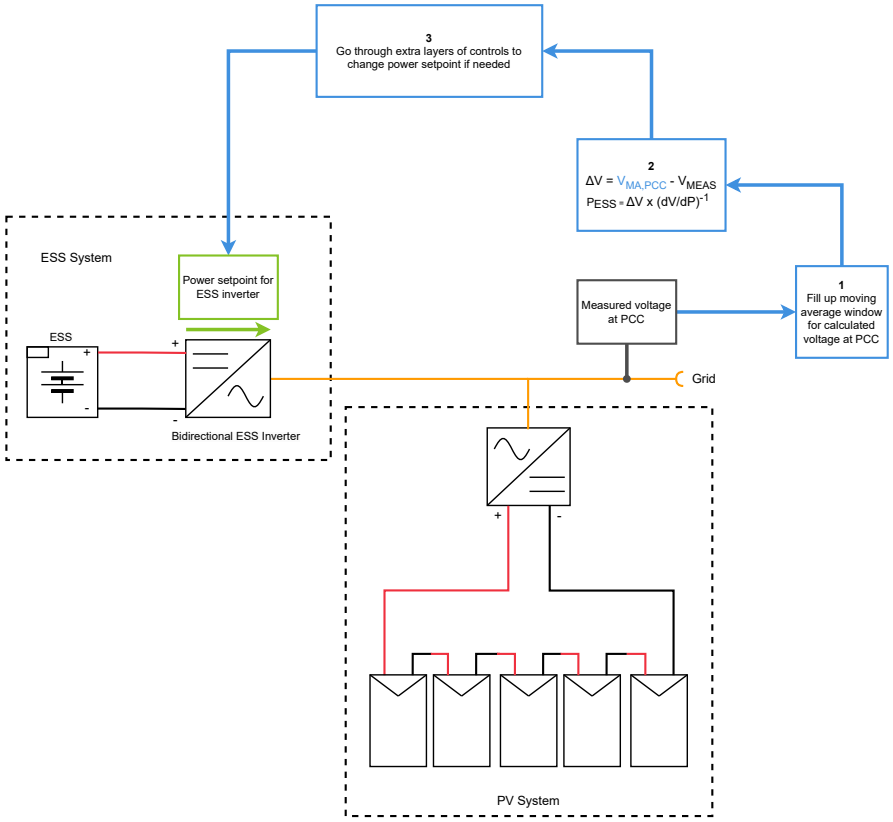

Figure 3.13: Voltage control sequence of action.

3.6. Simulation setting and assumptions

It is important to point out that the simulation to test the performance of the control algorithms was done in Matlab and the setting for the simulation was done for an AC connected ESS. The reason for the latter is due to the availability of the data provided was only measurements at the output of the PV inverter and did not contain measurements at the DC input of the PV inverter or did not disclose which PV inverter was used to derive the efficiency value. The data was taken from a PV system, for which the specifications are highlighted in table 3.1.

It is important to note that throughout the simulation the data used for bench marking the performance of the control algorithms was the PV data where the power fluctuations was measured to be the worst throughout that year. This data is from August 4th 2017 and the PV power and voltage at PCC profile is given in figure 3.14a and figure 3.14b respectively. In section 3.7.5 and 3.8.5, the data of other days in different seasons are used to benchmark the energy usage of the control algorithm. The inverter used for the simulation is modelled after the Victron Multiplus II ESS inverter, which has nominal efficiency of 94 % [C.1.10]. The reason why this particular inverter was chosen and eventually used in the test setups is further explained in section 4. Finally, it is assumed that for the simulation for the control algorithm implementation the inverter response time is instant and thus delivers the power based on the read-in power setpoint right away.

	Specifications
PV capacity (kWp)	3.48
Measured voltage sensitivity	0.0010674
Sampling rate (seconds)	2
Measured visible flickers	306
Measured annoying flicker	7

Table 3.1: Specification of the data from the PV system used for the simulation.

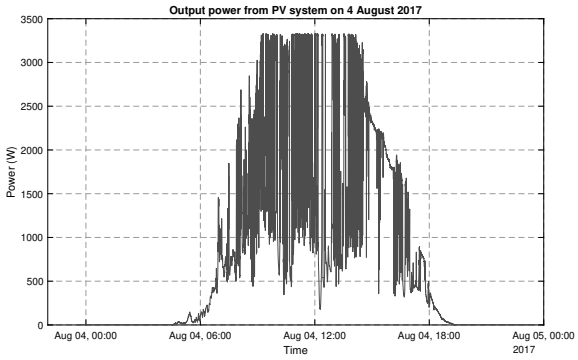

(a) PV output data used for the simulation.

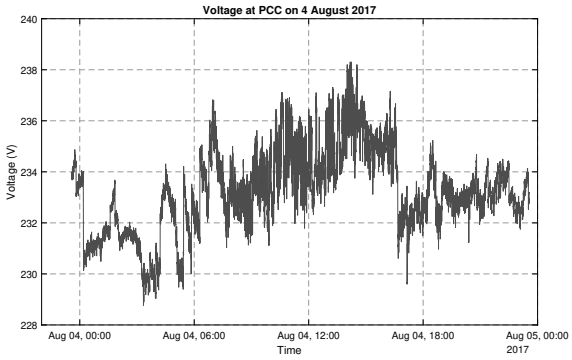

(b) Voltage at PCC data used for the simulation.

Figure 3.14: System design and simulation results from Kakimoto et al.

3.7. Simulation results of power control

For the simulation of the power control, the outline of the simulation results are as follow.

1. Firstly the simple moving average algorithm and the moving average with optimised weights are both simulated to illustrate the power to energy ratio performance between the two. Then the flicker avoidance performance of both types of moving average are also compared between the two. After this the final window size to be used for the eventual implementation within the test setups is chosen

2. Consequently the window of operation check is implemented and the power to energy ratio and flicker avoidance performance is analysed for the moving average algorithm with optimised weights with the chosen window size.

3. After establishing the window of operation, the SoC power reduction curve is implemented. Different charge and discharge correction factors are simulated and the effect it has on the performance metrics is analysed. After this step, the final charge and discharge correction factor is chosen.

4. After the SoC power reduction curve, the idle charge/discharge layer is implemented in the simulation. Different values for the idle charge and discharge are analysed and eventually the final values for this control layer is chosen.

5. Finally a full simulation is done with all of the control layer and the flicker avoidance performance metric is analysed with and without the control algorithm. Furthermore the control algorithm is applied to other days in different seasons to benchmark the power to energy ratio performance metric.

Furthermore, the matlab script used for simulating power control is available in the appendix at section A.2.2

3.7.1. Moving average type simulation results

For this part of the simulation, the simple moving average and the moving average with the optimised weights are applied throughout the whole dataset. From the calculated power that the ESS has to deliver, the maximum charge and discharge power is calculated. Furthermore, the ESS energy used throughout the whole day is calculated, this would then lead to the power to energy ratio being calculated for both types of moving averages with different window sizes. Table 3.2 illustrates the simulation results using the simple moving average and table 3.3 illustrates the simulation results using the moving average with optimised weights.

Window size (# elements)	Maximum discharge power (W)	Maximum charge power (W)	ESS energy usage (Wh)	Power to energy ratio
15	2682.79	-2506.70	154.99	17.31
30	2716.37	-2570.45	214.14	12.68
45	2701.67	-2615.58	255.08	10.59
60	2738.75	-2632.97	283.94	9.65
90	2778.92	-2622.36	327.33	8.49

Table 3.2: Simulation results using the simple moving average.

Window size (# elements)	Maximum discharge power (W)	Maximum charge power (W)	ESS energy usage (Wh)	Power to energy ratio
15	2715.84	-2463.54	115.40	23.54
30	2676.81	-2508.82	160.55	16.67
45	2648.97	-2529.86	194.91	13.59
60	2627.21	-2571.73	221.83	11.84
90	2700.45	-2607.66	261.64	10.32

Table 3.3: Simulation results using the moving average with optimised weights.

Based on the simulation results of both moving average types, the following conclusions can be formulated. The ESS energy used by the simple moving average control algorithm is higher than that of the moving average algorithm using the optimised. When analyzing how much less energy usage this is, it was calculated that the moving average control algorithm using optimised weights uses ~ **23%** less energy than the simple moving average control algorithm. This comes as no suprise as the simple moving average type lags more behind the moving average type with optimised weights. An example of this is given in figure 3.15.

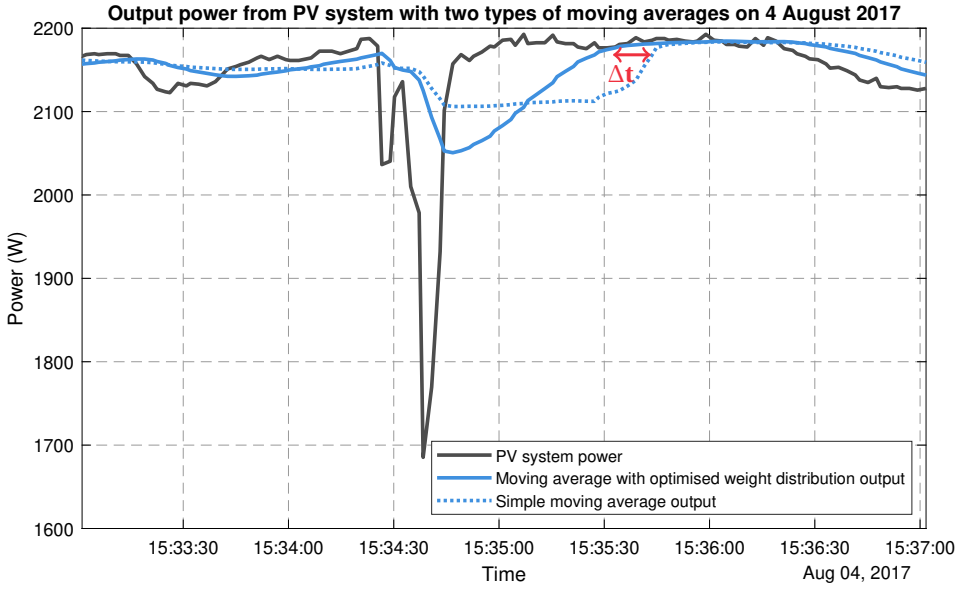

Figure 3.15: PV output power compared to the simple moving average output and the moving average with optimised weights output.

As can be seen from the figure, after the PV power fluctuates and returns back to nominal values the simple moving average takes a certain amount of time to reach the same nominal value as the PV output power. When compared to the moving average with optimised weights, this is achieved much faster than the simple moving average. The difference in time (highlighted by Δt) is around 15 seconds in this example. Furthermore as explained in section 3.4, the ESS must deliver power based on the difference between the moving average output and the PV output power. During the timeframe of 15 seconds using the simple moving average, the ESS must deliver ~ 40 W unnecessarily for 15 seconds while the moving average using optimised weights already reached the nominal PV power and thus no ESS power has to be discharge using this moving average type. Knowing this, the amount of energy discharged unnecessarily by the simple moving average was calculated as follow.

$$\Delta E_{\text{simple}} = \frac{15 \cdot 40}{3600} \approx 0.167\text{Wh} \tag{3.18}$$

This value may not seem significant since this is a very low energy usage difference between the two types of simple moving average, yet due to the very frequent power fluctuations from the PV system data this will thus accumulate to a large difference of energy usage between the two moving average types. This thus confirms the hypothesis made in section 3.2.1 regarding energy usage from both types of moving average considered and gives a good basis to consider the weight distribution for the moving average introduced by Raudys et al for this research.
Though the energy usage of the moving average control algorithm with optimised weights is less than the simple moving average control algorithm, the power to energy ratio of both types of moving averages are not above the expected value of 70. This due to the maximum discharge and charge power value being the same and independent of the type of moving average and window size. Furthermore, the energy usage of both types of moving averages is quite high aswell. For this reason, the other control layers has to be implemented in order to increase the power to energy ratio and lower the overal energy usage

of the ESS.
After analyzing the energy usage of both types of moving averages, the measured visible and annoying flickers were measured before and after applying both types of moving averages. After applying the control algorithm, the voltage at PCC is calculated using equation 3.7.1.

$$V_{\text{PCC,after}} = V_{\text{PCC,before}} + P_{\text{ESS,AC}} \cdot \frac{\text{dV}}{\text{dP}} \tag{3.19}$$

With $V_{\text{PCC,before}}$ being the measured voltage at PCC before applying the control algorithm. Using the voltage sensitivity ($\frac{\text{dV}}{\text{dP}}$) and the power from the ESS at the inverter output($P_{\text{ESS,AC}}$), the voltage at PCC after applying the control algorithm is calculated ($V_{\text{PCC,after}}$). From this, the change in the voltage at PCC is again calculated and then mapped onto the voltage flicker curve to measure if there are any visible or annoying flicker that have occurred. Table 3.4 and 3.5 illustrates the results after applying both types of moving average with different window sizes.

Window size (# elements)	Amount of visible flickers	Amount of annoying flickers
15	114	0
30	112	0
45	114	0
60	113	0
90	111	0

Table 3.4: Voltage flickers after applying the simple moving average with different window sizes.

Window size (# elements)	Amount of visible flickers	Amount of annoying flickers
15	125	0
30	113	0
45	111	0
60	112	0
90	112	0

Table 3.5: Voltage flickers after applying the moving average with optimised weights with different window sizes.

From both tables, the following conclusions can be derived. Firstly for both types of moving averages, the amount of visible and annoying flicker reduction is almost the same. With the total reduction for both visible and annoying flicker combined being around ~ **65%**. Finally, It can be observed that for both moving average types the amount of visible and annoying flicker reduction remains the same regardless of the window size used.
Based on the above mentioned conclusions and the conclusions highlighted in section 3.7.1, the main takeaway is that both types of moving averages reduce the same amount of visible and annoying flickers, yet the moving average with the optimised weights uses less energy from the ESS to achieve this. This clearly shows that the moving average with the optimised weights has a better performance and thus will be used for the control algorithm moving forward. Another takeway is that the window size does not reduce the amount of flickers, yet only increases the amount of used ESS energy. Based on this, it was decided to use a window size of 30 elements for power control as this showed a great balance between energy used and amount of flicker reduction. The performance of this window size is highlighted in table 3.3 and 3.5.

3.7.2. Window of operation check simulation results

For this part of the simulation, the window of operation check is applied to the simulation of the control algorithm. In essence, the ESS would only within a certain time window during which there would be sunlight and the PV system outputs power. Since the dataset is based on measurements from the 4th of August 2017, the window of operation would be between 5 AM till 10 PM since this is during the summer period as highlighted in section 3.2.2. The flicker reduction simulation results can be seen in table 3.6. The window size used for the simulation was the chosen 30 elements.

Window of operation	Amount of visible flickers within operating window	Amount of annoying flickers within operating window	Amount of visible flickers outside operating window	Amount of annoying flickers outside operating window
Before	103	0	10	0
After	103	0	10	0

Table 3.6: Effect on voltage flicker reduction after implementing window of operation check.

Based on this results above, it can be observe the total flicker events only increased as result of applying the window of

operation check. This is due to the flicker events occurring outside the window of operation not being fixed by the control algorithm. Furthermore, the ESS energy used was not reduced as a result of applying the window of operation check and stayed around 160Wh. Nonetheless, this control layer was still implemented as for the scope of this project, it is important to fix the voltage flickers caused by PV systems and not voltage flickers caused by (for example) load connections while the PV system is not proving any power.

3.7.3. SoC power reduction curve simulation results

As explained in section 3.2.3, in order to avoid the ESS from being overcharged or overdischarged when operating a control layer must be added to reduce the charge and discharge power based on the SoC of the ESS. Furthermore, this would result in lower energy usage from the control algorithm. By implementing what is called a discharge/charge correction factor, the charge and discharge power is reduced based on the measured energy usage (or SoC) and the correction factor used. Since the goal is to be as energy efficient as possible and achieving a power to energy ratio that is higher than 70, the threshold for which the power reduction curve reduces the power sent to the ESS is set at ± 5 Wh. Table 3.7 and 3.8 illustrates the simulation results using different correction factors for charge and discharge.

Charge and discharge correction factor	Maximum discharge power (W)	Maximum charge power (W)	ESS energy usage (Wh)	Power to energy ratio
0	2676.81	-2508.82	160.55	16.67
0.001	2525.68	-2508.82	156.40	24.76
0.005	2442.84	-2508.82	141.50	58.17
0.01	2511.48	-2508.82	125.83	77.93
0.02	2671.05	-2508.82	26.00	102.72

Table 3.7: Energy usage of the ESS after applying different correction factors for the SoC power reduction curve.

As can be observed from both tables, the ESS energy used reduces as the correction factor increases due to the discharge power decreasing aswell highlighted by the measured maximum discharge power. As a result the power to energy ratio also increases, even to values above the desired value of 70 when a correction factor of higher than 0.01 is applied.
Furthermore the measured flicker events also changes as the correction factor increases. Yet by increasing the correction factor to higher values, it was measured that although the energy usage reduces greatly the amount of flicker events increases as the power is reduced such that it will not compensate the amount of power needed to avoid a flicker event anymore. Based on these results, it was decided to use a correction factor for charge and discharge of 0.01 as it deemed to be the optimized value that has ensured a high power to energy ratio and high reduction of the amount of flicker events. The performance using this correction factor value is highlighted in both tables.

Charge and discharge correction factor	Amount of visible flickers within operating window	Amount of annoying flickers within operating window
0	103	0
0.001	98	0
0.005	95	0
0.01	96	0
0.02	98	0

Table 3.8: Voltage flickers after applying different correction factors for the SoC power reduction curve.

3.7.4. Idle charge and discharge simulation results

For this layer of the control algorithm, the main goal is to essentially maintain the energy usage of the ESS at a minimum by charging or discharging the ESS (based on the measured energy usage or SoC) whenever a low enough power setpoint is sent to the ESS. Based on preliminary simulations, the power threshold to perform idle charge or discharge is set at ± 50W and just like for the SoC power reduction curve the energy usage threshold is set at ± 5Wh. Table 3.9 and 3.10 illustrates the simulation results for different idle charge and discharge values.

Idle charge power (W)	Idle discharge power (W)	Maximum discharge power (W)	Maximum charge power (W)	ESS energy usage (Wh)	Power to energy ratio
-25	25	2676.81	-2508.82	27.27	98.16
-50	50	2676.81	-2508.82	27.14	98.62
-100	100	2676.81	-2508.82	27.26	98.20
-100	50	2676.81	-2508.82	27.07	98.90

Table 3.9: Energy usage from the ESS after applying different idle charge and discharge power values.

Idle charge power (W)	Idle discharge power (W)	Amount of visible flickers within operating window	Amount of annoying flickers within operating window
-25	25	100	0
-50	50	101	0
-100	100	101	0
-100	50	101	0

Table 3.10: Voltage flickers after applying different idle charge and discharge power values.

Based on these results, it can be observed that once the idle charge/discharge is applied the energy usage reduction is around 5Wh and does not seem to change when the idle charge and discharge power values are increased. Furthermore, the discharge and charge power does not change aswell (given by the maximum charge and discharge power values) when this control layer is also applied even though the SoC power reduction curve is applied to the simulation aswell.
The main reason for this is that the energy usage is successfully being kept at a minimum with the idle charge/discharge control layer. Because of this the energy usage does not reach values for which the SoC power reduction curve control layer has to significantly reduce the charge or discharge power. The reason why the energy usage reduction is maintained at 5Wh is due to the energy usage already being close to the ± 5 Wh threshold and thus the control algorithm does not need to perform the idle charge/discharge for prolonged periods of time. Figure 3.16 illustrates the energy usage throughout the day and as can be seen the energy usage stays very close to the -5Wh threshold.
Furthermore, the highest power to energy ratio was achieved when using an idle charge power of -100W and an idle discharge power of 50W with a value of 98.90. This is well above the desired power to energy ratio of 70 goal set earlier in this report.
When analyzing the voltage flicker reduction performance of this control layer in table 3.10, it can be observed that the idle charge and discharge control layer does not greatly affect the flicker reduction performance of the overall control algorithm. Although some extra flicker events were caused by this control layer compared when compared to the previous control layer, this can be due to the ESS power switching back and forth to perform idle charge or discharge when close to the power and energy threshold. This can cause flicker of its own. For this reason it was opted not go for higher values for idle charge and discharge as this could further increase the flicker events.
Based this result from the table above and the results from table 3.9 and 3.10, it was decided to use an idle charge power of -100W and an idle discharge power of 50W. The performance of this idle charge and discharge values are highlighted in both tables.

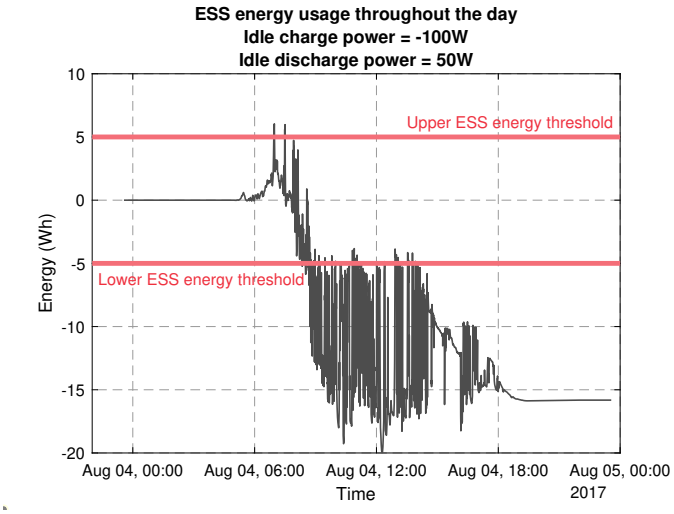

Figure 3.16: Energy usage throughout the day with idle charge and discharge

3.7.5. Summary of simulation results and performance results during different seasons.

Based on all of the results given in the preceding sections, a summary of the results is given in table 3.11 and 3.12. Firstly, it can be observed that with all of the control layers implemented using the moving average with optimised weights the energy usage was reduced with 87% compared to a control algorithm using only the simple moving average. Furthermore, the power to energy ratio with all of the control layers was 98.90, this is well within the goal set for this performance metric of having a value higher than 70. This is significantly higher than 12.68 power to energy ratio achieved with a control algorithm using only the simple moving average. The effect that each control layer has on the energy usage is compared to the simple moving average and is illustrated in figure A.1.

	ESS energy usage (Wh)	Energy usage reduction relative to the simple moving average	Power to energy ratio
Moving average with optimised weights	160.55	25	16.67
Window of operation check	160.55	25	16.67
SoC power reduction curve	32.23	85	77.93
Idle charge and discharge	27.07	87	98.90

Table 3.11: Summary of the energy usage when each each control layer is applied.

	Amount of visible flickers within operating window	Amount of annoying flickers within operating window	Amount of visible flickers outside operating window	Amount of annoying flickers outside operating window
Moving average with optimised weights	103	0	10	0
Window of operation check	103	0	10	0
SOC power reduction curve	96	0	10	0
Idle charge and discharge	101	0	10	0

Table 3.12: Summary of the voltage flicker reduction when each each control layer is applied.

When analysing the flicker reduction performance of the novel control algorithm, almost the same of amount of flicker reduction was achieved compared to a simple moving average control algorithm. The total amount of flicker events went from 313 to 111 with the novel control algorithm while the simple moving moving average control algorithm also reduced the amount of flicker events from 313 to 111. Furthermore, it was measured that the average voltage flicker values above the visible and annoying flicker curve were reduced from 1.039V to 0.46V. The final flicker reduction performance when mapped onto the flicker curve before and after applying the control algorithm can be seen in figure 3.17.

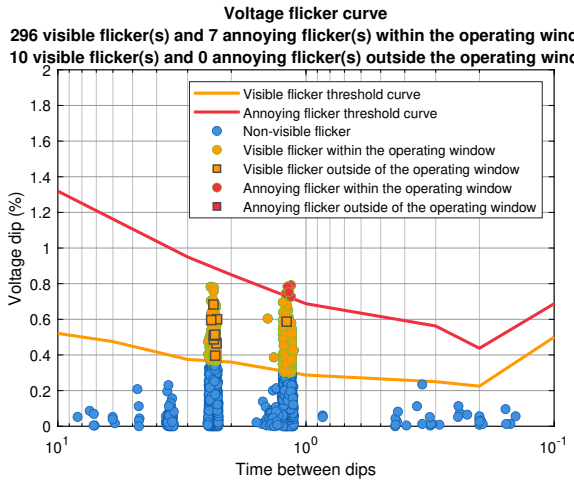

(a) Voltage flickers measured before applying power control.

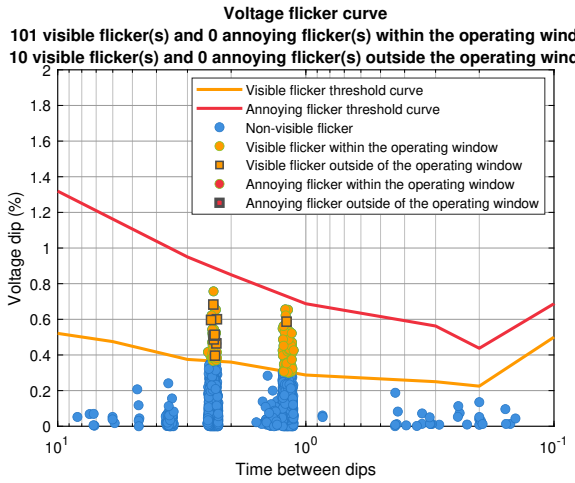

(b) Voltage flickers measured after applying power control.

Figure 3.17: Voltage flickers measured before and after applying power control.

In order to ensure that the energy usage using this novel control algorithm is still kept to a minimum throughout the year, it was decided to pick out several other days in other season in order to test the performance of the control algorithm implementation. Consequently, the window of operation was changed for each of the simulated days as these days are within other seasons. Table 3.13 illustrates the simulation results, it was decided to choose the days within the seasons that had the highest energy usage as this is considered worst case scenarios for the control algorithm implementation. Finally, the matlab script used for simulating power control for different days in other seasons is available in the appendix at section A.2.3

Season	Chosen Date	Maximum discharge power (W)	Maximum charge power (W)	ESS energy usage (Wh)	Power to Energy ratio
Winter	March 9th 2017	2285.05	-2208.32	25.41	89.91
Spring	June 9th 2017	2600.90	-2333.23	29.79	87.31
Fall	October 6th 2017	1691.33	-1910.57	24.10	79.29

Table 3.13: Energy usage from the ESS when using power control in different days from different seasons.

As can be seen from the results in the table, the energy usage is kept at a minimum for all of the simulated days and are close to the energy usage value of the simulated summer day which was the absolute worst case scenario for the control algorithm. Furthermore, the power to energy ratio was slightly lower than the simulated summer day. This can be due to the lower irradiance level during other seasons compared to the higher irradiance levels during the summer time. Nonetheless, the power to energy ratio is still higher than the desired value of 70. Thus with the power control algorithm, the flicker reduction within the operating window was ~ 67% with the power to energy being around 99. With this, the power to energy ratio goal set for the control algorithm has been met while the flicker reduction goal has not been completely met. The final parameters of the control algorithm which will be implemented into the experimental setup is given in table 3.14.

Parameter	Value
Window size for moving average	30
Window of operation	5AM till 10PM
Charge correction factor SoC reduction curve	0.01
Discharge correction factor SoC reduction curve	0.01
Energy threshold lower limit (Wh) SoC reduction curve	-5
Energy threshold upper limit (Wh) SoC reduction curve	5
Idle charge power (W) Idle charge and discharge	-100
Idle discharge power (W) Idle charge and discharge	50
Energy threshold lower limit (Wh) Idle charge and discharge	-5
Energy threshold upper limit (Wh) Idle charge and discharge	5
Power threshold lower limit (W) Idle charge and discharge	-50
Power threshold upper limit (W) Idle charge and discharge	50

Table 3.14: Final parameter list for the control algorithm implemented for power control.

3.8. Simulation results of voltage control

As explained in section 3.5, voltage control reacts to the change in the voltage at PCC in order to send a power setpoint to the ESS inverter. For the following sections, the same procedure for the simulation results applies as explained in section 3.7. For voltage control, the voltage at PCC profile used is the one illustrated in figure 3.14b which was the day where the worst PV power fluctuations occurred. Furthermore, the matlab script used for simulating voltage control is available in the appendix at section A.2.1.

3.8.1. Moving average type simulation results

For this part of the simulation, the two types of moving averages are applied to the voltage profile. After which the ESS power that needs to be delivered is calculated using the equations 3.16 and 3.17 as described in section 3.5. Furthermore using the energy consumption equation described in equation 3.13 section 3.4, the energy usage from the ESS can be calculated along with the power to energy ratio. Table 3.15 and 3.16 illustrates power/energy usage performance for both types of moving averages with different window sizes.

Window size (# elements)	Maximum discharge power (W)	Maximum charge power (W)	ESS energy usage (Wh)	Power to energy ratio
6	2863.46	-2223.10	213.22	13.43
12	3194.19	-2466.09	274.15	11.65
18	3308.65	-2498.75	321.12	10.30
24	3337.22	-2552.39	359.66	9.28
30	3312.07	-2691.76	393.35	8.42

Table 3.15: Simulation results using the simple moving average.

Window size (# elements)	Maximum discharge power (W)	Maximum charge power (W)	ESS energy usage (Wh)	Power to energy ratio
6	2463.56	-1773.62	164.94	14.94
12	2848.98	-2179.81	212.41	13.41
18	3023.85	-2364.04	248.16	12.18
24	3167.33	-2437.74	278.12	11.39
30	3237.77	-2483.44	304.13	10.65

Table 3.16: Simulation results using the moving average with optimised weights.

Based on these results, it can be seen that the energy usage using the moving average with optimised weights is less than the energy usage using the simple moving average. The reduction was calculated to be an average of ~ 22%, which is comparable to the simulation results from power control as highlighted in section 3.7.1. Furthermore, the power to energy ratio for the moving average using the optimised weights is also higher than the power to energy ratio of the simple moving average.
Another takeaway from these simulation results, is that the maximum charge/discharge power and energy usage for both types of moving averages is higher for voltage control than for power control. Thus is due to relatively low measured voltage sensitivity of the circuit, which would thus result higher power values and consequently higher energy usage. Furthermore as with power control, the larger the window size the higher energy usage becomes.
For the flicker reduction performance, the same methodology of mapping the voltage fluctuations onto the flicker curve was used to assess this performance metric. The difference in this case between power control and voltage control, is that the calculated voltage at PCC using voltage control is the 'new' voltage at PCC as described as the variable $V_{\text{PCC,after}}$ in equation 3.7.1. Table 3.17 and 3.18 illustrates the flicker reduction performance for both types of moving averages using different sized windows.

Window size (# elements)	Amount of visible flickers	Amount of annoying flickers
6	0	0
12	0	0
18	0	0
24	0	0
30	0	0

Table 3.17: Voltage flickers after applying the simple moving average with different window sizes.

Window size (# elements)	Amount of visible flickers	Amount of annoying flickers
6	6	0
12	0	0
18	0	0
24	0	0
30	0	0

Table 3.18: Voltage flickers after applying the moving average with optimised weights with different window sizes.

Based on the results given above, the flicker reduction for both types of moving averages is for almost all window sizes 100 %. This is significantly more than what was achieved with power control as with this type of control the voltage fluctuations at PCC are actively fixed while with power control the voltage fluctuations at PCC are indirectly fixed by compensating for the power fluctuations from the PV system. Based on these results and the results from table 3.16 and 3.18, it was decided to choose a moving average window of 12 elements for voltage control. This is mainly due to it striking a balance between flicker reduction and minimal energy usage.

3.8.2. Window of operation check simulation results

When applying the window of operation check, the same procedure is applied to voltage control as was done for power control. Table 3.19 illustrates the flicker reduction results after applying the window of operation check.

Window of operation	Amount of visible flickers within operating window	Amount of annoying flickers within operating window	Amount of visible flickers outside operating window	Amount of annoying flickers outside operating window
Before	0	0	0	0
After	0	0	10	0

Table 3.19: Effect on voltage flicker reduction after implementing window of operation check.

For the flicker reduction performance, it can be seen that all of the flickers within the window of operation are fixed yet when the window of operation is applied some flickers are not fixed that were otherwise reduced before applying the window of operation check. Nonetheless as highlighted in section 3.7.2 for power control, this control layer is still implemented for the control algorithm as the goal is to only reduce the voltage flickers that are caused by power fluctuations from PV systems. Furthermore the energy usage after applying the window of operation check was ~ 180 Wh, which is a significant reduction when compared to an energy usage of 212 Wh without applying the window of operation check. This occurs due to the

control algorithm still operating throughout the night as the voltage at PCC still fluctuates throughout the night, while there is no PV output power during the night.

3.8.3. SoC power reduction curve simulation results

Again for this part of the simulation, the same procedure used for the simulation of power control which was explained in section 3.7.3 is applied for voltage control aswell. This means that the same energy threshold is used for this simulation aswell. Furthermore, different correction factors are used and the effect it has on the flicker reduction and energy usage was analysed. Table 3.20 and 3.21 illustrates the simulation results for different correction factors used.

Charge and discharge correction factor	Maximum discharge power (W)	Maximum charge power (W)	ESS energy usage (Wh)	Power to energy ratio
0	2848.98	-2179.81	179.84	15.84
0.001	2607.82	-2179.81	98.46	26.49
0.005	2468.98	-2179.81	38.32	64.43
0.01	2442.88	-2179.81	25.76	94.83
0.02	2444.62	-2179.81	19.08	128.12
0.05	2584.37	-2179.81	14.56	177.49

Table 3.20: Energy usage of the ESS after applying different correction factors for the SoC power reduction curve.

Charge and discharge correction factor	Amount of visible flickers within operating window	Amount of annoying flickers within operating window
0	0	0
0.001	0	0
0.005	0	0
0.01	0	0
0.02	0	0
0.05	1	0

Table 3.21: Voltage flickers after applying different correction factors for the SoC power reduction curve.

Based on these results, it can be seen that the energy usage reduces significantly as the correction factor increases. Consequently, the power to energy ratio increased with higher correction factor values. This was also observed from the simulation results for power control.
Furthermore up until a correction factor of 0.02, the flicker reduction is not affected by the increasing correction factor value and thus a total elimination of the voltage flickers within the operating window is achieved while implementing this control layer.
For choosing the final correction factor value, the correction factor values of 0.01 and 0.02 are considered to be values to choose from with 0.02 being the better option due to a slightly lower energy usage. Yet due to 0.01 being chosen as the correction factor for power control, it would be wise to do same for voltage control as then a proper comparison can be done between the two control algorithms using the same parameters for the control layers. For this reason, the correction factor used for voltage control was chosen to be 0.01 with the performance of this value being highlighted in both tables.

3.8.4. Idle charge and discharge simulation results

Much like the preceding sections regarding the other control layers, the same procedure done for power control is applied for the idle charge and discharge control layer for voltage control. Meaning that the energy usage (± 5 Wh) and power (± 50 W) threshold for operation is the same as for both power and voltage control. Table 3.22 and 3.23 illustrates the simulation results for energy usage and flicker reduction for different idle charge and discharge values respectively.

Idle charge power (W)	Idle discharge power (W)	Maximum discharge power (W)	Maximum charge power (W)	ESS energy usage (Wh)	Power to energy ratio
-25	25	2646.93	-2179.81	20.56	128.77
-50	50	2813.25	-2179.81	18.31	153.62
-100	100	2848.98	-2179.81	14.98	190.17
-100	50	2848.98	-2179.81	14.98	190.17

Table 3.22: Energy usage from the ESS after applying different idle charge and discharge power values.

Based on the simulation results shown, it can be observed that the energy usage reduces as the idle charge power increases

with the power to energy ratio increasing aswell. Furthermore using 50W or 100W idle discharge power does not affect the energy usage of the control algorithm. Furthermore, the maximum charge and discharge values stay the same as the idle charge and discharge power values increases. The reason for this is the same as discussed in section 3.7.4 and the energy usage throughout the day is illustrated in figure 3.18 for an idle charge and discharge value of -100 and 50 W. As can be seen the energy usage remains around the -5 Wh threshold and thus the SoC power reduction curve control layer does not have a significant impact on the power values.
Finally as can be seen below, the flicker reduction is not affected by the different idle charge and discharge power values. As was done for power control, it was opted not to further increase the power values as this would cause flickers of its own for PV system where the voltage sensitivity is higher. Based on these results, the chosen value for idle charge and discharge power was -50 W and 100 W with the performance of both values being highlighted in both tables.

Idle charge power (W)	Idle discharge power (W)	Amount of visible flickers within operating window	Amount of annoying flickers within operating window
-25	25	0	0
-50	50	0	0
-100	100	0	0
-100	50	0	0

Table 3.23: Voltage flickers after applying different idle charge and discharge power values.

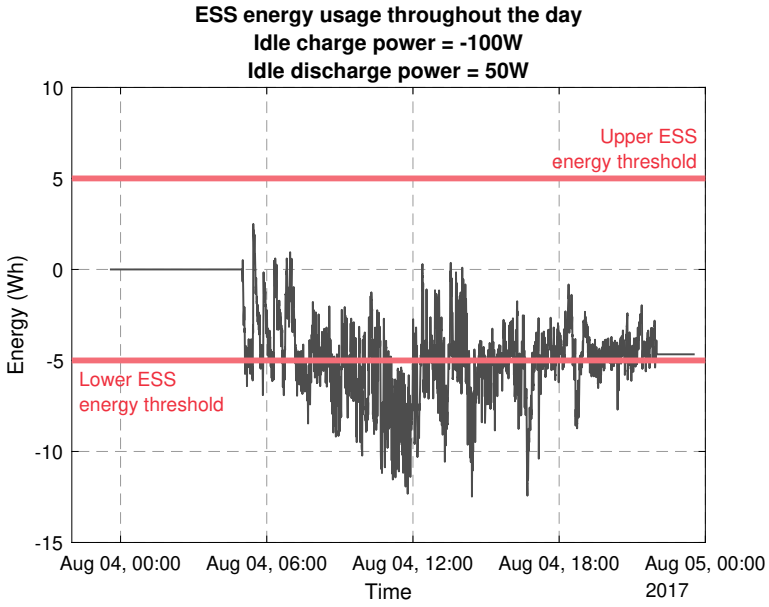

Figure 3.18: Energy usage throughout the day with idle charge and discharge.

3.8.5. Summary of simulation results and performance results during different seasons

Based on all of the results given in the preceding sections, a summary of the results is given in table 3.24 and 3.25.

	ESS energy usage (Wh)	Energy usage reduction relative to the simple moving average	Power to energy ratio
Moving average with optimised weights	212.41	23	13.41
Window of operation check	179.84	34	15.84
SoC power reduction curve	25.76	91	94.83
Idle charge and discharge	14.98	95	190.17

Table 3.24: Summary of the energy usage when each each control layer is applied.

Firstly, it can be observed that the control algorithm with all of the control layers implemented using the moving average with optimised weights the energy usage was reduced with 95% compared to a control algorithm using only the simple moving average. Furthermore, the power to energy ratio with all of the control layers was 190.17, this is well within the goal set for this performance metric of having a value higher than 70 and almost two times higher than what was achieved with almost the same parameters for the control algorithm. This power to energy ratio is significantly higher than the 11.65 power to energy ratio achieved with a control algorithm using only the simple moving average. The effect that each control layer has on the energy usage is compared to the simple moving average and is illustrated in figure A.2.

	Amount of visible flickers within operating window	Amount of annoying flickers within operating window	Amount of visible flickers outside operating window	Amount of annoying flickers outside operating window
Moving average with optimised weights	0	0	10	0
Window of operation check	0	0	10	0
SOC power reduction curve	0	0	10	0
Idle charge and discharge	0	0	10	0

Table 3.25: Summary of the voltage flicker reduction when each each control layer is applied.

Furthermore as seen from table 3.25, all of the visible and annoying flickers within the operating window were eliminated using this control algorithm. Finally, it was measured that the average voltage flicker values above the visible and annoying flicker curve were reduced from 1.039V to 0.127V. The final flicker reduction performance when mapped onto the flicker curve before and after applying the control algorithm can be seen in figure 3.19.

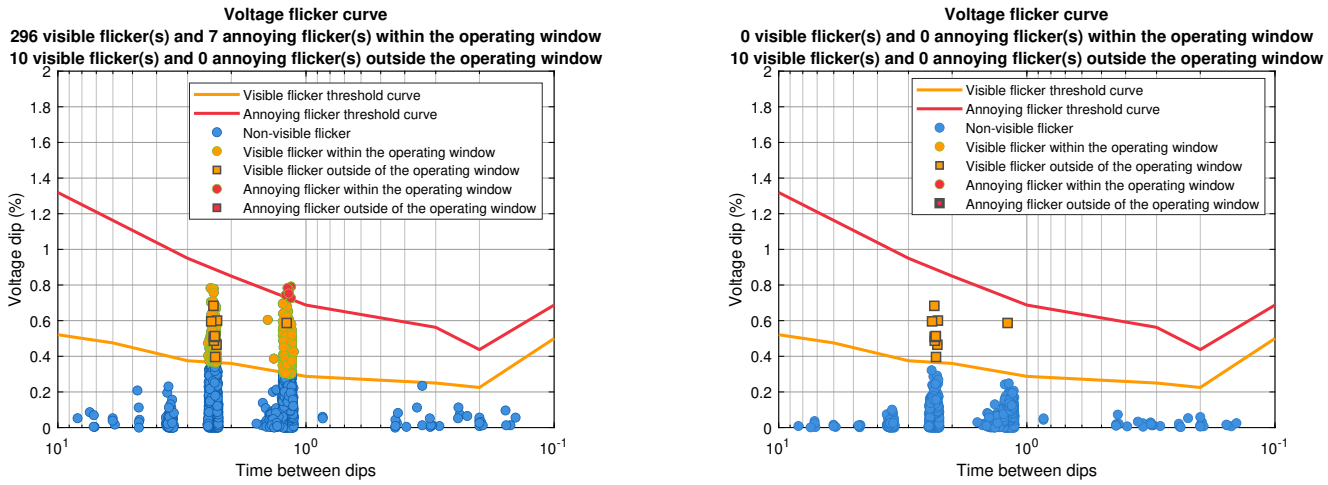

(a) Voltage flickers measured before applying voltage control.

(b) Voltage flickers measured after applying voltage control.

Figure 3.19: Voltage flickers measured before and after applying voltage control.

Based on the results given in the table above, the control algorithm was applied to other days in other season to benchmark the energy usage performance. For this, the same dates that were used for power control were also used for voltage control. This was done as these dates represent the worst case scenario in each of the seasons. Table 3.26 illustrates the simulation results using different dates from different seasons. Finally, the matlab script used for simulating voltage control for other days in different seasons is available in the appendix at section A.2.4.

Season	Chosen Date	Maximum discharge power (W)	Maximum charge power (W)	ESS energy usage (Wh)	Power to Energy ratio
Winter	March 9th 2017	2673.30	-2924.62	21.19	138.03
Spring	June 9th 2017	3000.78	-2094.23	20.82	144.10
Fall	October 6th 2017	2750.44	-2525.40	17.64	155.93

Table 3.26: Energy usage from the ESS when using power control in different days from different seasons.

As can be seen from the results, the energy usage is slightly higher in the other days of the season than the worst case date in the summer. Nonetheless the power to energy ratio for these dates are still higher than 70 and considerably higher than what was achieved with power control. Furthermore, the energy usage for these dates using voltage control is slightly lower than the energy usage using power control. Thus with the voltage control algorithm, the flicker reduction within the operating window is 100% with the power to energy being around 190. With this, the goals set for the control algorithm has been met. The final parameters for the control algorithm which will be implemented into the experimental setups is given in table 3.27.

Parameter	Value
Window size for moving average	12
Window of operation	5AM till 10PM
Charge correction factor SoC reduction curve	0.01
Discharge correction factor SoC reduction curve	0.01
Energy threshold lower limit (Wh) SoC reduction curve	-5
Energy threshold upper limit (Wh) SoC reduction curve	5
Idle charge power (W) Idle charge and discharge	-100
Idle discharge power (W) Idle charge and discharge	50
Energy threshold lower limit (Wh) Idle charge and discharge	-5
Energy threshold upper limit (Wh) Idle charge and discharge	5
Power threshold lower limit (W) Idle charge and discharge	-50
Power threshold upper limit (W) Idle charge and discharge	50

Table 3.27: Final parameter list for the control algorithm implemented for voltage control.

4

Experimental setup design

For the experimental setup design, the university presented several opportunities to make use of already installed PV systems at the Electrical Engineering Mathematics Computer Science (EEMCS) faculty building. The first PV system used is the PV system installed on the second floor of the low rise building of the EEMCS faculty (highlighted by the red rectangle in figure 4.1). This PV system was used for the AC connected ESS experimental setup and the specifications of the PV system and experimental setup is explained in section 4.1. The second PV system used is the PV system installed for the E-bike charging station outside of the EEMCS building (highlighted by the orange circle in figure 4.1). This charging station was primarily used for charging electric bikes using power generated from the PV panels. Since this charging station is not being used often, it was offered to be used for experiments and thus the PV system and the setup aswell was used for the DC connected ESS experimental setup. This is due to the BESS from the charging station being connected at the DC bus. The specifications of the PV system and experimental setup is explained in section 4.2. As can be seen from the figure, the PV systems used for the experimental setups are in the near vicinity of eachother, meaning that it is expected that the clouds passing over one PV system has the same effect on the other PV system. Finally, a GUI was made for both experimental setups in order to increase ease of use for running experiments for which this is explained in section 4.3.

Figure 4.1: Locations of PV systems used for the experimental setups. The map is a satellite image of the EEMCS faculty.

4.1. AC connected ESS experimental setup

As stated before, the university has presented the possibility of using one of the PV system for the research. The current setup consist 7 PV panels connected in series with a PV inverter connected to feed the grid. Figure 4.3a and 4.3b illustrates the PV panels used for the setup and the built experimental setup respectively. The peak power of all of the PV panels is around 1.5 kW with the maximum DC voltage being around 400V. Furthermore each panels is connected to what is called a power optimizer from SolarEdge [C.1.1]. These power optimizers are DC/DC converters with a built in MPPT and ensure that the maximum power of each solar panels are achieved in a decentralized manner. Figure 4.2 illustrates the experimental setup

design for this research.

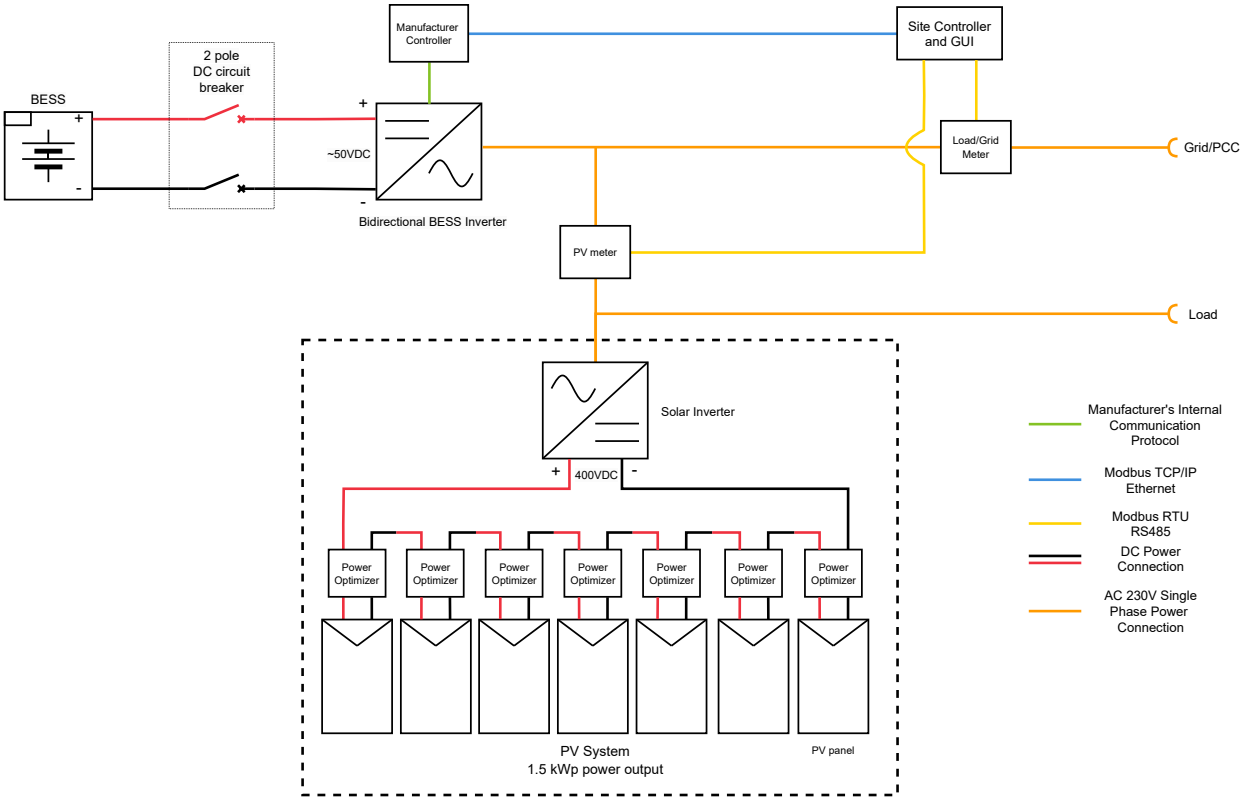

Figure 4.2: AC connected ESS experimental setup design.

The main task of each component in the experimental setup are as follow.

- **BESS**
  The BESS ensures that it delivers the necessary active power to reduce the power and voltage fluctuation at PCC. The system has a energy capacity for which it can deliver and is monitored by the site controller. The site controller ensures that the BESS is not overdischarged or overcharged and sets the active power command for BESS accordingly. Furthermore the site controller also ensures that if the BESS is operating outside of its SOA, then the site controller immediately sets the power setpoint to zero and throws an error to stop operating. The actual BESS used for the setup is indicated in figure 4.3b by the blue arrow.

- **Bidirectional BESS inverter**
  The bidirectional BESS inverter ensures that the DC power from and to the BESS can be converted to an AC power for a proper power delivery to the grid. It is important for this inverter to be able to be controlled by the site controller, as the site controller calculates how much active power the BESS has to deliver. The actual bidirectional BESS inverter used for the setup is indicated in figure 4.3b by the red arrow.

- **PV meter**
  This meter measures the active power from the PV system and communicates the measurements to the site controller.

- **Load/grid meter**
  This meter measures the active power delivered to the loads and grid. Most importantly this meter also measures the voltage at the load and grid connection, for which it is then possible to see if there any voltage fluctuations/flicker occuring. This meter also communicates these measurements to the site controller.

- **Solar Inverter**
  The main task of the solar inverter is to convert the DC power supplied by the PV panels to AC power that can be delivered to the grid and loads. The actual solar inverter used for the setup is indicated in figure 4.3b by the orange arrow.

- **Power Optimizer**
  As explained at the beginning of this section, the power optimizer is a DC/DC converter with a built-in MPPT. These devices ensure that each individual PV panel can deliver its maximum power.

- **Manufacturer controller**
  The manufacturer controller is a controller which acts as an interface between the site controller and the inverter or other devices. This is needed as the chosen manufacturer's inverter (Victron Energy) can only be controlled by the site controller using the manufacturer's controller in between.

- **Site controller**
  The main tasks of the site controller is to read in the measurements from the PV, BESS and load/grid meter. Based on the measurements it calculates how much active power the BESS has to deliver to compensate for the power fluctuations from the PV system and thus the voltage fluctuations measured at the load meter or at PCC. Based on the calculated values, the site controller then communicates with the bidirectional BESS inverter how much active power the BESS needs to charge or discharge. Furthermore the site controller shall be equipped with a GUI in order to simplify the operations needed to operate with the experimental setup. This GUI shall be further explained in section 4.3.

(a) PV panels used for the AC connected ESS experimental setup.

(b) Devices connected to the AC connected ESS experimental setup.

Figure 4.3: Pictures of the actual AC connected ESS experimental setup.

Based on this, table 4.1 illustrates the specific components used in the experimental setup. The components highlight by blue are the components already available and installed at the ESP lab in the EEMCS faculty.

PV panels	7 X CSun 260-6P
Power optimizer	7 X SolarEdge P300-400
Solar inverter	SolarEdge SE3000
PV meter	Carlo Gavazzi EM540
Load/Grid meter	Carlo Gavazzi EM540
Manufacturer Controller	Victron Energy Cerbo S-GX
Bidirectional BESS inverter	Victron Energy Multiplus-II 48/3000/35-32
BESS	1 X ATEPS AB5050
Site Controller	Personal laptop

Table 4.1: Components used for the AC connected ESS experimental setup.

The specifications of the chosen BESS are given below in table 4.2. As highlighted in section 2.2, Nickel-Manganese-Cobalt (NMC) cells were considered as an option for the BESS due to their low cost with its main drawbacks being the low cycle lifetime and power to energy ratio. Nonetheless this type of cell chemistry is still suitable for the experimental setup and eventual implementation in the future. As a safety precaution, a DC circuit breaker [C.1.2] was installed in between the input of the inverter and the BESS in order to disconnect both poles whenever a fault occurs.

ATEPS AB5050	Values
Nominal voltage (V)	50
Maximum discharge current (A)	100
Maximum charge current (A)	50
Nominal capacity (Wh)	2500
Number of cells in series	14
Cell chemistry	NMC
Power density (W/kg)	434.7
Energy density (Wh/kg)	108.7
Power to energy ratio	4

Table 4.2: Specifications of the ATEPS AB5050 battery module [C.1.3].

For this experimental setup, the PV power measurements come from the PV meter. It is important to note that there is a load connection just before the PV meter for which the load power is not being measured and thus the complete PV yield is not being measured. This can be seen from figure 4.2. Fortunately, the load power is consistently around 190W which is used to power on the different equipment in the lab. This offset in the PV power was adjusted accordingly in the GUI software by summing the measured power from the PV meter with 190W.
Furthermore, the voltage and power measurements at PCC come from the Load/Grid meter and between this meter and the connection with the bidirectional BESS inverter the cable length installed was around 7.5 meters. This is was done in order to create a large enough voltage sensitivity with fluctuating power ($^{dV}/_{dP}$) as highlighted in section 1.1.
When these measurements are eventually used by the site controller, the calculated power setpoint is first sent to the manufacturer controller and then communicated to the bidirectional BESS inverter. The amount of power that is being drawn from the BESS is measured by the bidirectional BESS inverter, which then communicates this value back via the manufacturer controller to the site controller.
The main communication protocol used in the experimental setup is the modbus protocol. This protocol is based on a request/receive basis and thus ensures that the measurements from the components are measured in real time.
Finally based on the specifications of the BESS and the parameters chosen for the control algorithm, the final parameters were adjusted to reflect SoC values instead of energy values as this is the main metric measured from the BESS in the experimental setup. This is given in section B.1.1 and B.1.2. Thus this is the final parameters list implemented for this experimental setup.

4.2. DC connected ESS experimental setup

For the DC connected ESS experimental setup, an opportunity was presented by the university to make use of the E-bike Charging Station outside next to the faculty. The setup consist of a PV system that is rated for 2.5kWp and a BESS connected at the DC side with the PV system. Figure 4.4 illustrates the single line diagram of the e-bike charging station, for which this was taken from Chandra Mouli et al [43].

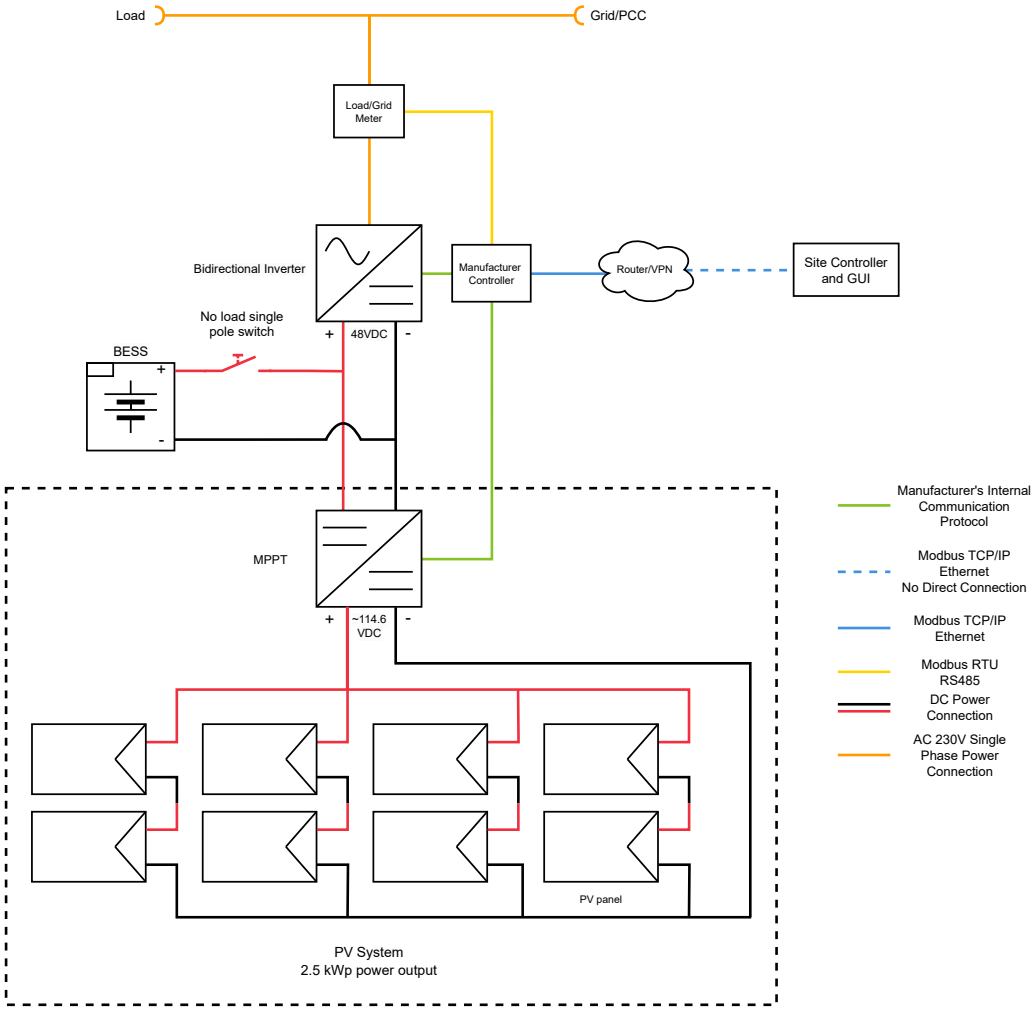

Figure 4.4: DC connected ESS experimental setup design for the research.

Figure 4.5a illustrates the PV panels used for the setup. Figure 4.5c and 4.5b shows the ESS and built experimental setup respectively. The components used for the station are the same used for the AC connected ESS experimental setup (Victron Energy inverter), which gives the opportunity to read in measurements and send power setpoints to the inverter. The type of components used for this setup are the same as the previous setup, yet there are some key differences. These are the following.

- Each PV panel does not come equipped with a power optimizer, instead there is a centralized DC/DC converter with a built-in MPPT. Each PV panel are connected to form a PV system, the output of this PV system is then connected to the DC/DC converter. The actual MPPT used for the experimental setup is highlighted in figure 4.5b by the orange arrow
- Since both the BESS and the PV system are connected to the same DC bus to the inverter, the inverter converts the DC power from both the BESS and PV system to AC power. This is different from the AC connected ESS experimental setup where the inverter only had to convert the DC power from the BESS. The actual bidirectional inverter used for the DC connected ESS experimental setup is highlighted in figure 4.5b by the red arrow.
- The type of BESS used for this setup are lead acid batteries from Victron Energy. These were not considered as a BESS used for this application due to it's low energy and power density. Yet since this type of BESS is already installed and can supply sufficient power for this application, it was decided to make use of this lead-acid BESS. The specifications of one of the lead acid battery module is given in table 4.3.

Victron Energy Gell Accu	Values
Nominal voltage (V)	12
Maximum discharge current (A)	220
Maximum charge current (A)	220
Nominal capacity (Wh)	2640
Cell chemistry	Lead acid
Power density (W/kg)	40.6
Energy density (Wh/kg)	40.6
Power to energy ratio	1

Table 4.3: Specifications of the Victron Energy Gell Accu [C.1.4].

- There is no direct connection between the site controller and the rest of the setup, but rather a VPN connection with the IP address of the manufacturer controller to the site controller.
- Each device within the setup communicates all of its measurements to the manufacturer controller. The manufacturer controller then communicates all of its measurements (via the VPN connection) to the site controller and thus acts as an interface between the setup and the site controller.

(a) PV panels used for the DC connected ESS experimental setup.

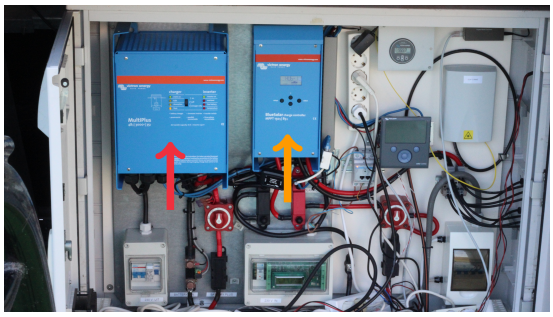

(b) Picture of the actual DC connected ESS experimental setup with all of the devices.

(c) Picture of the lead acid BESS connected to the DC experimental setup.

Figure 4.5: Pictures of the actual DC connected ESS experimental setup.

The components used for this setup is given in table 4.4 below and was taken from Chandra Mouli et al [43].

PV panels	8 X Sunpower X20-327-BLK,
DC/DC converter with MPPT	Victron Energy BlueSolar 150/85
Bidirectional inverter	Victron Energy Multiplus 48/3000 Bidirectional
Load/Grid meter	Carlo Gavazzi ET340
Manufacturer controller	Victron Energy Color Control GX
BESS	4 X Victron Energy Gell Accu 12V 220Ah
Site Controller	Secure TU Delft computer

Table 4.4: Components used for the DC connected ESS experimental setup.

For this setup, the PV power measurements come from the MPPT which is the output power of the device. The voltage and power measurements at PCC come from the Load/Grid meter. These measurements are then all communicated to the manufacturer controller and then to the site controller.
Based on these measurements, the site controller then computes a power setpoint value for the BESS. Due to the PV system and BESS being connected to the same DC bus, the final power setpoint is calculated to be the computed ESS power setpoint plus the measured PV power at the time instance.
One important aspect of the setup to note is that the LV cable length to the grid connection is unknown, yet the workaround is to measure the sensitivity by switching off the battery and only measure the effect the PV system has on the voltage fluctuations. This is further explained in section 5.1.
Similarly to the AC connected ESS experimental setup, the main communication protocol used for the setup is the modbus protocol.
Finally much like what was explained in section 4.1, the final parameters were adjusted to reflect SoC values instead of energy values as this is the main metric measured from the BESS in the experimental setup. This is given in section B.1.3 and B.1.4. Thus this is the final parameters list implemented for this experimental setup.

4.3. GUI design

For the GUI design, the main reason why this was done is again to make running multiple experiments as easy as possible. From illustrating real time values of each component in the experimental setups to exporting data, the GUI is designed such that all of that can be done in a fraction of second. The GUI front-end design for the AC and DC experimental setups is given in figure 4.6 and 4.7 respectively. Though the GUI design for both experimental setups look different from each other, the same control algorithm and overall software design is the same but with a few features that differ due to the difference in the design of the setup. The matlab code for both GUI's can be found in the appendix at section B.3.2 and B.3.1
As can also be seen from the GUI design for the experimental setups, there are several buttons which the user has to click that will perform a specific task. These are explained in the following sections.

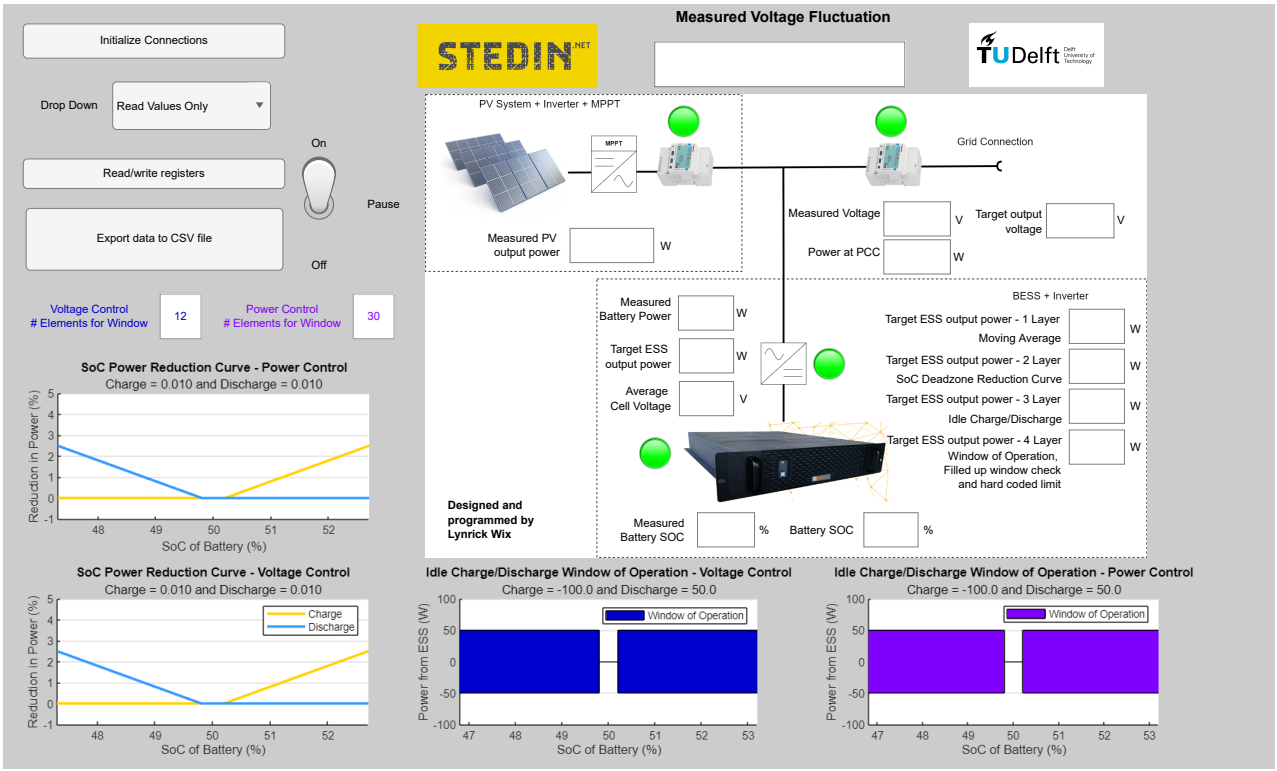

Figure 4.6: GUI for the AC connected ESS experimental setup.

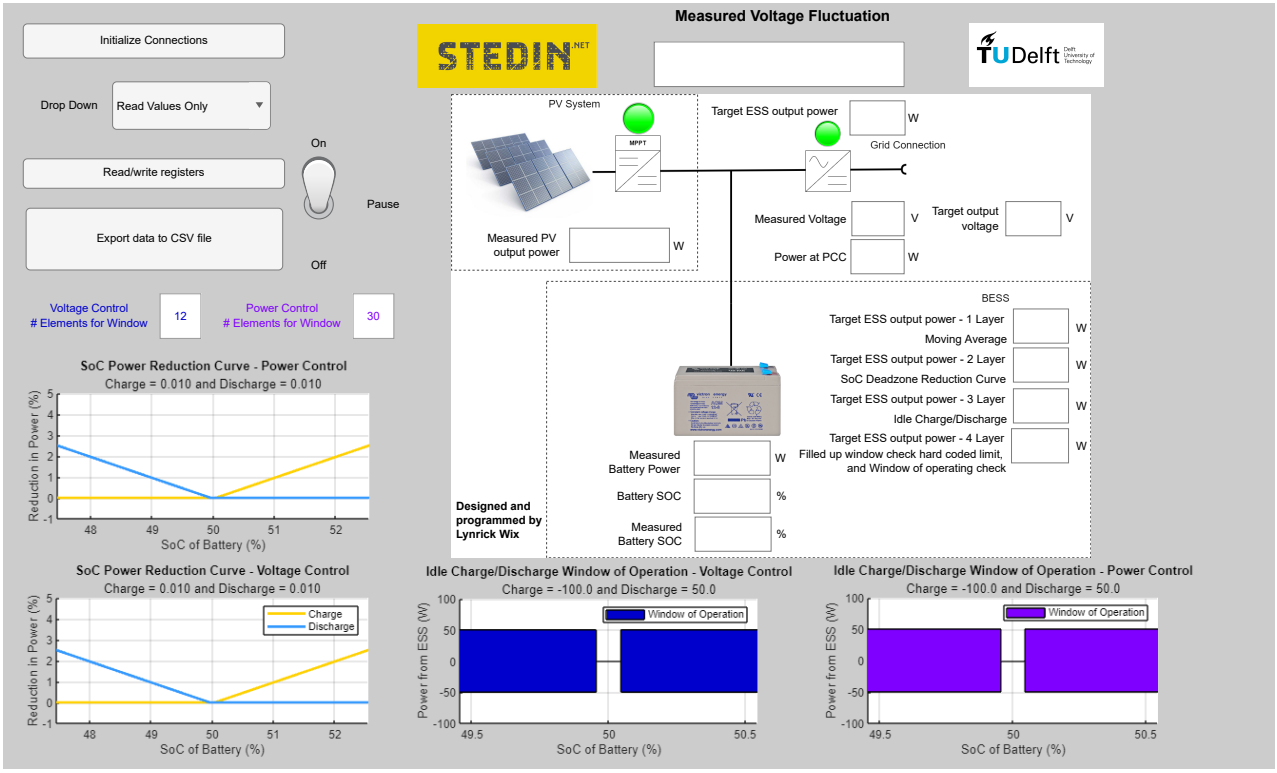

Figure 4.7: GUI for the DC connected ESS experimental setup.

4.3.1. 'Initialize Connections' button

This button firstly reads in a Comma-Seperated Values (CSV) configuration file made for the experimental setup which contains information regarding the communication link for the connected components in the setup, parameters for the control algorithm and the modbus mapping to read in measurements from the components in the setup. The configuration files for both experimental setups can be found in section B.2.2 and B.2.1.
After reading in the configuration file, the software makes a communication link between all of the connected components in the setup. Immediately after this, the software requests the state of each connected component using the modbus mapping from configuration file. If the component is in an error state, then the light indicating the state of the components turns to red. If not, then the light turns green which can be seen from both figures above each component given in the schematic.
Then after this, the parameters for the control algorithms are displayed onto the GUI in an illustrative way. The window sizes are indicated onto the screen. The SoC power reduction curve is indicated in the same manner as figure 3.7 and the idle charge and discharge is illustrated by showing the conditions for which it should operate as explained in equation 3.10.

4.3.2. Drop down menu for choosing control algorithm

After the communication link is established and each connected component is in a safe to operate state, the user can then choose the control algorithm by clicking the drop down menu and selecting one of the following options.

- **Reading Values Only**
  This option is to give the user the option to only let the PV operate without the BESS operating simultaneously. This was very important as this ensured the data collected from this option would help calculate the voltage sensitivity of the setup for which this was calculated for both setups in section 5.1. Furthermore, it also provides a reference point to measure the voltage flicker reduction performance metric of both control algorithms for both experimental setups.

- **Voltage Control**
  This option would let the voltage control algorithm implementation operate and would routinely send power setpoint modbus messages to the inverter based on the measured voltage at PCC.

- **Power control**
  This option is similar to the already mentioned voltage control option, yet this option would let the power control algorithm implementation operate and send modbus messages to the inverter based on the measured output power from the PV system.

4.3.3. 'Read/write registers' button

The functionality of this button is to start the experiment with the chosen control algorithm. It first reads in the measurements from the connected components in the experimental setup and are used for the control algorithm. Then after going through each control layer, a power setpoint command is then written to the inverter. While this is occurring, the measured values and also the calculated values from the control algorithm are all displayed onto the GUI. Furthermore these values are also continuously added to an array that can be used to export the data for post processing.
Finally, the data is being sampled at a 2 second rate. This is mainly due to the inverter delay which is further explained in section 5.5.

4.3.4. 'Pause' and 'Export data to CSV file' button

For these two buttons, the sequence for the user is to be able to pause any experiment at any given moment, export the data and then continue the experiment if desired to do so.
By having the 'Pause' button to pause or continue the experiment, the user is able to change which control algorithm implementation to operate with by first pausing the experiment, change which control algorithm implementation to use and then continue the experiment.
When exporting the data, there are two files that are exported. The first one being the actual data collected throughout the whole experiment. The other file is the configuration file that was loaded in. The reason why this is also exported is for the user to know which parameters for the control algorithm was used for each experiment. That way there would no confusion as to what parameters were used for an experiment when the parameters would constantly changed for each experiment. It can also be used to debug any issues when analyzing the data.

4.3.5. Safety features implemented through the GUI

Since the setups present some risk when conducting an experiment due to risk of short circuits or battery pack thermal runaway, there were safety electronics in place to prevent this from happening as explained in section 4.1. Also there were safety features implemented through the GUI software as well. These are as follow.

- While the values are read in by the software and the written to the inverter, the status of each component is continuously checked by the software. If one component goes into an error state, then the status light changes to red and then the software stops writing values to the inverter and thus stops the experiment.
- Since there is quite a bit of data being illustrated onto the GUI, it was decided to color code the values that are being used by the chosen control algorithm implementation for the moving average control layer. Meaning that when the power control algorithm is operating, the power setpoint and measured PV output power values are colored purple. For voltage control operation, the measured voltage at PCC and power setpoint are colored blue. Furthermore whenever an experiment starts, the measured battery power is continuously plotted in real time in a separate window. An example of this is illustrated in figure 4.8. This is all done in order to facilitate the user to spot any values that are deemed to high for safe operation and can thus interrupt the experimental if needed through the 'Pause' button. The 'Pause' button ensures that no values are written to the inverter anymore and thus stops the experiment.

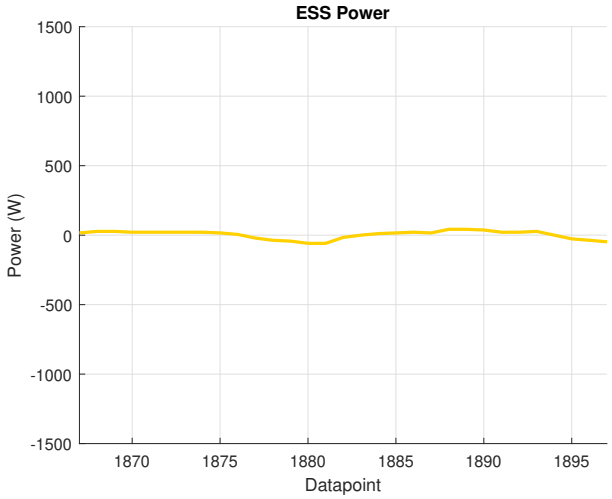

Figure 4.8: Example of the measured ESS power that is continuously plotted in real time.

- Whenever the experiment is running outside of the window of operation, the BESS is not suppose to deliver any power at all. In order to ensure that does not occur as this would potentially lead to overdischarging the BESS, the inverter is set to a sleeping mode (which is called 'Passthru' mode by the manufacturer). In this sleeping mode, the BESS was

measured to barely or not at all discharge any power.

- Due to the AC experimental setup using a lithium ion battery pack, this presents an even greater risk than the DC experimental setup which uses a lead acid battery pack. With this in mind, it is always great practice for lithium ion battery packs to measure the cell voltages of the battery cells connected in series in the battery pack. Since it wasn't possible to directly communicate with the battery pack, the battery pack voltage and current was measured through the input of the BESS inverter. Based on the datasheet of the battery pack (highlighted in table 4.2), there are 14 cells connected in series and thus the average cell voltage is then calculated based on the measured battery pack voltage. Should the average cell voltage exceed 4.1V or is below 3.0V then the status light for the battery pack turns red. This value range is well within the cell voltage range of 2.75 till 4.2 V highlighted in the battery cell datasheet for the battery module[C.1.5]. Furthermore if the SoC of the battery packs exceeds 90% or is below 10%, then the status light also turns red. All of these scenerios then ofcourse leads to the software not writing any power setpoint to the inverter anymore and thus stops the experiment.
- At the beginning of each test, the start SoC of the BESS is set at 50%. This is to minimize the risk of the BESS being overcharged or overdischarged. Furthermore, the measured and calculated SoC is constantly being monitored by the software with the latter being used for the control layers of the control algorithm. The reason is due to low resolution of the measured SoC being 0.5% increments, which does not suffice for proper operation of the control algorithm.
- In order to not overstress the inverter or cause the circuit breaker in the faculty to trip by accident or overstress the BESS, the power setpoint maximum for the AC experimental setup is limited to 1500W for discharge and 1250W for charge when operating in voltage and power control mode. The same is done for the DC experimental setup where only the discharge power is limited to 500W. This is not is needed for power control mode as the power control algorithm ensures that the BESS delivers the power that the PV system is not delivering at the moment.

5

Experimental results

Based on the setup design from the preceding chapter, the experimental setups were built and/or commissioned. After this, the voltage sensitivity of each experimental setup is measured and is discussed in section 5.1 after which this is applied to the setups. Then the experiment results from these setups are extensively discussed with the key performance metric being discussed for each setup and control algorithm implementation used. These are discussed in section 5.2 and 5.3. Finally a summary and limitations of the experimental setups are discussed in section 5.5.

5.1. Measured voltage sensitivity

For measuring the voltage sensitivity of both experimental setups, the same procedure as explained in section 3.3 is applied with the data collected from both experimental setups when only the PV system is delivering power. Figure 5.1 illustrates a summary of the procedure to measure the voltage sensitivity as explained in section 3.3.

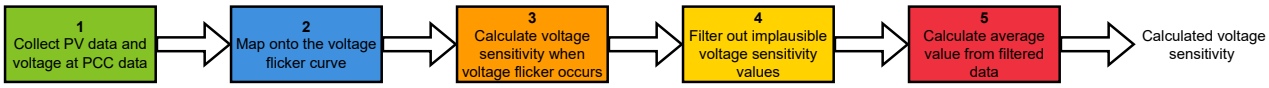

Figure 5.1: Summary of the procedure to measure the voltage sensitivity as explained in section 3.3.

For the AC connected ESS experiemental setup, this was done by letting the ESS inverter go into the sleeping mode. Thus the ESS does not deliver any power and only the PV system delivers power. On the other hand for the DC connected ESS experimental setup, letting the inverter go into the sleeping mode would force the PV system to fully curtail its power delivery to 0W. This is due to how the PV system is installed as given in figure 4.4. Since writing a zero power setpoint also did not work due to the ESS consistently delivering power, the ESS was thus manually switched off using the no-load single pole switch illustrated in figure 4.4 and thus only the PV system will deliver power. Following these procedures for both setups, the data was collected and the voltage sensitivity was measured. Table 5.1 illustrates the voltage sensitivity for both experimental setups.

Experimental setup	Measured voltage sensitivity
AC connected ESS	0.002761
DC connected ESS	0.003509

Table 5.1: Measured voltage sensitivity for both experimental setups.

5.2. Voltage flicker avoidance

In this section, the voltage flicker avoidance performance for both test setups and both control algorithm implementations is analysed. The main goal is that the ESS and control algorithm ensure that whenever a PV power fluctuation or PCC voltage fluctuation occurs, then this immediately compensated for.
Firstly, a reference measurement is done to illustrate how much the PV power should fluctuate to cause a visible voltage flicker for each setup. This is done by a shade experiment onto the PV panels illustrated in figure 5.2. The shade experiment is done by moving a set of wooden planks up and down over the PV panels that will then shade the panels and cause the power from the PV panels to drop. From this the voltage fluctuations is also analysed.
Then the performance of each control algorithm is analysed when the same shade experiment is again performed when

the control algorithm is operating with the ESS. The response of the control algorithm and ESS is therefore analysed. This experiment was done in order to properly compare the performance of both control algorithms to a reference measurement without needing to wait for the weather conditions to be exactly the same for all three measurements.

Figure 5.2: Illustration of how the shade experiments were conducted. The planks were moved up and down along the PV panels by pulling on a rope that is attached to the planks and runs all the way behind the PV system.

5.2.1. AC connected ESS experimental setup

For the AC connected ESS experimental setup, it important to point out that a shade experiment was planned out but due to the location of the panels and safety risks it was decided not to this experiment. Fortunately, enough data was collected to properly compare the performance of the control algorithm to a reference measurement as the same conditions that caused PV power fluctuation in the reference measurement were also observed in other days where the control algorithm implementations were operating. Figure 5.3 illustrates the reference measurement from this setup.

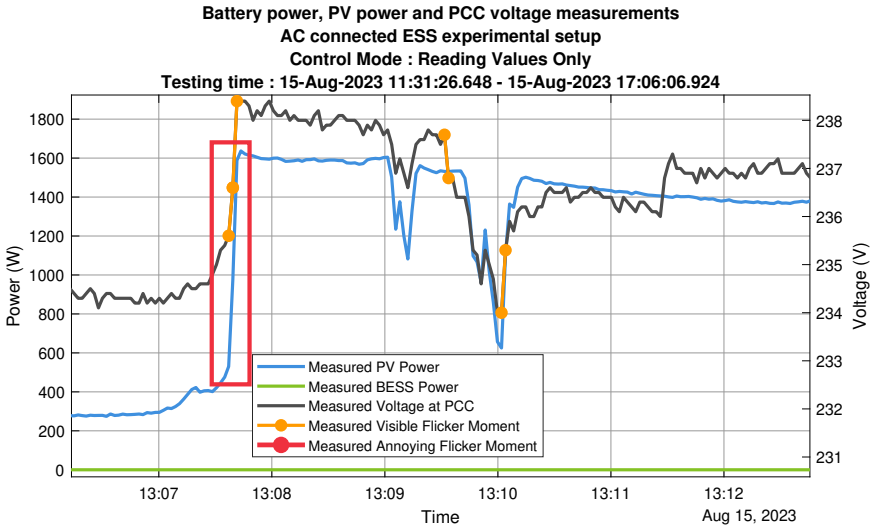

Figure 5.3: Reference measurement from the the PV system from the AC connected ESS experimental setup. A 400 W increase resulted in a visible voltage flicker highlighted by the red rectangle.

As can be seen from the figure above and highlighted by the red rectangle, a power fluctuation of 400W would already cause of visible voltage flicker with a measured voltage dip of around 1.0V. This was measured throughout the reference data aswell and with this established the performance of each control algorithm in the same experimental conditions was observed from collected data from other days. Figure 5.4 and 5.5 illustrates the results when power and voltage control was operating respectively.

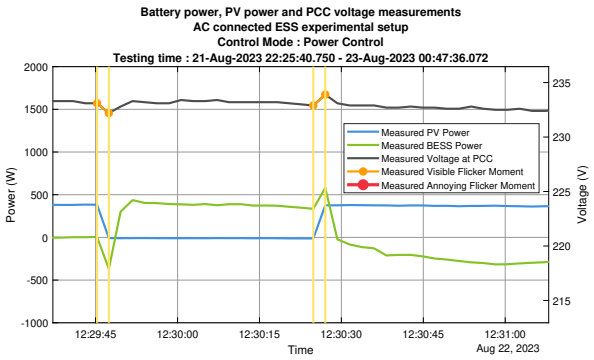

(a) Example of when the PV power fluctuated with the control algorithm response operating in power control and the measured voltage at PCC given.

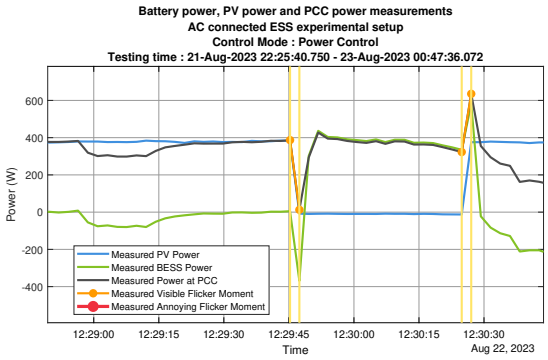

(b) Example of when the PV power fluctuated with the control algorithm response operating in power control and the measured power at PCC given.

Figure 5.4: Power control performance for the AC connected ESS experimental setup.

As can be seen from both sets of figures, whenever the PV power or the voltage at PCC dips then an immediate power setpoint is sent to the inverter to take action. This highlighted by the data in between the two yellow lines. Unfortunately, the inverter reacted a bit to slow and thus the power delivery occurs in the next measurement cycle as can be seen from the measured BESS power. Because of this phenomena, the voltage flicker was not avoided and thus a flicker event occurred. Furthermore, the power at PCC is not completely smoothed out when operating with power control as can be seen from figure 5.4b and at times due to late power delivery from the inverter another visible flicker occurred right after. The latter can be seen from the voltage control results in figure 5.5b. This is due to the power at PCC fluctuating due to the PV power dip and then the BESS power delivery right after. Thus the voltage at PCC fluctuates aswell, causing voltage flicker events to occur. The delay of the inverter is further investigated and discussed in section 5.5.

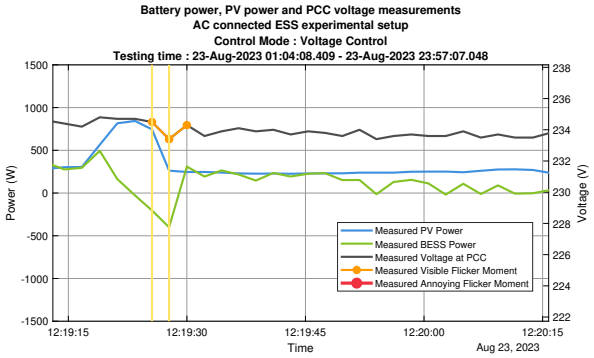

(a) Example of when the PV power fluctuated with the control algorithm response operating in voltage control and the measured voltage at PCC given.

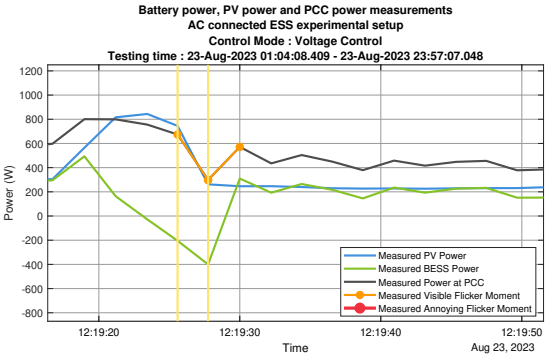

(b) Example of when the PV power fluctuated with the control algorithm response operating in voltage control and the measured power at PCC given.

Figure 5.5: Voltage control performance for the AC connected ESS experimental setup.

5.2.2. DC connected ESS experimental setup

As explained in the previous section, a shade experiment was planned for both experimental setups. Fortunately due to the location of the PV panels for the DC connected ESS experimental setup, it was possible to perform this shade test for this setup and is illustrated in figure 5.2. Furthermore as highlighted at the beginning of this chapter, the BESS had to manually be switched off to perform the reference measurement and the results obtained can be seen in figure 5.6.

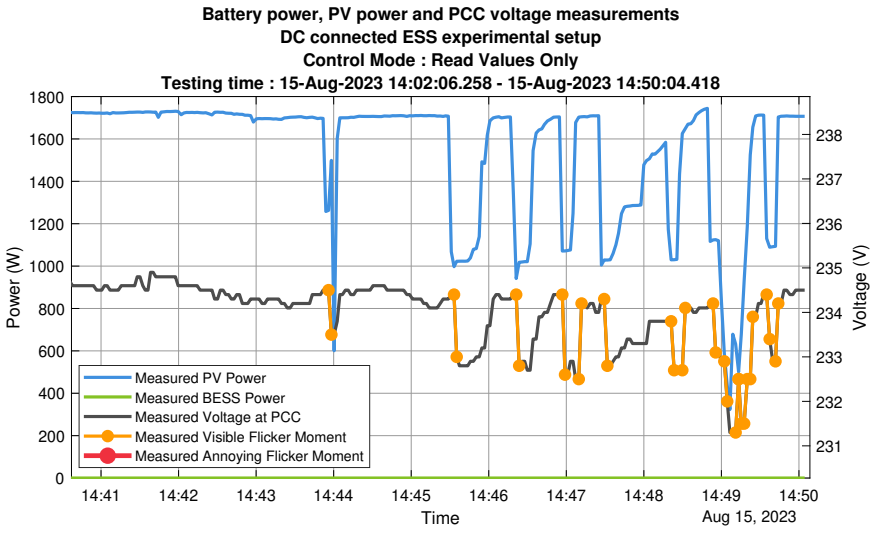

Figure 5.6: Reference measurement from the shade experiment onto the PV system from the DC connected ESS experimental setup.

As can be seen from the reference measurements, the shading procedure was done multiples times and this was done in order to establish an average power and voltage dip values. From this, it was established that whenever there is a PV power dip of around 600W a visible voltage flicker occurs with the voltage dip being around 1.6V. With this in mind, the same shade test was done with the battery turned on and the two different control algorithm implementations operating as well. Figures 5.7 and 5.8 illustrates the experiment results when power and voltage control mode is operating respectively.

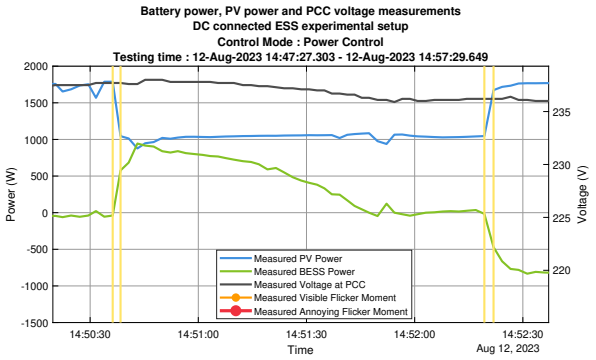

(a) Example of when the PV power fluctuated with the control algorithm response operating in power control and the measured voltage at PCC given.

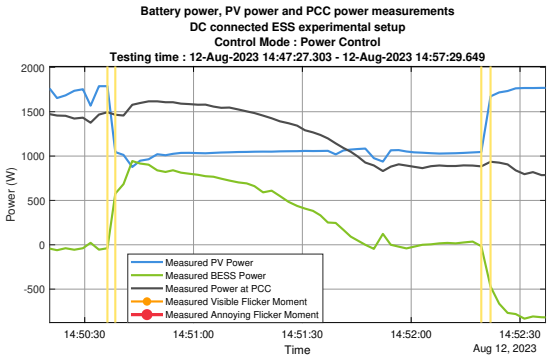

(b) Example of when the PV power fluctuated with the control algorithm response operating in power control and the measured power at PCC given.

Figure 5.7: Power control performance for the DC connected ESS experimental setup.

As can be seen from figure 5.7a, when power control is operating then the BESS delivers power right away whenever the PV power fluctuates. This is highlighted again with the data in between the two yellow lines given in the figure. Thus the power at PCC is also successfully smoothed out using power control as highlighted by figure 5.7b. On the other hand when operating with voltage control, the BESS also successfully delivers power on time yet the due to the BESS power fluctuating a voltage flicker event occurred as can be seen in figure 5.8a. This is due to when the BESS is fluctuating, the power at PCC also fluctuates as given in figure 5.8b and thus the voltage at PCC also fluctuates. This was common recurrence when analysing experimental data from other days. Furthermore due to the inverter used for this experimental setup being the same type and made by the same manufacturer there was still an issue with the inverter response time as highlighted in the previous section. The reason why the power control and voltage control experiment was successful for this experimental setup is further investigated and explained in section 5.5.

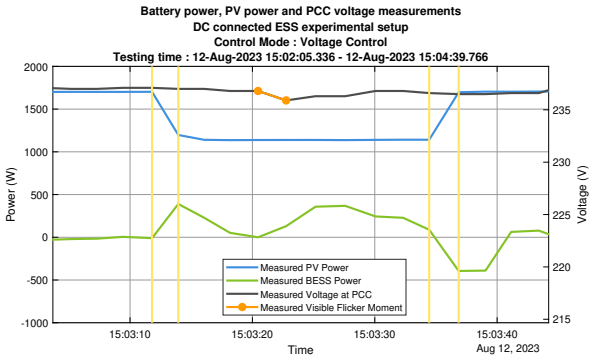

(a) Example of when the PV power fluctuated with the control algorithm response operating in voltage control and the measured voltage at PCC given.

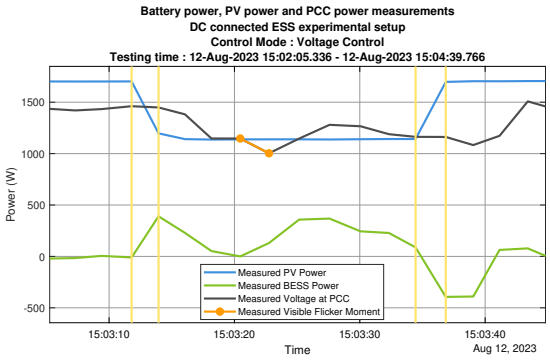

(b) Example of when the PV power fluctuated with the control algorithm response operating in voltage control and the measured power at PCC given.

Figure 5.8: Voltage control performance for the DC connected ESS experimental setup.

5.2.3. Full day experiment

Based on the performance of the control algorithms for both experimental setups, it was then decided to perform a full day experiment. Essentially the experiment starts at night the day before, runs throughout the day with PV system delivering power and the control algorithm operating. Then the experiment is stopped around the same time as it was started the day before and the data is exported.

Furthermore one control algorithm is tested on both experimental setups on the same day, since both PV systems are in near proximity of each other the same PV power delivery profile is expected for both setups. Thus it is important to point out that the results from one control algorithm tested on both setups can be compared with each other, but not the results from both control algorithm implementations tested on one setup. This is due to both control algorithm implementations not being tested on the same day on one experimental setup. With this in mind, the experiment was performed with the voltage flicker curves from the experiments given in figure 5.9.

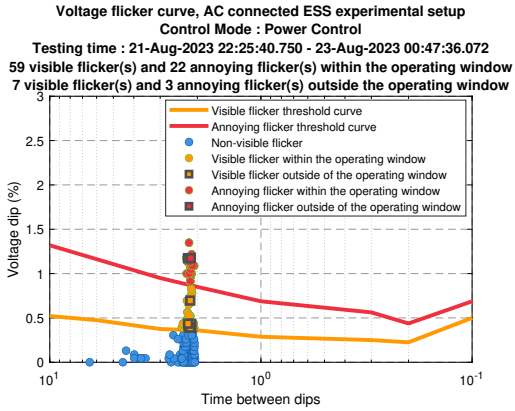

(a) Voltage flickers measured throughout the day from the AC connected ESS experimental setup operating in power control mode.

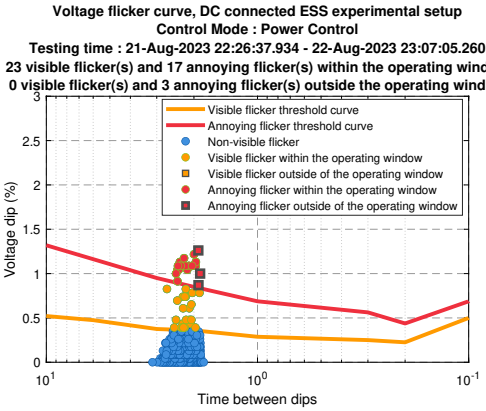

(b) Voltage flickers measured throughout the day from the DC connected ESS experimental setup operating in power control mode.

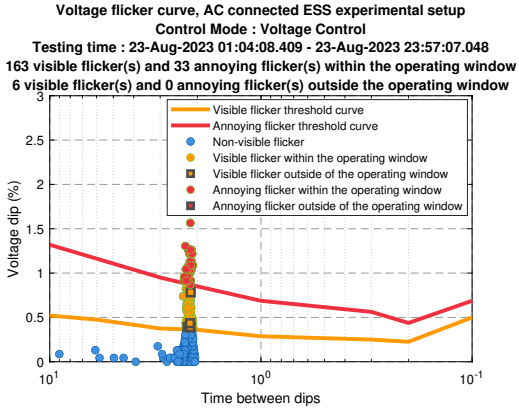

(c) Voltage flickers measured throughout the day from the AC connected ESS experimental setup operating in voltage control mode.

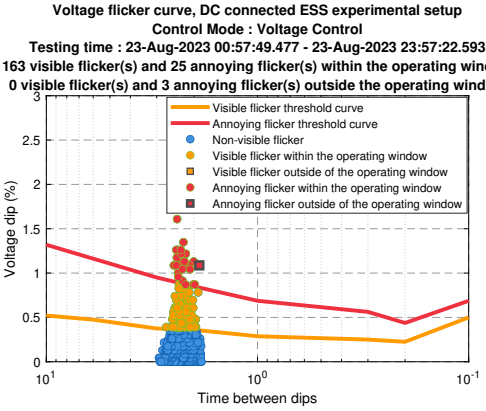

(d) Voltage flickers measured throughout the day from the DC connected ESS experimental setup operating in voltage control mode.

Figure 5.9: Voltage flickers measured from both experimental setup operating in power and voltage control mode.

As can be seen from figure 5.9a and 5.9b and in terms of the amount of visible and annoying flickers within the operating window, power control operated the best with the DC connected ESS experimental setup when compared the AC connected ESS experimental setup. For voltage control as given in figure 5.9c and 5.9d, both setups performed equally with almost the same amount of visible and annoying flickers. This is can be due to the reasons discussed in section 5.2.1 and 5.2.2.
Furthermore throughout the experiment, it was observed that there were voltage flickers occurring that was not caused by the PV or the BESS (and thus the PCC) power fluctuating. Figure 5.10a and 5.10b illustrates an example of this for both setups where two consecutive annoying flicker moments occured around the same time at both experimental setups. These occurances can be caused by load connections, MV voltage fluctuating or other external factors. It is important to note this as this occurred several times during the experiment and is documented in the results. Though it did not occur a significant amount of time to have an influence on the experiment results. In the case given in figure, the reason behind the annoying flickers occurring is presumed to be due to the on-load tap changer transformer changing between taps to increase or decrease the voltage at MV level by a few percent. This would then result in a sudden change in the voltage at LV level aswell.

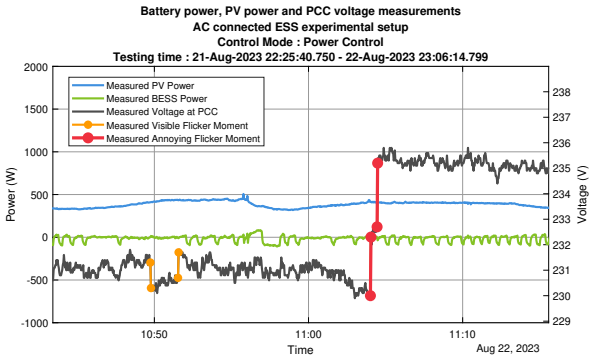

(a) Two sequential annoying flicker events measured from the AC connected ESS experimental setup.

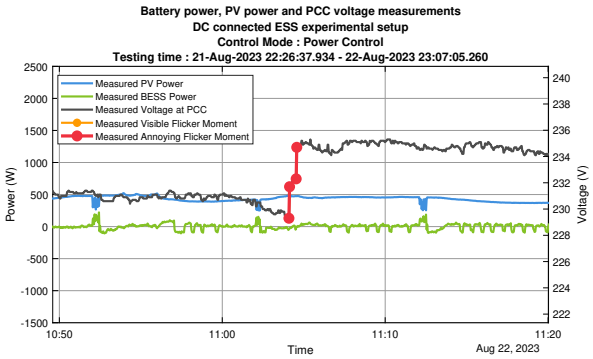

(b) Two sequential annoying flicker events measured from the AC connected ESS experimental setup.

Figure 5.10: Two sequential annoying voltage flickers measured by both experimental setups.

5.2.4. Summary of results

Based on the results given in the preceding sections, the main takeaway is that due to the inverter delay both setups were not able to avoid many voltage flickers from occurring. The sole outlier of this being mostly the DC connected ESS experimental setup operating in power control mode, yet there is a reason as to why for this particular operation the voltage flickers were avoided and is further discussed in section 5.5 regarding the limitations of the experimental setups.
As for now, it can be concluded that in terms of voltage flicker avoidance performance, the DC connected ESS experimental setup operating in power control mode had the best performance. Due to it having less voltage flickers occurring than the AC connected ESS experimental setup. Furthermore when the experimental setups operate in voltage control mode, the amount of voltage flickers that occurred was almost the same due to inverter delay. Thus the power delivery from the BESS causes a voltage flicker event.

5.3. Energy usage

As explained in section 5.2.3, a full day test was performed for both setups using both control algorithms on separate dates. Not only was the voltage flicker performance analysed for both setups, but also the energy usage was measured throughout the experiment. As can be recalled from the goals set for this research, it is important to keep the energy usage at a minimum in order to achieve a power to energy ratio of higher than 70. In the following section, the results of the energy usage for each experimental setups is discussed.

5.3.1. AC connected ESS experimental setup

For the AC connected ESS experimental setup, the energy usage throughout the day for power and voltage control are given in figure 5.11a and 5.11b respectively.

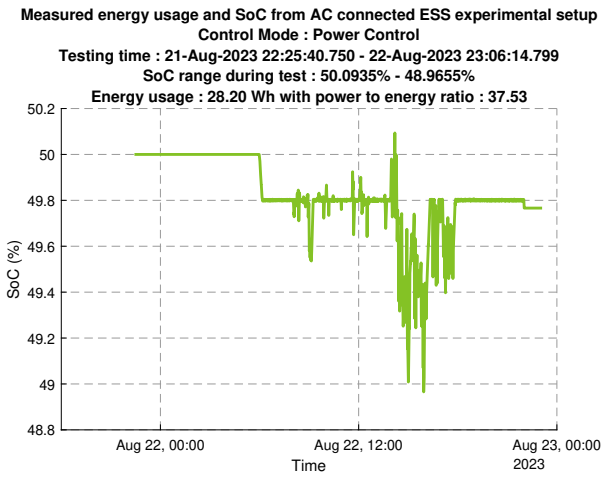

(a) SoC of the BESS from the AC connected ESS experimental setup operating in power control mode.

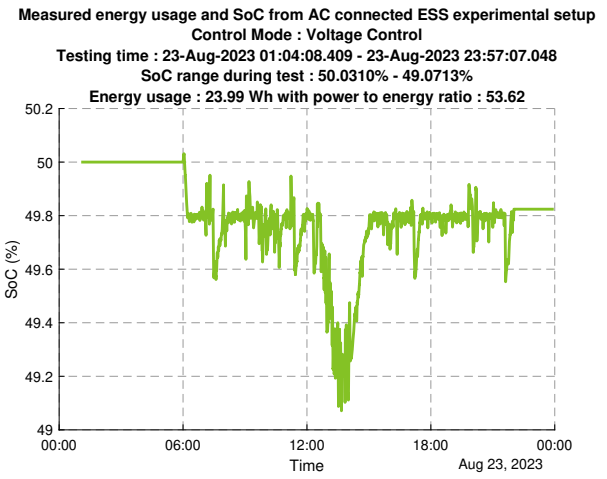

(b) SoC of the BESS from the AC connected ESS experimental setup operating in voltage control mode.

Figure 5.11: SoC of the BESS from the AC connected ESS experimental setup.

As can be seen from the results, for both experiments the energy usage stays well within the 49.8% SoC threshold for this setup since this is the threshold of operation for the SoC power reduction curve and idle charge/discharge control layer. The measured energy usage throughout the day reached a maximum of 28.2 and 23.99Wh when operating in power and voltage control mode respectively. With this in mind, the power to energy ratio was calculated to be around 37.53 for power control and 53.62 for voltage control. This is not higher than 70, yet this is due to the battery still discharging even when there is a zero power set point sent to the inverter. This issue is further investigated in section 5.5.

5.3.2. DC connected ESS experimental setup

Much like for the AC connected ESS experimental setup, the energy usage was measured for power and voltage control operation. Figure 5.12a and 5.12b illustrates the results obtained for power and voltage control respectively.

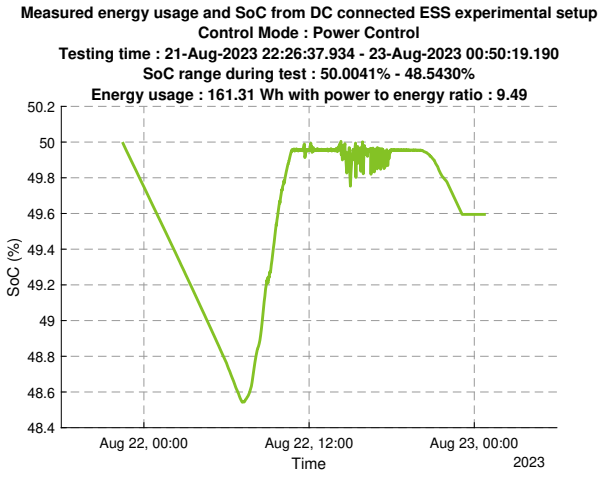

(a) SoC of the BESS from the DC connected ESS experimental setup operating in power control mode.

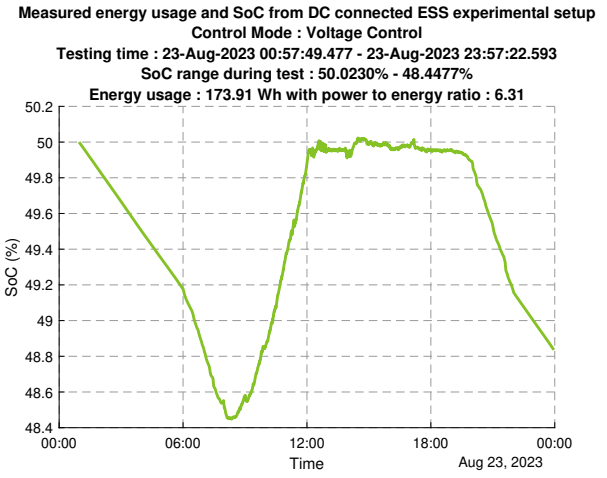

(b) SoC of the BESS from the DC connected ESS experimental setup operating in voltage control mode.

Figure 5.12: SoC of the BESS from the DC connected ESS experimental setup.

As can be seen above, the energy usage from both experiments using this experimental setup is significantly higher than what was measured with the AC connected ESS experimental setup. The measured energy usage was 161.31 Wh and 173.91 Wh for power and voltage control mode respectively. This results in the power to energy ratio being around 9.49 and 6.31 for power and voltage control respectively. These values for the power to energy ratio is way below than 70 and the reason for this is due to the BESS discharging even if the inverter is in the sleeping mode when outside of the window of operation. This can be clearly seen from both figures as the energy usage increases linearly throughout the night. It is expected that due to various devices connected in this experimental setup, the BESS is thus delivering power to all of these devices. Furthermore as explained in section 5.3.1, even if a zero power setpoint is sent to the inverter the BESS still discharges power and for this experimental setup it is no less different. This issue is further investigated in section 5.5.

Though a majority of the energy usage comes from throughout the night, it was still investigated how much energy usage there would be if hypothetically speaking the BESS did not discharge at all when the inverter went into the sleeping (as seen from the AC experimental setup). For this it was decided to measure the energy usage within a timeframe where it was deemed that the hypothetical situation given occurred. This is highlighted in figure 5.13a and 5.13b for power and voltage control mode. The energy usage was remeasured within a timeframe which corresponds to in between the two red lines in the figures. When analysing the energy usage within this timeframe, almost the same energy usage behaviour was observed when compared to the energy usage measured throughout the day for the AC connected ESS experimental setup. This was the case as around this timeframe the energy usage was kept around the 49.955% SoC threshold for this setup. This is the threshold for operation for the SoC power reduction curve and idle charge/discharge control layer and the same was observed from the AC connected ESS experimental setup. Thus this timeframe was deemed to be a good hypothetical checkup of what the energy usage could be for the DC connected ESS experimental setup had the BESS not discharge any power when the inverter was in sleeping mode.
Given the explanation above regarding the choice for the timeframe, the energy usage was remeasured to be around 27.26 Wh and 13.29 Wh for power and voltage control mode. This is also given in figure 5.13a and 5.13b. Based on the measured energy usage, the power to energy ratio was measured to be around 56.16 and 82.64 for power and voltage control respectively. The latter achieving the goal of reaching a power to energy usage of above 70 with the former being below the value of 70.

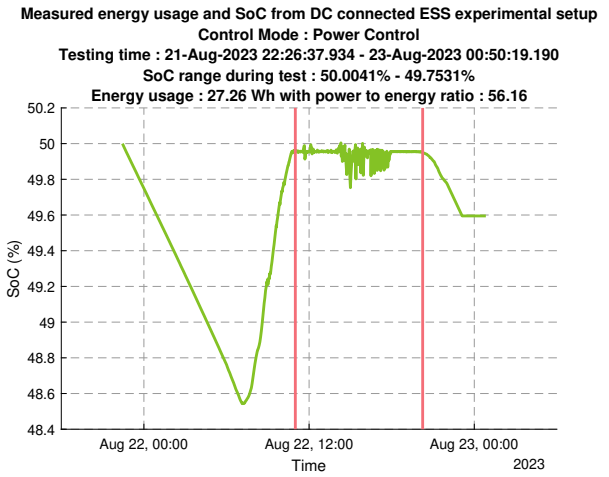

(a) SoC of the BESS from the DC connected ESS experimental setup operating in power control mode with the window of analysis given between the two red lines.

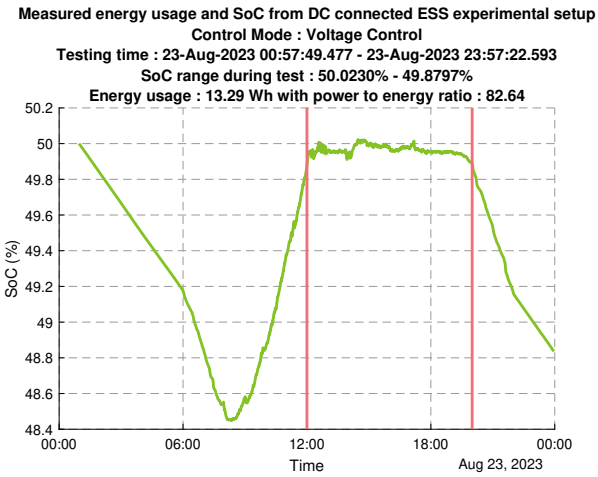

(b) SoC of the BESS from the DC connected ESS experimental setup operating in voltage control mode with the window of analysis given between the two red lines.

Figure 5.13: SoC of the BESS from the AC connected ESS experimental setup with the window of analysis given

5.3.3. Summary

Based on the results regarding the energy usage given in the preceding sections, the main takeaway is that the inverter does not actually enact a zero power setpoint and thus the BESS still discharges some power. Nonetheless, the AC connected ESS experimental setup had the best performance in terms of energy usage. While the DC connected ESS experimental setup had significant higher energy usage in comparison. Had the BESS not discharge throughout the night, the energy usage from the DC connected ESS experimental setup would have been lower. It can also be observed that the energy usage from the AC connected ESS and the DC connected ESS experimental setup are almost the same (when using the new timeframe for the DC connected ESS experimental setup) due to it being tested on the same day. While the energy usage when operating in voltage control mode from the DC experimental setup is lower than from the AC experimental setup, yet this is most likely due to the BESS discharge power being limited to 500 W for the DC connected ESS experimental setup while for the AC connected ESS experimental setup this was limited to 1500 W.

5.4. Comparison between the experimental setups and control algorithm implementations

Based on the experimental results from the experimental setups, this can be summarized in the following tables in this section. For the shade experiment, table 5.2 summarizes the results. The results indicate if the ESS successfully avoided a visible flicker from occurring while operating in either power or voltage control for both experimental setup.

	AC	DC
Power control	No	Yes
Voltage control	No	Yes*

Table 5.2: Summary of the shade test for both experimental setups operating in either power or voltage control.

Based on the results from table 5.2, it can be concluded that the DC experimental setup was more successful in avoiding a voltage flicker from occurring than the AC experimental setup. The reason for this is further explained in section 5.5 regarding the limitations of the experimental setups. Although (as highlighted by the asterisk) for the DC experimental setup operating in voltage control mode, a visible flicker occurred after the ESS successfully avoided the voltage flicker due to the ESS not discharging anymore.
Based on the results from the DC experimental setup, a comparison between the control algorithm implementation can also be done. When operating power control, the ESS was able to successfully avoid a voltage flicker. When operating in voltage control on the other hand, this was not entirely the case as it created its own visible voltage flicker moment due to ESS no longer discharging. For a future outlook, it would also be more feasible to implement power control instead of voltage control due to varying voltage sensitivity value per household. This would result in more procedures to measure the voltage sensitivity before implementing this control mode, while this is not needed for power control.
For the summary of the full day experiment to analyse the voltage flicker avoidance performance, table 5.3 illustrates a summary of the results.

	Visible flicker		Annoying flicker	
	AC	DC	AC	DC
Power control	59	23	22	17
Voltage control	163	163	33	25

Table 5.3: Summary of the full day experiment to analyse the voltage flicker avoidance performance for both experimental setups operating in either power or voltage control.

Based on the results, it can be deduced that the DC experimental setup operating in power control mode performed better than the AC experimental setup operating in power control mode due to lower visible and annoying voltage flicker count. For both experimental setups operating in voltage control mode, the performance is observed to be same between the two experimental setups. This result is mainly due to the fluctuating power setpoint sent to the inverter and the resultant inverter response time delay, which is further explained in section 5.5. For the summary of the full day experiment to analyse ESS energy usage performance, table 5.4 summarizes the results from this experiment.

	ESS energy usage (Wh)		Power to energy ratio	
	AC	DC	AC	DC
Power control	28.20	27.26*	37.53	56.16*
Voltage control	23.99	13.29*	53.62	82.64*

Table 5.4: Summary of the full day experiment to analyse the ESS energy usage performance for both experimental setups operating in either power or voltage control.

Based on the results, the main conclusion is that the DC experimental setup had the lower energy usage and achieved a higher power to energy ratio than the AC experimental setup. Yet as highlighted by the asterisk, this was only after filtering out the 'noise' from the data due to the connected loads. Nonetheless, the ESS energy usage from the AC experimental setup is still considered to be very low and though it did not exceed the desired power to energy ratio of 70 a slightly larger sized SESS can be used.

5.5. Limitations of experimental setups

For this section, the limitations of the experimental setups are explained thoroughly and its effect on the experimental results are also explained.

5.5.1. Inverter response time delay

As explained in the previous sections, the chosen inverter has a delay in between reading the power setpoint value and actually delivering the power based on the setpoint. Based on experimental results, this was measured to be around 2-4 seconds and is highlighted by figure 5.14 where different values for the power setpoint is sent to the inverter.

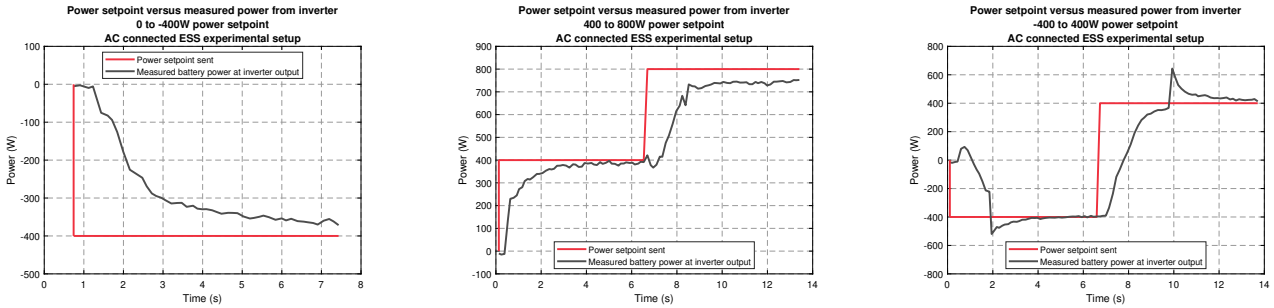

(a) 0 to -400 W power setpoint experiment.

(b) 400 to 800 power setpoint experiment.

(c) -400 to 400 W power setpoint experiment.

Figure 5.14: Power setpoint experiment with the inverter from the AC connected ESS test setup.

As can be seen from the figures, the inverter has an internal ramprate which ensures that it takes a few seconds for power delivery to reach the power setpoint. From the inverter datasheet, the manufacturer claims that the power ramprate is internally set to a maximum of 400W/s yet based on the measurements given in figure 5.14 the ramprate is lower than 400W/s. Due to this internal delay of the inverter, in most cases it was not possible for the ESS to deliver power on time to avoid a voltage flicker from occurring. So whenever an experiment is done, it seems as though that the ESS is delivering power based on the setpoint that was previously sent and not the power setpoint that sent at that exact moment. Thus a lag was measured in the measurements due to the inverter delay. This was mostly the case for the AC connected ESS experimental setup, but for the DC connected ESS experimental setup this was not the case as the voltage flickers that would have been caused by the PV power fluctuations were mitigated using power control as highlighted in section 5.2.2.
An explanation for this is that the setpoints sent to the inverter for the DC experimental setup operating in power control mode does not vary allot when a PV power fluctuation occurs. This is mainly due to the power setpoint sent is the power that the ESS must deliver with the PV power measured at that moment. Due to this the power setpoint remains relatively constant during the PV power fluctuation moments, this can be seen from figure 5.15a. And due to this, the inverter delay does not affect the performance of the control algorithm and this is especially the case for the DC connected ESS experimental setup where the BESS is connected at DC bus with no power electronics in between. Thus the BESS will deliver power immediately whenever the PV power fluctuates as it will compensate for whatever the PV power lacks to reach the required power setpoint. Although if during the day the PV power fluctuates allot, this would also result in a varying power setpoint sent to the inverter when operating in power control mode. This would also result in the BESS causing voltage flickers aswell. Yet this was not observed from the data from the DC experimental setup operating in power control mode as the PV power did not fluctuate constantly on that specific day.
This is the case for the DC experimental setup operating in power control mode, yet this is not the case when operating in voltage control mode. This is due to the power setpoint varying allot even when with the slightest change in voltage at PCC and thus the inverter delay effect was observed. The varying power setpoint values can also be seen from the AC connected ESS experimental setup as the power setpoint sent is the power that the ESS has to deliver. Thus the power setpoint varies allot when the PV power fluctuates as highlighted in figure 5.15b.

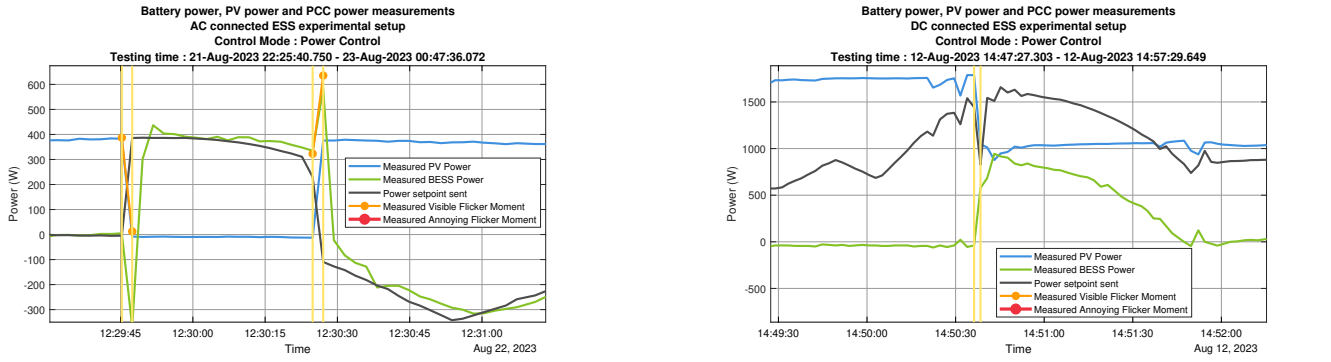

(a) Power setpoints sent to the inverter from the AC connected ESS experimental setup whenever a PV power fluctuation occurred.

(b) Power setpoints sent to the inverter from the DC connected ESS experimental setup whenever a PV power fluctuation occurred.

Figure 5.15: Power setpoints sent to the inverter from both experimental setups whenever a PV power fluctuation occurred.

5.5.2. Inverter power setpoint reaction

Sending a power setpoint of zero to the inverter did not result in the inverter delivery no power. It was measured that the BESS still discharged power when the power delivery should have been zero. This was the case for both setups. Figure 5.16 illustrates an example of this for the AC connected ESS experimental setup.

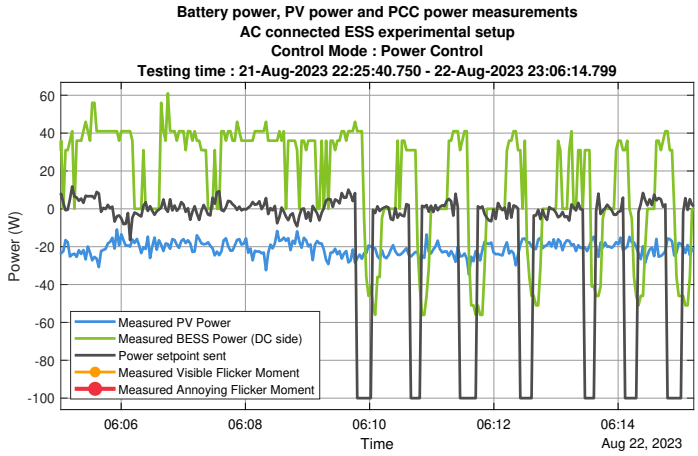

Figure 5.16: Example of the inverter from the AC connected ESS experimental setup not delivering zero power when the setpoint was 0 W.

The assumption was that this was due to a measurement error as the measured BESS power was measured at the input of the inverter using the modbus register for that inverter. Yet when the BESS was disconnected from the setup (DC and AC experimental setups), the measured power was zero even when the power setpoint was zero aswell. This was also the case when the inverter went into sleeping mode for the AC connected ESS experimental setup. This indicates that the BESS is indeed discharging power even when the power setpoint is set at zero. The same was also observed for the DC connected ESS experimental setup when the inverter went into sleeping mode where the BESS also discharged power unnecessarily. This unnecessary discharge of the BESS resulted in significant amounts of energy usage of the BESS.

5.5.3. Measurement devices limitation

Another takeaway from the experimental setups are the measurement devices. Though the modbus protocol has a data transmission speed of upwards of 1000 bits/s, the update rate of the values in the registers from the devices could vary per device. This is the case for the grid/load meter used for the experimental setups. The AC connected ESS experimental setup makes use of the Carlo Gavazzi EM540 meter for which the meter updates its registers every 100 ms [C.1.6]. The DC connected ESS experimental setup uses the Carlo Gavazzi ET340 for the grid/load meter which updates its registers every 2 seconds. This is significantly slower than the EM540 and this may have resulted in the voltage control not operating properly due to its dependency on the PCC voltage for operation. This could also have resulted in the reason why power control operation for the DC experimental setup was such a success as the voltage fluctuation may have been missed whenever the registers were updated.
Furthermore, the load/grid meter for both experimental setups also has a one decimal resolution with measured values for the voltage at PCC. This can consequently result in unnecessary visible or annoying flickers being measured. An example of this could be whenever the PV power fluctuates and causes a voltage dip of 0.8 V at PCC. This voltage dip is just under the visible flicker curve threshold of 0.9 V (samplerate is 2 seconds). Since the meter has a resolution of 1 decimal for measured voltage values, it is assumed that a further dip of 0.05 V caused by the BESS would result in the meter registering a total dip of 0.9 V since it would round the values up. This would then be considered as a visible flicker. The amount of power from the BESS needed to cause a 0.05 V dip is calculated using the voltage sensitivity of the DC connected ESS experimental setup.

$$\Delta P_{\text{BESS}} = \frac{\text{dV}}{\text{dV}/\text{dP}} = \frac{0.05}{0.002761} \approx 18.1W \tag{5.1}$$

Since it was already explained in section 5.5.2 that the inverter does not exactly deliver the power as read in for the power setpoint and that it would only take 18.1 W for the explained scenario to register a visible flicker, having 1 decimal resolution for the measured voltage at PCC would only facilitate in false positives for observed visible or annoying voltage flickers. Having a higher resolution measurement devices for the experimental setups would reduce the chances of false positives from occurring.

5.5.4. Connected loads at the DC connected ESS experimental setup

Based on the paper from Chandra Mouli et al [43] regarding the DC connected ESS experimental setup, there are connected loads at the DC bus and at AC bus as well. These loads are DC/DC converters or other devices which serves to keep the charging station operational. This as a result would discharge power from the BESS in order to supply the loads. This is thus an explanation as to why the energy usage from the DC connected ESS experimental setup is significantly higher the energy usage from the AC connected ESS experimental setup as there is no loads connected in this experimental setup.

6

Conclusion and Recommendation for future research

In this chapter, the conclusion for this research is explained based on the results from the previous chapters with final thoughts of this research given as well. Furthermore a recommendation for future research on this topic is given and explained thoroughly.

6.1. Conclusion

For this section regarding the conclusion, the main goal and sub goal for this thesis is elaborated if the goal was achieved or not.

6.1.1. Voltage fluctuation below visible flicker using ESS and control algorithm

The main goal of this thesis is to make use of an ESS and control algorithm to reduce the voltage fluctuations caused by PV systems in order for the voltage fluctuations not to be categorized as a visible flicker. The designed control algorithm was implemented in two ways.

The first being in what is called power control, where the control algorithm uses the measured PV system power to predict the next PV system power value. The other implementation is what is called voltage control, where the control algorithm makes use of the measured voltage at PCC and thus predicts the next value for the voltage at PCC.

Simulation results from section 3.7 and 3.8 showed that for power control the amount of flickering that occurs due to the PV system was reduced with 65%, while for voltage control this was reduced with 100%.

For the experimental setup to validate the control algorithm functionalities, the type of ESS used was a BESS and there were two connection types for the BESS. The first being an AC connected BESS which was explained in section 4.1 and a DC connected BESS which was explained in section 4.2. Thus for the experimental results, we achieve four different variants of implementation for the experimental setup type and control algorithm implementation.

Results from the shade experiment and collected data showed that due to a delay in response from the inverter, the ESS delivered power too late to avoid a voltage flicker from occurring for most variant. The exception from this phenomena is the DC connected ESS experimental setup operating in power control mode. This is due to the inverter delay coming mainly due to a fluctuating power setpoint sent to the inverter. The power setpoint sent to the DC connected ESS experimental setup operating in power control mode fluctuates the least and thus is affected the least from this limitation.

Based on the simulation and experimental results, it can be concluded that from the simulation results the main goal was achieved using voltage control. Yet a practical implementation of the control algorithm with an ESS showed that due to the limitations of the inverter the main goal for this thesis was not completely achieved. Only with the DC connected ESS experimental setup operating in power control mode, the voltage flicker avoidance performance was at its best.

6.1.2. Minimization of the ESS energy usage with the control algorithm

For this subgoal, the idea is to have a use case of a SESS in the future for this application. Though this type of ESS suffers from very low energy density. Due to this low energy density, the designed control algorithm must ensure that the energy usage from the ESS has to remain very low and minimized as much possible in order for this control algorithm to be used in combination with an SESS in the future. The main metric to show a use case of an SESS is achieving power to energy ratio of higher than 70.

Not only did the control algorithm consist of a moving average algorithm as its main component for the algorithm, but it also consisted of three other control layers with the main goal of these layers being minimizing the energy usage of the ESS. The other control layers are explained in section 3.2. Simulation results from this control algorithm operating in power and

voltage control mode showed the energy usage was minimized by choosing the most optimal parameters for each control layer. For power control as highlighted in section 3.7.5, the energy usage was around 27 Wh with a power to energy ratio of around 99. For voltage control as highlighted in section 3.8.5, the energy usage was measured to be around 15 Wh with a power to energy ratio of around 190. This surpasses the goal of achieving a power to energy ratio of higher than 70.
For the experimental results on the other hand highlighted in section 5.3, the energy usage for both implementation of the control algorithm and both types of experimental setup was slightly higher than expected. This resulted in a lower measured power to energy ratio with power to energy ratio for most variants being below 70. This is due to limitations of the experimental setups, such as the connected loads at the DC connected ESS experimental setup and the inverter for both setups not completely following the power setpoint. Nonetheless, the ESS energy usage values and thus the power to energy ratio from the experiments for all four variants are still very low and are promising results.

6.1.3. Design, build and commission two experimental setups

For this subgoal of this thesis, in order to verify the practical implementation of the control algorithm an experimental setup has to be built. The experimental has to also mimic a household with a PV system connected to it and thus the experimental setups has to come equipped with an actual PV system. Furthermore for connecting the ESS, two types of connection are considered for this. One being a DC connected ESS and the other an AC connected ESS. Thus two experimental setups has to designed, built and commissioned.
The design for the DC connected ESS experimental setup is explained in section 4.2 and it consist of an already existing setup which is the E-bike charging station outside of the EEMCS faculty. This experimental setup was commissioned to be operational with the designed control algorithm. The design for the AC connected ESS experimental setup is explained in section 4.1 and consists of an already existing PV system installed at the ESP lab. The setup was built using a BESS connected with a bidirectional inverter, then this was connected to the same AC bus as the PV system to the grid. Then setup was commissioned to be operational with the designed control algorithm.
Finally, each experimental setup comes equipped with a GUI which interfaces with the site controller which in turn communicates with all of the devices within the experimental setup. This was done to make running experiments, visualizing data during the experiments and exporting the data as easy as possible.
Based on this the goal of designing, building and commissioning two experimental setups was achieved as both setup were fully operational, comes equipped with a GUI and mimics a household with a PV system connected as there is an actual PV system used for both setups.

6.1.4. Compare the performance of both experimental setup with both implementation of the control algorithm

This sub goal was conceived in order to give a judgement as to which control algorithm implementation and which type of ESS connection is best to make use of in a future application. The metric used for this judgement are the voltage flicker avoidance and energy usage minimization performance. Based on section 5.5, the comparison done to establish which connection type for the ESS and control algorithm implementation is the best showed that the DC connected ESS setup operating in power control mode had the best voltage flicker avoidance performance. The lowest energy usage and also the highest power to energy ratio also came from the DC connected ESS type, yet some of the 'noise' from the data due to the connected loads had to filtered out to calculate the true energy usage. Furthermore, it could be also suggested that for future application a power control implementation is more feasible as the ease of implementation is higher than that of the voltage control implementation. This is due to less components and parameters needed for the power control implementation.

6.2. Recommendation for future research

In this section, a few research topics to continue this research are given and explained thoroughly. These recommendations should not be seen as the only recommendations for future research, but only as recommendations that were conceived based on what was done for this research.

6.2.1. Fast responding inverter

Based on the performance of the inverter used for the experimental setups (explained in section 5.5), a design for a fast responding single phase inverter should be considered for this application.
As mentioned before, there was a limitation due to the inverter response and the design for the inverter should tackle this for this application. In section 5.4, it was highlighted that due to the inverter response time the BESS delivered power 2 seconds too late and thus two flicker moments occurred. Furthermore, a simulation was done where a time lag was introduced to the power delivered by the ESS and the results are given in figure 6.1. Based on the results, the amount of visible and annoying flicker almost doubled due to the ESS not delivering power on time. This proves that if the inverter has a delay and does not deliver power from the ESS in a timely manner, then the ESS used for this application will only cause more flickers rather than avoiding flickers from occurring in the first place. Thus this gives more reasons to investigate and design a single phase inverter that has a fast response time with the power delivery.

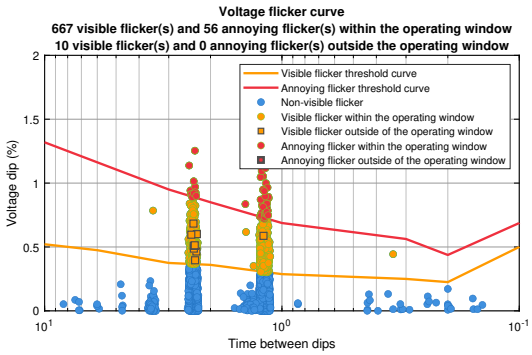

(a) Voltage flicker performance when operating in power control mode with a time lag. The amount of visible flickers is 667 and annoying flickers is 56.

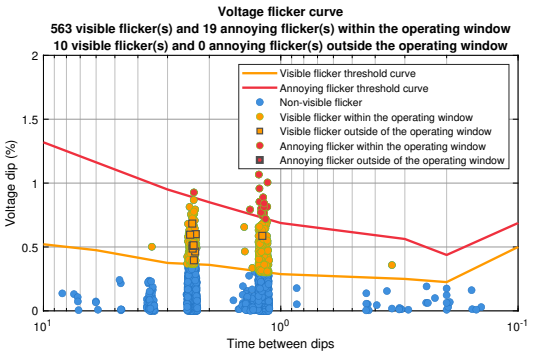

(b) Voltage flicker performance when operating in voltage control mode with a time lag. The amount of visible flickers is 563 and annoying flickers is 19.

Figure 6.1: Simulation results for both control algorithm implementations with a time lag introduced for the power delivered by the ESS.

6.2.2. Implementation of a SESS

In the next phase after implementing a fast responding single phase inverter an SESS should implemented for this application. The main metric to look into when comparing this implementation with a BESS implementation is the efficiency values, resultant energy usage and cycle lifetime. For a SESS implementation, another aspect for the inverter used with the SESS is to have a wide input voltage range. The wide input voltage range is mainly due to the linear Open Circuit Voltage (OCV) versus SoC characteristic curve of a SESS, which for a typical SESS varies from 0V to max voltage through the SoC range. This is illustrated in figure 6.2a.

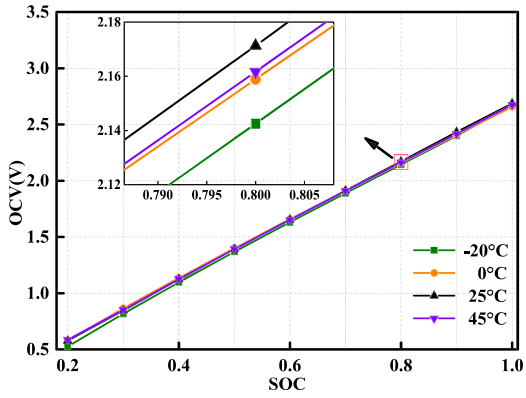

(a) Example of the OCV versus SoC curve of a supercapacitor cell at different temperatures [44].

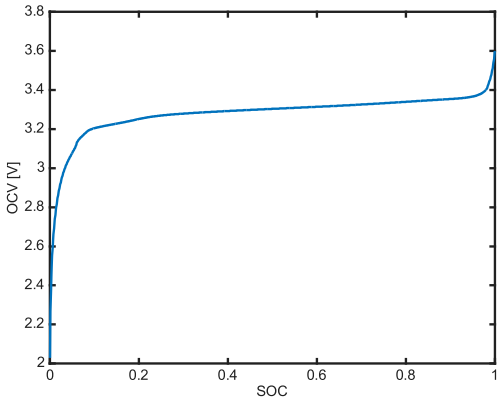

(b) Example of the OCV versus SoC curve of a Lithium-Iron-Phosphate (LFP) cell [45].

Figure 6.2: OCV versus SoC curve of the different types of ESS.

In order to utilize the full range of the SESS capacity, the input voltage range of the inverter should at least cover 80% of the voltage range of the SESS. If not, then there is a risk of needing to add another supercapacitor module in parallel and thus this increases the cost of the ESS for this application. This can be avoided by either having a wide input voltage range inverter or having a built in DC/DC converter stage which regulates the voltage which is then connected to the inverter stage. Either way, the main compromise that should be looked into for both designs should be the lower efficiency values that can be achieved. As the voltage of the supercapacitor lowers due to lower SoC values while also delivering the same power demand, the higher the current delivered by the SESS and thus more heat losses are generated (I^2R relation). Part of the heat losses is being dissipated in the SESS itself. This would then also subsequently result in the SESS operating at higher temperature values, which could lead to faster degradation over its cycle lifetime [46].

This type of effect on the ESS is not entirely observed when using a BESS, since the voltage of a BESS is much more constant and does not fluctuate greatly within its SoC range. Figure 6.2b illustrates the OCV versus SoC curve of a Lithium-Iron-Phosphate (LFP) battery cell. This would then result in a more consistent and lower discharge/charge current throughout its SoC range and thus would then result in lower operating temperatures of the BESS. It also eliminates the necessity of having a wide input voltage range inverter, since for a BESS the voltage range is more constant than a SESS.

Thus in the future, a comprehensive comparison based on experimental results should be done between a SESS and BESS implementation. The result of this comparison will shed light if a SESS is the most optimal ESS to use for this application.

6.2.3. Cost analysis

Another method for establishing if a SESS is the most optimal ESS to use for this application is to do a thorough cost analysis when a SESS or BESS is used to compensate for PV system power fluctuation. The cost analysis includes the cost of the PV system itself, the ESS and the devices used for the ESS such as the bidirectional inverter. An indicative cost analysis was done and can be found in appendix D. The following categorization was done to distinguish the different types of ESS implementation for this application.

1. SESS or BESS implementation.
2. DC or AC connected ESS.
3. Upgraded or integrated solution. An upgraded solution is defined as the ESS being installed later on after the PV system is installed, resulting in two installation moments. An integrated is defined as the ESS and the PV system being installed together with some of the devices being a combination of other devices. The latter would then result in a lower component count of the entire system.

Based on the assumptions made for the indicative cost analysis and cost of the different devices on the marker, the cost of each different ESS implementation was calculated and given in figure 6.3.

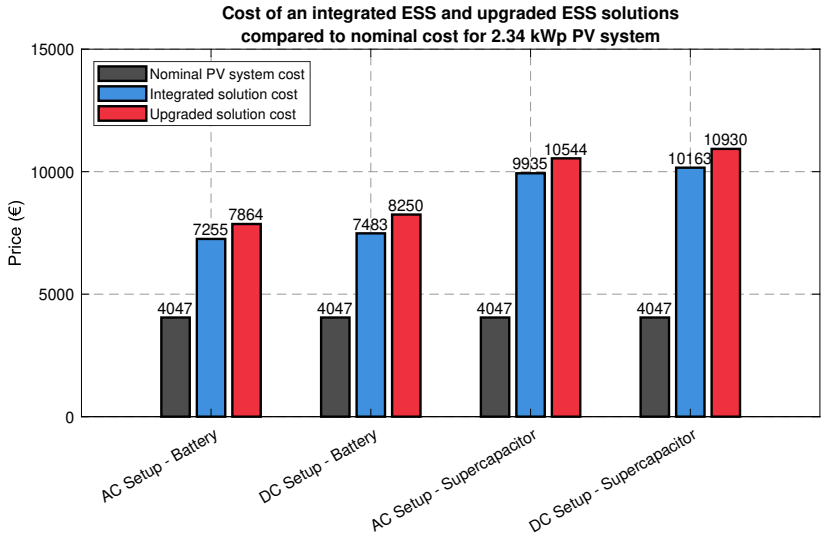

Figure 6.3: Summary of the cost for different ESS implementations.

Based on the figure above, an integrated AC connected BESS solution is the most cost effective solution. Overall a BESS solution is much more cost effective than a SESS solution, costing on average 3000 euros less.
Again this is a very indicative cost analysis, thus it does not take into many other details and these details can be seen as an improvement or recommendation for a more thorough cost analysis in the future. These are the following.

- Return of investment using either a BESS or SESS and how using the ESS for arbitrage can reduce time for return of investment. The latter would then indicate that if it is lucrative for the consumer to implement an ESS for this application. Furthermore, the ESS could also be used to store excess PV energy to be used later at night as a means to also make it lucrative to invest in an ESS. Both of these implementation of the ESS is unfortunately not possible with a SESS due to its low energy density.
- A more thorough research as to how the installation cost for the PV system and ESS is calculated and how it affects the upgraded or integrated solution cost calculation.
- Calculating the cost of a SESS or BESS sized specifically for this application and how this would affect the overal cost. For now, the BESS and SESS used for the cost analysis are ones that are readily available on the market and are not specifically sized for this application. This would then lead to the BESS or SESS being oversized and thus would result in higher cost. If the SESS or BESS was sized specifically for this application, then the capacity of the BESS or SESS would be lower and thus lowering the overal cost.
- Researching how the expected cost of the SESS in the future would reduce. If the expectation of it is that the prices for SESS would reduce in the future then it would make implementing SESS more lucrative in the future. The same could be done for integrated devices that are made out of a combination of other devices. Based on a superficial research done for establishing the cost for integrated devices, it was found that the cost of this is the same as the cost of the

devices (which was used for the combination for the integrated device) separately[47]. Yet a research could be done to predict if an integrated device' price would reduce in the future and if several devices are combined with each other what functionalities and features are actually needed for this application. The latter is expected to lower the cost of the integrated devices, since it has lower amounts of functionalities and features to achieve its main functionality for this application.

6.2.4. Sensitivity analysis of the control algorithm with experimental setups

Based on the experimental setup design explained in chapter 4 and the experimental results explained in chapter 5, it can be observed that the experimental setups has its limitations and that the setups are not built with the same measurement devices. Another key limitation of the experimental setups is ironically the implementation of actual PV systems within the setups. The disadvantage of using an actual PV system for this research is the inherent variability that a PV system brings everyday. As the weather is not the same every single day, the PV power profile is also not the same everyday. This resulted in only the performance between the experimental setups being compared with another, but not the performance between the control algorithm implementations as highlighted in section 5.2.3. Due to the experiments being done on separate dates, resulting in a different PV power profiles. This also resulted in a sensitivity analysis not being possible with the experimental setups. Although this was done during the simulation part for validating the control algorithm in chapter 3, yet the optimal parameters chosen for the control algorithm based on the simulation results does not always result in the parameters being optimal in a practical setting since simulation and experimental results can differ from each other. Hence performing a sensitivity analysis in a practical setting would be beneficial for future research.
How this can be done is to firstly replace the PV system with a programmable single phase power supply connected to an ESS. The reason for this combination of components is that it would mimic the idea of a PV system being a power generating source. The programmable single phase power supply is then fed with PV power data, much like the PV power profile given in figure 1.2a, which the power supply then uses as a power setpoint and discharges power from the ESS. Then a separate ESS can be used with the control algorithm to compensate for the PV power fluctuations and avoid any voltage flickers from occurring. This experimental setup can be done for both a DC and AC connected ESS and a visual representation for an AC connected ESS setup of this kind is given in figure 6.4. This type of experimental setup is based of a paper published by Alam et al[3], where a programmable power supply was also used to mimic a PV system. Though the difference between the presented experimental setup idea and the one presented in the paper is that the authors opted to use a grid connected programmable power supply instead of having a separate standalone energy source for the programmable power supply.
The main idea of implementing such an experimental setup is to then perform a proper sensitivity analysis and compare the performance of both control algorithm in a practical setting since the PV power profile is the same for all experiments.

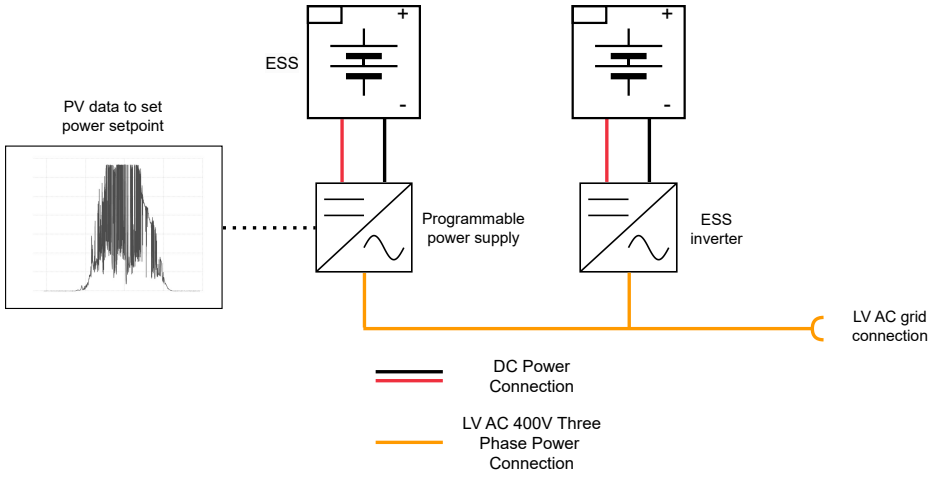

Figure 6.4: AC connected ESS experimental setup example to perform the sensitivity analysis.

6.2.5. Simulation of the control algorithm with an ESS at a distribution level

One way to also tackle the voltage flickers at a residential LV level is to implement the control algorithm with an ESS at the distribution level. An indicative representation of this is given in figure 6.5, with the control algorithm essentially controlling only the ESS inverter. The advantage of this is that the ESS is implemented through the DSO as this is within their scope to implement and thus the cost of the ESS does not lay with the homeowners. Yet a disadvantage of this implementation is that the complexity to coordinate how much power the ESS should deliver increases as the PV systems are more distributed with the power fluctuations of each PV systems needed to be taken into account.
In order to investigate this in the future, a simulation has to be set up which mimics the distribution setup from figure 6.5 and then implement the control algorithm with the ESS. The main result is to check if at a distribution level the ESS can successfully avoid any voltage flickers from occurring when the PV systems from different households fluctuate.

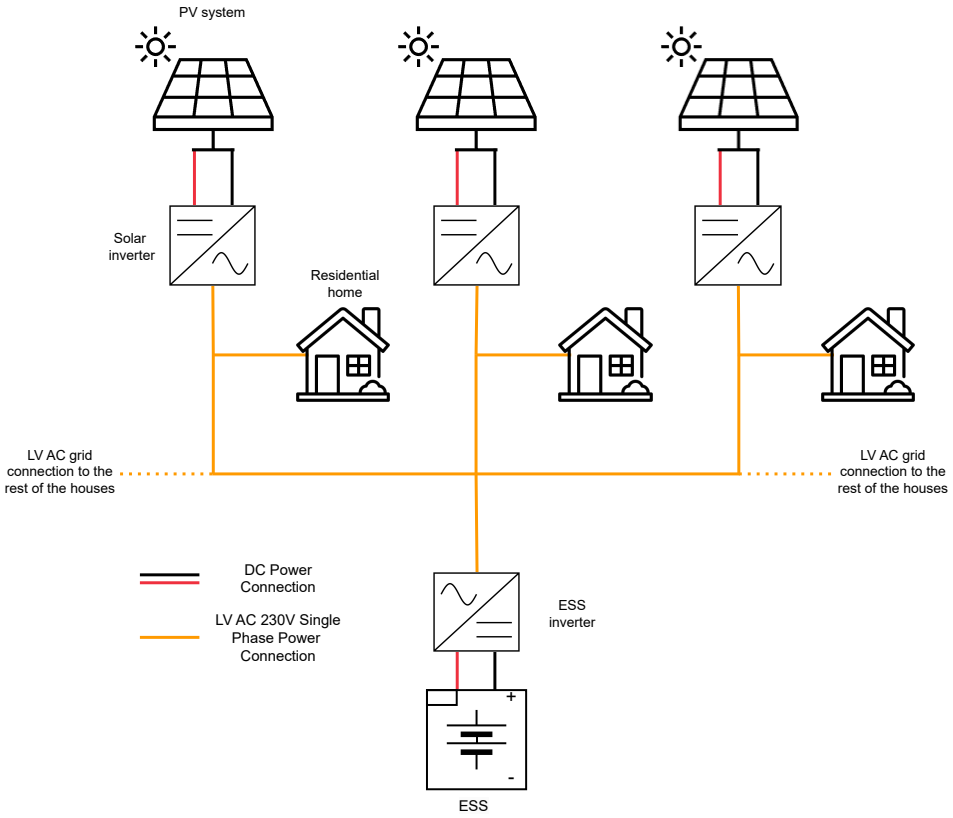

Figure 6.5: ESS and control algorithm implementation at a distribution level.

6.2.6. Simulation of the control algorithm with an ESS at a utility level

This recommendation comes after the literature research done where several authors presented simulation results where an ESS was used at a utility level to compensate for the fluctuating output power of the solar park [21][19][18] and other authors presented that at times solar parks causes voltage flickers at a distribution level [14][15]. Thus a next step would be to simulate the designed control algorithm with an ESS at utility level. An indicative representation of an ESS implementation at a utility level is illustrated in figure 6.6. In the paper published by Wang et al [18], a solar park with a BESS installed to compensate for the fluctuations was simulated and based on the simulation results it showed that many voltage flickers were avoided using a BESS at a utility level. The author presented a different control algorithm to be used for the simulation, so a next step would be to test this with the designed control algorithm from this thesis and check if the voltage flickers could be avoided with this control algorithm.

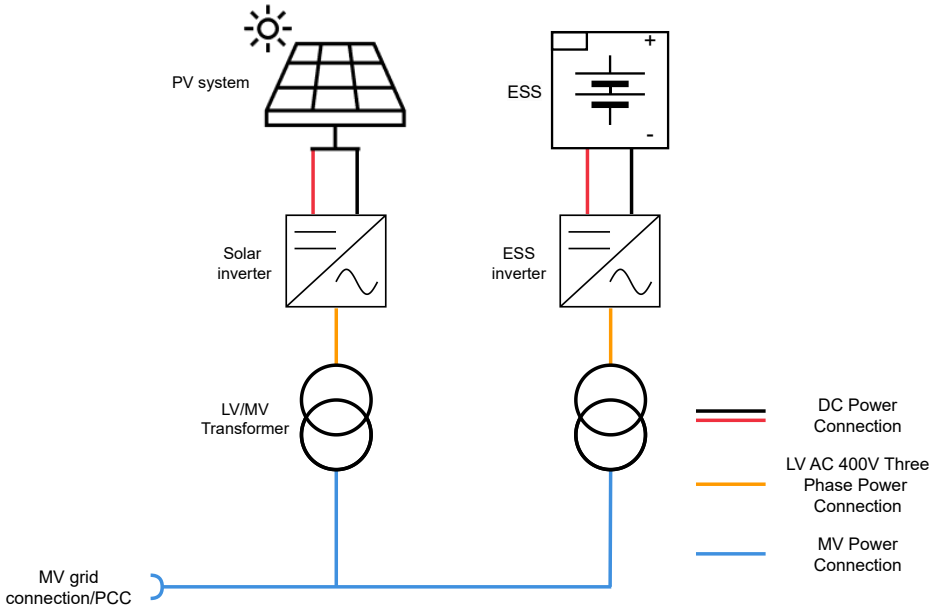

Figure 6.6: Indicative representation of an ESS implementation at a utility level.

6.3. Final thoughts

Throughout this report and research, it was shown that the voltage flickers caused PV systems due to clouds passing over the panels can be minimized by making use of an ESS coupled with a control algorithm at a household LV level. Although simulation results showed that this was possible, experimental results showed that this was only possible with the DC connected ESS experimental setup operating in power control mode under special circumstances.

Furthermore, the control algorithm was able to minimize the energy usage of the ESS based on simulation results. Though from experimental results a higher ESS energy usage was measured and thus a lower power to energy ratio was achieved for the different control implementation and different experimental setups. Though it is important to note that this measured ESS energy usage is still considered to be very low. Based on this result and the result of the voltage flicker avoidance performance, it can be concluded that for future implementation a DC connected ESS operating in power control mode is the most feasible to implement due to it having the best performance.

For future implementation, it was also suggested that the power control was the best most feasible to implement than voltage control. In order to make the same judgement for the type of ESS connection and ESS type for future application, an indicative cost analysis was done in appendix D. In short, the cost of an AC connected BESS is slightly lower than that of a DC connected BESS yet both are 3000 euros more expensive that installing just of PV system. Which for now is not that lucrative for homeowners to buy for only one application of the BESS. In the future, a cost reduction could be done in the integration of several components or the cost of the ESS itself. To make it more lucrative, the BESS could be used for arbitrage aswell or storing excess PV energy to be used later at night. Though this is not possible with a SESS due to its low energy density. As a consequence when an SESS is used for this application, the SESS is only limited to only this application and thus might not be feasible to implement in the future due to the possibility of it not being lucrative for homeowners to invest in. Furthermore, the SESS has high cost of implementation (highlighted in section 6.2.3) and brings technical challenges (highlighted in section 6.2.2) aswell. From this, it can be deduced that for the foreseeable future a BESS is the most feasible to implement for this application than a SESS.

Thus now or in the near future to have a successful ESS implementation for avoiding voltage flickers from occurring due to a PV system at a household level, the ESS implementation should be a DC connected BESS operating in power control mode due to the reasons mentioned above.

Bibliography

[1] QualTech. The history of flicker limits, 2011.

[2] Naoto Kakimoto, Hiroyuki Satoh, Satoshi Takayama, and Kouichi Nakamura. Ramp-rate control of photovoltaic generator with electric double-layer capacitor. IEEE Transactions on Energy Conversion, 24:465–473, 2009.

[3] M. J.E. Alam, K. M. Muttaqi, and D. Sutanto. A novel approach for ramp-rate control of solar pv using energy storage to mitigate output fluctuations caused by cloud passing. IEEE Transactions on Energy Conversion, 29:507–518, 2014.

[4] Els Stultiens. 2 miljoen huizen in nederland hebben zonnepanelen, 12 2022.

[5] Novar. Zonnepark dorhout mees, 9 2023.

[6] Erik Schuurmans. The effect of solar pv on voltage flicker in the lv grid, 2020.

[7] Sandro Corsi. Advances in Industrial Control. Springer', 2015.

[8] C. A.G. Medeiros and J. C. De Oliveira. Effects of voltage fluctuation associated to flicker limits on equipments performance. volume 1, pages 347–352. IEEE Computer Society, 2002.

[9] Arnold Wilkins, Jennifer Veitch, and Brad Lehman. Led lighting flicker and potential health concerns: Ieee standard par1789 update. pages 171–178, 2010.

[10] IEC. Nen-en-iec 61000-4-15 : Testing and measurement techniques - flickermeter - functional and design specifications. IEC, 2011.

[11] IEC. IEC 61000-3-7 : Limits – Assessment of emission limits for the connection of fluctuating installations to MV, HV and EHV power systems. Institute of Electrical and Electronics Engineers, 2008.

[12] IEC. Iec 61000-3-11 : Limits – limitation of voltage changes, voltage fluctuations and flicker in public low-voltage supply systems - equipment with rated current 75 a and subject to conditional connection. IEC, 2000.

[13] W. Mombauer. Flicker caused by phase jumps. European Transactions on Electrical Power, 16(6):545–567, 2006.

[14] Yun Seng Lim and Jun Huat Tang. Experimental study on flicker emissions by photovoltaic systems on highly cloudy region: A case study in malaysia. Renewable Energy, 64:61–70, 2014.

[15] Shahinur Rahman, Masood Moghaddami, Arif I Sarwat, Temitayo Olowu, and Mohammadsaleh Jafaritalarposhti. Flicker estimation associated with pv integrated distribution network.

[16] N. B.G.(Nico) Brinkel, M. K.(Marte) Gerritsma, T. A.(Tarek) AlSkaif, I. (Ioannis) Lampropoulos, A. M.(Arjan) van Voorden, H. A.(Henk) Fidder, and W. G.J.H.M.(Wilfried) van Sark. Impact of rapid pv fluctuations on power quality in the low-voltage grid and mitigation strategies using electric vehicles. International Journal of Electrical Power and Energy Systems, 118, 6 2020.

[17] Prabha Ariyaratna, Kashem M. Muttaqi, and Danny Sutanto. A novel control strategy to mitigate slow and fast fluctuations of the voltage profile at common coupling point of rooftop solar pv unit with an integrated hybrid energy storage system. Journal of Energy Storage, 20:409–417, 12 2018.

[18] Licheng Wang, Feifei Bai, Ruifeng Yan, and Tapan Kumar Saha. Real-time coordinated voltage control of pv inverters and energy storage for weak networks with high pv penetration. IEEE Transactions on Power Systems, 33:3383–3395, 5 2018.

[19] Hannan Ahmad Khan, Mohd Zuhaib, and Mohd Rihan. Voltage fluctuation mitigation with coordinated oltc and energy storage control in high pv penetrating distribution network. Electric Power Systems Research, 208, 7 2022.

[20] M. Jan E. Alam, Kashem M. Muttaqi, and Danny Sutanto. Battery energy storage to mitigate rapid voltage/power fluctuations in power grids due to fast variations of solar/wind outputs. IEEE Access, 9:12191–12202, 2021.

[21] Javier Marcos, Iñigo de La Parra, Miguel García, and Luis Marroyo. Control strategies to smooth short-term power fluctuations in large photovoltaic plants using battery storage systems. Energies, 7:6593–6619, 2014.

[22] Amin, Riyanto Trilaksono Bambang, Arief Syaichu Rohman, Cees Jan Dronkers, Romeo Ortega, and Arif Sasongko. Energy management of fuel cell/battery/supercapacitor hybrid power sources using model predictive control. IEEE Transactions on Industrial Informatics, 10:1992–2002, 11 2014.

[23] Ronald Staubly and Robert Rounds. Gridscale energy storage flywheel system, 2011.

[24] Greenfields Energy. Flywheel energy storage system (fess).

[25] Kris Likit-Anurak, Kasemsak Uthaichana, Konlayutt Punyawudho, and Yottana Khunatorn. The performance and efficiency of organic electrolyte redox flow battery prototype. volume 118, pages 54–62. Elsevier Ltd, 2017.

[26] Declan Bryans, Véronique Amstutz, Hubert H. Girault, and Léonard E.A. Berlouis. Characterisation of a 200 kw/400 kwh vanadium redox flow battery. Batteries, 4, 2018.

[27] David Linden and Thomas B Reddy. Handbook of batteries, Fifth edition, volume 33. 2018.

[28] Portfolio management energy from smart grid deliverable: Report/white paper on ultracapacitor technology unlocking new possibilities through innovative energy storage the role of ultracapacitors in the energy transition, 2020.

[29] Kasun Subasinghage, Kosala Gunawardane, Nisitha Padmawansa, Nihal Kularatna, and Mehdi Moradian. Modern supercapacitors technologies and their applicability in mature electrical engineering applications, 10 2022.

[30] Yuliya Preger, Heather M. Barkholtz, Armando Fresquez, Daniel L. Campbell, Benjamin W. Juba, Jessica Romàn-Kustas, Summer R. Ferreira, and Babu Chalamala. Degradation of commercial lithium-ion cells as a function of chemistry and cycling conditions. Journal of The Electrochemical Society, 167:120532, 1 2020.

[31] Marc Wentker, Matthew Greenwood, and Jens Leker. A bottom-up approach to lithium-ion battery cost modeling with a focus on cathode active materials. Energies, 12, 2 2019.

[32] Ana Irina Stroe, Daniel Loan Stroe, Vaclav Knap, Maciej Swierczynski, and Remus Teodorescu. Accelerated lifetime testing of high power lithium titanate oxide batteries. pages 3857–3863. Institute of Electrical and Electronics Engineers Inc., 12 2018.

[33] Sina Orangi and Anders Hammer Strømman. A techno-economic model for benchmarking the production cost of lithium-ion battery cells. Batteries, 8, 8 2022.

[34] Javier Marcos. Predicting pv plant power fluctuations and optimising energy storage, 10 2014.

[35] Samson G. Tesfahunegn, Øystein Ulleberg, Preben J.S. Vie, and Tore M. Undeland. Pv fluctuation balancing using hydrogen storage - a smoothing method for integration of pv generation into the utility grid. volume 12, pages 1015–1022. Elsevier Ltd, 2011.

[36] Yushu Sun, Zhenxing Zhao, Min Yang, Dongqiang Jia, Wei Pei, and Bin Xu. Overview of energy storage in renewable energy power fluctuation mitigation. CSEE Journal of Power and Energy Systems, 6:160–173, 3 2020.

[37] Shivashankar Sukumar, Marayati Marsadek, K. R. Agileswari, and Hazlie Mokhlis. Ramp-rate control smoothing methods to control output power fluctuations from solar photovoltaic (pv) sources—a review, 12 2018.

[38] Aistis Raudys and Židrina Pabarškaitė. Optimising the smoothness and accuracy of moving average for stock price data. Technological and Economic Development of Economy, 24:984–1003, 1 2018.

[39] Tomonobu Senjyu, Manoj Datta, Atsushi Yona, Toshihisa Funabashi, and Chul Hwan Kim. Pv output power fluctuations smoothing and optimum capacity of energy storage system for pv power generator. Renewable Energy and Power Quality Journal, 1:35–39, 3 2008.

[40] Abdelkader Abbassi, Mohamed Ali Dami, and Mohamed Jemli. Statistical characterization of capacity of hybrid energy storage system (hess) to assimilate the fast pv-wind power generation fluctuations. pages 467–472. Institute of Electrical and Electronics Engineers Inc., 7 2017.

[41] Dwi Riana Aryani, Jung Su Kim, and Hwachang Song. Suppression of pv output fluctuation using a battery energy storage system with model predictive control. International Journal of Fuzzy Logic and Intelligent Systems, 17:202–209, 2017.

[42] Wei Ma, Wei Wang, Xuezhi Wu, Ruonan Hu, Fen Tang, and Weige Zhang. Control strategy of a hybrid energy storage system to smooth photovoltaic power fluctuations considering photovoltaic output power curtailment. Sustainability (Switzerland), 11, 3 2019.

[43] Gautham Ram Chandra Mouli, Peter Van Duijsen, Francesca Grazian, Ajay Jamodkar, Pavol Bauer, and Olindo Isabella. Sustainable e-bike charging station that enables ac, dc andwireless charging from solar energy. Energies, 13, 7 2020.

[44] Jing Ren, Yonghong Xu, Hongguang Zhang, Fubin Yang, Yifang Yang, Xu Wang, Peng Jin, and Denggao Huang. State of charge estimation of ultracapacitor based on forgetting factor recursive least square and extended kalman filter algorithm at full temperature range. Heliyon, 8, 11 2022.

[45] Sergio Mendoza, Ji Liu, Partha Mishra, and Hosam K. Fathy. Statistical quantification of least-squares battery state of charge estimation errors. volume 1. American Society of Mechanical Engineers, 2016.

[46] Donal B. Murray and John G. Hayes. Cycle testing of supercapacitors for long-life robust applications. IEEE Transactions on Power Electronics, 30:2505–2516, 5 2015.

[47] Top Systems. Multiplus ii top systems webshop, 10 2023.

A

Appendix, Simulation

A.1. Simulation results

A.1.1. Energy usage throughout the day with different layers - Power control

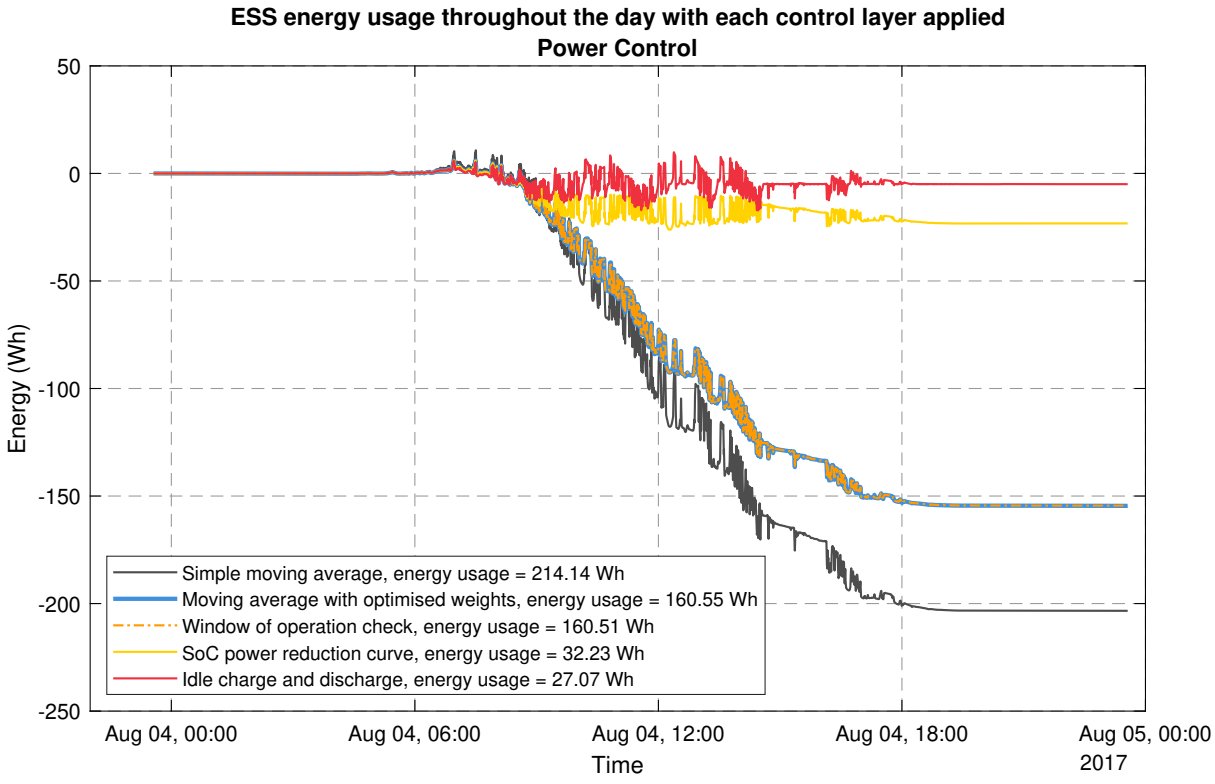

Figure A.1: Energy usage with different control layers applied using power control

A.1.2. Energy usage throughout the day with different layers - Voltage control

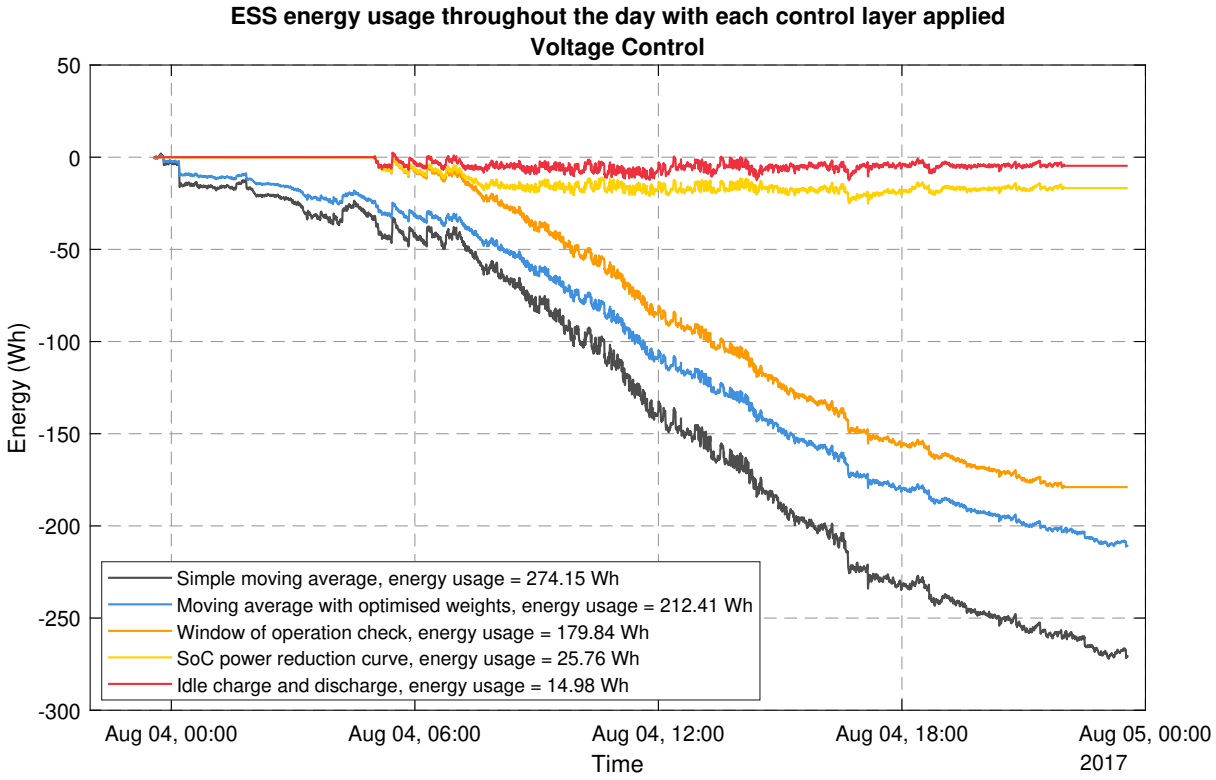

Figure A.2: Energy usage with different control layers applied using voltage control

A.2. Matlab script for simulation

A.2.1. Voltage control simulation Matlab script

File of this script can be found in the auxiliary document for all of the scripts or given upon request to the author of this thesis.

A.2.2. Power control simulation Matlab script

File of this script can be found in the auxiliary document for all of the scripts or given upon request to the author of this thesis.

A.2.3. Full year power control simulation Matlab script

File of this script can be found in the auxiliary document for all of the scripts or given upon request to the author of this thesis.

A.2.4. Full year voltage control simulation Matlab script

File of this script can be found in the auxiliary document for all of the scripts or given upon request to the author of this thesis.

A.2.5. Voltage flicker curve mapping Matlab script

File of this script can be found in the auxiliary document for all of the scripts or given upon request to the author of this thesis.

B

Appendix, Experimental setup & results

B.1. Final parameters used for the experimental setups

B.1.1. Power control for AC connected ESS experimental setup

Parameter	Value
Window size for moving average	30
Window of operation	5AM till 10PM
Charge correction factor SoC reduction curve	0.01
Discharge correction factor SoC reduction curve	0.01
SOC lower limit (%) SoC reduction curve	49.8
SOC upper limit (%) SoC reduction curve	50.2
Idle charge power (W) Idle charge and discharge	-100
Idle discharge power (W) Idle charge and discharge	50
SOC lower limit (%) Idle charge and discharge	49.8
SOC upper limit (%) Idle charge and discharge	50.2
Power threshold lower limit (W) Idle charge and discharge	-50
Power threshold upper limit (W) Idle charge and discharge	50

Table B.1: Final parameters for power control for the AC connected ESS experimental setup

B.1.2. Voltage control for AC connected ESS experimental setup

Parameter	Value
Window size for moving average	12
Window of operation	5AM till 10PM
Charge correction factor SoC reduction curve	0.01
Discharge correction factor SoC reduction curve	0.01
SOC lower limit (%) SoC reduction curve	49.8
SOC upper limit (%) SoC reduction curve	50.2
Idle charge power (W) Idle charge and discharge	-100
Idle discharge power (W) Idle charge and discharge	50
SOC lower limit (%) Idle charge and discharge	49.8
SOC upper limit (%) Idle charge and discharge	50.2
Power threshold lower limit (W) Idle charge and discharge	-50
Power threshold upper limit (W) Idle charge and discharge	50

Table B.2: Final parameters for voltage control for the AC connected ESS experimental setup

B.1.3. Power control for DC connected ESS experimental setup

Parameter	Value
Window size for moving average	30
Window of operation	5AM till 10PM
Charge correction factor SoC reduction curve	0.01
Discharge correction factor SoC reduction curve	0.01
SOC lower limit (%) SoC reduction curve	49.955
SOC upper limit (%) SoC reduction curve	50.045
Idle charge power (W) Idle charge and discharge	-100
Idle discharge power (W) Idle charge and discharge	50
SOC lower limit (%) Idle charge and discharge	49.955
SOC upper limit (%) Idle charge and discharge	50.045
Power threshold lower limit (W) Idle charge and discharge	-50
Power threshold upper limit (W) Idle charge and discharge	50

Table B.3: Final parameters for power control for the DC connected ESS experimental setup

B.1.4. Voltage control for DC connected ESS experimental setup

Parameter	Value
Window size for moving average	12
Window of operation	5AM till 10PM
Charge correction factor SoC reduction curve	0.01
Discharge correction factor SoC reduction curve	0.01
SOC lower limit (%) SoC reduction curve	49.955
SOC upper limit (%) SoC reduction curve	50.045
Idle charge power (W) Idle charge and discharge	-100
Idle discharge power (W) Idle charge and discharge	50
SOC lower limit (%) Idle charge and discharge	49.955
SOC upper limit (%) Idle charge and discharge	50.045
Power threshold lower limit (W) Idle charge and discharge	-50
Power threshold upper limit (W) Idle charge and discharge	50

Table B.4: Final parameters for voltage control for the DC connected ESS experimental setup

B.2. Configuration file for experimental setups

B.2.1. Configuration file for DC experimental setup

ESS Inverter Modbus Type	tcpip				
ESS Inverter IP	192.168.11.3				
ESS Inverter Port	502				
PV Meter Modbus Type	rtu				
PV Meter COM Port					
Grid Meter Modbus Type	rtu				
Grid Meter COM Port					
Sensitivity	0.003508772				
Ateps Wh	11040				
Ateps Start SoC	50				
VOLTAGE CONTROL					
Correction Factor Discharge	0.01				
Correction Factor Charge	0.01				
SoC Lower Limit	49.955				
SoC Upper Limit	50.045				
Window Voltage Control Nr Elements	12				
Idle Charge Power - Voltage Control	-100				
Idle Discharge Power - Voltage Control	50				
SoC Lower Limit - SoC Deadzone	49.955				
SoC Upper Limit - SoC Deadzone	50.045				
Power Threshold Idle - Voltage	50				
POWER CONTROL					
Correction Factor Discharge	0.01				
Correction Factor Charge	0.01				
SoC Lower Limit	49.955				
SoC Upper Limit	50.045				
Window Power Control Nr Elements	30				
Idle Charge Power - Power Control	-100				
Idle Discharge Power - Power Control	50				
SoC Lower Limit - SoC Deadzone	49.955				
SoC Upper Limit - SoC Deadzone	50.045				
Power Threshold Idle - Power	50				
ESS INVERTER - MODBUS MAPPING	Address	Type	Scalefactor	Unit ID	Register type
ESS Inverter - Set Power	37	int16	1	246	holdingregs
ESS Inverter - Error Check	32	uint16	1	246	inputregs
ESS Inverter - Output Voltage	15	uint16	10	246	inputregs
ESS Inverter - Output Current	18	int16	10	30	inputregs
ESS Inverter - Output Power	23	int16	0.1	30	inputregs
PV METER - MODBUS MAPPING	Address	Type	Scalefactor	Unit ID	Register type
PV Meter - Output Power	789	uint16	10	100	inputregs
PV Meter - Error Check	788	uint16	1	100	inputregs
GRID METER - MODBUS MAPPING	Address	Type	Scalefactor	Unit ID	Register type
Grid Meter - Output Voltage	2616	uint16	10	30	inputregs
Grid Meter - Output Power	2600	int16	1	30	inputregs

B.2.2. Configuration file for AC experimental setup

ESS Inverter Modbus Type	tcpip				
ESS Inverter IP	169.254.1.2				
ESS Inverter Port	502				
PV Meter Modbus Type	serialrtu				
PV Meter COM Port	COM5				
Grid Meter Modbus Type	serialrtu				
Grid Meter COM Port	COM4				
Sensitivity	0.00276115				
Ateps Wh	2500				
Ateps Start SoC	50				
VOLTAGE CONTROL					
Correction Factor Discharge	0.01				
Correction Factor Charge	0.01				
SoC Lower Limit	49.8				
SoC Upper Limit	50.2				
Window Voltage Control Nr Elements	12				
Idle Charge Power - Voltage Control	-100				
Idle Discharge Power - Voltage Control	50				
SoC Lower Limit - SoC Deadzone	49.8				
SoC Upper Limit - SoC Deadzone	50.2				
Power Threshold Idle - Voltage	50				
POWER CONTROL					
Correction Factor Discharge	0.01				
Correction Factor Charge	0.01				
SoC Lower Limit	49.8				
SoC Upper Limit	50.2				
Window Power Control Nr Elements	30				
Idle Charge Power - Power Control	-100				
Idle Discharge Power - Power Control	50				
SoC Lower Limit - SoC Deadzone	49.8				
SoC Upper Limit - SoC Deadzone	50.2				
Power Threshold Idle - Power	50				
ESS INVERTER - MODBUS MAPPING	Address	Type	Scalefactor	Unit ID	Register type
ESS Inverter - Set Power	37	int16	1	227	holdingregs
ESS Inverter - Error Check	32	uint16	1	227	inputregs
ESS Inverter - Output Voltage	15	uint16	10	227	inputregs
ESS Inverter - Output Current	18	int16	10	227	inputregs
ESS Inverter - Output Power	842	int16	1	100	inputregs
PV METER - MODBUS MAPPING	Address	Type	Scalefactor	Unit ID	Register type
PV Meter - Output Power	40	int16	10	1	inputregs
PV Meter - Error Check	20498	uint16	1	1	inputregs
GRID METER - MODBUS MAPPING	Address	Type	Scalefactor	Unit ID	Register type
Grid Meter - Output Voltage	6	int16	10	1	inputregs
Grid Meter - Output Power	40	int16	10	1	inputregs
Grid Meter - Error Check	20498	uint16	1	1	inputregs
BATTERY - MODBUS MAPPING	Address	Type	Scalefactor	Unit ID	Register type
Battery - Pack Voltage	840	uint16	10	100	inputregs
Battery - Pack Current	841	int16	10	100	inputregs
Battery - SOC	30	uint16	10	227	inputregs

B.3. Matlab script for GUI and data processing

B.3.1. GUI Matlab code for DC connected ESS experimental setup

File of this script can be found in the auxiliary document for all of the scripts or given upon request to the author of this thesis.

B.3.2. GUI Matlab code for AC connected ESS experimental setup

File of this script can be found in the auxiliary document for all of the scripts or given upon request to the author of this thesis.

C

Appendix, Datasheets

C.1. Datasheets

C.1.1. Power optimizer datasheet

Scroll down for datasheet

Power Optimizer

Voor Europa

P370 / P401 / P404 / P485 / P500 / P505 / P601

POWER OPTIMIZER

Vermogensoptimalisatie op paneelniveau

- Speciaal ontworpen om te werken met SolarEdge-omvormers
- Geavanceerd onderhoud met monitoring op paneelniveau
- Beperkt alle soorten mismatch-verlies van panelen, fabriekstoleranties tot gedeeltelijke schaduw
- Superieur rendement (99,5%)
- Flexibel systeemontwerp voor maximale benutting van oppervlakte
- Spanningsafschakeling op paneelniveau voor de veiligheid van installateurs en brandweer
- Snelle installatie met één schroef

/ Power Optimizer

P370 / P401 / P404 / P485 / P500 / P505 / P601

Optimizer model (geschikte paneeltypes)	P370 (60&70 cels-panelen)	P401 (60&70 cels-panelen)	P404 (voor 60-cels en 72-cels, korte strings)	P485 (voor hoogspanning spanelen)	P500 (voor 72-cels-panelen)	P505 (voor panelen met hogere stroom)	P601 (voor 1 x PV-paneel met hoog vermogen)	EENHEID
INGANG								
Nominaal DC-ingangsvermogen[1]	370	420	405	485	500	505	600	W
Absoluut maximale ingangsspanning (Voc bij laagste temperatuur)	60		80	125	80	83	65	Vdc
MPPT-werkbereik	8 - 60		12,5 - 80	12,5 - 105	8 - 80	12,5-83	12,5 - 65	Vdc
Maximale kortsluitstroom (Isc)	11	12,5	11,75	11	10,1	14		Adc
Maximaal rendement	99.5							%
Gewogen rendement	98,8						98.6	%
Overspanningscategorie	II							
OUTPUT TIJDENS BEDRIJF (POWER OPTIMIZER AANGESLOTEN OP WERKENDE SOLAREDGE-OMVORMER)								
Maximale uitgangsstroom	15							Adc
Maximale uitgangsspanning	60		80		60	80		Vdc
OUTPUT TIJDENS STAND-BY (POWER OPTIMIZER LOSGEKOPPELD VAN SOLAREDGE-OMVORMER OF SOLAREDGE-OMVORMER UIT)								
Veilige uitgangsspanning per power optimizer	1 ± 0,1							Vdc
REGELGEVING								
Emissies	FCC Deel 15 Klasse B, IEC61000-6-2, IEC61000-6-3							
Veiligheidsnormen	IEC62109-1 (veiligheidsklasse II), UL1741							
RoHS	Ja							
Brandveiligheid	VDE-AR-E 2100-712:2018-12							
INSTALLATIESPECIFICATIES								
Maximaal toegestane systeemspanning	1000							Vdc
Afmetingen (b x l x h)	129 x 153 x 27,5 / 5,1 x 6 x 1,1	129 x 153 x 29,5 / 5,1 x 6 x 1,16	129 x 153 x 42,5 / 5,1 x 6 x 1,7	129 x 159 x 49,5 / 5,1 x 6,2 x 1,9	129 x 153 x 33,5 / 5,1 x 6 x 1,3	129 x 162 x 59 / 5,1 x 6,4 x 2,3	129 x 153 x 52 / 5,1 x 6 x 2	mm
Gewicht (inclusief kabels)	655		775 / 1,7	845 / 1,9	750 / 1,7	1064		gr
Ingangsconnector	MC4(2)			Enkele of dubbele MC4[2][3]	MC4(2)			
Lengte ingangskabel	0,16 / 0,52, 0,9 / 2,95		0,16					m
Uitgangsconnector	MC4							
Lengte uitgangskabel	1,2						1,4 / 4,5	m
Bedrijfstemperatuur [4]	-40 tot +85							°C
Beschermingsklasse	IP68							
Relatieve vochtigheid	0 - 100							%

(1) Het nominale vermogen van het zonnepaneel bij STC zal de optimizer 'Nominaal DC-ingangsvermogen' niet overschrijden Panelen met maximaal +5% vermogenstolerantie zijn toegestaan
(2) Neem contact op met SolarEdge indien u ander type connectoren wilt gebruiken.
(3) Gebruik voor de dual versie voor parallelle aansluiting van twee panelen de P485. In het geval van een oneven aantal PV panelen in één string is het toegestaan om één dual versie P485 Power Optimizer op één PV paneel te installeren. Als u een enkel paneel koppelt, sluit u de ongebruikte ingangen af met het meegeleverde paar afdichtingen
(4) Voor een omgevingstemperatuur van boven de +70 °C wordt power de-rating toegepast. Raadpleeg de technische notitie Power Optimizers Temperatuur de-rating voor meer details

PV-systeemontwerp met behulp van een Solaredge-omvormer[5]		SolarEdge Home Wave 1-Fase	SolarEdge Home 3-Fase (voor korte strings)	3-Fase 230/400V	3fase voor het 277/480V net	
Minimale stringlengte (power optimizers)	P370, P401, P500	8	9	16	18	
	P404, P485, P505, P601	6	8	14 (15 met SE30K)	14	
Maximale stringlengte (power optimizers)		25	20	50	50	
Maximaal nominaal vermogen per string		5700[6]	5625 [6]	11250 [7]	12750[8]	W
Parallelle reeksen van verschillende lengtes of oriëntaties		Ja				

(5) Het is niet toegestaan om P404/P485/P505/P601 in één string met P370/P401/P500 te combineren
(6) Als het nominale AC-vermogen van de omvormer ≤ maximaal nominaal vermogen per string, dan zal het maximale vermogen per string het maximale DC-ingangsvermogen van de omvormer kunnen bereiken. Zie: https:/ /www.solaredge.com/sites/default/files/se-power-optimizer-single-string-design-application-note.pdf
(7) Voor het 230/400V-net: het is toegestaan tot 13.500 W per string te installeren als het maximale vermogensverschil tussen elke string niet meer dan 2000 W bedraagt.
(8) Voor het 277/480 V-net: het is toegestaan tot 15.000 W per string te installeren als het maximale vermogensverschil tussen elke string niet meer dan 2000 W bedraagt

CE

C.1.2. DC circuit breaker datasheet

Scroll down for datasheet

Product data sheet
Characteristics

M9F22263
Multi 9 - C60SP - MCB - 2P - 63 A - C Curve - 480Y/277 V - 5 kA - UL 1077

Main

Range	Multi 9
Product name	Multi 9 C60
Product or component type	Miniature circuit-breaker
Device short name	C60SP
Device application	Distribution
Poles description	2P
Number of protected poles	2
[In] rated current	63 A at 25 °C conforming to EN/IEC 60947-2
Network type	AC
Trip unit technology	Thermal-magnetic
Curve code	C
Breaking capacity	10 KA AIR at 240 V AC conforming to UL 1077 10 KA AIR at 240 V AC conforming to CSA C22.2 No 235 6 KA Icu at 440 V AC conforming to EN/IEC 60947-2 10 KA Icu at 415 V AC conforming to EN/IEC 60947-2 20 KA Icu at 240 V AC conforming to EN/IEC 60947-2 6 KA Icu at 440 V AC conforming to GB 14048.2 10 KA Icu at 415 V AC conforming to GB 14048.2 20 KA Icu at 240 V AC conforming to GB 14048.2 5 KA AIR at 480Y/277 V AC conforming to UL 1077 5 kA AIR at 480Y/277 V AC conforming to CSA C22.2 No 235
Suitability for isolation	Yes conforming to EN/IEC 60947-2
Standards	EN/IEC 60947-2 GB 14048.2 UL 1077 CSA C22.2 No 235
Product certifications	IEC CCC UR CSA

Complementary

[Ue] rated operational voltage	240 V AC 50/60 Hz 415 V AC 50/60 Hz 440 V AC 50/60 Hz
Magnetic tripping limit	8.5 x In +/- 20 % AC
[Ics] rated service breaking capacity	4.5 KA 75 % conforming to EN/IEC 60947-2 - 440 V AC 7.5 KA 75 % conforming to EN/IEC 60947-2 - 415 V AC 15 KA 75 % conforming to EN/IEC 60947-2 - 240 V AC 4.5 KA 75 % conforming to GB 14048.2 - 440 V AC 7.5 KA 75 % conforming to GB 14048.2 - 415 V AC 15 kA 75 % conforming to GB 14048.2 - 240 V AC
[Ui] rated insulation voltage	500 V AC conforming to EN/IEC 60947-2
[Uimp] rated impulse withstand voltage	6 kV conforming to EN/IEC 60947-2
Contact position indicator	Yes
Control type	Toggle
Local signalling	ON/OFF indication
Mounting mode	Clip-on

Mounting support	DIN rail
9 mm pitches	4
Height	81 mm
Width	36 mm
Depth	72 mm
Colour	Grey
Mechanical durability	20000 cycles
Electrical durability	10000 cycles
Provision for padlocking	Padlockable
Connections - terminals	Tunnel type terminal (top or bottom)1…35 mm² (AWG 18...AWG 2) - rigid Tunnel type terminal (top or bottom)1…25 mm² (AWG 18...AWG 3) - flexible with ferrule Tunnel type terminal (top or bottom)1…25 mm² (AWG 18...AWG 3) - flexible
Wire stripping length	14 mm for top or bottom connection
Tightening torque	3.5 N.m top or bottom
Earth-leakage protection	Without

Environment

IP degree of protection	IP20 conforming to IEC 60529 IP40 (modular enclosure) conforming to IEC 60529
Pollution degree	3 conforming to EN/IEC 60947-2
Tropicalisation	2 conforming to IEC 60068-1
Relative humidity	95 % at 55 °C
Operating altitude	0...2000 m
Ambient air temperature for operation	-30…70 °C
Ambient air temperature for storage	-40…80 °C

Offer Sustainability

Sustainable offer status	Green Premium product
REACh Regulation	REACh Declaration
EU RoHS Directive	Compliant EU RoHS Declaration
Mercury free	Yes
RoHS exemption information	Yes
China RoHS Regulation	China RoHS Declaration
Environmental Disclosure	Product Environmental Profile
WEEE	The product must be disposed on European Union markets following specific waste collection and never end up in rubbish bins

C.1.3. ATEPS battery module datasheet

Scroll down for datasheet

ATEPS NEDERLAND BV

ADVANCED TECHNOLOGIES FOR ENERGY & POWER SYSTEMS

Solutions For Energy Storage

ATEPS is based around a number of core technologies that all focus on the preservation and storage of energy.

We have developed unique solutions for peak-shaving, energy storage and fuel saving for CHP's that can be delivered quickly and starts saving your energy cost energy cost almost instantly.

In many cases these installations can be offered including financing and do not need any capital investments on your side. Therefore these solution are risk-free for any user; risk free both financially and technically since any changes to your existing application can be undone in a matter of minutes should you desire to do so.

Our service devision keeps an eye on all the units and service and optimization can often be done without user interference.

19" Lithium battery

ATEPS Netherlands BV has developed a 19" battery with a height of 2U, which can be used in many applications. Due to the universal design of the battery it can easily be integrated into existing installations such as:

- **Energy Storage System**
- **Backup in ICT systems**
- **Emergency power supply for telecommunication systems**

The batteries are interconnected via the backplane so there are no voltage-carrying parts on the front of the battery, an important safety feature.

For applications where the voltage should be available to the front, this can be achieved by means of a 1U high connection-unit.

Depending on the backplanes used, the batteries can be connected in series or parallel or a combination of these whereby a maximum of 16 modules can be inserted in tot rack. Thereby systems with different voltages and capacities can be easily configured.

A 19" BMU is available for integration in the same cabinet that controls all batteries in this rack. The BMU communicates to external devices via RS485 or the ATEPS Energy Management System that also controls the converters in ESS applications.

An SD card can be inserted in the BMS to update firmware in the batteries and can be used to log battery data for later analyses of the battery parameters.

ESS Project Planning

Important at the outset of any ESS project is a clear understanding of the current operational cost and the cost of ownership. Using advanced analytical tools, a prediction on obtainable cost savings are made that will form the basis for the Return on Investment calculations.

The ESS system can be combined with different solar installations, wind generators or in combination with fuel cells and the creation of hydrogen.

Depeding on the size of the ESS, installation is done using an external power-house or as a single or small row of cabinets. Installation is simple and will be handled by qualified Ateps engineers in a mater of hours or days.

Service, updates and frequent reporting is part of the system so the ESS application will hardly be noticed other than in your monthly energy bills!

More information:

ATEPS Nederland BV
Panovenweg 34
5708 HR Helmond
The Netherlands

Tel: +31 (0)492 - 792707
www.ateps.com
info@ateps.com

Specifications

Type	AB5050
Nominal voltage	50V
Capacity	50Ah
Technologies	Li-NiMnCoO$_2$
Dimensions	19" x 2U x 550mm
Weight	23kg
BMU	External - 4U
Nom. discharge current	50A
Max. discharge current	100A standard - 200A in special cabinet
Nom. Charge current	25A
Max. Charge current	50A standard - 100A in special cabinet
Integrated sensors	14 x Voltage, Current, 7 x Temperature
Communication	RS485 with secure protocol
Temp. range in use	0°C to +45°C
Temp. range storage	-10°C to +55°C
System Vmax	1050V (42U cabinet, batteries connected in series)
System Ah max.	1050Ah (42U cabinet, batteries connected in parallel)
Diagnostics	3-color LED
Service USB	Cell voltage, temperatures, current
Safety	Packs designed for 1500V and in accordance with, UN 3480, UN 38.3 and UL2054
BMS	Smart BMS with automatic battery ID distribution and communication to EMS

Each cell individually fused

19" batteries

Batteries in 19" racks

ESS Application

C.1.4. Victron lead acid battery module

Scroll down for datasheet

Gel en AGM accu's

Altijd stroom

www.victronenergy.com

AGM accu
12V 90Ah

1. VRLA technologie

VRLA staat voor Valve Regulated Lead Acid. Dit houdt in dat de accu's gesloten zijn. Alleen als gevolg van verkeerd laden en/of kapotte cellen zal er gas via een veiligheidsventiel ontsnappen.
VRLA accu's zijn onderhoudsvrij gedurende hun gehele levensduur.

2. Gesloten (VRLA) AGM accu's

AGM staat voor Absorbent Glass Mat. In deze accu's is de elektrolyt door middel van capillaire werking geabsorbeerd in een glasvezel mat die geklemd is tussen de platen. Zoals uitgelegd wordt in ons boek 'Altijd Stroom', zijn AGM accu's in vergelijking met Gel accu's meer geschikt voor het leveren van hoge stroom gedurende korte tijd.

3. Gesloten (VRLA) Gel accu's

Hier is de elektrolyt als gel geïmmobiliseerd. In vergelijking met AGM accu's hebben Gel accu's over het algemeen een langere levensduur, zowel bij 'float' als bij 'cycling' gebruik.

4. Lage zelfontlading

Door het gebruik van loodcalcium roosters en zeer zuivere materialen kunnen Victron VRLA accu's lange periodes zonder laden moeiteloos aan. De zelfontlading is minder dan 2% per maand bij een temperatuur van 20°C. Deze ontlaadsnelheid verdubbeld bij iedere temperatuur verhoging van 10°C. Victron VRLA accu's kunnen zodoende tot een jaar lang bewaard worden zonder dat zij opnieuw geladen hoeven te worden; mits dit bij een relatief lage temperatuur gebeurt.

5. Uitzonderlijk ontlaadherstel

Victron VRLA accu's herstellen zich zeer goed, zelfs na diepe en langdurige ontladingen. Niettemin heeft herhaaldelijk diep en langdurig ontladen een negatieve invloed op de levensduur van alle loodzwavelzuuraccu's. Victron accu's vormen hierop geen uitzondering.

6. Accu ontlaadkarakteristieken

De nominale capaciteit van Victron 'Deep Cycle' accu's verwijst naar een ontlading van 20 uur (een ontlaadstroom van 0,05C).
De nominale capaciteit van Victron Tubular Plate Long Life accu's verwijst naar een ontlading van 10 uur.
De effectieve capaciteit neemt af naarmate de ontlaadstroom hoger wordt (zie tabel 1).

Ontlaadtijd (constante stroom)	Eind spanning V	AGM Deep Cycle %	Gel Deep Cycle %	Gel Long Life %
20 uur	10,8	100	100	112
10 uur	10,8	92	87	100
5 uur	10,8	85	80	94
3 uur	10,8	78	73	79
1 uur	9,6	65	61	63
30 min.	9,6	55	51	45
15 min.	9,6	42	38	29
10 min.	9,6	38	34	21
5 min.	9,6	27	24	
5 sec.		8 C	7 C	

Tabel 1: Effectieve capaciteit als een functie van de ontlaadtijd (de laatste regel geeft niet de capaciteit maar de maximaal toelaatbare ontlaadstroom weer).

7. Het effect van temperatuur op de levensduur

Een hoge temperatuur heeft een zeer negatief effect op de levensduur. De levensduur van Victron accu's als een functie van temperatuur is weergegeven in tabel 2.

Gemiddelde temperatuur	AGM Deep Cycle jaren	Gel Deep Cycle jaren	Gel Long Life jaren
20°C / 68°F	7 - 10	12	20
30°C / 86°F	4	6	10
40°C / 104°F	2	3	5

Tabel 2: Levensduur overzicht van Victron accu's in 'float'

Victron Energy B.V. | De Paal 35 | 1351 JG Almere | The Netherlands
General phone: +31 (0)36 535 97 00 | E-mail: sales@victronenergy.com
www.victronenergy.com

8. Het effect van temperatuur op de capaciteit

Zoals wordt weergegeven in grafiek 1, vermindert de capaciteit aanzienlijk bij lage temperaturen.

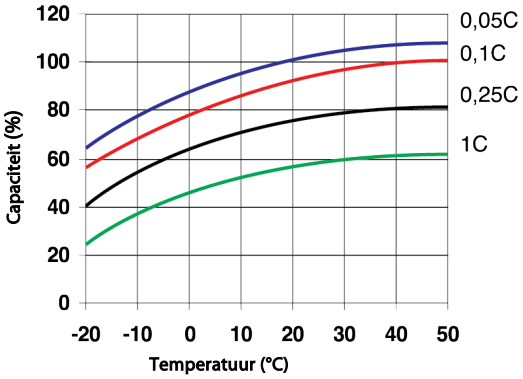

Grafiek 1: Het effect van temperatuur op de capaciteit

9. Levenscyclus van Victron accu's

Accu's verouderen door ontladen en herladen. Het aantal cycli hangt af van de ontladingsdiepte. Dit wordt weergegeven in grafiek 2.

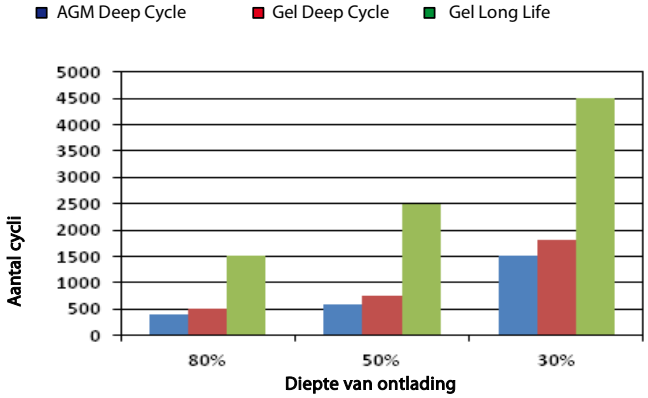

Grafiek 2: Levensduur bij cyclisch gebruik

10. Acculaden in het geval van cyclus gebruik: de 3-traps laadkarakteristiek

De meest voorkomende laadcurve die gebruikt wordt om VRLA accu's te laden in het geval van cyclisch gebruik is de 3-traps laadkarakteristiek. Hierbij wordt een constante stroom fase (de 'bulk' fase) gevolgd door twee constante spanning fases ('absorbtion' en 'float'); zie grafiek 3.

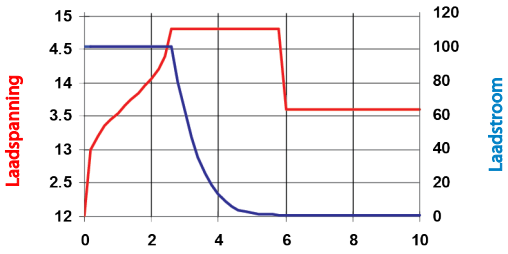

Grafiek 3: De 3-traps laadcurve

Tijdens de 'absorbtion' fase wordt de laadspanning op een relatief hoog niveau gehouden zodat de accu volledig geladen kan worden binnen een redelijk tijdsbestek. De derde en laatste fase is de 'float' fase: de spanning wordt verlaagd tot 'standby' niveau. Dit is voldoende om te compenseren voor de zelfontlading.

Nadelen van de traditionele 3-traps laadkarakteristiek:

- Tijdens de bulk fase wordt de stroom op een constant en dikwijls hoog niveau gehouden, zelfs nadat de gasspanning (14,34V voor een 12V accu) is overschreden. Dit kan leiden tot een te hoge gasdruk in de accu. Een deel van het gas zal ontsnappen via de veiligheidsventielen. Dit verlaagt de levensduur van de accu.
- Daarna wordt de 'absorbtion' spanning toegepast. Dit gebeurt gedurende een vast tijdsbestek, onafhankelijk van hoe diep de laatste ontlading is geweest. Een volledige 'absorbtion' periode, na een ondiepe ontlading, zal de accu overbelasten. Ook dit verlaagt de levensduur van de accu (bijvoorbeeld door versnelde corrosie van de positieve platen).
- Uit onderzoek is gebleken dat de levensduur van een accu verhoogd kan worden door de 'float' spanning te verlagen op momenten dat de accu niet gebruikt wordt.

11. Acculaden: een langere levensduur met Victron 4- traps adaptief laden

Victron heeft de adaptieve laadkarakteristiek ontwikkeld. De 4-traps adaptieve laadcurve is het resultaat van jaren lang onderzoek .

De Victron adaptieve laadcurve is dé oplossing voor de drie voornaamste problemen van de 3-traps laadkarakteristiek:

- Battery Safe mode
  Om excessieve gasvorming te verkomen, heeft Victron de 'Battery Safe Mode' ontwikkeld. De 'Battery Safe Mode' zal de mate van spanningsvermeerdering begrenzen zodra de gasspanning bereikt is. Uit onderzoek is gebleken dat dit interne gasvorming zal verlagen tot een veilig niveau.

- Variabele 'absorbtion' tijd
  Gebaseerd op de duur van de 'bulk' fase, berekent de lader hoe lang hij de accu in 'absorbtion' houdt.
  Als de 'bulk' tijd kort is, betekent dit dat de accu al bijna volledig geladen was. Zodoende zal de 'absorbtion' tijd kort zijn. Een langere 'bulk' tijd zal ook resulteren in een langere 'absorbtion' tijd.

- Storage mode
  Na voltooiing van de 'absorbtion' periode is de accu volledig geladen en wordt de spanning verlaagd naar 'float' of 'standby' niveau. Als er gedurende de hierop volgende 24 uur geen ontlading plaatsvindt, wordt de spanning nog verder verlaagd en gaat de accu in 'storage' modus. De lagere 'storage' spanning vermindert corrosie van de positieve platen.
  Eén keer per week wordt de laadspanning gedurende een korte periode verhoogd naar het 'absorbtion' niveau om te compenseren voor de zelfontlading (Battery Refresh mode).

12. Acculaden in het geval van 'standby' gebruik: constante spanning 'float' laden

Als een accu niet regelmatig diep ontladen wordt, kan een 2-traps laadcurve gebruikt worden. Tijdens de eerste fase wordt de accu geladen met een begrensde stroom (de 'bulk' fase). Zodra een vooraf ingestelde spanning wordt bereikt, wordt de accu op die spanning gehouden (de 'float' fase). Deze laadmethode wordt gebruikt voor startaccu's in voertuigen, en in ononderbroken stroomvoorzieningen.

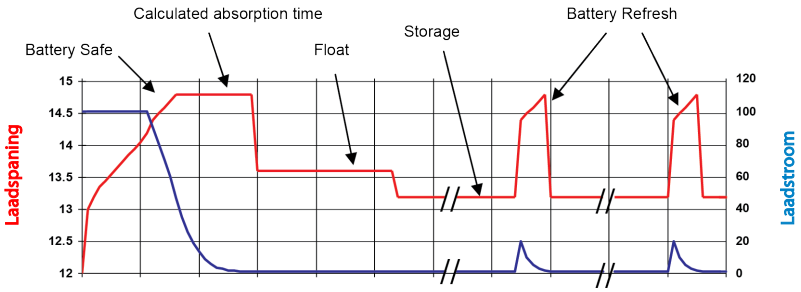

Grafiek 4: 4-traps adaptieve laadcurve

13. Optimale laadspanning van Victron VRLA accu's

De aangeraden laadspanning instellingen voor een 12V accu zijn weergegeven in Tabel 3.

14. Het effect van temperatuur op de laadspanning

Als de temperatuur hoger wordt moet de laadspanning verlaagd worden.
Temperatuur compensatie is vereist wanneer verwacht wordt dat de temperatuur van de accu gedurende langere tijd lager is dan 10°C/50°F of hoger dan 30°C/85°F.
De aangeraden temperatuur compensatie voor Victron VRLA accu's is -4 mV/Cel (-24 mV/°C voor een 12V accu).
Het middelpunt voor temperatuur compensatie is 25°C/70°F.

15. Laadstroom

De laadstroom moet bij voorkeur niet hoger zijn dan 0,2C (20A voor een 100 Ah accu). De temperatuur van een accu zal met meer dan 10°C toenemen als de laadstroom 0,2C overschrijdt en dan is temperatuur compensatie noodzakelijk.

	Float **Bedrijf** (V)	Cycle bedrijf Normaal (V)	Cycle bedrijf Snelherlading (V)
Victron AGM 'Deep Cycle'			
Absorption		14,2 - 14,6	14,6 - 14,9
Float	13,5 - 13,8	13,5 - 13,8	13,5 - 13,8
Storage	13,2 - 13,5	13,2 - 13,5	13,2 - 13,5
Victron Gel 'Deep Cycle'			
Absorption		14,1 - 14,4	
Float	13,5 - 13,8	13,5 - 13,8	
Storage	13,2 - 13,5	13,2 - 13,5	
Victron Gel 'OPzV Tubular'			
Absorption		14,0 - 14,2	
Float	13,5 - 13,8	13,5 - 13,8	
Storage	13,2 - 13,5	13,2 - 13,5	

Tabel 3: Aangeraden laadspanningen

12 Volt Deep Cycle AGM							Algemene specificaties
Artikel nummer	**Ah**	**V**	**l x b x h mm**	**Gewicht kg**	CCA @0°F	RES CAP @80°F	Technologie: vlakke plaat AGM Aansluiting: koper
BAT406225084	**240**	6	320 x 176 x 247	31	700	270	Nominale Capaciteit: 20u ontlading bij 25°C Float levensduur: 12 jaar bij 20°C Cyclus levensduur: 400 cycli bij 80% ontlading 600 cycli bij 50% ontlading 1500 cycli bij 30% ontlading
BAT212070084	**8**	12	151 x 65 x 101	2,5			
BAT212120086	**14**	12	151 x 98 x 101	4,4			
BAT212200084	**22**	12	181 x 77 x 167	5,8			
BAT412350084	**38**	12	197 x 165 x 170	12,5			
BAT412550084	**60**	12	229 x 138 x 227	20	280	80	
BAT412600084	**66**	12	258 x 166 x 235	24	300	90	
BAT412800084	**90**	12	350 x 167 x 183	27	400	130	
BAT412101084	**110**	12	330 x 171 x 220	32	500	170	
BAT412121084	**130**	12	410 x 176 x 227	38	550	200	
BAT412151084	**165**	12	485 x 172 x 240	47	600	220	
BAT412201084	**220**	12	522 x 238 x 240	65	650	250	
BAT412124081	**240**	12	522 x 240 x 224	67	650	250	

12 Volt Deep Cycle GEL							Algemene specificaties
Artikel nummer	**Ah**	**V**	**l x b x h mm**	**Gewicht kg**	CCA @0°F	RES CAP @80°F	Technologie: vlakke plaat GEL Aansluiting: koper
BAT412550104	**60**	12	229 x 138 x 227	20	250	70	Nominale Capaciteit: 20u ontlading bij 25°C Float levensduur: 12 jaar bij 20°C Cyclus levensduur: 500 cycli bij 80% ontlading 750 cycli bij 50% ontlading 1800 cycli bij 30% ontlading
BAT412600100	**66**	12	258 x 166 x 235	24	270	80	
BAT412800104	**90**	12	350 x 167 x 183	26	360	120	
BAT412101104	**110**	12	330 x 171 x 220	33	450	150	
BAT412121104	**130**	12	410 x 176 x 227	38	500	180	
BAT412151104	**165**	12	485 x 172 x 240	48	550	200	
BAT412201104	**220**	12	522 x 238 x 240	66	600	220	
BAT412126101	**265**	12	520 x 268 x 223	75	650	250	

Andere capaciteiten en aansluitpolen: op aanvraag

Victron Energy B.V. | De Paal 35 | 1351 JG Almere | The Netherlands
General phone: +31 (0)36 535 97 00 | E-mail: sales@victronenergy.com
www.victronenergy.com

C.1.5. Battery cells used for ATEPS module datasheet

Scroll down for datasheet

圆柱锂离子电芯规格书

SPECIFICATION OF PRODUCT

Cylindrical Lithium-ion Rechargeable Cell

电芯型号：SW18650-26HPA

Model: SW18650-26HPA

Document No. **文件编号**	SW/PS-RD-XX-021		**Date** **生效日期**	2021-04-20	
Originator **拟制**		**Checked By** **审核**		**Approved By** **批准**	
Customer confirmation:(Signature and seal) **客户确认：（签字并加盖公章）**					

东莞市振华新能源科技有限公司
Sinowatt Dongguan Limited

http://www.sinowatt.com

Address 地址：No.7,Xingyuan Rode,Yuquan Industrial Park,Fenggang Town,Dongguan,Guangdong

广东省东莞市凤岗镇玉泉工业区兴园路 7 号

Tel 电话：+86-0769-82695588 **Fax 传真：**+86-0769-89330788 **Email：**sales@sinowatt.com

Change the resume 更改履历			
Version No 版本	Revised description 修订描述	Reviser 修订人	Revision date 修订日期
A0	First issue 首次发行	赵 川	2021/04/20

Contents

目录

1 Scope 适用范围 2

2 Description and model 说明及型号 2

3 Nominal Specifications 基本规格参数 2

4 Appearance 外观 3

5 Standard Test Conditions 标准测试条件 4

5.1 Environmental Conditions 环境测试条件 4

5.2 Measurement Apparatus 测试设备要求 4

6 Environmental Safety characteristics 环境安全性能 4

7 Safety characteristics 安全性能 6

8 Warranty 产品责任书 7

9 Warning 注意事项 7

Attached drawing 1 Outline Dimensions 8

附图 1：规格尺寸外形图 8

1 Scope 适用范围

This specification describes the type and size, performance, technical characteristics, warning and caution of the lithium ion rechargeable cell. The specification only applies to SW18650-26HPA cell supplied by Sinowatt Dongguan Limited.

本规格书规定了东莞市振华新能源科技有限公司生产的型号为 SW18650-26HPA 锂离子二次电芯的技术要求和测试方法及注意事项。

2 Description and model 说明及型号

2.1 Description 产品名称：Cylindrical Li-ion rechargeable cell 圆柱锂离子二次电芯

2.2 Model 电芯型号：SW18650-26HPA

3 Nominal Specifications 基本规格参数

Item 项目	Specification 参数	Remark 备注
Model 型号	SW18650-26HPA	
Rated Capacity 标称容量	2600mAh	After standard charging, then at 0.2C_5 discharge to 2.75V, 25℃ 标准充电后，25℃0.2C_5放电至 2.75V
Min Capacity 最低容量	2550mAh	
Platform Voltage 平台电压	3.60V	
Standard Charging 标准充电	CC-CV, Std.0.2C_5, 4.2V, cut-off at 1/50C_5,8.0hrs 25℃±2℃ 0.2 C_5恒流恒压充电至 4.2V，截止电流 1/50C_5，充电时间不大于 8 小时	C_5, nominal capacity C_5为 5 小时率额定容量
Charging Current (Max.) 最大充电电流	0℃~10℃ 0.2C_5 10℃~45℃ 0.5C_5	
Standard Discharging 标准放电	CC,0.2C_5，cut-off at 2.75V 0.2C_5恒流放电至 2.75V	
Max. continuous discharge 最大持续放电	3C_5	25℃
Max. instantaneous discharge 最大瞬时放电	5C_5	25℃
AC Impedance 交流阻抗	≤20mΩ	AC 1kHz 交流频率 1kHz
Cycle Life 循环寿命	500th cycle>80% of 1st Cycle Capacity 500 次循环后放电容量>80%首次放电容量	25℃,0.5C_5 charge, 1/20C_5 cut off;Discharge:1.0C_5 to 2.75V 0.5C_5充电，恒压 1/20C_5截止，1C_5放电至 2.75V
Discharge Characteristics (by rate of discharge) 倍率放电性能	0.2 C_5 ＝100% 0.5 C_5 ≥96% 1.0 C_5 ≥94% 3.0 C_5 ≥90% 5.0 C_5 ≥88%	Cells are to be charged per standard charge profile. The discharge capacity of each cell at respective discharge rate shall be compared with the discharge capacity at 0.2C_5 标准充电后按不同倍率放电容量同 0.2C_5放电容量的百分比

C.1.6. Victron compatible energy meters datasheet

Scroll down for datasheet

Energiemeter Selectiegids

www.victronenergy.com

ET112

ET340

EM540

B21

B23 B24

Venus OS ondersteunt meerdere types van energiemeters, waarvan enkele opgeslagen worden door Victron en anderen die rechtstreeks van de producenten, zoals Carlo Gavazzi of ABB, gekocht moeten worden.

De Energiemeters worden gebruikt in systemen met een GX-apparaat om het vermogen van een PV-omvormer, een AC-aggregaat of als een netstroommeter te meten in een ESS-installatie. Het kan ook gebruikt worden om AC-belastingen te meten.

De meeste energiemeters maken verbinding met een GX-apparaat via RS485, ofwel via een bedrade verbinding via onze RS485 naar USB interface ofwel draadloos via onze Zigbee-naar-USB en Zigbee-naar-RS485-omzetters. Diens gegevens worden dan weergegeven op een GX-apparaat en ons VRM-portaal. Alternatief kan de EM24-ethernetmeter gebruikt worden, op voorwaarde dat de meter verbinding maakt met een lokaal netwerk, op een zodanige manier dat het GX-apparaat het kan bereiken.

Bepaal eerst, om een selectie te maken, of u een meter met één of drie fasen nodig heeft:

Welke energiemeter geselecteerd moet worden hangt af van de installatie, het aantal fasen dat u wenst te meten en de maximale stroom per fase.**Voorbeelden:** Gebruik voor een driefasige netaansluiting een meter met drie fasen. Gebruik voor een driefasige PV-omvormer ook een meter met drie fasen. Gebruik voor een netaansluiting met een enkelvoudige fase een meter met een enkelvoudige fase. En in een installatie met een netaansluiting met een enkelvoudige fase, die tevens een PV-omvormer heeft die moet worden gemeten met een energiemeter, kunt u twee ET112's of de ET340 gebruiken. Gebruik, wanneer de toepassing het max. stroomgehalte overschrijdt, een energiemeter met stroomtransformatoren. Let op dat de meeste PV-omvormers "direct-uitlezing" hebben door het Victron-systeem en hebben dus niet nodig dat hun output gemeten wordt door een energiemeter.

Selecteer nu, op basis van de stroom, het model:

Vereiste	Metingstype	Oplossing
Enkelvoudige fase tot 100 A	Direct/Shunt	ET1XX / EM1XX / ABB B21
Drie fasen tot 65 A/fase	Direct/Shunt	ET340 / EM24 / EM340 / EM540 / ABB B23
Enkelvoudige fase met meer dan 100 A/fase	Stroomtransformatoren (CT)	Niet beschikbaar, gebruik een CT-oplossing met drie fasen
Drie fasen met meer dan 65 A/fase	Stroomtransformatoren	EM24* / EM330 / EM530 / ABB B24

* EM24DINAV53DISX alleen, niet opgeslagen door Victron

Kies tussen RS485 of Ethernet-verbinding:

De Ethernet-modus past beter in installaties waar een Ethernet-netwerk beschikbaar is. In plaats van een RS485-draad te moeten trekken tussen de hoofd-AC-distributiekaart en het opslagsysteem, kan het bestaande Ethernet worden gebruikt. Het nadeel is dat dit afhankelijk is van het goed functioneren van het netwerk – in het geval van problemen schakelt het opslagsysteem over naar de inactieve modus: doorgeefluik.

De EM24, EM3XX, EM5XX en ABB meters gebruiken vectorregistratie om energie te tellen. Deze methode heeft de voorkeur in veel landen, zoals Duitsland en Oostenrijk en de meeste andere landen. De andere energiemeters gebruiken rekenkundige registratie. Raadpleeg Veelgestelde vragen V8 in de Victron Energiemeter-handleidingen voor meer informatie over de verschillen in energietelling.

Energiemeter	Handleiding	Onderdeelnummer	Weergave	Fasen	Maximale stroom	Metingstype	Communicatie	Vernieuwen gehalte [4]	Opmerkingen
ET112	ET112	REL300100000	Nee	1	100 A	Direct/Shunt	RS485	750 ms	ET112DINAV01XS1X
ET340	ET340	REL300300000	Nee	3	65 A per fase	Direct/Shunt	RS485	2000 ms	ET340DINAV23XS1X
EM540	EM540	REL200100100	LCD	3	65 A per fase	Direct/Shunt	RS485	100 ms	EM540DINAV23XS1X
EM24 Ethernet	EM24 Ethernet	REL200200100	LCD	3	65 A per fase 5 A per fase	Direct/Shunt CT's	Ethernet	600 ms	EM24DINAV23XE1X EM24DINAV53XE1X [3]
Andere energiemeters met GX-firmware ondersteuning									
EM111	EM111	Niet opgeslagen	LCD	1	45 A	Direct/Shunt	RS485	750 ms	
EM112	EM112	Niet opgeslagen	LCD	1	100 A	Direct/Shunt	RS485	750 ms	
EM330 [1]	EM330	Niet opgeslagen	LCD	3	5 A per fase	CT's	RS485	1200 ms	EM330DINAV53HS1X27 EM330DINAV53HS1PFB27
EM340 [1]	EM340	Niet opgeslagen	LCD	3	65 A per fase	Direct/Shunt	RS485	-	EM340DINAV23XS1X27 EM340DINAV23XS1PFB27
EM530 [1]	EM530	Niet opgeslagen	LCD	3	5 A per fase	CT's	RS485	100 ms	EM530DINAV53XS1X
EM24 RS485 [1]	EM24 RS485	Niet opgeslagen	LCD	3	65 A per fase	Direct/Shunt	RS485	600 ms	EM24DINAV93XISX
ABB B21 [1, 2]	B21	Niet opgeslagen	LCD	1	65 A	Direct/Shunt	RS485	480 ms	2CMA100155R1000 Zilver
ABB B23 [1, 2]	B23	Niet opgeslagen	LCD	3	65 A per fase	Direct/Shunt	RS485	480 ms	2CMA100169R1000 Zilver
ABB B24 [1, 2]	B24	Niet opgeslagen	LCD	3	6 A per fase	CT's	RS485	480 ms	2CMA100183R1000 Zilver

[1] geselecteerde modellen worden ondersteund - [2] Zigbee-verbinding wordt niet ondersteund – [3] geen voorraad bij Victron – [4] Ververssnelheid = hoe vaak geeft de energiemeter een nieuwe waarde in de registers.Let op dat de (VenusOS) vertraging (de tijd die het kost om te lezen aan 9600 baud) tussen 180 en 250 ms ligt.

Victron Energy B.V. | De Paal 35 | 1351 JG Almere | Nederland
E-mail: sales@victronenergy.com | **www.victronenergy.com**

C.1.7. Pylontech LFP battery pack datasheet

Scroll down for datasheet

US2000C Pylontech Lithium

Low voltage 48V Lithium Battery

US2000C - 2,4 kWh Modules

Pylontech's US2000C lithium battery is the new version of the already known US2000.
The simplicity and modularity of the 2.4 kWh capacity US2000C make it suitable to realize storage systems of small and large capacities that can be expanded according to current and future energy needs.
Among the new features there is the built-in **Soft-Start** function able to reduce the peak current when inverter need to start from battery.
The US2000C battery has an integrated BMS that can manage and monitor cell information including voltage, current and temperature.

Features:

- The more **stable and safer internal molecular structure** of LFP batteries, allows an increase in combustion temperature equal to 600 ° C compared to 300 ° C of NMC and LCO;
- 95% **depth of discharge** (DOD), available for the inverter which completely follow Pylontech latest protocol to operate;
- Support wake up by 5~12V signal from RJ45 port;
- Support upgrade battery module from upper controller via CAN or RS485 communication;
- **Dual active protection on BMS level;**
- Ability to work under different temperature conditions;
- **Monitoring and assistance included, 10 year warranty.**

Each element, 50 Ah and 2 rack units height, is easily installed in special rack cabinets supplied on request by Energy Srl.

For the storage systems with EPS anti black out mode you must follow all ENERGY srl instructions about the minimum quantity of modules installed.

energy®
SAVE YOUR PLANET
www.energysynt.com

Technical data
Lithium battery

Model	US2000C
ELECTRICAL DATA	
Cell Technology	Li-ion (LFP)
Voltage [V]	48
Recommend Charge Current [A]	25
Nominal Capacity [Wh]	2400
Operating Voltage [V]	44,5 - 53,5
DOD [%]	95
BUS	
Communication Bus	RS485, CAN
Communication protocol	YD/T 1363.3-2005
DIMENSIONS AND WEIGHT	
Height [mm]	89 (2U)
Width [mm]	442
Depht [mm]	410
Weight [kg]	22,5
GENERAL DATA	
Operation Life at 25 °C	15+ years
Life Cycles	>6000 25°C - 95% DoD
Discharging Temperature [°C]	-10…50
Charging Temperature [°C]	0…50
Storage Temperature [°C]	-20…60
Protection Class	IP20
Eartquake Certificate	GR-1089
Transport Certificate	UN 3090
EMC	IEC62619, IEC63056 UL1642, IEC61000-6-2, IEC61000-6-3, UN38.3
Environmental Certification	GB/T 2423
Transfer Certificate	TÜV, CE, UN38.3

Energy Srl
Registered office:
Piazza Manifattura, 1
38068, Rovereto TN - Italy
Tel. +39 0464 350812 - Fax +39 0464 350512

www.energysynt.com
www.retiintelligenti.com

Energy Srl
Operations/Warehouse:
Via Seconda Strada, 26
30030, Z.I. Loc. Galta di Vigonovo (VE) - Italy
info@energysynt.com
Tel. +39 049 2701296 - Fax +39 049 8599098

C.1.8. SkelMod 102V88F EDLC Supercapacitor module datasheet

Scroll down for datasheet

SKELETON TECHNOLOGIES

DATA SHEET

SkelMod 102V 88F

+ 102V DC nominal voltage
+ Ultra-low ESR
+ Long lifetime - 1 million duty cycles
+ Integrated Ultracapacitor Management System for effective cell balancing
+ CAN bus communication
+ 19 inch rack system compatible

CE

SMA102V88FAF TECHNICAL SPECIFICATIONS	UNIT	VALUE
Electrical		
Nominal voltage	V	102
Absolute maximum voltage	V	108
Rated capacitance	F	88
Rated DC 10ms ESR	mΩ	6.2
Rated DC 1s ESR	mΩ	7.6
Specific energy[3]	Wh/kg	4.8
Energy density[4]	Wh/L	4.3
Maximum series voltage	VDC	1500*
Rated maximum peak current (for 1 s duration)[1]	A	2689
Typical short circuit current	kA	21.25
Maximum stored energy[2]	Wh	127.1
Rated nominal power (DC 10ms ESR):		
Power[5]	kW	419.5
Specific power[6]	kW/kg	15.8
Power density[7]	kW/L	14.2
Rated practical power (DC 1s ESR):		
Power[5]	kW	342.2
Specific power[6]	kW/kg	12.9
Power density[7]	kW/L	11.6
Cells in total	pcs	36
Cell type		SCA3200
Life*		
Life at 102 V and maximum operating temperature	Hours	1500
Shelf life @ RT, uncharged	Years	10
Projected cycle life @ RT between 102 V and 56 V	Cycles	1 000 000
Temperature		
Operating temperature range	ºC	-20 to +60*
Storage temperature range	ºC	-40 to +50
Ultracapacitor management system		
Nominal auxiliary supply voltage	V	24
Auxiliary supply voltage range	V	16-33
Constant current consumption at 24V DC	A	0.07**
Cell balancing method	Controlled resistive balancing	
Temperature monitor	6 NTC sensors	
Voltage monitor	Individual Cell	
Communication interface	CAN bus 2.0B	
Connectors		
Power connector	Ø 13.5 mm Trough hole	
Signal connectors	D-sub DE-9 Male D-sub DE-9 Female	
Connector location	Front	

SMA102V88FAF TECHNICAL SPECIFICATIONS	UNIT	VALUE
Standards		
International protection marking (for enclosure)	IEC 60529, IP 20	
Isolation protection	IEC 62477-1, OVC2, PD2	
EMC immunity	IEC 61000-6-2	
EMC emissions	IEC 61000-6-3	
Thermal parameters* **		
Thermal resistance given at ΔT 30 °C (R_{th})	°C/W	0.065
Thermal capacitance (C_{th})	kJ/°C	25
Maximum continuous current (at ΔT 15 °C)	A	172
Maximum continuous current (at ΔT 30 °C)	A	245
Maximum continuous current (at ΔT 40 °C)	A	281
Physical parameters		
Typical mass	kg	26.5
Typical volume	L	29.6

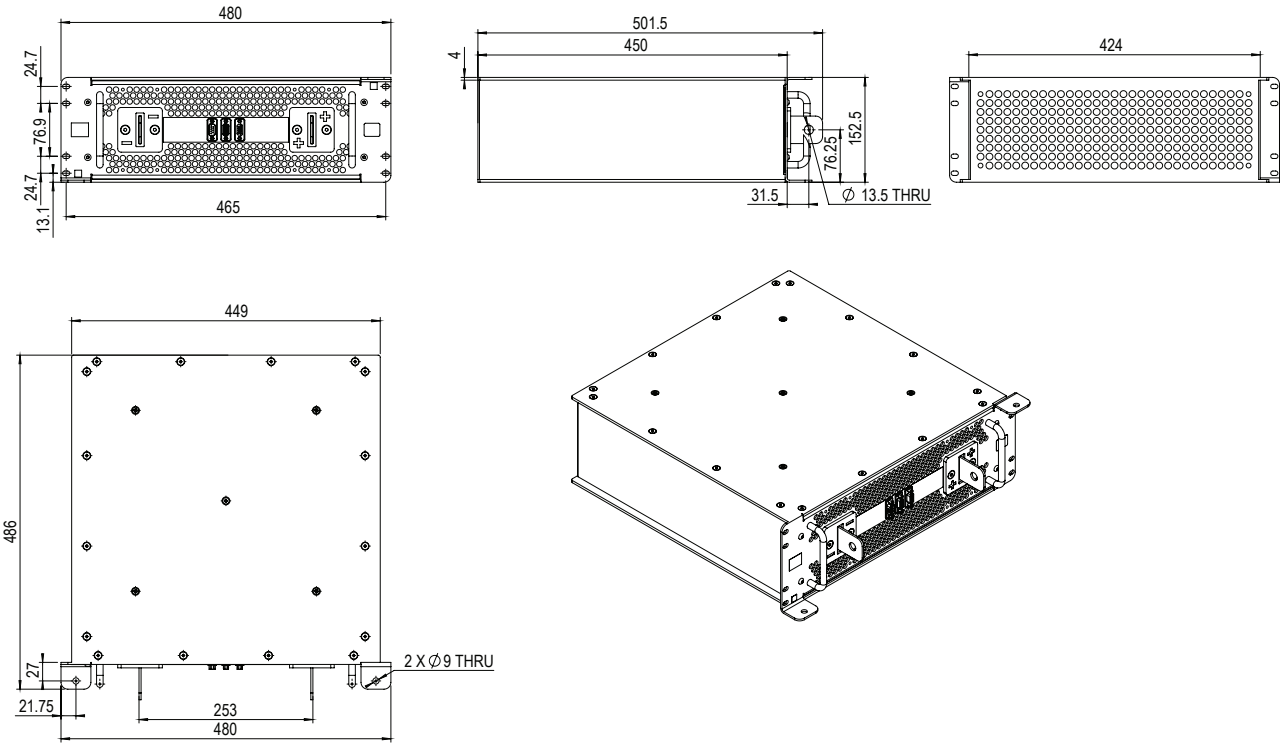

** For maximum series voltage IE32 (EN 60721-3-3) requirements must be followed. For lower temperature contact Skeleton Technologies*

*** Inrush current for the auxiliary supply: 0.18A*

**** Thermal parameters given for cooling airflow rate of 85CFM*

1 Maximum peak current(1s)= $\frac{C \times 1/2 \times V}{C \times ESR + 1\,s}$

2 $E_{stored} = \frac{1/2 \times C \times V^2}{3600}$

3 $E_{specific} = \frac{E_{stored}}{mass}$

4 $P_{density} = \frac{P_{max}}{volume}$

5 $E_{density} = \frac{E_{stored}}{volume}$

6 $P_{max} = \frac{V^2}{4 \times ESR}$

7 $P_{specific} = \frac{P_{max}}{mass}$

8 $R_{th} = \frac{\Delta T}{DC\ 1s\ ESR \times I^2}$

Standard markings

+ Name of Manufacturer, Part number, Serial number, Rated voltage
+ Rated capacitance, Negative and positive terminals, Warning marking
+ Total energy in watt-hours

Notes

+ All information provided on this data sheet and all subsequent ultracapacitors sales and testing are subject to Standard Terms of Service (ToS) available on www.skeletontech.com, document General Terms of Sale for Skeleton Technologies OÜ

Skeleton Technologies GmbH

Sales and Headquarters
Schücostraße 8, 01900 Großröhrsdorf, Germany
info@skeletontech.com

www.skeletontech.com

SKELETON TECHNOLOGIES

C.1.9. Eltek 48V DC/DC Converter datasheet

Scroll down for datasheet

ELTEK
A Delta Group Company

Wide input DC/DC converters

The Flatpack2 DC/DC converters add new flexibility to the Flatpack2 power systems. Secondary $24V_{DC}$ or $48V_{DC}$ outputs can be provided from the main voltage battery. Application requiring galvanic isolation between the loads can now also be addressed.

The galvanic isolated CAN bus can be connected to a supplying Eltek power system's control system allowing monitor and control of the DC/DC converters without adding a separate controller.

FLATPACK2 DC/DC 1350W

18-75V/24V & 18-75V/48V

Doc 241115.60x.DS3 – v2.3

APPLICATIONS

TELECOM – MOBILE / WIRELESS

- RADIO BASE STATIONS/ CELL SITES
- LTE / 4G / WIMAX
- MICROWAVE

TELECOM – FIXED

- TELEPHONY SERVERS / SWITCHES
- FIBER OPTICS
- MICROWAVE
- CABLE
- BROADBAND

POWER UTILITIES

- CONTROL & PROTECTION
- PLC AND ALARM SYSTEMS
- SIGNALING

RAILWAY & METRO

- CONTROL & PROTECTION
- SIGNALING SYSTEMS
- SAFETY SYSTEM

6U SYSTEM

FLATPACK2 DC/DC POWER RACK (PN: 273820)

MONITORING USING COMPACK INTERFACE KIT (PN: 242100.900)

KEY FEATURES

- WIDE INPUT RANGE
- OR-ING PROTECTION ON OUTPUT
- BOOST MODE
- QUICK TRIP PULSE
- HIGH EFFICIENCY
- MODULE KEYING
- SEAMLESSLY INTEGRATED IN CONTROL SYSTEM

STATUS OF DC/DC CONVERTERS IN SMARTPACK2 WEB

FLATPACK2 DC/DC 1350W

18-75V/24V & 18-75V/48V

Model	1350W 18-75/24V	1350W 18-75/48V
Part number	241115.600	241115.602
INPUT DATA		
Voltage range	20 - 75 V_{DC} (shutdown < 16.5V_{DC})	
Current (maximum)	70 A_{DC} (85 A_{DC} during boost)	
Protection	Fuse and reversed polarity protection	
OUTPUT DATA		
Voltage (default)	26 V_{DC}	53 V_{DC}
Voltage (adjustable range)	24 - 28 V_{DC}	48 - 58.5 V_{DC}
Power (maximum) @ V_{IN} > 26 V_{DC} / V_{IN} = 18 V_{DC} Power boost 15s / 10min recovery (V_{IN} > 25V_{DC})	1350 W / 910 W 2000W	
Current (maximum) Current boost 15s / 10min recovery (V_{IN} > 25V_{DC})	56 A 84 A	28 A 42 A
Static Voltage regulation (0 - 100% load)	±1%	±0.5%
Dynamic Voltage regulation	±5.0% for 10-90% or 90-10% load variation, regulation time < 30ms	
Ripple, 20MHz bandwidth	< 200 mV_{pp}	
Protection	Short circuit proof , OR-ing diode, High temperature protection, Hot plug-in inrush current limiting, Over voltage Shutdown	
OTHER SPECIFICATIONS		
Efficiency	Up to 91.7 %	Up to 93.8 %
Isolation	1.2 kV_{DC} - input to chassis 1.9 kV_{DC} - input to output 1.0 kV_{DC} - output to chassis	1.9 kV_{DC} - CAN to chassis 1.9 kV_{DC} - CAN to input 1.9 kV_{DC} - CAN to output
Alarms: Red LED 'on'	Low and high input voltage shutdown, High and low temperature shutdown, Converter Failure, Overvoltage shutdown on output, Fan failure, Low output voltage alarm	
Warnings: Yellow LED 'on'	Converter in power de-rate mode, Remote output current limit activated, Input voltage out of range, flashing at overvoltage, Loss of CAN communication with controller	
Normal (module running): Green LED 'on'		
MTBF (Telcordia SR-332 Issue I method III (a))	>315 000 (@ $T_{ambient}$: 25 °C)	>315 000 (@ $T_{ambient}$: 25 °C)
Operating temperature	-40 to +75°C (-40 to +185°F), humidity 5 - 95% RH non-condensing	
Temperature de-rating above 55°C (131°F)	1350W to 1250W @ 65°C (149°F) and 800W @ 75°C (167°F)	
Storage temperature	-40 to +85°C (-40 to +185°F), humidity 0 - 99% RH non-condensing	
Dimensions[WxHxD] / Weight	109 x 41.5 x 327mm (4.25 x 1.69 x 13") / < 1.95 kg (4.3 lbs)	
DESIGN STANDARDS		
Electrical safety	UL 60950-1, EN 60950-1	
EMC	EN 61000-6-1 / -2 / -3 / -4 ETSI EN 300 386 V.1.4.1	
Environment	ETSI EN 300 019: 2-1 (Class 1.2), 2-2 (Class 2.3) & 2-3 (Class 3.2) RoHS (2011/65/EU) and WEEE (2002/96/EC) compliant	

Eltek — Gråterudveien 8, PB 2340 Strømsø, 3003 Drammen, Norway Phone: +47 32 20 32 00

C.1.10. Victron Multiplus II datasheet

Scroll down for datasheet

MultiPlus-II Omvormer/Lader

230 V

► Victron online product pagina

https://ve3.nl/6H

Een MultiPlus met ESS-functionaliteit (Energy Storage System)

De MultiPlus-II is een multifunctionele omvormer/oplader met alle functies van de MultiPlus, plus een externe stroomsensoroptie die de PowerControl en PowerAssist-functies uitbreidt tot 50 A of 100 A.
De MultiPlus-II is bij uitstek geschikt voor professionele scheepvaart, zeilsport, voertuig- en landgebaseerde toepassingen zonder netaansluiting.
Het heeft ook een ingebouwde anti-eilandbedrijf-functie en een groeiende lijst met goedkeuringen van landen voor ESS-toepassingen. Er zijn verschillende systeemconfiguraties mogelijk. Voor meer gedetailleerde informatie, zie de ESS ontwerp en configuratiehandleiding.

PowerControl en PowerAssist - Het verhogen van de capaciteit van het stroomnet of een stroomgenerator

Er kan een maximale stroomnet- of generatorstroom worden ingesteld. De MultiPlus-II zal dan rekening houden met andere AC-belastingen en alle extra stroom gebruiken voor het opladen van de accu, waardoor wordt voorkomen dat de generator of het stroomnet worden overbelast (PowerControl-functie).
PowerAssist neemt het principe van PowerControl naar een hoger niveau. Waar piekvermogen vaak slechts voor een beperkte periode vereist is, compenseert de MultiPlus-II voor de ontoereikende generator-, wal- of stroomnetvoeding met stroom van de accu. Wanneer de belasting afneemt, wordt het reservevermogen gebruikt om de accu op te laden.

Zonne-energie: Wisselstroom beschikbaar, zelfs tijdens een stroomstoring

De MultiPlus-II kan zowel in een netonafhankelijke PV als in een op het elektriciteitsnet aangesloten PV en andere alternatieve energiesystemen worden gebruikt. Het is compatibel met zowel zonnelader-controllers als netontwikkelingsomvormers.

Twee AC-uitgangen

De hoofduitgang heeft geen pauze-functionaliteit. De MultiPlus-II neemt de voeding naar de aangesloten belastingen over, in het geval van een stroomstoring of wanneer de walstroom/generatorspanning wordt losgekoppeld. Dit gebeurt zo snel (in minder dan 20 milliseconden) dat computers en andere elektronische apparatuur zonder onderbreking kunnen blijven werken.
De tweede uitgang is alleen actief wanneer wisselstroom beschikbaar is op de ingang van de MultiPlus-II. Belastingen die de accu niet zouden moeten ontladen, zoals een boiler bijvoorbeeld, kunnen op deze uitgang worden aangesloten.

Vrijwel onbeperkte stroom dankzij parallelle (niet voor 8k-, 10k- en 15k-modellen) en driefasige werking

Tot wel 6 Multi's kunnen parallel werken om een hoger uitgangsvermogen te bereiken. Zes 48/5000/70 eenheden kunnen bijvoorbeeld een uitgangsvermogen van 25 kW / 30 kVA leveren met een laadcapaciteit van 420 Ampère.
Naast de parallelle verbinding kunnen drie eenheden van hetzelfde model worden geconfigureerd voor een driefasige uitvoer. Maar dat is nog niet alles: tot wel 6 sets van drie units kunnen parallel worden aangesloten voor een 75 kW / 90 kVA omvormer en meer dan 1200 ampère laadcapaciteit.

Configuratie, bewaking en controle op locatie.

Instellingen kunnen binnen enkele minuten worden gewijzigd met de VEConfigure-software (computer of laptop en een MK3-USB-interface nodig).
Er zijn verschillende bewaking- en controle-opties beschikbaar: Color Control GX, Venus GX, Octo GX, CANvu GX, laptop, computer, Bluetooth (met de optionele VE.Bus Smart dongle), Battery Monitor, Digital Multi Control Panel.

Configuratie en bewaking op afstand

Installeer een Color Control GX of een ander GX-product om verbinding te maken met internet.
Operationele gegevens kunnen kosteloos worden opgeslagen en weergegeven op onze VRM-website (Victron Remote Management).
Na aansluiting op het internet kunnen systemen op afstand worden geopend en instellingen worden gewijzigd.

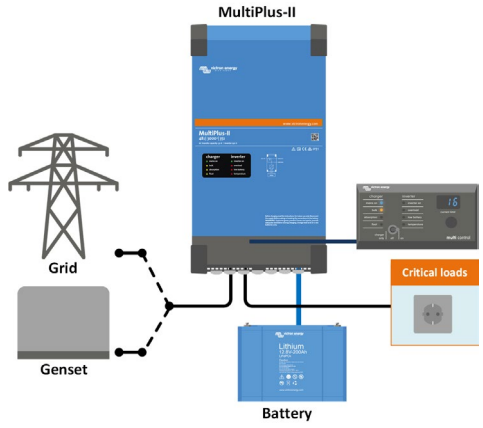

Standaard scheepvaart, mobiele of netonafhankelijke-toepassingen
Belastingen die moeten worden uitgeschakeld wanneer er geen AC-ingangsvermogen beschikbaar is, kunnen worden aangesloten op een tweede uitgang (niet getoond). De PowerControl- en PowerAssist-functie houden rekening met deze belastingen om de AC-ingangsstroom te beperken tot een veilige waarde wanneer wisselstroom beschikbaar is.

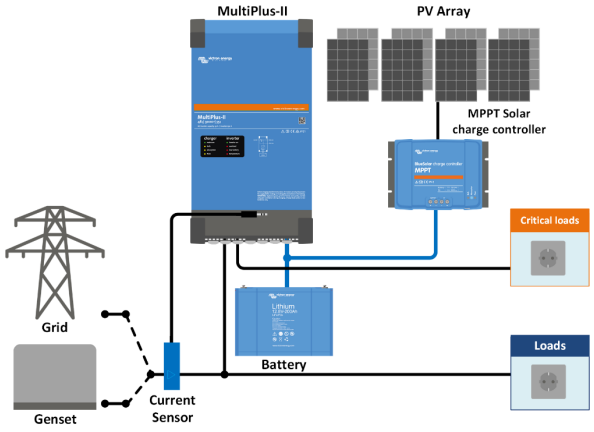

Stroomnet parallelle topologie met MPPT-zonnelaadcontroller
De MultiPlus-II zal gegevens van de externe AC-stroomsensor gebruiken (moet apart worden besteld) of die van de vermogensmeter om het eigen verbruik te optimaliseren en, indien nodig, om netvoeding te voorkomen. In het geval van een stroomstoring, zal de MultiPlus-II de minimale belasting blijven leveren.

GX Touch en Cerbo GX
Biedt intuïtieve systeembesturing en bewaking
Naast systeembewaking en -besturing biedt de Cerbo GX toegang tot onze gratis website voor bewaking op afstand: het VRM Online-portaal

VRM-portaal
Onze gratis website voor het op afstand bewaken (VRM) toont al uw systeemgegevens door middel van een begrijpelijke grafische interface. Systeeminstellingen kunnen op afstand via het portaal worden gewijzigd. Waarschuwingsnotificaties kunnen via email ontvangen worden.

VRM-app
Bewaak en beheer uw Victron Energy-systeem vanaf uw smartphone en tablet. Beschikbaar voor zowel iOS als Android.

VE.Bus Smart dongle
Meet de accuspanning en -temperatuur en maakt bewaking en controle mogelijk via een smartphone of een ander Bluetooth-apparaat.

MultiPlus-II 230V	12/3000/120-32 24/3000/70-32 48/3000/35-32	24/5000/120-50 48/5000/70-50	48/8000/ 110-100	48/10000/ 140-100	48/15000/ 200-100
PowerControl & PowerAssist	Ja				
Transfer-schakelaar	32 A	50 A	100 A	100 A	100 A
Maximale AC-ingangsstroom	32 A	50 A	100 A	100 A	100 A
OMVORMER					
DC-ingangsspanningsbereik	12V - 9,5–17 V	24V - 19–33V	48V – 38-66 V		
Uitgang	Uitgangsspanning: 230 VAC ± 2 % Frequentie: 50 Hz ± 0,1 % (1)				
Cont. uitgangsvermogen bij 25 °C 3)	3000 VA	5000 VA	8000 VA	10000 VA	15000 VA
Cont. uitgangsvermogen bij 25 °C	2400 W	4000 W	6400 W	8000 W	12000 W
Cont. uitgangsvermogen bij 40 °C	2200 W	3700 W	5500 W	7000 W	10000 W
Cont. uitgangsvermogen bij 65 °C	1700 W	3000 W	4000 W	6000 W	7000 W
Maximaal schijnbaar feed-in-vermogen	3000 VA	5000 VA	8000 VA	10000 VA	15000 VA
Piekvermogen	5500 W	9000 W	15000 W	18000 W	27000 W
Maximale efficiëntie	93 % / 94 % / 95 %	96 %	95 %	96 %	95 %
Nullastvermogen	13 / 13 / 11 W	18 W	29 W	38 W	55 W
Nullastvermogen in AES-modus	9 / 9 / 7 W	12 W	19 W	27 W	39 W
Nullastvermogen in Zoekmodus	3 / 3 / 2 W	2 W	3 W	4 W	6 W
LADER					
AC-ingang	Ingangsspanningsbereik: 187-265 VAC Ingangsfrequentie: 45 – 65 Hz				
'Absorptie'-laadspanning	14,4 / 28,8 / 57,6 V				
'Float'-laadspanning	13,8 / 27,6 / 55,2 V				
Opslagmodus	13,2 / 26,4 / 52,8 V				
Maximale acculaadstroom (4)	120 /70 / 35 A	120 / 70 A	110 A	140 A	200 A
Accu temperatuursensor	Ja				
ALGEMEEN					
Hulpuitgang	Ja (32 A)		Ja (50 A)		
Externe AC-stroomsensor (optioneel)	50 A		100 A		
Programmeerbaar relais (5)	Ja				
Beveiliging (2)	a - g				
VE.Bus-communicatiepoort	Voor parallelle (niet voor 8k-, 10k- en 15k-modellen)en driefasige werking, bewaking- en systeemintegratie op afstand				
Communicatiepoort voor algemene doeleinden	Ja, 2x				
Op afstand bediende aan/uit-functie	Ja				
Bedrijfstemperatuurbereik	-40 tot +65 °C (koeling met behulp van ventilator)				
Luchtvochtigheid (geen condensvorming)	max 95 %				
BEHUIZING					
Materiaal & Kleur	staal, blauw RAL 5012				
Beschermingscategorie	IP22				
Accu-aansluiting	M8 bouten		Vier M8 bouten (2 plus- en 2 min-aansluitingen)		
230 V AC-aansluiting	Schroefklemmen 13 mm² (6 AWG)		Bouten M6		
Gewicht	19 kg	30 kg	42 kg	49 kg	80 kg
Afmetingen (hxbxd)	546 x 275 x 147 499 x 268 x 141 499 x 268 x 141	607 x 330 x 149 565 x 320 x 149	642 x 363 x 206	677 x 363 x 206	810 x 405 x 217
NORMEN					
Veiligheid	EN-IEC 60335-1, EN-IEC 60335-2-29, EN-IEC 62109-1, EN-IEC 62109-2				
Emissie, immuniteit	EN 55014-1, EN 55014-2 EN-IEC 61000-3-2, EN-IEC 61000-3-3 IEC 61000-6-1, IEC 61000-6-2, IEC 61000-6-3				
Ononderbroken voeding	Raadpleeg de certificaten op onze website				
Eilandbedrijf-beveiliging	Raadpleeg de certificaten op onze website				

1) Kan worden aangepast tot 60 Hz
2) Beveiligingssleutel:
a) kortsluiting bij uitgang
b) overbelasting
c) accuspanning te hoog
d) accuspanning te laag
e) temperatuur te hoog
f) 230 VAC op omvormeruitvoer
g) ingangsspanning met een te hoge rimpel

3) Niet-lineair belasting, topfactor 3:1
4) Tot 25 °C omgevingstemperatuur
5) Programmeerbaar relais dat kan worden ingesteld voor algemene waarschuwingsnotificaties, DC-onderspanning of genset-start/stop-functie. AC-classificatie: 230 V / 4 A, DC-classificatie: 4 A tot 35 VDC en 1 A tot 60 VDC

Verbindingsgebied

Stroomsensor 100 A: 50 mA
Om PowerControl en PowerAssist te implementeren en om het eigen verbruik te optimaliseren met externe stroomdetectie.
Maximumstroom: 50 A tot 100 A.
Lengte van de verbindingskabel: 1 m.

Digitaal Multicontrolepaneel
Een handige en goedkope oplossing voor bewaking op afstand, met een draaiknop om de PowerControl- en PowerAssist-niveaus in te stellen.

Victron Energy B.V. | De Paal 35 | 1351 JG Almere | Nederland
Email: sales@victronenergy.com | **www.victronenergy.com**

C.1.11. Victron Multiplus II - GX datasheet

This product is a combination of the Victron Multiplus II and the Victron CCGX manufacturer controller. Scroll down for datasheet

MultiPlus-II GX Omvormer/Acculader

MultiPlus-II 24/3000/70-32 GX, 48/3000/35-32 GX & 48/5000/70-50 GX

Een MultiPlus-II met LCD en GX-functionaliteit

De MultiPlus-II GX integreert een MultiPlus-II omvormer/acculader en een GX apparaat met een 2 x 16 character-scherm.

Scherm en Wi-Fi

Het scherm leest de parameters van de accu, omvormer en zonne-oplaadcontroller.
Dezelfde parameters zijn toegankelijk met een smartphone of een ander Wi-Fi-apparaat.

GX-apparaat

Het geïntegreerde GX-apparaat omvat:

- Een BMS-Can interface. Dit kan gebruikt worden om verbinding te maken met een compatibele CAN-bus beheerde accu. Merk op dat dit geen VE.Can compatibele poort is.
- Een USB-poort.
- Een Ethernet-poort.
- Een VE.Direct-poort.

Toepassingen

De MultiPlus-II GX is bedoeld voor toepassingen waarbij extra interfacing met andere producten en/of bewaking op afstand vereist is, zoals off-grid of op het netwerk aangesloten energieopslagsystemen en bepaalde mobiele toepassingen.

Parallelle en driefasige werking

Er is slechts één GX-eenheid nodig in het geval van parallelle en driefasige werking.

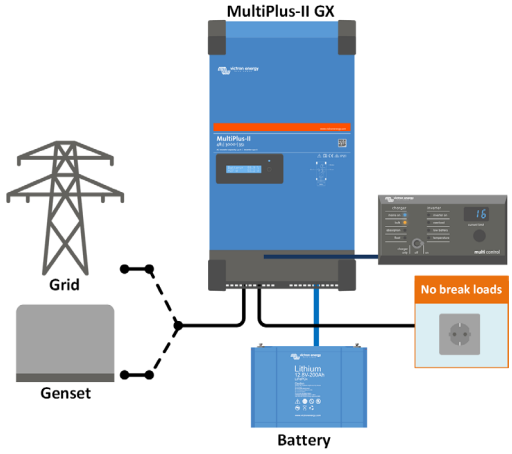

Standaard marine, mobiele of off-grid toepassing

Ladingen die moeten worden uitgeschakeld wanneer er geen wisselstroom beschikbaar is, kunnen worden aangesloten op een tweede uitgang (niet weergegeven). Met deze ladingen wordt rekening gehouden door de PowerControl- en PowerAssist-functie om de wisselstroom te beperken tot een veilige waarde wanneer deze beschikbaar is.

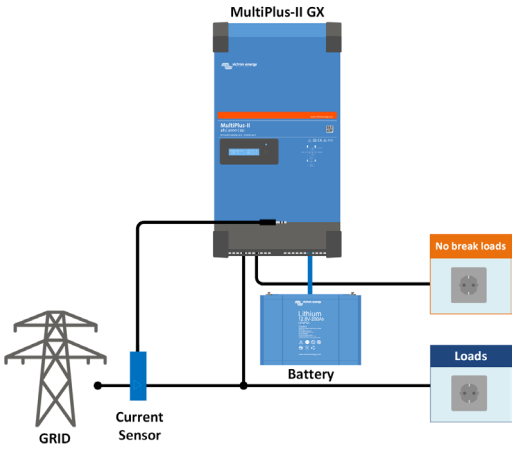

Standaard mobiele of off-grid-applicatie met externe stroomsensor

Maximaal stroombereik: 50 A resp 100 A

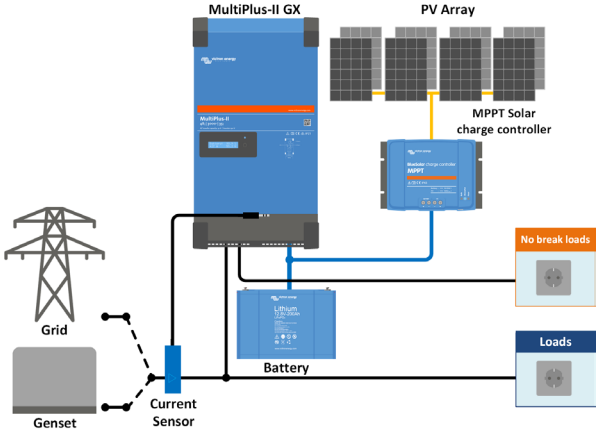

Raster-parallelle topologie met MPPT zonnelaadregelaar

De MultiPlus-II gebruikt gegevens van de externe wisselstroomsensor (apart te bestellen) of vermogensmeter om het zelfverbruik te optimaliseren en, indien nodig, netvoeding te voorkomen. In het geval van een stroomstoring zal de MultiPlus-II de minimale lading blijven leveren

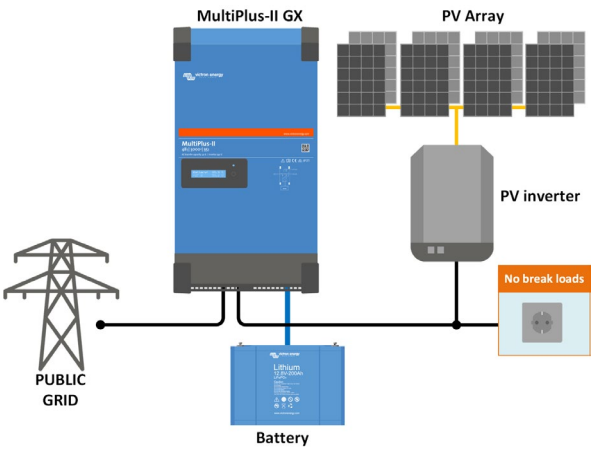

Raster in-line topologie met PV-omvormer

PV-vermogen wordt direct omgezet in AC.
De MultiPlus-II zal overtollig PV-vermogen gebruiken om de accu op te laden of om stroom terug te voeren naar het net en zal de accu ontladen of stroom van het net gebruiken om een tekort aan PV-vermogen aan te vullen. In het geval van een stroomuitval, zal de MultiPlus-II het netwerk loskoppelen en de lading blijven leveren.

VRM-portaal
Onze gratis externe monitoring-website (VRM) geeft al uw systeemgegevens weer in een uitgebreid grafisch formaat. Systeeminstellingen kunnen op afstand worden gewijzigd via het portaal. Waarschuwingen kunnen per email worden ontvangen.

VRM-app voor Wi-Fi
Monitor en beheer uw Victron Energy-systeem vanaf uw smartphone en tablet. Beschikbaar voor zowel iOS als Android.

GX GSM
Een mobiele modem; biedt mobiel internet voor het systeem en verbinding met Victron Remote Management (VRM).
Optioneel: GSM-antenne buiten en GPS-antenne.
Voer voor meer details *GX GSM* in het zoekvak op onze website in

MultiPlus-II GX	24/3000/70-32	48/3000/35-32	48/5000/70-50
PowerControl & PowerAssist	Ja		
Transfer-schakelaar	32 A		50 A
Maximale AC-ingangsstroom	32 A		50 A
Hulpuitgang	Ja (32 A)		
OMVORMER			
DC-ingangsspanningsbereik	19 – 33 V	38 – 66 V	
Uitgang	Uitgangsspanning: 230 VAC ± 2 % Frequentie: 50 Hz ± 0,1 % (1)		
Cont. uitgangsvermogen bij 25 °C (3)	3000 VA		5000 VA
Cont. uitgangsvermogen bij 25 °C	2400 W		4000 W
Cont. uitgangsvermogen bij 40 °C	2200 W		3700 W
Cont. uitgangsvermogen bij 65 °C	1700 W		3000 W
Maximaal schijnbaar feed-in-vermogen	3000 VA		5000 VA
Piekvermogen	5500 W		9000 W
Maximale efficiëntie	94 %	95 %	96 %
Nullastvermogen	13 W	11 W	18 W
Nullastvermogen in AES-modus	9 W	7 W	12 W
Nullastvermogen in Zoekmodus	3 W	2 W	2 W
LADER			
AC-ingang	Ingangsspanningsbereik: 187-265 VAC Ingangsfrequentie: 45 – 65 Hz		
'Absorptie'-laadspanning	28,8 V	57,6 V	
'Float'-laadspanning	27,6 V	55,2 V	
Opslagmodus	26,4 V	52,8 V	
Maximale acculaadstroom (4)	70 A	35 A	70 A
Accu temperatuursensor	Ja		
ALGEMEEN			
Interfaces	BMS-Can, USB, ethernet, VE.Direct, WiFi		
Externe AC-stroomsensor (optioneel)	50 A		100 A
Programmeerbaar relais (5)	Ja		
Beveiliging (2)	a - g		
VE.Bus-communicatiepoort	Bewaking- en systeemintegratie op afstand voor parallelle en driefasige werking,		
Communicatiepoort voor algemene doeleinden	Ja, 2x		
Op afstand bediende aan/uit-functie	Ja		
Bedrijfstemperatuurbereik	-40 tot +65 °C (koeling met behulp van ventilator)		
Luchtvochtigheid (geen condensvorming)	max 95 %		
BEHUIZING			
Materiaal & Kleur	staal, blauw RAL 5012		
Beschermingscategorie	IP22		
Accu-aansluiting	M8 bouten		
230 VAC-aansluiting	Schroefklemmen 13 mm² (6 AWG)		
Gewicht	19 kg		30 kg
Afmetingen (hxbxd)	506 x 275 x 147		565 x 323 x 148
NORMEN			
Veiligheid	EN-IEC 60335-1, EN-IEC 60335-2-29, EN-IEC 62109-1, EN-IEC 62109-2		
Emissie, immuniteit	EN 55014-1, EN 55014-2 EN-IEC 61000-3-2, EN-IEC 61000-3-3 IEC 61000-6-1, IEC 61000-6-2, IEC 61000-6-3		
Ononderbroken voeding	IEC 62040-1		
Eilandbedrijf-beveiliging	Raadpleeg de certificaten op onze website		

1) Kan worden aangepast tot 60 Hz
2) Beveiligingssleutel:
a) kortsluiting bij uitgang
b) overbelasting
c) accuspanning te hoog
d) accuspanning te laag
e) temperatuur te hoog
f) 230 VAC op omvormeruitvoer
g) ingangsspanning met een te hoge rimpel
3) Niet-lineair belasting, topfactor 3:1
4) Tot 25 °C omgevingstemperatuur
5) Programmeerbaar relais dat kan worden ingesteld voor algemene waarschuwingsnotificaties, DC-onderspanning of genset-start/stop-functie. AC-classificatie: 230 V / 4 A, DC-classificatie: 4 A tot 35 VDC en 1 A tot 60 VDC

Verbindingsgebied

Huidige sensor 100 A: 50 mA
Om PowerControl en PowerAssist te implementeren en het zelfverbruik te optimaliseren met externe stroomdetectie.
Maximumstroom: 50 A resp. 100 A.
Lengte van de aansluitkabel: 1 m.

Digitaal Multibedieningspaneel
Een handige en voordelige oplossing voor monitoring op afstand, met een draaiknop om PowerControle- en PowerAssist-niveaus in te stellen.

Victron Energy B.V. | De Paal 35 | 1351 JG Almere | Nederland
Email: sales@victronenergy.com | **www.victronenergy.com**

C.1.12. PV system cost for Delft

Scroll down for datasheet

Informatiepakket Zonnepanelenactie gemeente Delft

Beste lezer,

Een dak met zonnepanelen levert u als bewoner duurzame energie, en al snel €700 tot €1.000 voordeel per jaar op. U bespaart zo flink op uw maandelijkse energierekening én draagt uw steentje bij aan het milieu. Om u hierbij te helpen, organiseert Regionaal Energieloket samen met gemeente Delft een zonnepanelenactie voor haar inwoners. Regionaal Energieloket organiseert regelmatig acties voor energiebesparende maatregelen en werkt hierbij samen met betrouwbare aanbieders uit de regio.

In dit informatiepakket leest u meer over de zonnepanelen en de actieprijzen. Regionaal Energieloket en de gemeente organiseren ook een informatieavond. U bent van harte uitgenodigd! Tijdens de avond kunt u uw vragen stellen aan Regionaal Energieloket, de gemeente en de installateur. U vindt de datum van de informatieavond op de website van Regionaal Energieloket. U kunt zich hier aanmelden voor de informatieavond en vrijblijvend inschrijven voor de zonnepanelenactie.

Over Regionaal Energieloket

Regionaal Energieloket helpt woningeigenaren met het verduurzamen van de woning. Het is ons doel om woningeigenaren te informeren over duurzame maatregelen voor de woning en hen te ondersteunen bij het treffen van maatregelen. Wij werken in opdracht van de gemeente Delft.

Heeft u alvast een vraag? Bel of mail Regionaal Energieloket gerust!

Fardeau Gradus
Projectmanager Regionaal Energieloket

088 525 4110
projecten@regionaalenergieloket.nl

Over deze zonnepanelenactie

Installateurs uit de regio zijn uitgenodigd om een aanbod in te dienen. Onafhankelijke adviseurs van Regionaal Energieloket hebben de aanbiedingen beoordeeld en het beste aanbod gekozen. Wij zoeken namelijk altijd naar een hoogwaardig aanbod met de beste prijs-kwaliteitverhouding. Dit is **niet noodzakelijk** het goedkoopste aanbod. In de beoordeling van het aanbod zijn ruim 50 aspecten meegenomen, verdeeld over de volgende thema's:

Bedrijf

- Certificaten
- Ervaring
- Capaciteit

Producten

- Kwaliteit zonnepanelen
- Kwaliteit omvormers

Prijs

- Pakketprijzen
- Betalingsvoorwaarden

Garanties

- Productgaranties
- Installatiegarantie

Voordelen voor u als woningeigenaar

Zonnepanelen aanschaffen via deze actie heeft een aantal voordelen. U krijgt een kwalitatieve installatie van een vakkundige installateur tegen een aantrekkelijke prijs. Regionaal Energieloket ziet toe op een goede uitvoering van de werkzaamheden.

1. **Kwaliteit**
   Er is veel werk gestoken in de selectie van een leverancier en de aangeboden producten. Het beste aanbod is gekozen op basis van ervaring, prijs-kwaliteitverhouding en garanties. Ook voeren we steekproefsgewijs controles uit bij geplaatste installaties om de kwaliteit te borgen.

2. **Prijsvoordeel**
   Regionaal Energieloket neemt een deel van het werk van de installateur uit handen zodat de installateur efficiënter kan werken. De installateur berekent dit voordeel door in de prijs.

3. **Maatwerk**
   Elke woning is anders. Daarom ontvangt u altijd een persoonlijk advies en een offerte. Collectief voordeel in combinatie met het benodigde maatwerk.

Een compleet verzorgde installatie

Het aanbod in deze actie bestaat uit een volledig werkend zonnepanelensysteem. Installatie van het systeem is inclusief **zonnepanelen**, **omvormer**, **montage**, **bekabeling** en **aansluiting** van het systeem op uw meterkast. De zonnepanelen kunnen op zowel een schuin als een plat dak worden geïnstalleerd. Hieronder leest u meer over het aanbod in deze actie.

Installateur

Enie.nl is geselecteerd als leverancier voor deze actie. Enie.nl heeft in 9 jaar al honderden installaties voor particulieren verzorgd. Ze zijn aangesloten bij Holland Solar en InstallQ. De installateurs zijn VCA gecertificeerd en werken via de geldende veiligheidsvoorschriften en richtlijnen. Regionaal Energieloket voert steekproefsgewijs onafhankelijke keuringen uit om hierop toe te zien.

Zonnepanelen

De panelen die zijn geselecteerd voor deze actie zijn van het merk Jinko Solar met een vermogen van 390 Wattpiek (Wp). Het zijn volledig zwarte monokristallijne panelen. De panelen scoren goed op prijs/kwaliteitsverhouding.

Meer weten over zonnepanelen? Ga naar onze kennisbank.

***Tip:** U kunt tijdens uw adviesgesprek met de installateur onderzoeken welke panelen het meest geschikt zijn voor uw situatie. Ook kan de installateur u adviseren hoeveel panelen u kunt plaatsen. De prijzen en garanties zijn verderop dit informatiepakket te vinden.*

Een compleet verzorgde installatie (II)

Omvormers

Een omvormer zet de opgewekte zonnestroom om in bruikbare elektriciteit. Standaard is dit een 'stringomvormer' waarbij de zonnepanelen in serie geschakeld worden. Valt er schaduw op (een groot deel van) de panelen gedurende de dag? Of heeft het dak verschillende hellingshoeken? Dan zijn 'power optimizers' een goed idee. Ze zorgen voor een optimale opbrengst per paneel. Bij power optimizers wordt ook een stringomvormer gebruikt maar zijn de panelen parallel geschakeld. In deze actie wordt beide aangeboden:

- Stringomvormer: Growatt
- Power optimizers: SolarEdge

Tip: *De adviseur denkt graag met u mee welk type omvormer het beste is voor uw situatie. De prijzen en garanties zijn te vinden verderop in dit informatiepakket.*

Meterkast

Binnenhuis worden de zonnepanelen aangesloten op de meterkast. Vanaf een bepaald minimum aan opgewekte stroom is het wettelijk verplicht om een extra groep aan te leggen in de meterkast. Voor extra veiligheid en zekerheid, legt de installateur een vrije groep aan bij de installatie. Op pagina 12 vertellen we u meer over de aanpassingen die u kunt verwachten aan de meterkast en bijkomende kosten.

Tip*: als u de meterkast laat aanpassen als onderdeel van de zonnepaneleninstallatie mag u de 21% btw over de kosten terugvragen bij de Belastingdienst.*

Het proces van deze actie

1

Vrijblijvend Inschrijven

U kunt zich via de website van Regionaal Energieloket inschrijven. Ga naar www.regionaalenergieloket.nl en vul uw postcode in. U vindt daar ook de einddatum voor inschrijving. Wacht niet te lang met inschrijven; als u zich eerder inschrijft bent u ook eerder aan de beurt. Er is bovendien beperkte capaciteit beschikbaar van de installateur.

2

Inplannen adviesgesprek

U ontvangt een e-mail van Enie.nl met een link waarmee u zelf een afspraak plant voor een online / telefonisch adviesgesprek.

3

Woningopname en adviesgesprek

Enie.nl heeft speciale software waarmee zij op afstand een goede offerte kunnen opstellen. Zij vragen u wat foto's aan te leveren. Zo bouwt de adviseur een goed beeld op van uw woning. De adviseur kan uw vragen beantwoorden en denkt graag mee over de juiste oplossing voor uw woning en wensen.

4

Persoonlijke offerte

De adviseur geeft u een persoonlijke offerte. De offerte volgt de prijzen zoals u die vindt in dit informatiepakket.

5

Installatie

Als u akkoord geeft op de offerte, bent u officieel akkoord met de opdracht. U plant samen met Enie.nl een dag in waarop de werkzaamheden worden uitgevoerd (max. 3 maanden na akkoord offerte, tenzij anders overeengekomen). De installatie van het volledige zonnepanelensysteem neemt 1 tot 2 dagen in beslag.

Genieten en besparen!

Pakketprijzen (1 van 2)

Schuin dak met basispaneel Trina Solar en GroWatt omvormer

U bepaalt samen met de installateur hoeveel panelen u wilt laten plaatsen. De keuze is van meerdere factoren afhankelijk, zoals de mogelijkheden van het dak (ruimte, schaduw, etc.) en uw (toekomstige) elektriciteitsverbruik. De meerprijs voor installatie op een plat dak bedraagt 32,5 euro per paneel exclusief btw.

Aantal panelen	Totaal vermogen (Wattpiek)	Type omvormer (GroWatt)	Prijs incl. groepskorting (incl. btw)	Prijs incl. groepskorting (excl. btw)*	Gemiddelde opbrengst (kWh/jaar)	Jaarlijkse Besparing (euro's)**
6	2.340	Growatt MIN 2500TL-XE Inverter 1PH	€3.532	€2.919	1.989	€935
7	2.730	Growatt MIN 2500TL-XE Inverter 1PH	€3.853	€3.184	2.321	€1.091
8	3.120	Growatt MIN 3000TL-XE Inverter 1PH	€4.140	€3.422	2.652	€1.246
9	3.510	Growatt MIN 3000TL-XE Inverter 1PH	€4.419	€3.652	2.984	€1.402
10	3.900	Growatt MIN 3600TL-XE Inverter 1PH	€4.757	€3.931	3.315	€1.558
11	4.290	Growatt MIN 4200TL-XE Inverter 1PH	€5.196	€4.294	3.647	€1.714
12	4.680	Growatt MIN 4600TL-XE Inverter 1PH	€5.501	€4.547	3.978	€1.870
13	5.070	Growatt MIN 5000TL-XE Inverter 1PH	€5.728	€4.734	4.310	€2.025
14	5.460	Growatt MIN 5000TL-XE Inverter 1PH	€6.001	€4.960	4.641	€2.181
15	5.850	Growatt MIN 5000TL-XE Inverter 1PH	€6.480	€5.355	4.973	€2.337
16	6.240	Growatt MIN 6000TL-XE Inverter 1PH	€6.865	€5.673	5.304	€2.493
17	6.630	Growatt MIN 6000TL-XE Inverter 1PH	€7.017	€5.800	5.636	€2.649
18	7.020	Growatt MIN 6000TL-XE Inverter 1PH	€7.339	€6.065	5.967	€2.804
19	7.410	Growatt MIN 6000TL-XE Inverter 1PH	€7.782	€6.431	6.299	€2.960
20	7.800	Growatt MIN 6000TL-XE Inverter 1PH	€8.149	€6.735	6.630	€3.116

* Particulieren die niet actief zijn als ZZP-er kunnen in veel gevallen de btw op zonnepanelen op dit moment terugvragen bij de Belastingdienst. U kunt uw vragen ook aan de adviseur stellen.

** Op basis van het gemiddelde prijspeil voor stroom in 2022 van 47 cent per kWh.

Pakketprijzen (2 van 2)

Schuin dak met basispaneel Trina Solar en SolarEdge

U bepaalt samen met de installateur hoeveel panelen u wilt laten plaatsen. De keuze is van meerdere factoren afhankelijk, zoals de mogelijkheden van het dak (ruimte, schaduw, etc.) en uw (toekomstige) elektriciteitsverbruik. De meerprijs voor installatie op een plat dak bedraagt 32,5 euro per paneel exclusief btw.

Aantal panelen	Totaal vermogen (Wattpiek)	Type omvormer (SolarEdge)	Prijs incl. groepskorting (incl. btw)	Prijs incl. groepskorting (excl. btw)*	Gemiddelde opbrengst (kWh/jaar)	Jaarlijkse Besparing (euro's)**
6	2.340	SolarEdge SE2200 HD	€4.109	€3.396	2.106	€990
7	2.730	SolarEdge SE2200 HD	€4.442	€3.671	2.457	€1.155
8	3.120	SolarEdge SE3000 HD	€4.813	€3.978	2.808	€1.320
9	3.510	SolarEdge SE3500 HD	€4.944	€4.086	3.159	€1.485
10	3.900	SolarEdge SE3680 HD	€5.708	€4.717	3.510	€1.650
11	4.290	SolarEdge SE4000 HD	€6.081	€5.026	3.861	€1.815
12	4.680	SolarEdge SE4000 HD	€6.408	€5.295	4.212	€1.980
13	5.070	SolarEdge SE4000 HD	€6.655	€5.500	4.563	€2.145
14	5.460	SolarEdge SE5000 HD	€7.023	€5.804	4.914	€2.310
15	5.850	SolarEdge SE5000 HD	€7.464	€6.169	5.265	€2.475
16	6.240	SolarEdge 6000H	€7.966	€6.584	5.616	€2.640
17	6.630	SolarEdge 6000H	€8.287	€6.848	5.967	€2.804
18	7.020	SolarEdge 6000H	€8.752	€7.233	6.318	€2.969
19	7.410	SolarEdge 6000H	€9.024	€7.458	6.669	€3.134
20	7.800	SolarEdge 6000H	€9.490	€7.843	7.020	€3.299

* Particulieren die niet actief zijn als ZZP-er kunnen in veel gevallen de btw op zonnepanelen op dit moment terugvragen bij de Belastingdienst. U kunt uw vragen ook aan de adviseur stellen.

** Op basis van het gemiddelde prijspeil voor stroom in 2022 van 47 cent per kWh.

Maatwerk

Iedere woning is net anders. Hierdoor zijn er soms extra werkzaamheden nodig om de zonnepanelen goed en veilig te installeren. Wij hebben als Regionaal Energieloket een lijst met mogelijk meerwerk opgesteld en de kosten van te voren vastgelegd met de installateur. Zo weet u waar u aan toe bent en bent u verzekerd van maatwerk. U vindt de meerprijzen hieronder exclusief btw*. Als u in aanmerking komt mag u de btw over de volledige offerteprijs namelijk terugvragen van de Belastingdienst.

Omschrijving	Meerprijs exclusief btw*
Rolsteiger/dakrandbeveiliging	Inbegrepen
Kapot geraakte pannen vervangen (indien voorradig)	Inbegrepen
Basis hak- en breekwerk	Inbegrepen
Aanleggen eigen groep voor zonnepanelen	Inbegrepen
Leveren en aansluiten monitoring	Inbegrepen
Meerdere aparte dakvlakken	€100 per extra dakvlak
Steil dak (45-59 graden)	€7,50 per paneel
Verwijderen/verplaatsen pijpjes (indien mogelijk)	€100 per pijpje
Powerline	€50
Splitter voor ethernet	€50
Wifi versterker	€50
Nieuwe hoofdschakelaar	Tussen de €100 en €125
Ombouwen meterkast van 1-fase naar 3-fase	Tussen de €300 en €750
Hoogwerker (of plat dak vanaf tweede verdieping)	Maatwerk, ongeveer €350
Moeilijk bereikbaar dak	Vanaf €100
Hak en breekwerk: additionele wensen	Maatwerk
Nieuwe groepenkast	Maatwerk
Graafwerkzaamheden	Maatwerk
Extra werk dakconstructie	Maatwerk
Stroomverzwaring (1 naar 3 fase)	Netbeheerder (€200-€300)
Speciale maatwerkwensen klant	Tegen meerkosten in overleg

* Particulieren die niet actief zijn als ZZP-er kunnen in veel gevallen de btw op zonnepanelen op dit moment terugvragen bij de Belastingdienst. U kunt uw vragen ook aan de adviseur stellen.

D

Cost analysis

In this chapter, an indicative cost analysis is done for the two types of experimental setup using different types of ESS. This is done as the experimental setup built are indicative of what can be implemented in the future for a residential household with a PV system installed and the cost of these system designs should be analysed to establish the most cost effective solution. The first way this is done is to establish a common PV system found in many households and calculate how much the cost are for such a PV system. Then the cost for upgrading such a system is calculated using available products on the market. Then the cost for an integrated of a PV system with an ESS is calculated using the same available products. Then fnially the cost between the integrated solution and upgraded solution is compared to one another. This chapter is thus composed out of the following sections. Firstly, a common PV system found in many households is given with the assumptions made for the upgraded system given in section D.1. Secondly, section D.2 discusses the types of ESS used for both the upgraded and integrated solution and the reasoning behind using such ESS types. Furthermore, the connection type (DC or AC connection) is considered for both solution using both types of ESS. Based on this, the total cost is calculated for both ESS and connection types for the upgraded solution and is explained in section D.3. Finally the same procedure is done to calculate the total cost for the integrated solution using both ESS and connection types in section D.4. A summary of these findings is given in section D.5 with the most cost effective system design given aswell.

D.1. Existing PV system setup and assumptions made

For an existing PV system installed for a household, figure D.1 illustrates the electrical diagram of such a typical PV system. The following assumptions are made for this.

1. The PV system considered is a 2.34 kWp system with 6 solar panels installed (each outputting a maximum of 390 W).
2. It is assumed that the MPPT is built into the PV inverter and there is no individual power optimizer for each panel.
3. It is assumed that the main controller used is the Victron main controller used for the AC connected ESS experimental setup and the main controller has a setting to switch on power or voltage control.
4. It is asssumed that the ESS or main inverter used for the upgraded or integrated solution is the Victron inverter used for both experimental setup and does not suffer from the inverter delay explained in section 5.5. Thus the inverter reacts right away and avoids any voltage flickers from occurring.
5. For the upgraded solution, it is assumed that the PV inverter cannot communicate or interface with the the main controller. While for the integrated solution, it is assumed that this is possible.
6. For both solutions with a DC connected ESS, the DC bus voltage is rated for 48V.
7. The prices of the devices are in euros (€) and were last updated on the October 2 2023.
8. For the integrated solution, when integrating multiple devices with one another it assumed that the prices of the devices are added with each other to calculate the price of the integrated device. For example, if the main controller (€232) is integrated with the bidirectional inverter (€1084) then the total cost of this new integrated device would cost €1316.
9. For the profit made for the company when installing a BESS, the price of this is assumed to be 40% of the profit made for installing a PV system. This is due to the installation of the PV system being much more work than installing a BESS. The values used for this assumption are from the installation cost explained in the document from regionaal energieloket.

10. Based on the preceding assumption for the upgraded solution, the installation is taken into account twice as it is assumed that the homeowner installed the PV system first and then later on a BESS. For the integrated solution, the installation cost is only taken into account once and then the cost of this is adjusted based on the PV system needs and BESS integration cost.

Based on these assumptions, the cost for the PV system was based on a cost analysis from Regionaal Energieloket for the Delft municipality. Based on their cost analysis and assumptions, the total cost for the PV system was calculated to be around €4047. The PV system for this cost makes use of a Growatt MIN 2500TL-XE 1PH solar inverter C.1.12, which cost around €400 on the market, with six Trina Solar 390 Wp solar panels connected to the inverter. One solar panels costs around €150 on the market.

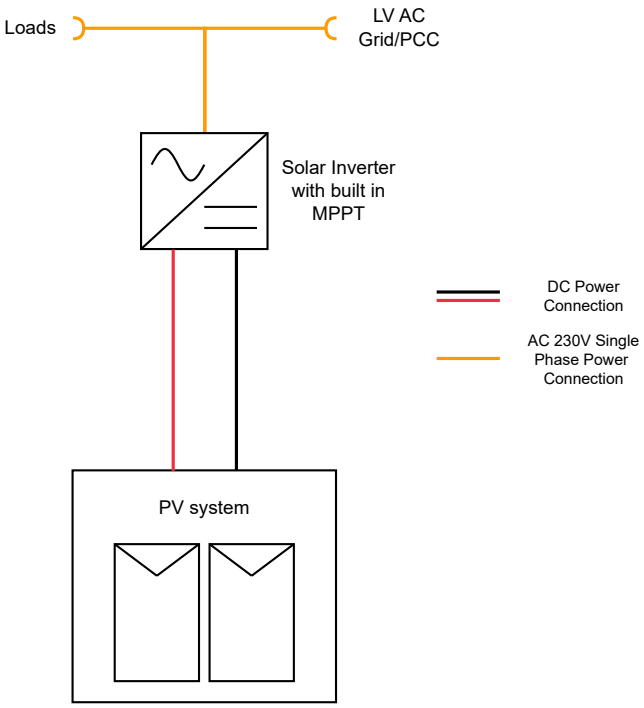

Figure D.1: Typical PV system installed for a household.

D.2. Types of ESS considered

For the types of ESS considered for the implementation for both solutions, the two main types of ESS considered are the BESS and SESS. This is mainly based on the findings from section 2.2. The type of SESS considered for implementation is the EDLC supercapacitor as it has the highest cycle lifetime and power to energy ratio. For the cost analysis, the SkelMod 102V88F from Skeleton Technologies [C.1.8] is used. For the implementation of this SESS, a DC/DC converter has to be connected to the SESS in order to be connected to either the DC or AC bus with the PV system. This is due to the wide voltage range of the supercapacitor as the SoC of the supercapacitor changes and is highlighted in figure D.2a. If a DC/DC converter is not connected to the SESS then in a case where the SESS is connected the same DC bus with the PV system then the DC bus voltage varies allot and thus a improper operation of the PV system can be observed. In the case when the SESS is connected to the same AC bus with the PV system, then the inverter connected to the SESS will no operate properly due to the Victron inverter having a input voltage range for operation of between 38-66 V. For the cost analysis, the Eltek 48V 18-75V DC-DC Converter from Eltek is used as the DC/DC converter [C.1.9]. This DC/DC converter has a wide input voltage range with a 48V output, this results in about 50% of SESS capacity being used (or around 65 Wh) which is well within the values measured for the energy usage from the experimental setups highlighted in section 5.5.
For the type of BESS considered, an LFP battery pack is used for the implementation of both solutions. The reason behind this is not only due to its high power density and cycle lifetime compared to the rest of the types of BESS, but also the characteristic voltage versus SoC curve for LFP cells provides an advantage for implementation. Figure D.2b illustrates this characteristic voltage versus SoC curve and as can be observed between the range of 10% to 95% SoC the cell voltage of the LFP cell remains fairly constant. This is advantageous to implement on a DC bus as then the DC bus voltage remain fairly constant even when the LFP battery pack is connected without any DC/DC converter in between. This can be achieved when the BESS operates around 50% SoC, highlighted by the red line in figure D.2b, as due to the low energy usage the pack voltage of the BESS will not fluctuate. This is mainly due to the cell voltage of the LFP cells remain constant around this SoC range. Furthermore this type of BESS can be easily implemented with the Victron inverter which has a limited input voltage range for operation as highlighted before. For the cost analysis the Pylontech US2000C LFP battery pack from Pylontech is

considered [C.1.7].

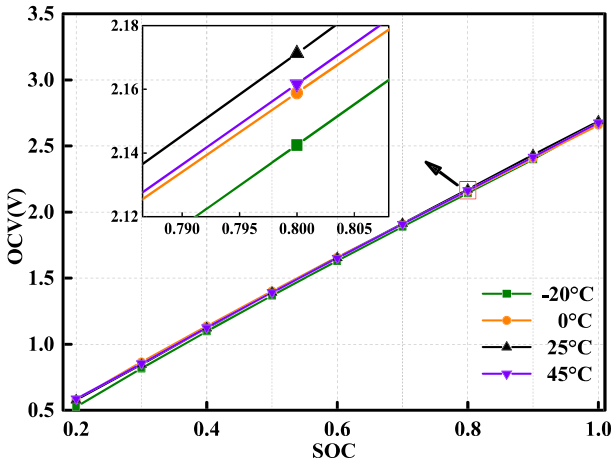

(a) Example of the OCV versus SoC curve of a supercapacitor cell at different temperatures [44].

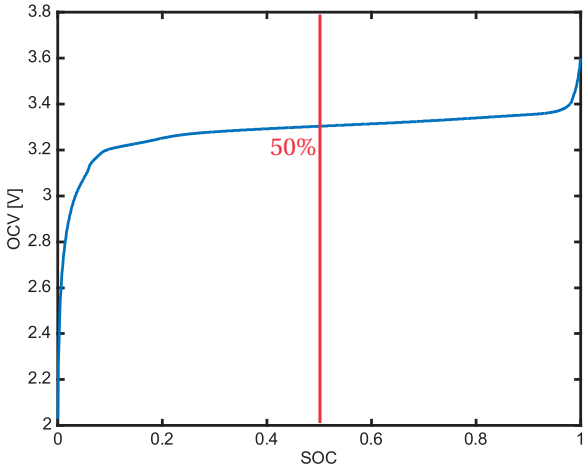

(b) Example of the OCV versus SoC curve of a LFP cell [45].

Figure D.2: OCV versus SoC curve of the different types of ESS used for the cost analysis.

D.3. Cost of an upgraded solution

For the upgraded solution, it was assumed (based on section D.1) that the solar inverter installed in the household cannot communicate or interface with the main controller. Based on this, extra measurement devices which can communicate and interface with the main controller has to be installed.

D.3.1. AC connected BESS system cost

For the AC connected BESS system as an upgraded solution, figure D.3 illustrates the electrical diagram of this system and is comparable to the experimental setup commissioned for this research which is explained in section 4.1. The highlighted yellow devices in the diagram are the devices that needs to be installed when upgrading the system with a BESS for proper operation.

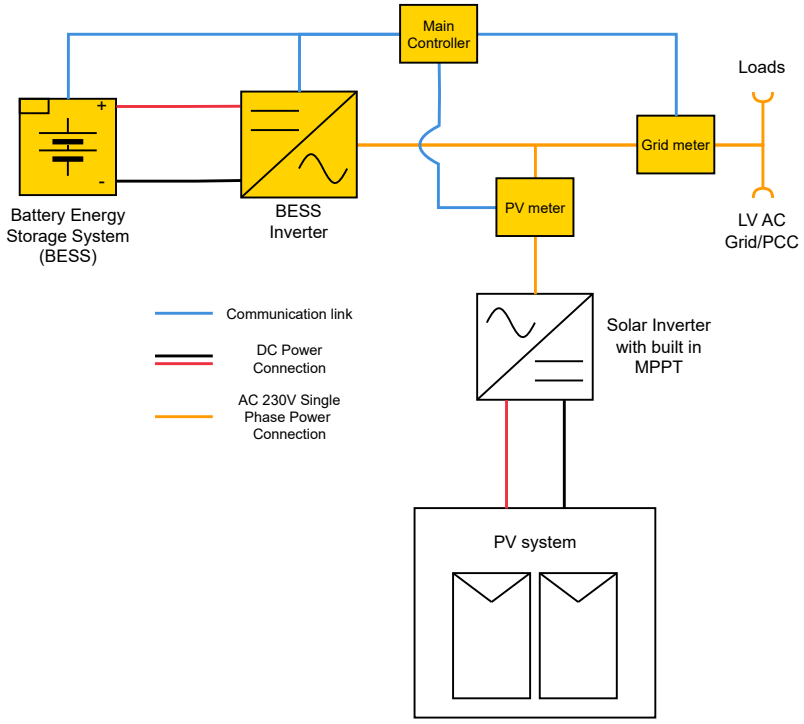

Figure D.3: Electrical diagram of an AC connected BESS for the upgraded solution. The devices highlighted in yellow are the devices that needs to be installed for the upgrade with a BESS.

Based on the highlighted devices that needs to be installed and the cost of installing the PV system, the total cost was calculated and is highlighted in table D.3.1. The total cost for this system is around €8089.80 and, taking into the base cost of the PV system from section D.1, this is 199.90% more costly than just installing a PV system for the household.

	Price (€)
BESS	900
Main Inverter	1084
Main Controller	232
PV Meter	242
Grid Meter	242
Installation cost	1117.8
PV system cost	4271
Total Price	8089.80

Table D.1: Cost of an AC connected BESS system upgrade.

D.3.2. DC connected BESS system cost

For the DC connected BESS system as an upgraded solution, figure D.4 illustrates the electrical diagram of this system and is also comparable to the experimental setup commissioned for this research which is explained in section 4.2. The highlighted yellow devices in the diagram are the devices that needs to be installed when upgrading the system with a BESS for proper operation.

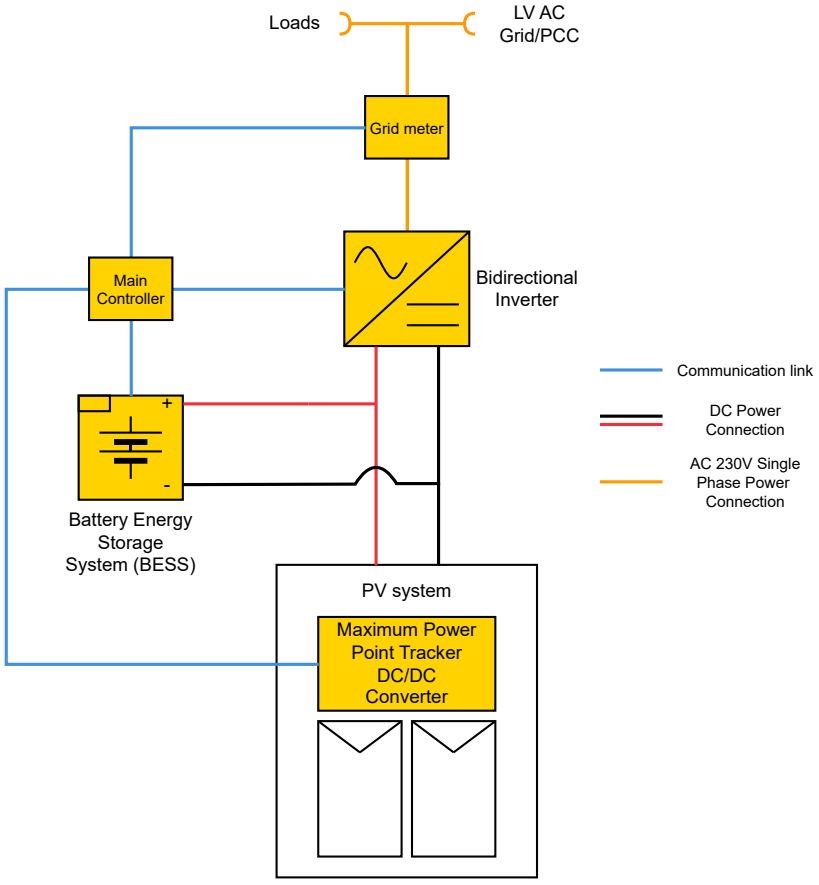

Figure D.4: Electrical diagram of an DC connected BESS for the upgraded solution. The devices highlighted in yellow are the devices that needs to be installed for the upgrade with a BESS.

Based on the highlighted devices from figure D.4 compared to a normal PV system given in figure D.1, it can be observed that the previously installed solar inverter has to be removed to install a MPPT DC/DC converter with a bidirectional inverter. Then the BESS is connected to the DC bus with the PV system to the bidirectional inverter, which is controlled by the main controller. Finally since the MPPT DC/DC converter is from Victron, this device can communicate all of its values to the main controller. The was done for the DC connected ESS experimental setup explained in section 4.2. Based on this, the total cost for this upgrade was calculated and is given in table D.3.2.

	Price (€)
BESS	900
Main Inverter	1084
Main Controller	232
MPPT DC/DC Converter	627.90
Grid Meter	242
Installation cost	1117.8
PV system cost	4271
Total Price	8475.70

Table D.2: Cost of an DC connected BESS system upgrade.

The total cost for this system is around €8475 and, taking into account the base cost of the PV system from section D.1, this is 209.43% more costly than just installing a PV system for the household.

D.3.3. AC connected SESS system cost

For this solution with a SESS and as highlighted in section D.2, the SESS has to first be connected to a DC/DC converter and then to the bidirectional SESS inverter. This can be observed from the electrical diagram for this solution in figure D.5. This is the main difference with the AC connected BESS upgraded solution explained in section D.3.1.

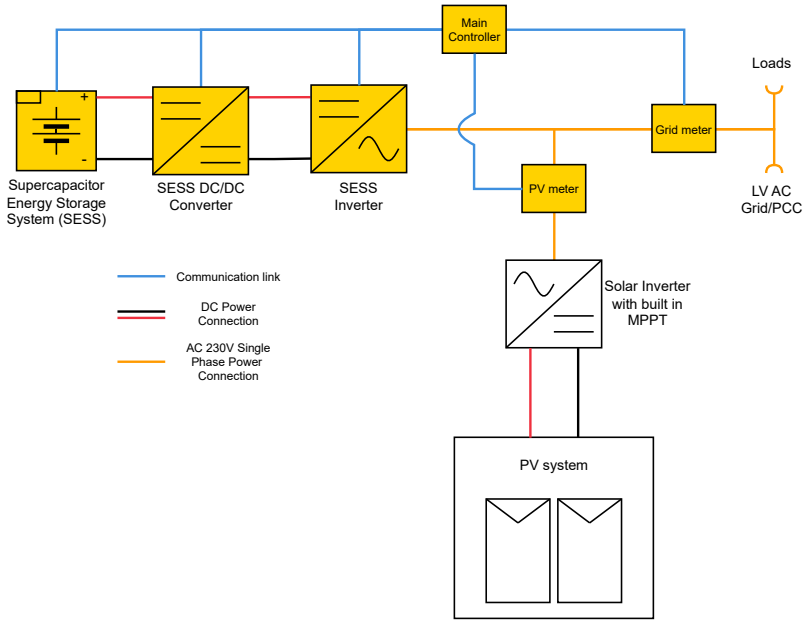

Figure D.5: Electrical diagram of an AC connected SESS for the upgraded solution. The devices highlighted in yellow are the devices that needs to be installed for the upgrade with a SESS.

Based on the figure above, the total cost for this system upgrade was calculated and is given in table D.3.3. The total cost for this system is around €10769.80 and ,taking into the base cost of the PV system from section D.1, this is 266.12% more costly than just installing a PV system for the household.

	Price (€)
SESS	3000
DC/DC SESS Converter	580
SESS Inverter	1084
Main Controller	232
PV Meter	242
Grid Meter	242
BESS installation cost	1117.80
PV system cost	4271
Total Price	10769.80

Table D.3: Cost of an AC connected SESS system upgrade.

D.3.4. DC connected SESS system cost

Much like the SESS solution presented in the previous, a DC/DC converter has to be connected between the SESS and the DC bus. This is the main difference between the DC connected BESS upgraded system apart from the different ESS type. Figure D.6 illustrates the electrical diagram for this upgrade solution.

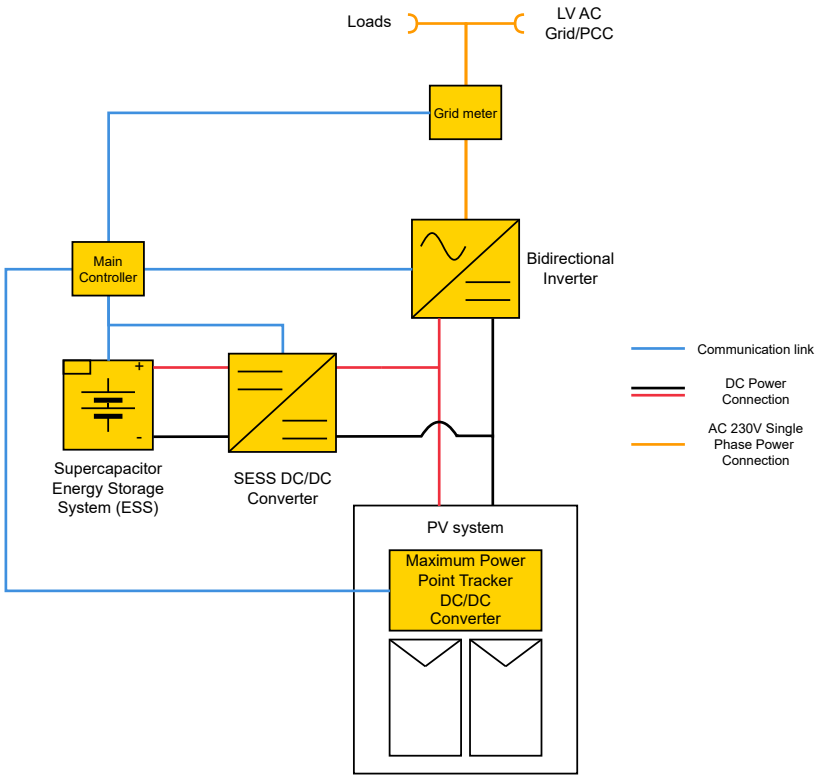

Figure D.6: Electrical diagram of an DC connected SESS for the upgraded solution. The devices highlighted in yellow are the devices that needs to be installed for the upgrade with a SESS.

Based on the figure above, the total cost for this system upgrade was calculated and is given in table D.3.4. The total cost for this system is around €11155.70 and ,taking into the base cost of the PV system from section D.1, this is 275.65% more costly than just installing a PV system for the household.

	Price (€)
SESS	3000
DC/DC SESS Converter	580
SESS Inverter	1084
Main Controller	232
MPPT DC/DC Converter	627.90
Grid Meter	242
Installation cost	1117.80
PV system cost	4271
Total Price	11155.70

Table D.4: Cost of an DC connected SESS system upgrade.

D.4. Cost of an integrated solution

For the integrated solution, it was assumed (based on the assumptions from section D.1), it was assumed that all of the devices from the system can communicate with the main controller. Furthermore, several devices are also integrated with each other to create one single device. This is to lower the device count for the system and thus achieve a more compact solution. Furthermore the installation cost and profit made for the company installing the system is accounted for once. This is due to the system already having the ESS integrated with the PV system and thus the installation only takes place once.

D.4.1. AC connected BESS system cost

For the AC connected BESS integrated solution, figure D.7 illustrates the electrical diagram of the integrated solution. It can be observed that the main controller and BESS inverter is integrated with each other as such solutions exist on the market [C.1.11]. Furthermore, every device in the system communicates all of its measurements to this device.

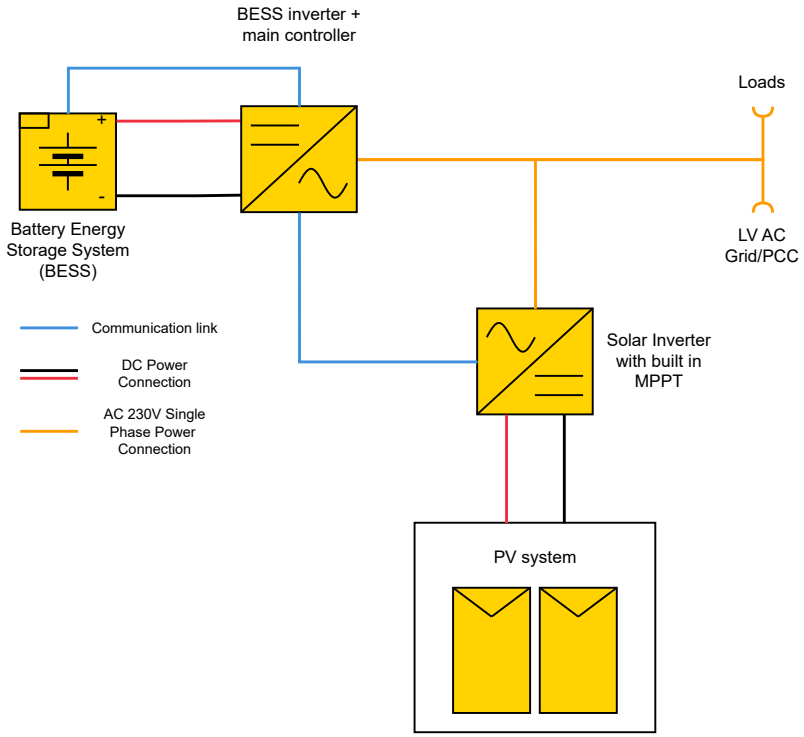

Figure D.7: Electrical diagram of an AC connected BESS for the upgraded solution. The devices highlighted in yellow are the devices that needs to be installed for the upgrade with a BESS.

Based on this, the total cost of this integrated solution was calculated and is given in table D.4.1. The total cost of this integrated solution amounts to €7255.80 and is around 179.29% more than the cost of a PV system.

	Price (€)
BESS	900
BESS Inverter	1316
ESS integrated with PV system cost	5039.80
Total Price	7255.8

Table D.5: Cost of an AC connected BESS integrated solution.

D.4.2. DC connected BESS system cost

For the DC connected BESS integrated solution, Furthermore as with the other DC connected solution, figure D.10 illustrates the electrical diagram of this solution.

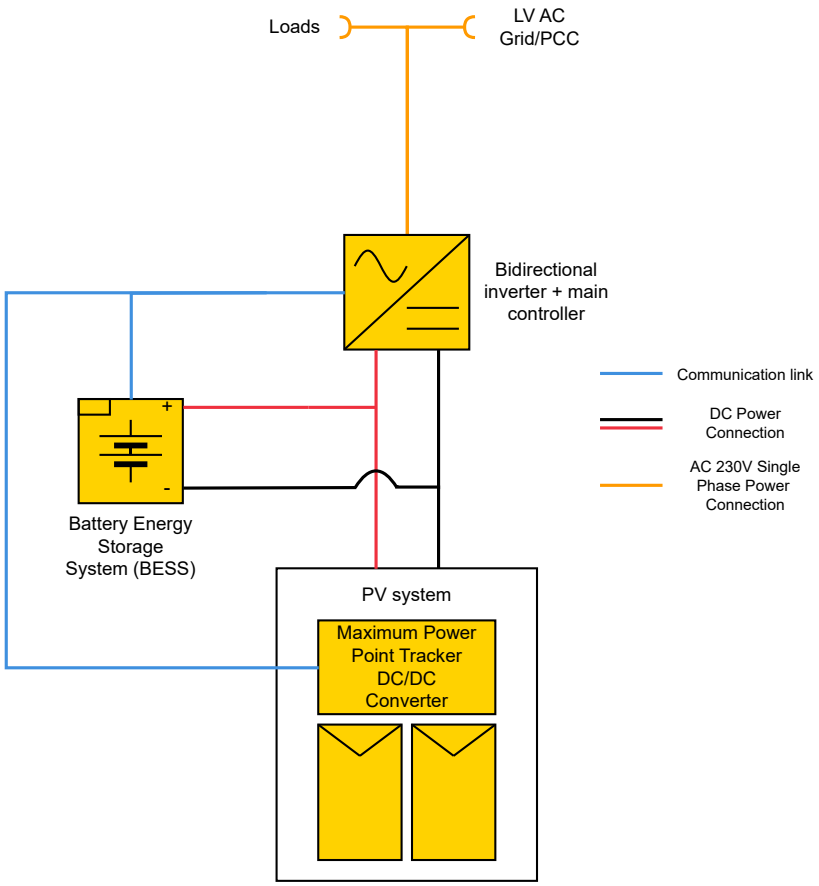

Figure D.8: Electrical diagram of an DC connected BESS for the upgraded solution. The devices highlighted in yellow are the devices that needs to be installed for the upgrade with a BESS.

The total cost of such a solution is tabulated in table D.4.2 and the total cost of this solution was calculated to be around €7483.70. This is around 184.92% more cost than the total cost of a PV system.

	Price (€)
BESS	900
Main inverter	1316
MPPT DC/DC converter	627.90
ESS integrated with PV system cost	4639.80
Total Price	7483.70

Table D.6: Cost of an DC connected BESS integrated solution.

D.4.3. AC connected SESS system cost

For the AC connected SESS integrated solution, the electrical diagram for this solution is given in figure D.9.

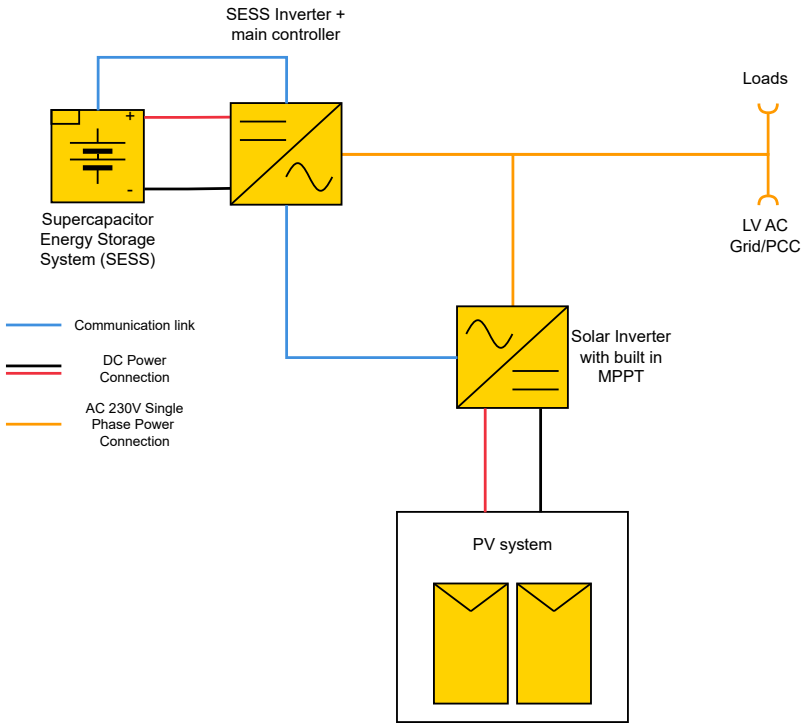

Figure D.9: Electrical diagram of an AC connected SESS for the upgraded solution. The devices highlighted in yellow are the devices that needs to be installed for the upgrade with a SESS.

The total cost of this solution is given in table D.4.3 and the total cost of the solution was calculated to be around €9935.90. This is around 245.51% more expensive than the total cost of a PV system.

	Price (€)
SESS	900
Main inverter	1896
ESS integrated with PV system cost	5039.80
Total Price	9935.80

Table D.7: Cost of an AC connected SESS integrated solution.

D.4.4. DC connected SESS system cost

For the DC connected SESS integrated solution, the main takeaway is that a DC/DC converter has to be connected between the DC bus and the SESS to keep the DC bus voltage constant. Furthermore as with the other DC connected solution, a MPPT DC/DC converter has to be connected to the PV system. Figure D.10 illustrates the electrical diagram of this solution. The total cost of such a soltion is tabulated in

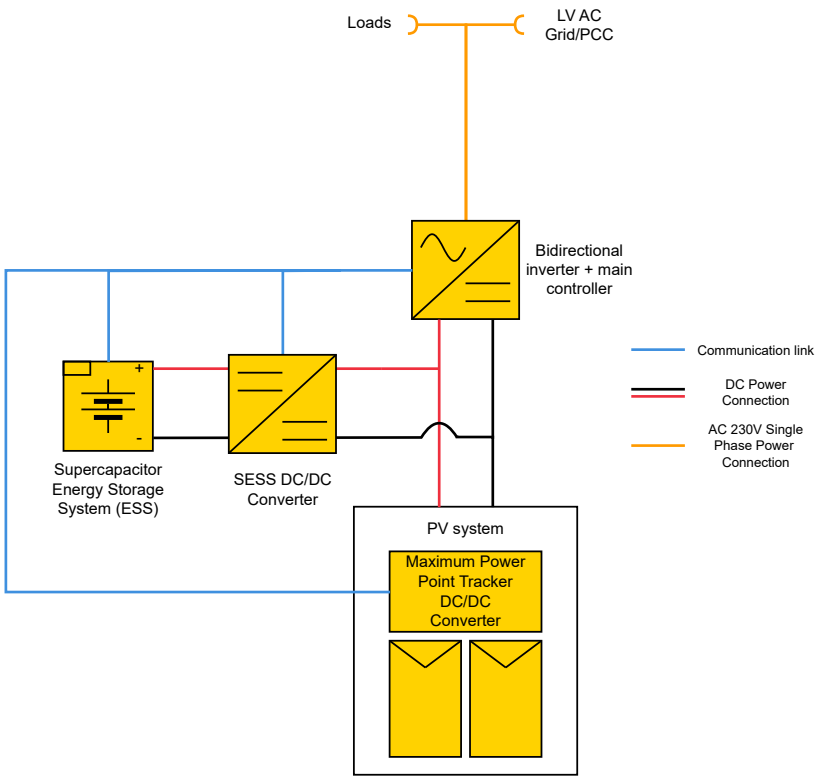

Figure D.10: Electrical diagram of an DC connected BESS for the upgraded solution. The devices highlighted in yellow are the devices that needs to be installed for the upgrade with a BESS.

The total cost of this solution is tabulated in table D.4.4 and the total cost was calculated to be around €10163.70. This is around 251.14% more expensive than the cost of a PV system.

	Price (€)
SESS	3000
SESS DC/DC converter	580
MPPT DC/DC converter	627.90
Main inverter	1316
ESS integrated with PV system cost	4639.80
Total Price	10163.70

Table D.8: Cost of an DC connected SESS integrated solution.

D.5. Summary of findings

Based on the findings from the previous sections, a summary of this is made and is illustrated in figure D.11. Based on the figure, the main conclusion is that an upgraded or integrated solution price do not differ significantly from eachother. This is due to the cost of an integrated device being the same as the cost of the separate devices. In the future, it is asssumed that this price would reduce making an integrated solution more lucrative for homeowners. The same can be said for the cost of the PV system, BESS and SESS. For the SESS since this type of ESS is not as widely used as BESS, the cost of a SESS is much higher since SESS are not as widely mass produced as BESS and currently there are less manufacturing plants for SESS than for BESS. All in all, the cost of implementing BESS for this particular application is around 3000 euros extra and with a SESS it is around 6000 euros extra than the cost of only installing a PV system.

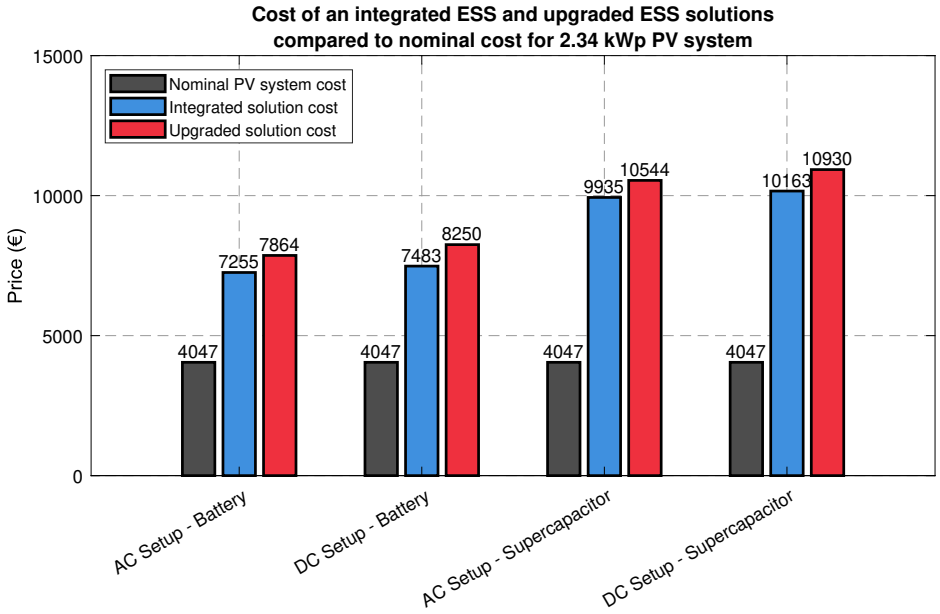

Figure D.11: Summary of the cost for an upgraded and integraded solution using BESS or SESS at two different connection points.